Using pharmacological and proteomic analysis to investigate molecular pathways in cellular senescence



Hannah Walters

Trinity College

University of Oxford

A thesis submitted for the degree of

Doctor of Philosophy

Trinity 2019

Abstract

Upon detection of genotoxic or other stress, cells can withdraw from the cell cycle and become senescent, a fate characterized by resistance to apoptosis, organelle dysfunction and pro-inflammatory secretion. Compelling evidence has highlighted a causal role for senescence in driving pathological ageing, alongside dysregulation of molecular pathways including mTOR and sirtuin signalling. In this thesis, I firstly report generation of a novel model of senescence based on acute treatment of primary human fibroblasts with the sirtuin 1/2 inhibitor Tenovin-6 (TnV6), characterized by permanent cell cycle arrest coincident with p21 upregulation and increased secretion of the SASP factor IL-6. Secondly, I used a range of senescence models and a panel of mTOR inhibitors to investigate mTOR signalling in senescence. Notably, acute treatment of senescent fibroblasts with the pan-mTOR inhibitor AZD8055 reversed multiple senescence phenotypes, including suppression of pro-inflammatory secretion, reduction in actin stress fibres, activation of mitophagy, decreased cellular hypertrophy and the stabilisation of nuclear structure. Furthermore, AZD8055 treatment also disrupted induction of senescence-associated proliferation arrest in a range of models of senescence including DNA damage-induced senescence, coincident with preventing upregulation of p21. In cells approaching replicative senescence, AZD8055 treatment substantially increased the replicative capacity; treatment also stabilized telomere length, in both wild-type and Werner syndrome patient fibroblasts. In addition, I created an unbiased molecular profile of replicative senescence using comparative proteomics, revealing the importance of actin remodelling in senescence, and its regulation through mTOR signalling. I subsequently noted a functional role for senescence-associated dysregulation of cytoskeletal remodelling in orchestrating direct cell-cell contact, and observed intercellular organelle transfer. My findings highlight mTOR signalling as a master regulator of both cell-autonomous and non-cell-autonomous aspects of cellular senescence.

Acknowledgements

Thanks to all members of the Cox lab past and present for a really enjoyable four years, in particular to Adam, Anitha, Sebastian and Gabriel for keeping every day interesting, to the many Part II students who have always been entertaining, and to Hayley whose cakes (and conversation!) are now sorely missed in the department. Thanks also to the Mellor lab for adopting me into their laser quest team. Above all, thanks to Lynne for guiding me through the past four years.

Thank you to my family and friends, especially Caz, Anu and Alex for all your solidarity and encouragement. Some have really gone above and beyond in their support (sorry Grandad, I think there are quite a lot of commas in here too). Tom, thanks for all your advice and reassurance (scientific and otherwise), for keeping me sane while writing, and for the continuous supply of G&T.

Most importantly, I am extremely grateful to the anonymous individual who funded the Oxford Graduate Scholarship in Cell Senescence. Making such a significant donation to support fundamental ageing research is an incredible act of generosity. I have immensely enjoyed working in such an exciting field and look forward to continuing to research senescence, building on the foundation of my DPhil training. Whoever you are, thank you.

Several portions of this thesis are reproduced from publications which I co-authored (all text and data presented here are my own work). In particular, part of the introduction is based on a recent review (Walters and Cox, 2018), Chapter 3 is based on a recent publication (Walters and Cox, 2019) and Chapter 4 builds on the findings of a previous publication (Walters et al., 2016).

Contents

Abstract ..... **ii**
Acknowledgements ..... **iii**
List of figures and tables ..... **ix**
List of abbreviations ..... **xiii**
1. Introduction **1**
1.1. Ageing as a public health concern 1
1.2. Factors affecting ageing 4
1.3. Cellular senescence 4
1.3.1. Senescence induction 5
1.3.2. Molecular players 5
1.3.3. Hallmarks of senescence 11
1.3.3.1. Morphological features 11
1.3.3.2. Organelle dysfunction in senescence 13
1.3.3.2.1. Mitochondrial dysfunction 13
1.3.3.2.2. Lysosome stress 14
1.3.3.2.3. ER stress 15
1.3.3.2.4. Altered plasma membrane 16
1.3.3.3. Senescent cell communication 17
1.3.3.3.1. Pro-inflammatory secretion (SASP) 17
1.3.3.3.2. Extracellular vesicles 19
1.3.3.3.3. Direct intercellular communication 20
1.3.3.4. DNA damage 20
1.3.3.4.1. DNA damage foci 20
1.3.3.4.2. Cytoplasmic chromatin fragments (CCFs) 22
1.3.3.4.3. DNA repair disorders and senescence 23
1.3.3.5. Chromatin changes 24
1.3.3.6. Resistance to apoptosis 26
1.3.4. Autophagy and senescence 27
1.3.5. Beneficial physiological roles of senescence 31
1.3.6. Senescence and ageing 33
1.3.7. Senescence-based therapies to promote healthy ageing 36
1.4. mTOR in senescence and ageing 43

1.4.1. mTOR signalling 43
1.4.2. mTOR in senescence 43
1.4.3. mTOR in ageing 47
1.4.4. mTOR inhibitors 47
1.4.5. mTOR inhibitors as therapeutics for age-related diseases 49
1.5. Aims of research 53
2. **Materials and methods 54**
2.1. Cell Culture 54
2.1.1. Routine subculture of primary human cell lines 54
2.1.2. Induction of senescence 57
2.1.2.1. Replicative senescence 57
2.1.2.2. DNA damage induced senescence 59
2.1.2.3. Oncogene-induced senescence 59
2.1.3. Drug treatments 59
2.2. Commercial cell culture-based assays 61
2.2.1. alamarBlue metabolic activity assay 61
2.2.2. Sulforhodamine B biomass assay 62
2.2.3. Click-iT EdU proliferation assay 62
2.2.4. Fluor de Lys® HDAC assay 62
2.2.5. Autophagy (CYTO-ID) 63
2.2.6. Cell cycle stage determination (Cell Cycle Clock) 63
2.3. IL-6 detection 64
2.3.1. IL-6 ELISA 64
2.3.2. HEK-BLUE IL6 reporter cell assay 64
2.4. Western blotting 65
2.5. Telomere analysis 65
2.5.1. Southern blotting (TeloTAGGG) 65
2.5.2. TeloFISH 67
2.6. Cell staining 67
2.6.1. Immunofluorescence 67
2.6.2. Mitochondria 68
2.6.3. Lysosomes 68
2.6.4. Actin 68
2.6.5. Tubulin 69
2.6.6. Plasma membrane 69
2.6.7. DNA 69

2.6.8. ROS 69
2.7. Microscopy 70
2.7.1. Phase contrast microscopy 71
2.7.2. Fluorescence microscopy 71
2.7.3. High-content imaging 71
2.8. Quantitative comparative proteomics 71
2.9. Statistical analysis 72
3. Generation of a novel model of primary human cell senescence through Tenovin-6 mediated inhibition of sirtuins 73
3.1. Introduction 74
3.2. Chapter aims 77
3.3. Results 77
3.3.1. TnV6 suppresses deacetylase activity 77
3.3.2. Low dose TnV6 treatment is cytostatic for primary cells and less toxic to cancer cells 79
3.3.3. Primary cells arrest in G1 on TnV6 treatment 83
3.3.4. Extended TnV6 treatment leads to increased cell size and senescent morphology in primary fibroblasts 85
3.3.5. Markers of cell senescence are elevated on TnV6 treatment 87
3.3.6. Extended TnV6 treatment induces SASP secretion from primary fibroblasts 91
3.3.7. Unexpected DNA damage following TnV6 treatment of primary cells 93
3.4. Discussion 95
3.5. Evaluation of TnV6-induced senescence as an experimental system 99
4. Reversal of phenotypes of cellular senescence by pan-mTOR inhibition 101
4.1. Introduction 102
4.2. Chapter aims 103
4.3. Results 104
4.3.1. Nanomolar dose AZD8055 is non-toxic and inhibits mTOR-dependent phosphorylation events 104
4.3.2. Morphological rejuvenation of senescent cells by acute pan-mTOR inhibition 105
4.3.3. Effects of pan-mTOR inhibition on lysosomal dysfunction 108
4.3.4. Major rearrangement of the actin cytoskeleton accompanies reversal of other senescent biomarkers 110
4.3.5. Loss of dysfunctional mitochondrial on pan-mTOR inhibition 112
4.3.6. Increase of autophagy and mitophagy on pan-mTOR inhibition in senescent fibroblasts 115
4.3.7. Reduced nuclear area and improved nuclear integrity on pan-mTOR inhibition 117

4.3.8. Pan-mTOR inhibition reduces pro-inflammatory secretion 120
4.3.9. Removal of treatment results in re-acquisition of senescent phenotypes 122
4.3.10. Reversal of phenotypes of cell senescence using a panel of mTOR inhibitors 124
4.3.11. Reversal of phenotypes of cell senescence in other models of senescence 126
4.4. Discussion 129
5. Pan-mTOR inhibition delays but does not reverse replicative, DNA damage and sirtuin inhibition induced senescence 136
5.1. Introduction 137
5.2. Chapter aims 139
5.3. Results 140
5.3.1. Deeply senescent cells do not re-start proliferation on extended pan-mTOR inhibition 140
5.3.2. Extension of primary human fibroblast replicative capacity on continuous or pulsed pan-mTOR inhibition 142
5.3.3. Pan-mTOR inhibition does not result in dramatic telomere elongation despite extension of replicative capacity 148
5.3.4. Premature senescence in Werner syndrome fibroblasts is attenuated by pan-mTOR inhibition 154
5.3.5. Pan-mTOR inhibition disrupts acutely-induced senescence 159
5.4. Discussion 168
5.4.1. Regulation of p21 and proliferation arrest by mTOR signalling 169
5.4.2. Crosstalk between mTOR and telomerase 172
5.4.3. Regulation of paracrine senescence? 174
5.4.4. Therapeutic options for Werner syndrome and healthy ageing 176
6. Comparative proteomic profiling of replicative senescence reveals proteome rejuvenation on pan-mTOR inhibition together with therapeutic candidates including actin reorganization 178
6.1. Introduction 179
6.1.1. Proteomics principles and methodology 179
6.1.2. Applications of comparative proteomics 180
6.2. Chapter aims 182
6.3. Results 183
6.3.1. Comparative proteomic profile of replicative senescence 183
6.3.2. Rejuvenation of the senescent proteome by acute pan-mTORC inhibition 196
6.3.3. Comparative proteomics analysis of replicative senescence identifies therapeutic candidate pathways and targets 204
6.3.3.1. Targeting actin reorganization 204
6.3.3.2. Targeting oxidative stress 208

6.4. Discussion 214
6.4.1. Actin organization and senescence 214
6.4.2. Oxidative stress and senescence 219
7. Altered actin organization networks in senescence direct intercellular organelle transfer 221
7.1. Introduction 222
7.2. Chapter aims 225
7.3. Results 225
7.3.1. Actin- and tubulin-based intercellular bridges connect senescent cells 225
7.3.2. Senescent nanotubes support intercellular mitochondrial transport 227
7.3.3. Direct intercellular communication in senescence is regulated by mTOR and Cdc42 signalling 233
7.4. Discussion 235
7.4.1. Physiological relevance of direct intercellular senescent contacts 237
7.4.2. Supercellularity in senescence: cell-cell bridges vs. cell-cell fusion 238
7.4.3. Targeting intercellular nanotubes in disease 239
7.4.4. Future work 240
8. Discussion 243
8.1. Summary 243
8.1.1. Exploring the mechanism of mTOR-dependent regulation of cellular senescence 244
8.1.2. Importance of actin remodelling in cellular senescence 246
8.2. Future work 247
8.2.1. mTORC1-specific inhibition 248
8.2.2. mTOR as senolytic target 249
8.2.3. Targeting mTOR to tackle bystander senescence *in vivo* 250
8.2.4. Targeting intercellular communication 251
8.3. Perspectives 252
8.3.1. Enhancing immunosurveillance 253
8.3.2. Therapeutic potential of targeting senescence in ageing 255
9. References 256
10. Supplementary Material 281

List of figures and tables

Number	Title	Page
Figure 1.1	Population ageing across the globe, its associated costs and risk factors	3
Figure 1.2	Telomere folding and the end-replication problem	7
Figure 1.3	A summary of molecular pathways governing the onset of cellular senescence	10
Figure 1.4	Regulation of autophagy and mitophagy	30
Table 1.1	Age-related diseases attenuated by senescent cell removal	37
Figure 1.5	Possible therapeutic targets in senescence	42
Figure 1.6	mTORC1 and mTORC2 regulation, crosstalk and downstream signalling consequences	46
Table 1.2	mTORC inhibitors as broad-spectrum therapeutics for age-related disease	51
Table 2.1	Details of the cell lines used in this thesis and appropriate media supplements	56
Figure 2.1	Induction of replicative senescence	57
Figure 2.2	Induction of DNA damage and oncogene-induced senescence	60
Table 2.2	Drugs used in this thesis	61
Table 2.3	Antibodies used in Western blotting and immunofluorescence	69
Figure 3.1	TnV6 strongly suppresses deacetylase activity in both primary and cancer cells	78
Figure 3.2	TnV6 exhibits dose-dependent toxicity in primary and cancer cells	80
Figure 3.3	Low dose TnV6 induces sustained proliferation arrest in primary human fibroblasts	82
Figure 3.4	Ablation of DNA replication in primary human fibroblasts on low dose TnV6 treatment	83
Figure 3.5	G1 phase arrest in primary human fibroblasts treated with TnV6	84

Figure 3.6	TnV6 induces p21 upregulation in primary human fibroblasts	85
Figure 3.7	Extended TnV6 treatment induces senescent morphology	87
Figure 3.8	Extended TnV6 treatment induces senescence-associated lysosomal dysfunction	88
Figure 3.9	TnV6 treatment results in nuclear area increase	89
Figure 3.10	Extended TnV6 treatment results in mitochondrial accumulation and actin stress fibres	90
Figure 3.11	IL-6 is upregulated in TnV6-treated cells	92
Figure 3.12	Extended TnV6 treatment induces DNA damage	94
Figure 4.1	A non-toxic dose of AZD8055 inhibits mTOR activity	105
Figure 4.2	AZD8055 rejuvenates senescent cell morphology	107
Figure 4.3	AZD8055 treatment reduces lysosomal dysfunction	109
Figure 4.4	AZD8055 treatment disrupts actin stress fibres in senescent fibroblasts	111
Figure 4.5	AZD8055 treatment reduces dysfunctional mitochondrial accumulation in senescent fibroblasts	114
Figure 4.6	AZD8055 treatment induces autophagy and mitophagy	116
Figure 4.7	Pan-mTOR inhibition reduces nuclear size and improves nuclear integrity in senescent fibroblasts	119
Figure 4.8	AZD8055 treatment reduces IL-6 secretion from senescent fibroblasts	121
Figure 4.9	Senescent phenotypes re-appear following AZD8055 treatment removal	123
Figure 4.10	Rapalogue treatment reverses phenotypes of senescence including lysosomal dysfunction, enlarged morphology, mitochondrial accumulation, actin stress fibres and IL-6 secretion	125
Figure 4.11	AZD8055 treatment rejuvenates morphology in a range of models of senescence	128
Figure 5.1	Pan-mTOR inhibition does not compromise proliferation arrest in deeply senescent fibroblasts	141

Figure 5.2	Pan-mTOR inhibition extends replicative capacity of human primary fibroblasts	145
Figure 5.3	Pan-mTOR inhibition prevents induction of senescence phenotypes	147
Figure 5.4	Telomere assessment over continuous passaging with and without AZD8055 treatment by TeloFISH	151
Figure 5.5	Telomere assessment over continuous passaging with and without AZD8055 treatment by Southern blotting	152
Figure 5.6	AZD8055 treatment prevents p21 upregulation in high CPD fibroblasts	153
Figure 5.7	Pan-mTOR inhibition extends proliferative capacity of Werner syndrome fibroblasts	156
Figure 5.8	Pan-mTOR inhibition disrupts phenotypes of senescence in Werner syndrome fibroblasts	157
Figure 5.9	Telomere length is stabilized on pan-mTOR inhibition in Werner syndrome fibroblasts	159
Figure 5.10	Pan-mTOR inhibition disrupts induction of DNA damage induced senescence	163
Figure 5.11	Pan-mTOR inhibition disrupts phenotypes of senescence induced by etoposide treatment	164
Figure 5.12	AZD8055 treatment prevents p21 upregulation on etoposide treatment	165
Figure 5.13	Pan-mTOR inhibition disrupts induction of TnV6-mediated senescence	167
Figure 6.1	Comparative proteomics methodology	181
Figure 6.2	Analysis of phenotypes of senescence in proliferating, peri-senescent and replicatively senescent fibroblasts for comparative proteomic analysis	184
Figure 6.3	Pathway analysis of comparative proteomics reveals important molecular drivers of senescence	187
Figure 6.4	GO analysis of comparative proteomics highlights important processes altered by replicative senescence	189
Figure 6.5	Important protein level changes in senescence	195

Figure 6.6	Pan-mTOR inhibition causes proteomic changes over the replicative lifespan of primary fibroblasts	200
Figure 6.7	Cytoskeletal remodelling is a therapeutic target in senescence	206
Figure 6.8	Inhibiting actin polymerisation through ROCK, PAK or Cdc42 disrupts phenotypes of senescence	208
Figure 6.9	Possible therapeutic targets upregulated in senescence	209
Figure 6.10	Upregulation of redox enzymes in replicative senescence	210
Figure 6.11	Auranofin induces oxidative stress in proliferating fibroblasts	211
Figure 6.12	Targeting oxidative stress in senescence using auranofin is mildly senolytic	213
Figure 7.1	Senescent cells are connected by thin intercellular contacts *in vitro*	226
Figure 7.2	Senescent intercellular contacts are composed of membrane, actin and tubulin	227
Figure 7.3	Mitochondria are present within senescent intercellular contacts	229
Figure 7.4	Mitochondria are motile within senescent intercellular contacts	230
Figure 7.5	Co-culture assay for analysis of intercellular mitochondrial transfer	231
Figure 7.6	Co-culture assay reveals evidence of intercellular mitochondrial transfer	233
Figure 7.7	Cdc42 and mTOR signalling control formation of intercellular bridges in senescent cells	235
Figure 8.1	mTOR as a central regulator of the cell-autonomous and non-cell-autonomous aspects of cellular senescence	245
Table S6.1	Statistical hits of pairwise comparisons from comparative proteomics of replicative senescence	281
Table S6.2	Statistical hits of pairwise comparisons from comparative proteomics of pan-mTOR inhibition	284

List of abbreviations

Abbreviation	Meaning
2DGE	2 dimensional gel electrophoresis
4-OHT	4'hydroxytamoxifen
5'TOP	5' terminal oligopyrimidine tract
AD	Alzheimer's disease
ADCC	antibody-dependent cell-mediated cytotoxicity
AGE	advanced glycation end products
ALT	alternative lengthening of telomeres
AMD	age-related macular degeneration
ANOVA	analysis of variance
ATP	adenosine triphosphate
AZD	AZD8055
BSA	bovine serum albumin
CAR-T	chimeric antigen receptors on cytotoxic T cells
CASIN	Cdc42 activity specific inhibitor
CCF	cytoplasmic chromatin fragment
CDP-Star	chemiluminescent substrate
cGAMP	cyclic guanosine monophosphate-adenosine monophosphate
ChIP-seq	chromatin immunoprecipitation sequencing
CHO	Chinese hamster ovary cells
CKI	cyclin-dependent kinase inhibitor
CM	conditioned media
CML	chronic myeloid leukaemia
COPD	chronic obstructive pulmonary disease
CPD	cumulative population doubling
CR	caloric restriction
CVD	cardiovascular disease
D+Q	dasatinib and quercetin (senolytic combination therapy)
DamID	DNA adenine methyltransferase identification
DAPI	4',6-diamidino-2-phenylindole
DC	dendritic cell
DCFDA	2',7'-dichlorodihydrofluorescein diacetate
DDIS	DNA damage induced senescence
DDR	DNA damage response
DIG	digoxigenin
DKC	dyskeratosis congenita
DMEM	Dulbecco's modified eagle's medium
DMSO	dimethyl sulfoxide
DN	diabetic nephropathy
DNA-SCARS	DNA segments with chromatin alterations reinforcing senescence
DR	dietary restriction

Abbreviation	Meaning
DRI-FOXO4	D-retro-inverse peptide of FOXO4
DSB	double strand break
ECM	extracellular matrix
ELISA	enzyme-linked immunosorbent assay
EMT	epithelial-mesenchymal transition
ER	endoplasmic reticulum
ER:Ras	estrogen receptor driven oncogenic Ras
ERAD	endoplasmic reticulum-associated protein degradation
ETC	electron transport chain
ETOP	etoposide
EV	extracellular vesicle
FACS	fluorescence-activated cell sorting
FASP	filter-aided sample preparation
FBS	fetal bovine serum
FDA	Food and Drug Administration (USA)
FISH	fluorescence in-situ hybridization
FITC	fluorescein isothiocyanate
gDNA	genomic DNA
GO	gene ontology
HAART	highly active antiretroviral therapy
HCI	high content imaging
HDAC	histone deacetylase complex
HEK-Blue	human embryonic kidney reporter cells
HGPS	Hutchinson-Gilford Progeria Syndrome
HIV	human immunodeficiency virus
HSC	hematopoietic stem cell
IDD	invertebral disc degeneration
IF	immunofluorescence
IF	intermediate filament
INK-ATTAC	transgene for inducible elimination of p16Ink4a-positive cells
IPA	Ingenuity Pathway Analysis
IPF	idiopathic pulmonary fibrosis
iPSC	induced pluripotent stem cells
IPTG	isopropyl-β-D-thiogalactoside
IR	ionizing radiation
IRES	internal ribosome entry site
ISR	integrated stress response
LAD	lamina-associated domain
LC-MS/MS	liquid chromatography – tandem mass spectrometry
LFQ	label-free quantification
MEF	mouse embryonic fibroblasts
MMP	matrix metalloprotease
MOMP	mitochondrial outer membrane permeabilization
MSC	mesenchymal stem cells
mtDNA	mitochondrial DNA

Abbreviation	Meaning
NAD	nicotinamide adenine dinucleotide
NK	natural killer cells
NLS	nuclear localization signal
NP	nucleus pulposus
NSG	NOD SCID γ (immunodeficient) mice
OA	osteoarthritis
OIS	oncogene-induced senescence
OSKM	OCT4, SOX2, KLF4, MYC reprogramming transcription factors
p16-3MR	trimodality reporter mice for inducible senescent cell ($p16^{+}$) removal
PANTHER	protein analysis through evolutionary relationships
PBS	phosphate buffered saline
PBS-T	phosphate buffered saline with 0.1% Tween (v/v)
PBS-T-BSA	phosphate buffered saline with 0.1% Tween (v/v) and 5% BSA(w/v)
PCR	polymerase chain reaction
PD	population doublings
PD	Parkinson's disease
PML	promyelocytic leukaemia protein nuclear bodies
PNA	peptide nucleic acid
PRO	proliferating
qPCR	quantitative polymerase chain reaction
RA	rheumatoid arthritis
rDNA	ribosomal DNA
RIPA	radioimmunoprecipitation assay buffer
RNA-seq	RNA-sequencing
ROS	reactive oxygen species
RPM	revolutions per minute
RS	replicative senescence
RSV	resveratrol
RT	room temperature
RTK	receptor tyrosine kinase
SA-β-gal	senescence-associated β-galactosidase
SAHF	senescence-associated heterochromatic foci
SASP	senescence-associated secretory phenotype
SCF	Skp1, Cullins, F-box multi-subunit E3 ubiquitin ligase complexes
SD	standard deviation
SEAP	secreted embryonic alkaline phosphatase
SEN	senescent
SILAC	stable isotope labelling by/with amino acids in cell culture
siRNA	small interfering RNA
SRB	sulforhodamine B
SSB	single strand break
TAD	topologically-associated domain
TCA	tricarboxylic acid
TID	type I diabetes
TIID	type II diabetes

Abbreviation	Meaning
TIS	tenovin-6-induced senescence
TNT	tunnelling nanotube
TnV6	tenovin-6
TRAP	telomerase repeated amplification protocol
TRF	telomere restriction fragment
TSA	trichostatin A
TSG	tumour suppressor gene
UPR	unfolded protein response
UTR	untranslated region
v/v	volume for volume
w/v	weight for volume
WGA	wheat germ agglutinin
WS	Werner syndrome

1. Introduction

1.1. Ageing as a public health concern

Prediction modelling of population trends has suggested that the number of people aged ≥65 in England and Wales will increase to 12.4 million by 2025, up from 10.4 million in 2015 (Guzman-Castillo et al., 2017). In this time, life expectancy is projected to increase, but the proportion of life expectancy with disability (morbidity period) is predicted to grow more in relative terms (Figure 1.1A). Hence elderly patients face a further increase in disease burden and decline in quality of life, comprising years of both physical and mental ill health (Niccoli and Partridge, 2012). This also constitutes a substantial strain on the economy, in the clinic, in social care and in support from relatives, which impacts women disproportionately (Sharma et al., 2016, Figure 1.1B). These changes are in line with global trends, despite vast discrepancies in life expectancy globally (Figure 1.1C) due to a range of environmental and social factors (Figure 1.1D), which can also cause remarkably local inequality (Figure 1.1E). Our current infrastructure is poorly equipped to cope with the increasing clinical and care demands of a growing elderly population. Urgent action needs to be taken in improving social care and in tackling disease risk factors including poor diets, smoking, alcohol consumption and lack of physical activity.

Moreover, there is vast unmet clinical demand for interventions that could prevent or treat age-related conditions, as well as for premature ageing disorders such as Werner syndrome and Hutchinson-Gilford Progeria. Intriguingly, the occurrence of such diseases that phenocopy normal human ageing at an accelerated rate also suggests the existence of a defined ageing process, which may be influenced by genes rather than driven by environmental factors alone. Indeed, meta-analysis data has suggested that heterozygous

carriers of DNA repair factor mutations such as ATM (which if homozygous would result in Ataxia Telangiectasia), who represent 1-2% of certain populations, are at increased risk of developing age-related diseases earlier in life, including cardiovascular disease, cataracts and cancer (van Os et al., 2016). Ongoing research is seeking to understand the factors driving ageing and excitingly, providing a number of possible interventions for a wide range of age-related diseases, through targeting the underlying causes of pathological ageing.

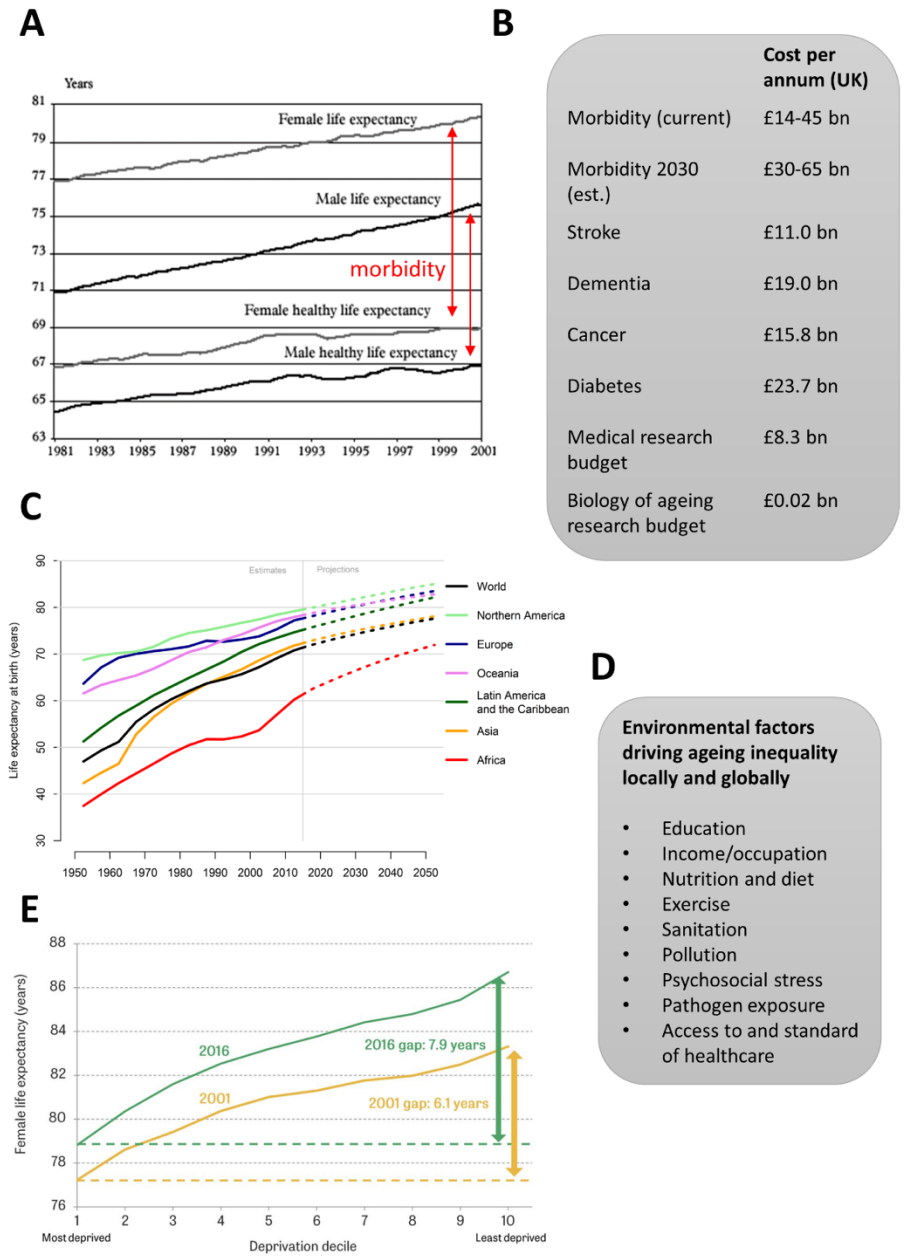


Figure 1.1. Population ageing across the globe, its associated costs and risk factors

A: life expectancy and healthy life expectancy in the UK 1981-2001, data source: Health Statistics Quarterly no. 15 Autumn 2002, edited to show morbidity period i.e. years of ill health before death. B: estimated or projected costs per annum (UK) for medical care and research budgets, data source: Office for National Statistics. C: estimated and projected life expectancy at birth globally and by continent, data source: United Nations (2017) World Population Prospects: the 2017 Revision. D: schematic showing environmental factors causing inequality in expected lifespans globally and locally. E: female life expectancy at birth by UK deprivation index decile, 2001 and 2016; figure reproduced from Bennett et al., 2018.

1.2. Factors affecting ageing

Organismal ageing is characterized by the gradual loss of physiological function over time, contributing to an increased risk of death. While this process appears inevitable throughout nature (with notable exceptions including Hydra and naked mole rats, Lees et al., 2016), important discoveries have shown that ageing is plastic and driven by a number of biochemical pathways and processes (Kenyon et al., 1993, Baker et al., 2011, Baker et al., 2016, Harrison et al., 2009, López-Otín et al., 2013). Such processes are 'antagonistically pleiotropic': while beneficial in youth, contributing to survival and reproduction, they can subsequently result in ageing, and the onset and progression of age-related disease. In this thesis, I investigate the interplay between central processes thought to drive ageing: stress signalling and cellular senescence (López-Otín et al., 2013).

1.3. Cellular senescence

Cellular senescence is an essentially permanent cell cycle arrest programme that cells undergo in response to a variety of stressors, which has been critically implicated in driving ageing (Baker et al., 2016). Senescence was first discovered as a limit to the replicative lifespan of primary cells in culture, in contrast to the unlimited proliferative capacity of cancer cells, highlighting the role of senescence as an important anti-cancer mechanism (Hayflick and Moorhead, 1961). However, senescence is now recognized as a universal anti-proliferative response to a range of stimuli, with both beneficial and detrimental consequences *in vivo* which depend on the nature of induction, the cell type, the surrounding microenvironment and the efficiency of senescent cell clearance (Yun, 2018). Senescent cells are refractory to mitogenic signalling and exhibit a range of phenotypic changes, including induction of a pro-inflammatory phenotype (the senescence-associated

secretory phenotype (SASP), Campisi, 2013). Senescence is an alternative fate to apoptosis in response to irreparable cellular damage; indeed senescent cells are highly resistant to apoptosis (Childs et al., 2014).

1.3.1. Senescence induction

A variety of stressors can induce cell senescence (reviewed in Muñoz-Espín and Serrano, 2014), including exhaustive telomere attrition (replicative senescence, Figure 1.1), as well as other irreparable DNA damage caused by endogenous or exogenous agents such as genotoxic chemotherapeutics. Stalling of DNA replication and oxidative stress are also able to induce senescence, both acting at least in part by causing DNA damage. Furthermore, oncogene activation (e.g. Ras (Serrano et al., 1997) or BRAF (Michaloglou et al., 2005)), or tumour suppressor inactivation (e.g. PTEN (Chen et al., 2005)) can also induce senescence in untransformed cells, as well as other stressors including protein misfolding, ER stress, ribosomal imbalances, viral infection, polyploidy, cell-cell fusion and mitochondrial dysfunction (Wiley et al., 2016). Further, proximity to other senescent cells can induce senescence via a bystander mechanism termed paracrine senescence (Nelson et al., 2012). It is not yet clear whether each of these types of senescence actually occur *in vivo* and if so, to what extent. However, by enforcing proliferative arrest upon recognition of damage or stress, cellular senescence is an important cell-autonomous anti-tumour mechanism that prevents the propagation of potentially damaged cells.

1.3.2. Molecular players

While a diverse range of stressors promote the induction of senescence, these upstream signals all converge on cell cycle regulatory pathways to elicit proliferation arrest. At the molecular level, the cyclin-dependent kinase inhibitors (CKI) $p21^{WAF1/CDKN1A}$, $p16^{INK4A/CDKN2A}$, $p15^{INK4B/CDKN2B}$ and $p27^{CDKN1B}$ (hereafter p21, p16, p15 and p27) all play important roles in enforcing and maintaining cell cycle arrest (Takahashi et al., 2007, Han et al., 2002).

In replicative senescence, telomeres that cap the ends of linear chromosomes are gradually eroded after multiple rounds of cell proliferation in the absence of telomerase activity, due to the end replication problem inherent in the mechanism of DNA replication (Levy et al., 1992, Figure 1.2A). A critically short telomere cannot correctly fold into its higher order structure for shelterin complex binding, which otherwise protects the chromosome end from recognition as a DNA double-strand break (DSB, Figure 1.2B). Critically short telomeres hence elicit a DNA damage response and activate p53 (Rossiello et al., 2014). As well as acting as molecular 'clocks' by monitoring proliferation events, telomeres also play an important role as a DNA damage sensor; the G-rich telomeric repeats (TTAGGG) are particularly sensitive to oxidative stress (Von Zglinicki, 2000) and shelterin components impede access to telomeric DNA for the DNA repair machinery (Fumagalli et al., 2012), while the G4 quadruplex structure may intrinsically impede DNA repair and replication machinery.

Upon sensing DNA damage such as telomere shortening, the DNA damage response (DDR) sensor kinases ATM and ATR signal through checkpoint kinases CHK1 and CHK2 to phosphorylate and activate several cell cycle proteins including p53. Through subsequent upregulation of p21 and inhibition of CDK-cyclin complexes (particularly CDK2, cyclins A and E), cell cycle arrest is enforced (d'Adda di Fagagna et al., 2003, Figure 1.3).

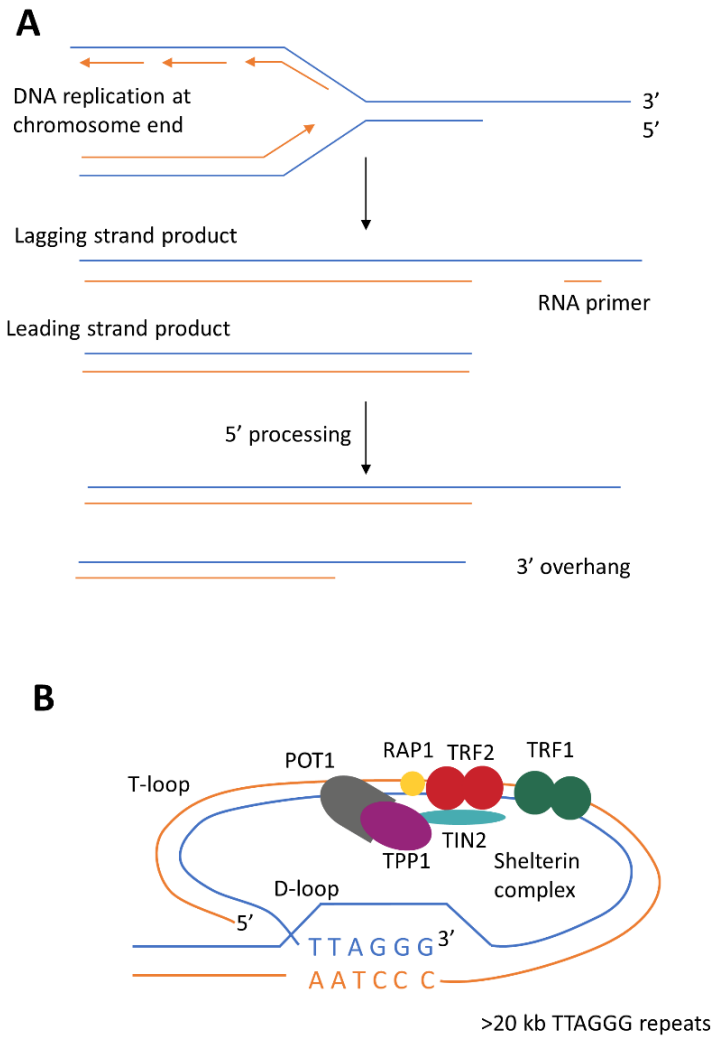


Figure 1.2 Telomere folding and the end-replication problem

A: schematic depicting the end-replication problem inherent in the mechanism of DNA replication. A semi-discontinuous bidirectional replication fork is shown, which due to the positioning of the final RNA primer on the lagging strand results (following 5’ end processing) in telomere shortening and a 3' overhang. B: schematic depicting telomere folding into D- and T-loops with strand invasion of the 3’ overhang for protection of the chromosome end. One shelterin complex is shown with constituent components (POT1, TPP1, TIN2, RAP1, TRF1 & TRF2); many shelterin complexes bind the telomere loops.

In contrast, senescence can also be caused through oxidative stress-induced DNA damage. For example, in epithelial cells, oxidative stress has been seen to result in the accumulation of single strand DNA breaks (SSB), which appear to remain unrepaired due to a decrease in PARP1 activity, resulting in large XRCC1 foci, p38 MAPK activation and upregulation of p16

(Nassour et al., 2016). Furthermore, high levels of intracellular ROS can also induce activation of p38 MAPK through the RAS-RAF-MEK-ERK signalling cascade, converging on p53 activation and upregulation of p21 or p16 to enforce cell cycle arrest (Borodkina et al., 2016).

Inflammatory signalling is also implicated in the onset of senescence through DNA damage. For example, TGFβ secretion by senescent cells in the SASP results in increased ROS levels in neighbouring cells, inducing DNA damage and activating p53 to elicit paracrine senescence (Acosta et al., 2013, Hubackova et al., 2012). Furthermore, ATM activation upon recognition of DNA damage can also activate p53 and induce senescence through expression of IFNβ (Yu et al., 2015), while IFNγ and TNF signalling can also induce p16-dependent arrest (Braumüller et al., 2013).

Upregulation of the CKI p16 is common to several types of senescence, including oncogene-induced senescence following Ras activation (Ras-OIS, Lin et al., 1998), where it blocks the activity of CDK4/6-cyclin D in G1 (Figure 1.3). Through CDK4/6 inhibition, p16 induces hypo-phosphorylation of Rb, a key regulator of cell cycle transition towards S-phase, thus enforcing a G1 phase proliferation arrest and preventing the onset of DNA replication. In addition, p16 cooperates with mitogenic signalling factors to induce a positive feedback loop between ROS and PKCδ that results in inhibition of cytokinesis (Takahashi et al., 2006).

While convergence on Rb through p16 induction results predominantly in G1 phase cell cycle arrest, not all senescent cells are arrested in G1 phase; G2 phase senescence can be induced through p21-mediated inhibition of mitotic CDK complexes (Baus et al., 2003, Herbig et al., 2004, Gire and Dulić, 2015). However, failure of this growth arrest can result in mitotic slippage, where passage through to the next cell cycle without completion of chromosome segregation or cytokinesis leads to cells with 4N DNA content undergoing arrest in the

subsequent cell cycle G1. Such arrest is reliant on p53/Rb for induction and p16 for maintenance (Johmura et al., 2014).

While oncogene-induced senescence was originally observed following expression of oncogenic RAS in human fibroblasts (Serrano et al., 1997), activation of other oncogenes such as BRAF have since been noted to induce senescence (Michaloglou et al., 2005). These activated oncogenes often induce senescence through stimulating rapid cell cycle progression resulting in DNA replication stress and damage to genomic DNA (Di Micco et al., 2006), through ROS (Irani et al., 1997), or by causing de-repression of the CDKN2A locus (Ruas and Peters, 1998). This locus is of particular importance in senescence; as well as encoding the cell cycle inhibitor p16, the CDKN2A locus also encodes p14 in an alternative reading frame, which stabilizes p53 through inhibition of the p53-targeting E3 ubiquitin ligase MDM2 (Kamijo et al., 1997, Shay et al., 1991).

The convergence of diverse upstream signals on negative regulators of cell cycle progression (CKI) underlines their importance in enforcing proliferation arrest in senescence. Indeed, loss of CKI expression can induce bypass of senescence and tumorigenesis (p21: Brown et al., 1997; p16: Sharpless et al., 2002; p16, Rb and p53: Beauséjour et al., 2003). *In vivo* analysis has revealed that expression of cyclin kinase inhibitors is also differentially regulated according to different environments, with p21-dependent but p16-independent senescence observed during mouse development (Muñoz-Espín et al., 2013), while p16-dependent senescence is induced during wound healing (Demaria et al., 2014) and in stem cells during ageing (Baker et al., 2016). Indeed, early *in vivo* experiments revealed senescence as a bona fide cellular stress response, rather than a tissue culture artefact (Collado et al., 2005, Chen et al., 2005 and Braig et al., 2005).

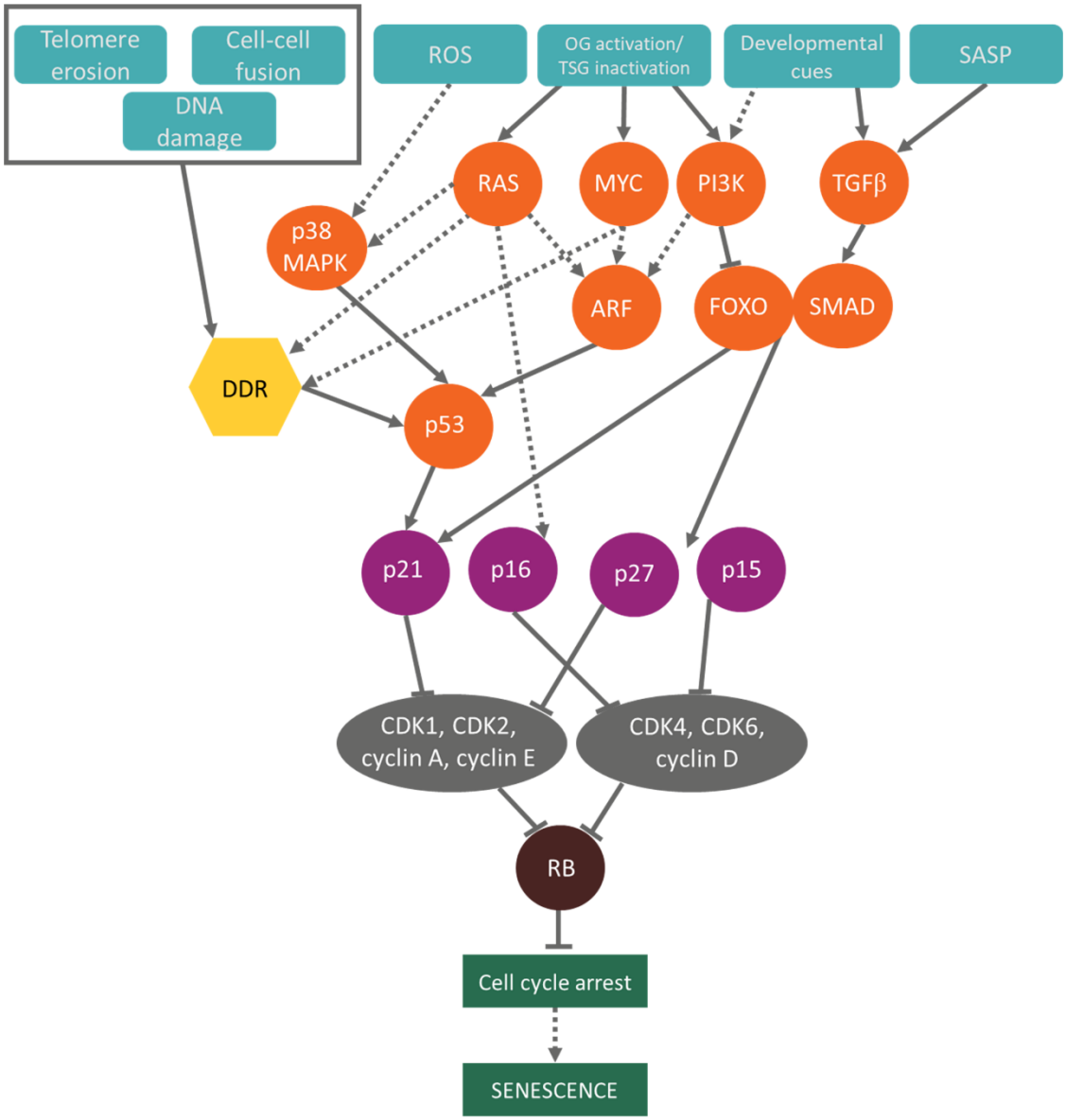


Figure 1.3. A summary of molecular pathways governing the onset of cellular senescence

Various signals that induce cellular senescence (blue) are shown acting through molecular pathways (orange), often converging on p53 activation and the DNA damage response (DDR, yellow) to bring about upregulation of CDK-cyclin inhibitors (CKIs, purple) resulting in maintenance of hypo-phosphorylation of Rb with subsequent G1 cell cycle arrest, which if sustained, results in cellular senescence. (Arrow head indicates activation, blunt-ended line indicates inhibition, dashed lines represent indirect signalling).

1.3.3. Hallmarks of senescence

Senescent cells are highly heterogeneous, exhibiting a range of phenotypes depending on factors including cell type, mode of induction (Nelson et al., 2012) and the time period since senescence onset. However, a number of senescence-associated phenotypes have been described which differentiate senescent cells from other cell cycle arrested cells, such as quiescent or terminally differentiated cells. These include morphological changes, organelle dysfunction, pro-inflammatory secretion and resistance to apoptosis, and highlight important biological features of senescence.

1.3.3.1. Morphological features

Senescent cells exhibit a dramatically enlarged, flattened, granular and highly irregular morphology compared to proliferating counterparts, at least *in vitro*. Though these morphological alterations represent an important and straightforward biomarker of senescence, the underlying molecular causes are not well understood. Cell morphology is regulated by the cytoskeleton, comprising tubulin-based microtubules, actin-based microfilaments and intermediate filament proteins. Filamentous actin stress fibres are often highly prominent in senescent cells (Nishio and Inoue, 2005). The ends of actin stress fibres are bound to focal adhesion plaques, comprising proteins such as vinculin and paxillin, which cross the cell membrane and contact the extracellular matrix. Intriguingly, these proteins are re-distributed upon senescence (Chen et al., 2000). Furthermore, small GTPases including Rac and Cdc42, integrins, and lipid raft proteins including caveolin-1 may also play important roles in regulating senescent morphology; knocking out caveolin-1 in senescent fibroblasts results in small, spindle-shaped morphology (Cho et al., 2004). Furthermore, upregulation and increased filamentation of the type III intermediate filament protein vimentin occurs on senescence, and overexpression of vimentin in proliferating cells confers senescent morphology (Nishio et al., 2001).

Changes in morphology and adhesion are important players in cancer metastasis and invasion (with tumour cells often appearing smaller and less adherent). Hence, it has been speculated that the enlargement of senescent cells may contribute to the barrier against tumorigenesis afforded by senescence. Indeed, recent work has demonstrated that the enlarged phenotype of senescent cells noted *in vitro* may be physiologically relevant *in vivo*. Through quantitatively identifying and characterizing senescent cells using flow cytometry and high content image analysis, senescent cells taken from aged mice tissue and tumours were shown to be larger than non-senescent cells (Biran et al., 2017). Furthermore, this enlargement of senescent cells *in vivo* may be functionally beneficial in some cases. For example, upon induction of senescence, glucose-stimulated insulin secretion from pancreatic beta cells rises, attributed to the increase in cell size, mitochondrial activity and glucose uptake (Helman et al., 2017), as well as possibly through constitutive mTOR activity in senescent cells driving increased protein synthesis (section 1.4). Notably however, senescence has also recently been implicated in the progression of type I diabetes (see Table 1.1, Thompson et al., 2019).

Changes in mechanical stiffness associated with cytoskeletal and extracellular matrix remodeling are also associated with senescence and ageing. Using laser-based optical cell stretching to investigate the viscoelastic biomechanics of dermal fibroblasts taken from human donors, increasing donor age was linked with cell stiffening and increased rigidity, coincident with a cellular shift from globular to filamentous actin shown by FACS analysis, but with no significant changes in vimentin or microtubule content (Schulze et al., 2010). These cytoskeletal changes are likely to contribute to the altered mechanical properties seen in ageing skin, also dependent on changes to the extracellular matrix such as altered collagen and elastin organization. Indeed, senescent cells are reported to accumulate in substantial quantities in ageing skin (Herbig et al., 2006; Lewis et al., 2011, see 1.3.6).

1.3.3.2. Organelle dysfunction in senescence

1.3.3.2.1. Mitochondrial dysfunction

Alongside cell senescence itself, mitochondrial dysfunction has been noted as a 'hallmark of ageing' (López-Otín et al., 2013) and the two are closely interrelated: mitochondrial dysfunction has been shown to play an important role in driving and maintaining senescence (Correia-Melo et al., 2016, Wiley et al., 2016, Passos et al., 2007). Furthermore, complex I dysfunction and increased ROS production are associated with ageing in many tissues (Kruse et al., 2016). Indeed, senescent cells exhibit a dramatic increase in mitochondrial mass; in DNA damage induced senescence (DDIS), this appears within 2-3 days of the peak of DNA damage, preceding the establishment of the secretory phenotype (Passos et al., 2010). The increased mitochondrial load may result from increased mitochondrial biogenesis, as the regulator of mitochondrial biogenesis, PCG1β, is indirectly induced by p53 activation in senescence (Dalle Pezze et al., 2014).

Senescent cells also show increased rates of respiration and oxygen consumption per cell. The mitochondrial gatekeeper protein pyruvate dehydrogenase (PDH) is highly activated in senescence, through simultaneous suppression of its inhibitory enzyme PDK1 and induction of the activating enzyme PDP2, and the resulting increase in PDH activity in the TCA cycle causes enhanced respiration (Kaplon et al., 2013). However, the fraction of ATP produced by oxidative phosphorylation in senescent cells decreases in favour of glycolysis, suggesting mitochondrial dysfunction. Indeed, mitochondria from senescent cells also show decreased membrane potential and increased production of ROS (Passos et al., 2007, Dalle Pezze et al., 2014), with mitochondrial dysfunction shown to result from persistent activation of p21 and signalling through TGFβ (Passos et al., 2010). Indeed, mitochondrial dysfunction and increased ROS production appear to be crucial in eliciting a stable proliferation arrest in senescence, as the production of ROS results in continuous occurrence of DNA damage foci

to maintain DDR activation, resulting in stabilization of proliferative arrest and establishment of senescence phenotypes (Passos et al., 2010).

The increased mitochondrial load and dysfunction associated with senescence suggests that senescent cells may accumulate dysfunctional mitochondria, possibly through failure of mitophagy, the selective autophagy pathway responsible for recycling dysfunctional mitochondria. In mitophagy, dedicated proteins including the serine/threonine PTEN-induced kinase PINK1 and the E3 ubiquitin ligase Parkin select mitochondria with reduced membrane potential for incorporation into autophagic vesicles by mediating their poly-ubiquitination (section 1.3.4 and Figure 1.4). Mutations in PINK1 and Parkin are associated with familial Parkinson's disease (PD), underlining an intriguing link between failure of mitophagy, senescence and PD (Truban et al., 2017). While evidence is conflicting about whether levels of general autophagy increase or decrease on senescence (section 1.3.4.), mitophagy appears to be compromised in senescence irrespective of mode of induction (Dalle Pezze et al., 2014). Failure of mitophagy could be driven through a number of mechanisms, including lysosomal dysfunction, impaired autophagy and/or overactive mTOR signalling, or through interaction of p53 with Parkin, which prevents its translocation to mitochondria (Ahmad et al., 2015). Further, the rate of mitochondrial fission and fusion events decreases on senescence due to downregulation of the fission mediators Drp1 and Fis1 (Mai et al., 2010), resulting in increased connectivity of the mitochondrial network and possibly causing sequestration of dysfunctional mitochondria, impairing their recycling (Dalle Pezze et al., 2014).

1.3.3.2.2. Lysosome stress

Upon induction of senescence, the cellular lysosomal content increases and lysosomal proteins are upregulated, either through enhanced lysosomal biogenesis or failure of lysosome recycling. Indeed, mTOR is constitutively active on senescence (Carroll et al.,

2017), activating TFEB and driving lysosome biogenesis. However, senescent cells also exhibit lysosomal accumulation of auto-fluorescent lipofuscin pigments (Cho et al., 2012) and recent reports suggest that lysosomal pH is increased in senescence due to failure of V-type ATPase proton pumps (Wang et al., 2018), suggestive of lysosomal dysfunction.

Due to the consistency of lysosomal dysfunction in senescence, a widely used biomarker for senescent cells is senescence-associated β-galactosidase (SA-β-gal) activity at suboptimal pH 6.0, reflecting lysosomal stress (Dimri et al., 1995). Using a chromogenic substrate X-Gal, which stains blue when cleaved by galactosidase, SA-β-gal is readily detectable and quantifiable, both *in vitro* and in *ex vivo* tissue sections. While it is not required for senescence and is detectable in certain other circumstances such as in quiescence (Yang and Hu 2005), SA-β-gal is a widely accepted senescence biomarker. Interestingly, the enzyme responsible for SA-β-gal activity is one of multiple transcripts encoded by GLB1, the expression of which is highly regulated, including negative transcriptional regulation through Notch signalling (itself implicated in senescence, Hoare et al., 2016, Parry et al., 2018, Teo et al., 2019).

1.3.3.2.3. ER stress

The endoplasmic reticulum (ER) is responsible for coordinating protein folding, and in situations where this is compromised (for example by mutations, viral infections, oxidative stress or a lack of chaperones), ER stress leads to accumulation and aggregation of unfolded or misfolded proteins. In response, the ER orchestrates either a degradation pathway (ER-associated protein degradation, ERAD), or a coordinated unfolded protein response (UPR) pathway where protein synthesis is attenuated and the ER is enlarged. Activation of the UPR can result in restoration of ER homeostasis, cell death or indeed, senescence (Pluquet et al., 2015). However, as well as possibly being a driver of cell senescence, the UPR may also be activated in senescent cells: following activation of oncogenic Ras, the ER was observed to

become dramatically enlarged and vacuolized (Denoyelle et al., 2006). These findings have since been replicated across many types of senescence (Pluquet et al., 2015). It is possible that the UPR is consistently activated in senescence due to the high demands of SASP factor production for pro-inflammatory secretion. Further, constitutive mTOR activity observed in senescent cells also predisposes to increased protein synthesis (Carroll et al., 2017) which may risk proteotoxicity.

Similarly, the integrated stress response (ISR) can also be induced by ER stress, or following nutrient deprivation, oncogene activation, hypoxia and infection, to restore homeostasis and cell survival (Pakos-Zebrucka et al., 2016). Through phosphorylation of eIF2α by one of several kinases, the ISR ensures global suppression of protein synthesis, but preferential translation of mRNAs of the transcription factor ATF4, involved in several cellular pathways including autophagy and cell cycle regulation (Lu et al., 2004). Interestingly, in renal tubular epithelial cells, ATF4 activity drives p16 upregulation and enforces senescence following ER stress, which has been implicated in the progression of diabetic nephropathy (Liu et al., 2015).

1.3.3.2.4. Altered plasma membrane

Upon induction of senescence, the composition and polarization of the plasma membrane are subject to changes; while the functional relevance of this is not yet fully understood, the plasma membrane is important in multiple processes including regulation of cell morphology, motility and intercellular signalling, for example in senescent – immune interplay. Indeed, cholesterol-enriched caveolae (specialized lipid rafts within small plasma membrane invaginations that mediate signal transduction) are increased on senescence through upregulation of caveolin-1, which influences cellular morphology and adherence (Volonte et al., 2015, section 1.3.3.1.). Interestingly, caveolin-1 upregulation has been shown to induce p53 activation and IL-6 secretion, through suppressing ATM activation and MDM2

inhibition (Volonte et al., 2015), suggesting a potential role for plasma membrane changes in senescence induction. Furthermore, changes to the plasma membrane may be responsible for an observed failure to form primary cilia in senescent cells, as well as membrane depolarization and mTOR activation (Carroll et al., 2017).

Changes to the lipids and proteins of the plasma membrane could also provide a useful source of senescence biomarkers: for example, an oxidized form of vimentin has been found to be specifically expressed at, and secreted from, the plasma membrane of senescent fibroblasts (Frescas et al., 2017). Furthermore, a proteomic screen of plasma membrane-associated proteins specifically expressed on senescence identified 107 senescence-specific candidate proteins, including the phosphatase DEP1 (associated with tumour suppressor mechanisms, Sacco et al., 2009). This screen also identified B2MG as upregulated upon senescence (Althubiti et al., 2014); B2MG is implicated in antigen presentation. Similarly, melanocytes that have entered OIS increase expression of MHC class II proteins, with antigen presentation thought to activate the adaptive immune system and promote tumour suppression (van Tuyn et al., 2017).

1.3.3.3. Senescent cell communication

1.3.3.3.1. Pro-inflammatory secretion (SASP)

Perhaps the most important and potentially deleterious phenotype of senescence is the pro-inflammatory secretion that accompanies the permanent growth arrest, known as the SASP (senescence-associated secretory phenotype). The SASP includes a range of growth factors (e.g. TGFβ, HGF, VEGF, PDGF), cytokines (e.g. IL-1, IL-6, IL-8), chemokines (e.g. MCP-1) and matrix-remodelling enzymes (e.g. cathepsins, MMPs) that are upregulated and secreted upon entry into senescence (Coppé et al., 2008, Acosta et al., 2008, Kuilman et al., 2008). Indeed, the SASP has a major role in directing the non-cell-autonomous functions of senescent cells (sections 1.2.4. and 1.2.5.): it can affect cell growth, motility, plasticity and

tissue architecture, and mediates recruitment and activation of immune cells such as monocytes/macrophages, T cells and NK cells to promote clearance of senescent cells (Sagiv et al., 2013), though there is also an important role for direct cell-cell signalling in immunomodulation (direct cell-cell membrane bridges: Biran et al., 2015 and Notch signalling: Hoare et al., 2016). However, the SASP also has a causal role in tumorigenesis, inflammation and the progression of a number of age-related diseases. For example, MMP3 and IL-6 are implicated in osteoarthritis progression (Jeon et al., 2018), while VEGF is involved in age-related macular degeneration (Cascella et al., 2017).

After induction of senescence, the SASP has been shown to develop dynamically *in vitro* and *in vivo* through a self-regulating hierarchy, with initiating factors coordinating SASP establishment, while later factors subsequently maintain pro-inflammatory secretion. In particular, IL-1 is essential for triggering SASP secretion in Ras-OIS (Acosta et al., 2013): IL-1α expression activates the SASP transcription factors C/EBPβ and NFκB, and IL-6/CXCR2-binding chemokines form positive feedback loops to reinforce inflammatory secretion. The SASP can also reinforce the initial senescence growth arrest: the TGFβ ligands VEGF, CCL2 and CCL20 regulate the CKIs p21 and p15 (Acosta et al., 2013), while IL-1 and TGFβ also increase ROS levels (Hubackova et al., 2012). As well as reinforcing the autocrine proliferative arrest, SASP factors can induce paracrine senescence, again through TGFβ and IL-1 driving a ROS-dependent mechanism in bystander cells (Acosta et al., 2013, Nelson et al., 2012). The dynamic nature of the developing pro-inflammatory phenotype highlights that rather than senescence reflecting a static endpoint, senescence may actually comprise a series of progressive and phenotypically diverse states acquired after the initial growth arrest. This further layer of complexity may help explain the heterogeneity observed in senescent cells even of the same origin, and underlines the need to both account for dynamics when investigating senescence *in vitro* and to elucidate the kinetics of the deleterious effects of senescence *in vivo*.

Interestingly, a thorough proteomic database of SASP factors secreted in Ras-OIS, DNA damage-induced senescence and atazanavir-induced senescence in both fibroblasts and epithelial cells has revealed that different inducers of senescence produce notably distinct secretory profiles. Of 1107 proteins identified in the overall senescent secretome, only 172 were common to all three forms (Basisty et al., 2019). Not only does this further highlight the heterogeneous nature of senescence, but these findings also suggest that different forms of senescence could produce distinct physiological outcomes through different SASP profiles mediating their non-cell-autonomous effects *in vivo*.

1.3.3.3.2. Extracellular vesicles

While many SASP factors are produced and directly secreted as soluble proteins, some factors require further processing. Some are initially expressed as transmembrane proteins and are subsequently released by ectodomain shedding, mediated by proteases such as ADAM17, a sheddase upregulated in OIS (Morancho et al., 2015). However, other SASP factors are secreted as cargo within extracellular vesicles (EV) such as exosomes, which provide endocrine as well as paracrine routes of communication. Indeed, the biogenesis of exosome-like vesicles carrying SASP factors released from senescent cells is p53-dependent (Lehmann et al., 2008) and increased secretion of extracellular vesicles alongside alterations in their contents and processing are observed in senescence (Borghesan et al., 2019).

Highlighting the functional relevance of EV secretion, EVs secreted from senescent cells have been shown to exert pro-proliferative effects on cancer cells *in vitro* (Takasugi et al., 2017). A possible mechanism for this is through oxidative inactivation of PTP1B phosphatase in senescent cells, which leads to enhanced phosphorylation of the receptor tyrosine kinase EphA2. This kinase, involved in cell proliferation, can then become enriched within extracellular vesicles and transmit pro-proliferative effects via EV uptake (Takasugi et al., 2017). However, exosome secretion may also play a role in preventing senescence. Indeed,

proliferating cells have been shown to secrete DNA of nuclear origin within exosomes, thus preventing activation of cytoplasmic DNA sensors and senescence, as a homeostatic mechanism to remove potentially harmful cytoplasmic DNA from cells (Takahashi et al., 2017, see 1.3.3.4.2).

1.3.3.3.3. Direct intercellular communication

As well as secreting a plethora of soluble and packaged signalling factors to facilitate intercellular communication, senescent cells have also been shown to directly communicate with neighbouring cells through actin-based cytoplasmic bridges, for example creating direct contacts with NK cells during immunosurveillance (Biran et al., 2015). These intercellular cytoplasmic bridges have been observed to permit direct intercellular protein transfer (Biran et al., 2015), which depends on cell-cell contact and actin polymerization, with factors that regulate actin polymerization such as Cdc42 implicated in the regulation of bridge dynamics and enriched in the pool of proteins transferred intercellularly (Biran et al., 2015). Furthermore, Notch signalling has also been shown to induce cell contact-dependent juxtracrine senescence (Teo et al., 2019).

1.3.3.4. DNA damage

1.3.3.4.1. DNA damage foci

Severe DNA damage such as double strand breaks (DSBs) occurring anywhere in the genome can induce senescence through eliciting a DNA damage response (DDR) and halting cell cycle progression through p53 activation and p21 upregulation (section 1.2.2.). This mechanism prevents the propagation of genomic instability and is exploited as a therapeutic tool in chemotherapy, with treatments such as camptothecin and etoposide (topoisomerase I&II inhibitors respectively) inducing DSB formation to cause apoptosis or senescence in tumour cells. Notably, these clinical treatments induce severe and long-term side effects through collateral damage of healthy cells. Whether induced by endogenous or exogenous causes,

DSBs lead to activation of ATM kinase which phosphorylates histone variant H2AX (present in 10-15% of nucleosomes) at serine 139 (γH2AX) in regions reaching over 1 kb surrounding the break (Rogakou et al., 1999). This provides a local platform for recruitment of further DDR proteins such as 53BP1, as well as creating DNA damage foci detectable by γH2AX immunofluorescence.

Upon senescence induction in primary fibroblasts by etoposide treatment, an initial peak of DNA damage (as assessed by number of γH2AX foci per nucleus) is observed up to 48 hours after treatment (~50% cells positive). Subsequently, alongside a gradual increase in SA-β-gal staining, the DNA damage load then falls to ~30% of nuclei positive for γH2AX foci after 8 days treatment (Biran et al., 2017). This indicates that an initial peak of DNA damage acts to induce senescence, and though some damage may be resolved through DNA repair pathway activity, senescent cells retain persistent, unrepaired DNA damage. These persistent DNA damage foci have been termed DNA-SCARS (DNA segments with chromatin alterations reinforcing senescence) and are differentiated from transient lesions through their association with nuclear PML bodies, accumulation of CHK2 and p53, and lack of RPA, RAD51, ssDNA and DNA synthesis (Rodier et al., 2011). Furthermore, these persistent lesions are required for SASP secretion (Rodier et al., 2009), indicating a role for the DNA damage response in orchestrating communication of the damage to the surrounding tissue. The DDR also coordinates degradation of G9a/GLP methyltransferase in senescence, leading to a global decrease in H3K9 dimethylation, including at promoters of the IL-6 and IL-8 genes, encoding two primary SASP components (Takahashi et al., 2012). DNA damage foci have also been observed in paracrine senescent cells, with retrograde signalling through TGFβ and ROS implicated in eliciting endogenous DNA damage to enforce proliferation arrest (Passos et al., 2010).

1.3.3.4.2. Cytoplasmic chromatin fragments (CCFs)

One mechanism the immune system employs to detect possible pathogenic infections operates by sensing microbial or viral DNA, using sensors such as cGAS (cyclic GMP-AMP (cGAMP) synthase), which detects cytosolic dsDNA. Through production of the secondary messenger cGAMP, cGAS triggers innate immune responses, activating STING (stimulator of interferon genes). STING in turn recruits IκB and TBK1 kinases to activate transcription factors IRF3 and NFκB respectively, leading to type I interferon expression and inflammatory cytokine production (Tanaka and Chen, 2012). However, as well as responding to infections, this pathway is also activated by tumour-derived DNA. Intriguingly, cytoplasmic chromatin fragments (CCFs) have also been observed in senescent cells; CCFs lack nuclear envelope components (they are lamin A/C negative) and are γH2AX positive (Ivanov et al., 2013). Live imaging analysis has shown that CCF production involves a chromatin fragment blebbing from an intact nucleus in a cell that is undergoing senescence, perhaps due to compromised nuclear integrity. Hence CCFs are distinct from lamin A/C positive micronuclei which are formed due to errors in chromosome segregation during mitosis (Ivanov et al., 2013). While CCFs are eventually processed by the autophagic/lysosomal pathway, they are also recognized by cGAS, and activate the subsequent innate immune pathway, causing interferon and cytokine production (Dou et al., 2017, Glück et al., 2017). The cGAS-STING pathway is activated in a number of different models of senescence including replicative and oncogene-induced senescence: in both models, around 20% of senescent cells were noted to harbour CCFs (Ivanov et al., 2013). Further experiments using cGAS knockout lines *in vitro* have revealed an important role for this pathway in regulating the expression of interferon and several key SASP components (including IL-6 and TNF-α) in senescent cells (Glück et al., 2017). Furthermore *in vivo*, STING-deficient mice exhibit impaired immunosurveillance of oncogenic RAS and lower tissue inflammation following ionizing radiation treatment, indicating an important role for cGAS-STING in inducing and regulating senescence.

However, while knocking out STING in mice reduced phenotypes of ageing such as hair greying, it also resulted in increased susceptibility to cancer (Dou et al., 2017). Therefore pharmacological inhibitors of STING used to target senescent cells also carry a substantial risk of compromising anti-tumour and anti-infection responses.

1.3.3.4.3. DNA repair disorders and senescence

DNA repair defects are intimately linked to senescence and ageing; disorders associated with compromised DNA repair capacity show premature senescence *in vitro* and premature ageing and cancer predisposition *in vivo*. Of these human progeroid disorders, the rare autosomal recessive disease Werner syndrome (WS) is the best characterized, with clinical symptoms including short stature, cataracts, early greying and loss of hair, scleroderma-like skin changes, ulceration and predisposition to cancer (Shamanna et al., 2017). WS results from mutations in the WRN gene, which encodes a RecQ helicase and 3'-5' exonuclease (Yu et al., 1996) with diverse roles in DNA metabolism, underlined through its interaction with many proteins involved in DNA replication and repair including PCNA and topoisomerase I (Lebel et al., 1999), DNA polymerase δ (Szekely et al, 2000), RPA (Brosh et al., 1999) and p53 (Blander et al., 1999). Indeed, WRN appears to participate in many aspects of DNA metabolism including transcription (Shiratori et al., 2002), telomere maintenance (Sun et al., 2017) and homology-dependent recombination, in particular in the resolution of stalled replication forks (Nehlin et al., 2000, Rodríguez-López et al., 2002). Mutations causing WRN destabilization or loss of the C-terminal nuclear localization signal (NLS) result in genetic instability (Fukuchi et al., 1989), hypersensitivity to DNA damaging agents (Lebel and Leder, 1998) and premature senescence *in vitro* (Martin et al., 1970) with elevated cancer risk and accelerated ageing *in vivo* (Cox and Faragher, 2007, Shamanna et al., 2017).

1.3.3.5. Chromatin changes

There are dramatic changes to chromatin structure during senescence, indeed an important biomarker of senescence is senescence-associated heterochromatic foci (SAHF, Narita et al., 2003), visualized as nuclear DAPI-dense foci. The function of SAHF may involve incorporation of proliferative genes (e.g. Rb) into repressive heterochromatin to enforce the irreversibility of proliferation arrest (Narita et al., 2003) and the histone chaperone proteins HIRA and ASF1a are key modulators of SAHF formation (Zhang et al., 2005, Zhang et al., 2007). Furthermore, proteins implicated in SAHF formation have been shown to localize to PML bodies (Ye et al., 2007), which increase in number and size during senescence (Pearson et al., 2000, Ferbeyre et al., 2000, Bischof et al., 2002). Notably however, not all senescent cells exhibit SAHF; they are predominantly found in OIS cells, but not in replicatively senescent or Hutchinson-Gilford progeria cells (Parry and Narita, 2016). Interestingly, ChIP-seq analysis has revealed that levels of repressive heterochromatin markers including H3K9me3 and H3K29me3 only change moderately upon induction of OIS (Chandra et al., 2012), suggesting a spatial rearrangement of pre-existing heterochromatin, rather than spreading of histone marks in SAHF establishment. Indeed, recent evidence suggests that further heterochromatic histone methylation changes (in particular H4K20me3) may reinforce, but not drive cell senescence (Nelson et al., 2016).

Alongside modifications to histones, changes to DNA methylation status are associated with senescence. Whole genome single nucleotide bisulfite sequencing revealed that on replicative senescence, DNA is globally hypo-methylated, in particular at heterochromatic regions such as gene-poor, late-replicating sequences and lamina-associated domains (LADs), but focally hyper-methylated at CpG islands and gene promoters, including those associated with cancer progression (Cruickshanks et al., 2013). Indeed, changes in the

methylation state of certain CpGs (clock CpGs) have been exploited to create an 'epigenetic clock' of ageing (Horvath, 2013).

Furthermore, changes in the nuclear lamina are associated with senescence and ageing: lamin A/C is mutated in Hutchinson-Gilford Progeria (HGPS) where a splice site mutation with consequent incorrect splicing results in formation of a mutant lamin C protein, progerin, which affects nuclear integrity. Interestingly, progerin is also increased in wild-type senescent cells (Cao et al., 2011) and accumulates with chronological age, possibly contributing to increased cardiovascular disease in the elderly (Olive et al., 2010), further HIV protease inhibitors that also inhibit the human ZMPSTE24 protease involved in LMNA post-translational processing induce senescence *in vitro* (e.g. azatanivir, Hernandez-Vallejo et al., 2013). Furthermore, lamin B1 is down-regulated in senescence (Freund et al., 2012) and may be degraded through autophagy (Dou et al., 2015). Using DamID to map binding sites in the genome using DNA adenine methyltransferase fusions (Steensel and Henikoff, 2000), interactions between the genome and the nuclear lamina have been shown to be reshaped upon entry into OIS, with loss of constitutive LADs, alongside re-localization of some genes and telomeres to the lamina (Lenain et al., 2017). Furthermore, a reduction of local connectivity in TADs (topologically associated domains, considered discrete regulatory transcription units) associated with heterochromatin has been observed during OIS using high-throughput chromatin conformation capture (3C) methods (Chandra et al., 2015), suggesting a possible mechanism for the vast changes in gene expression observed in senescence.

The HMGB (high mobility group box) proteins are major chromatin-associated non-histone proteins, acting as DNA chaperones for many processes involved in DNA metabolism, which are of particular importance in senescence. HMGB1 modulates gene expression within the nucleus, but on entry into senescence, oxidized HMGB1 re-localizes to the extracellular

milieu, dependent on p53 signalling (Davalos et al., 2013). Secreted HMGB1 is proposed to act as an alarmin, stimulating cytokine secretion. This re-localization results in re-shaping of nuclear TAD boundaries previously marked by HMGB1, and through interacting with many RNA binding proteins and RNA itself, it may also influence transcript splicing choices (Sofiadis et al., 2019). Furthermore, HMGB2 localizes to SASP gene loci during senescence, preventing their incorporation into repressive heterochromatin (Aird et al., 2016) and is in senescence-associated transcriptional remodelling (Zirkel et al., 2018).

1.3.3.6. Resistance to apoptosis

Conceptually, senescence is an alternative fate to apoptosis for damaged cells, and both are coordinated through several common molecular mediators. The choice between senescence and apoptosis in response to damage appears to depend on the severity and type of damage, as well as the cell type of origin. p53 expression and activation may be critical in this choice: lower levels of p53 stabilization and activation are required for induction of senescence, resulting in reduced expression of apoptosis proteins PUMA and NOXA, and increased expression of pro-survival Bcl-2 family proteins (Wang, 1995, Childs et al., 2014). However, this does not hold true for all models of senescence, such as IR-treated IMR90 fibroblasts, where PUMA and BIM are upregulated and BCL-2 expression is reduced; apoptosis is instead restrained by transcriptional regulation through FOXO4 (Baar et al., 2017). In this model, FOXO4 was shown to be upregulated in senescence, acting to sequester p53 in the nucleus and prevent induction of apoptosis (Baar et al., 2017). However, in other models anti-apoptotic factors such as BCL-2 are upregulated through chronic activation of the transcription factor CREB, while BCL-XL is upregulated through IRES-mediated translation (Ryu et al., 2007). Pro-apoptotic factors can be repressed on senescence, for example the Bax gene is found enriched with the repressive histone mark H3K20me3 in RS (Sanders et al., 2013).

p53 activity can lead to apoptosis indirectly via transcriptional activity or directly via interaction with apoptotic regulators such as Bax at mitochondrial membranes to promote cytochrome c leakage (Schuler et al., 2000, reviewed in Vaseva and Moll, 2009). Several separation-of-function mutations have been mapped in p53 which regulate the choice between apoptosis and senescence: mutation of K117 (an acetylation site) to arginine blocks apoptosis without compromising entry into senescence, while the triple mutant site p53-K117R/K161R/K162R is deficient in inducing both senescence and apoptosis (Li et al., 2012). The downstream effector of p53, p21, can also block apoptosis, by restricting JNK and caspase signalling under persistent DNA damage (Yosef et al., 2017).

Therefore once senescence is established, cells become highly resistant to apoptosis, through mechanisms involving upregulation of pro-survival/anti-apoptotic factors (Wang, 1995), downregulation of effectors of apoptosis and prevention of p53 stabilization to the levels required for apoptosis (Seluanov et al., 2001) and retaining p53 in the nucleus (Baar et al., 2017). Hence even on treatment with inducers of apoptosis such as H_2O_2 and staurosporine, senescent cells fail to undergo programmed cell death (Ryu et al., 2007). Interfering with the reliance of senescent cells on anti-apoptotic factors to avoid apoptosis presents the opportunity to induce apoptosis in senescent cells, and a novel class of 'senolytic' compounds are being developed (section 1.3.6.).

Therefore despite vast heterogeneity in terms of cell type, mode of induction and possibly even 'depth' of senescence, senescent cells share a number of defining phenotypes and characteristics which enforce proliferative arrest, promote intercellular communication (particularly with the immune system) and resist the alternative fate of apoptosis.

1.3.4. Autophagy and senescence

Macroautophagy (hereafter autophagy) is a selective homoeostatic degradation pathway for cellular components, which are directed via double-membrane vesicles (autophagosomes)

to lysosomes for degradation (Figure 1.4). Autophagy is activated in response to nutrient limitation and is suppressed by mTOR activity (section 1.4.) through the inhibitory phosphorylation of the autophagy-initiating kinase ULK1 (ATG1, Kim et al., 2011), as well as ATG13 and lysosomally-located TFEB (Kennedy and Lamming, 2016). The published literature contains some discrepancies about the association between autophagy and senescence. Adriamycin-induced senescent cells have been reported to exhibit fewer LC3-II puncta than untreated controls, coincident with mTOR activation; treatment with the mTOR inhibitor rapamycin rescued autophagosome formation (Sung et al., 2017). Further, co-treatment with the autophagy inhibitor Bafilomycin A1 increased the proportion of cells that positively stained for SA-β-gal (and hence are likely to be senescent) following adriamycin treatment (Sung et al., 2017). Indeed, a reduction in autophagy in senescence would appear to support senescence-associated hypertrophy and accumulation of organelles such as mitochondria.

However, to meet the demands of production and secretion of SASP factors, it has been proposed that while oppositely regulated by mTOR signalling, increased autophagy and increased protein synthesis may occur simultaneously in senescence by spatial coupling of mTOR (at least in OIS, Narita et al., 2011), with increased protein turnover through autophagy perhaps providing a continuous supply of free amino acids to drive constitutive mTOR activity in senescence (Carroll et al., 2017). While heterogeneity between different types of senescence could be responsible for these contrasting findings, an important caveat of the ER:Ras-OIS model is that expression of oncogenic Ras is driven by treatment with 4-hydroxytamoxifen, which has been shown induce autophagy (and autophagic cell death) in cancer cells (Kohli et al., 2013).

Decreased autophagy is linked to ageing: for instance, several proteins required for autophagy (Atg5, Atg7 and Beclin 1) are downregulated in normal human brain ageing (Lipinski et al., 2010) and in osteoarthritis (ULK1, Beclin 1 and LC3, Caramés et al., 2010),

while knock-in of an activated form of Beclin 1 delays the onset of cardiac and renal fibrosis in normally ageing C57/BL6 mice, and rescues the short lifespan of Klotho mutant mice (Fernandez et al., 2018). Increased autophagy may mediate the pro-longevity effects of caloric restriction (CR), as inhibition of autophagy prevents CR-mediated benefits (Rubinsztein et al., 2011). Activation of autophagy by spermidine also decreases immunosenescence (the functional decline of the immune system with age) and improves the response to influenza vaccination in mice (Puleston et al., 2014). Decreased autophagy in ageing may lead to the accumulation of protein aggregates in neurodegenerative disorders (Fujikake et al., 2018) and limit the removal of dysfunctional organelles such as mitochondria. Indeed, senescence-associated mitochondrial dysfunction, which may occur due to failure of mitophagy, has been implicated in liver steatosis through failure to efficiently metabolize fatty acids (Ogrodnik et al., 2017).

Autophagy has also been implicated as a mechanism for the antagonistic effects of SIRT6 expression on senescence in rat nucleus pulposus (NP) cells in a model of invertebral disc degeneration (IDD); SIRT6 expression declines in senescent NP cells, but when overexpressed, it attenuates senescence, and this effect depends on activation of autophagy and mTOR inhibition (Chen et al., 2018). Furthermore, an acetylcholine esterase inhibitor designed as a potential Alzheimer's treatment was shown to induce senescence in MCF-7 breast cancer cells, while simultaneously inducing the onset of autophagy but blocking autophagic flux, leading to the production of single-membrane autolysosomes with non-degraded cargo (Kucharewicz et al., 2018). Hence, initiation of autophagy with failure of autophagosome fusion with lysosomes may contribute to cell stress and senescence. These results taken in combination underline the complex role of mTOR signalling in regulating autophagy in senescence, and additionally highlight the inadequacy of standard markers of autophagy (autophagosome number or LC3-II/LC3-I ratio) as readouts for activation of such a complex pathway that is subject to further downstream regulation.

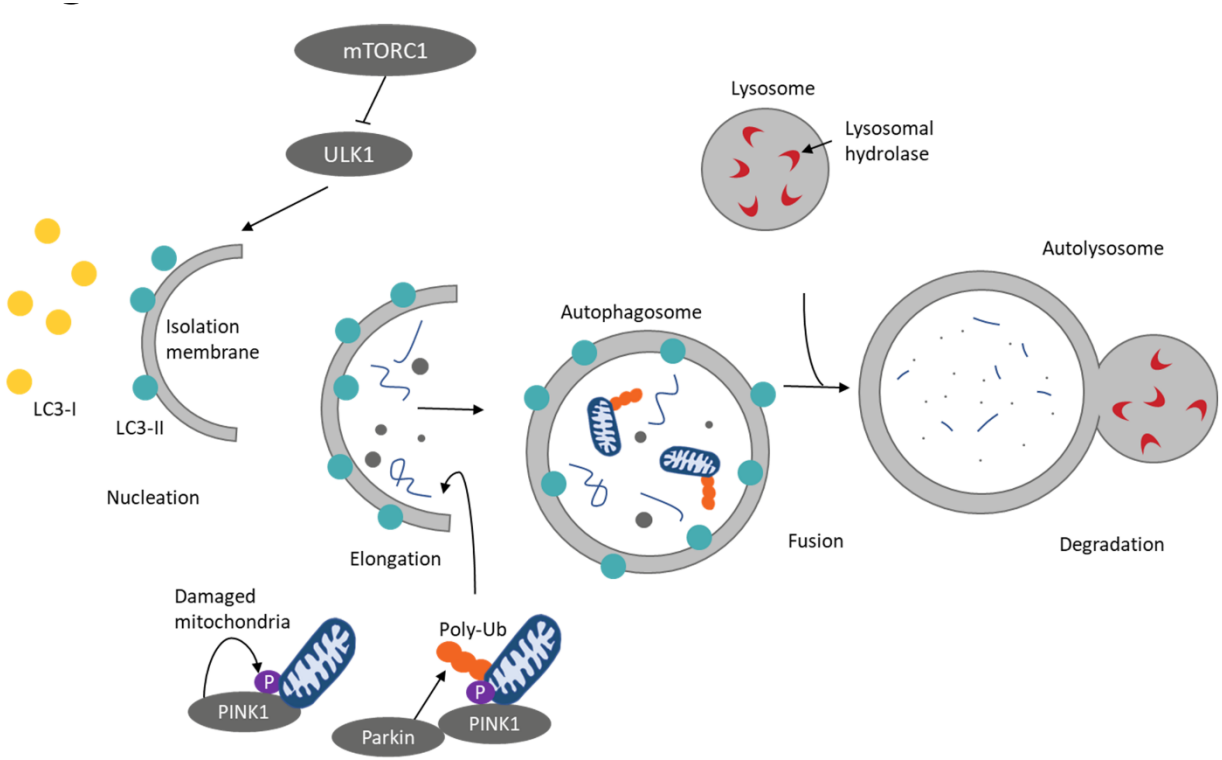


Figure 1.4 Regulation of autophagy and mitophagy

Schematic depicting regulation of autophagy and mitophagy. Cellular signalling to regulate autophagy (e.g. starvation, hypoxia or ER stress) converges on the ULK1 complex (ULK1, ATG13, FIP200 and AG101) which stimulates phagophore nucleation (details not shown). Through phosphorylation, mTORC1 suppresses ULK1 activity. In the conjugation of autophagic membranes, cytoplasmic LC3-I is converted into LC3-II, often used as a read out for autophagic membranes. As the isolation membrane elongates, it incorporates cargo to be degraded, such as protein aggregates or poly-ubiquitinated mitochondria (following PINK1 phosphorylation and E3 ubiquitin ligase Parkin-mediated ubiquitination, selecting dysfunctional mitochondria for removal). Following lysosomal fusion, cargo is degraded within the autolysosome by lysosomal hydrolase enzymes.

1.3.5. Beneficial physiological roles of senescence

As well as being noted for its role in pathological ageing and disease (see section 1.3.6 below), cellular senescence is also recognized to have several beneficial physiological roles, including acting as a barrier to tumorigenesis, for tissue remodelling during development and in tissue repair. Indeed, the capacity for unlimited proliferation is commonly regarded as an essential characteristic of cancer, necessary for sustaining tumour growth despite high cell death rates, and for the many rounds of clonal evolution in tumour progression. Therefore, cell senescence acts as a barrier to tumorigenesis by preventing propagation of potentially damaged cells, and bypass of senescence is regarded as an essential facet of tumour progression (Hanahan and Weinberg, 2000, 2011). Furthermore, senescence also operates as a tumour-suppressor mechanism through promoting immune surveillance: secretion of pro-inflammatory mediators from pre-malignant hepatocytes undergoing senescence has been shown to stimulate immune recruitment (macrophages and CD4+ T cells, Kang et al., 2011). Interestingly, as well as recruiting immune cells, the SASP can also directly regulate them: senescent hepatic stellate cells have been shown to drive macrophage polarization towards a pro-inflammatory M1 type, which contributes to tumour suppression (Lumjambio et al., 2013), though this may also account for chronic inflammation and macrophage polarity shifts associated with disease in later life. In parallel, senescence may constitute an important antiviral response: a number of viruses have evolved mechanisms for bypassing senescence including HPV (DiPaolo et al., 1993) and hepatitis B (Oishi et al., 2007). Indeed, one such mechanism relying on SV40 large T antigen (which binds and inactivates both p53 and Rb) is routinely exploited as a mechanism for cellular immortalization in culture.

As well as providing an important barrier to tumorigenesis and infection, senescence also appears to be beneficial in promoting pancreatic beta cell function through increased insulin secretory capacity, linked to the increase in protein production and/or cell size on

senescence (Helman et al., 2016) though recent data instead suggests a pathological role for senescence in type I diabetes (Thompson et al., 2019). Senescence is also highly important in wound healing (Jun and Lau, 2010): after wounding, an initial proliferative phase to refill the wound and deposit new extracellular matrix (ECM) occurs. Subsequently, fibroblasts progress to a myofibroblastic phenotype on entry to senescence, stop proliferating and balance ECM deposition with remodelling via metalloproteases, important SASP components. During wound healing, senescence appears to be induced by CCN1, which interacts with integrins to cause ROS production and p53 activation. The presence of senescent cells at the site of an acute wound also appears to accelerate its closure, through secretion of the SASP factor PDGF-AA from senescent cells (Demaria et al., 2014). While senescence is beneficial in wound healing, it is also noteworthy that chronic, non-healing wounds as seen in the elderly and in diabetic patients also have senescent traits (Vande Berg et al., 2005), suggesting that only transient induction of senescence is beneficial.

In embryonic development, senescent cells have been implicated in the structural degeneration of transient organ forms, such as the embryonic kidneys, by inducing macrophage-dependent elimination, as well as halting proliferation of specific cell types to balance growth, and through morphogenetic signalling (Muñoz-Espín et al., 2013, Storer et al., 2013). The senescent state induced during development appears to be DNA damage-independent but p21-dependent, with possible roles for ERK and TGFβ signalling, and interestingly, blocking senescence during development delays but does not prevent development, as apoptosis occurs instead to compensate (Davaapil et al., 2017). Senescence also plays an important role in development through contributing to placental formation during cytotrophoblast fusion, and to changes required for the onset of labour such as cervical remodelling and sterile inflammation (Cox and Redman, 2017).

Cell senescence is also robustly induced at wound margins during salamander limb regeneration: these senescent cells are efficiently cleared by macrophages (Yun et al., 2015), which are themselves required for regeneration following limb amputation, rather than wound repair without limb re-growth (Godwin et al., 2013). In non-regenerating animals, senescence may also restrict fibrosis following tissue injury (Krizhanovsky et al., 2008, Kong et al., 2012, Meyer et al., 2016). Conversely however, senescence is also implicated in the aetiology of idiopathic pulmonary fibrosis (IPF) – a lung disease associated with fibrotic scarring – as the condition is alleviated in the clinic by removal of senescent cells (dasatinib and quercetin (D+Q) section 1.3.7, Justice et al., 2019). Thus senescence may have both pro- and anti-fibrotic roles depending on the physiological context. Furthermore, senescence also plays important roles in tissue homeostasis (Ritschka et al., 2017) and possibly also in reprogramming (Abad et al., 2013, Mosteiro et al., 2016): senescence has been noted to enhance reprogramming efficiency, possibly through SASP secretion. However, while promoting cellular plasticity could promote tissue remodelling, it may also risk tumorigenesis.

1.3.6. Senescence and ageing

Senescent cells accumulate in various tissues with age in mammals, including the heart, lung, skin, spleen, liver and kidney (Wang et al., 2009, Yang and Fogo, 2010, Biran et al., 2017), and notably have been shown to accumulate within disease niches such as atherosclerotic plaques (Childs et al., 2016). Within such tissues, the senescent cell load can comprise a substantial proportion of total cells, for example >15% of cells were shown to be senescent using telomere dysfunction as a biomarker in aged baboon skin samples (Herbig et al., 2006) while in human sun-exposed geriatric skin, ~60% of fibroblasts in the papillary dermis were deemed senescent based on nuclear morphology (Lewis et al., 2011). Indeed, a number of cell types have been demonstrated to become senescent *in vivo*, including dermal fibroblasts (Dimri et al., 1995), crypt enterocytes and hepatocytes (Jurk et al., 2014), white

blood cells (Akbar et al., 2016), fat progenitors (Schafer et al., 2016), osteocytes (Farr et al., 2016) and possibly even neurons (Jurk et al., 2012). Several mechanisms could contribute to this accumulation of senescent cells with age, including an increased rate of senescence induction, decreased rate of clearance through reduced immune function, or loss of senescent markers for immune recognition causing immune evasion. Through secretion of pro-inflammatory factors and proteases, causing tissue dysfunction and loss of tissue regenerative potential, this accumulation of senescent cells appears to cause damage to tissue structure and loss of function with age.

Recently, a series of elegant experiments have conclusively demonstrated that senescent cells limit healthy lifespan and contribute to pathological ageing (Baker et al., 2011, Baker et al., 2016), using an inducible dimerization system to selectively induce apoptosis in senescent cells (INK-ATTAC). In this system, administration of the small molecule AP20187 leads to dimerization of a fusion protein expressed only in p16-expressing cells, consisting of FK506-binding protein and caspase 8, thus triggering apoptosis. In a mouse model deficient for the mitotic checkpoint protein Bub1b (*BubR1*$^{H/H}$) showing rapidly accelerated ageing, senescent cell removal was shown to extend lifespan and to blunt phenotypes of ageing including sarcopenia, cataracts and lipodystrophy (Baker et al., 2011). While this model was intriguing, the use of a prematurely ageing genetic mutant strain limited its applicability to normal ageing. However, Baker et al further demonstrated that elimination of senescent cells from naturally aged mice from midlife onwards through biweekly AP20187 administration caused extension in median lifespan, as well as preventing glomerulosclerosis, cardiomyocyte hypertrophy, diminished cardiac stress tolerance, cataracts, lipodystrophy and, crucially, cancer – demonstrating that removing senescent cells is anti-tumorigenic (Baker et al., 2016).

Subsequently, causal roles for cellular senescence have been demonstrated in a number of age-related diseases (Table 1.1). Furthermore, we have also begun to understand how the presence of senescent cells contributes to individual disease aetiology. Firstly, tissues with an increased senescent cell load may have a compromised replicative and repair capacity and may be subject to loss of specialised cell function, resulting in loss of tissue function. Secondly, accumulating senescent cells *in vivo* may contribute directly to sterile inflammation and age-related disease progression through secretion of pleotropic pro-inflammatory factors in the SASP. For example, in osteoarthritis, senescent cells promote an anti-regenerative environment through secretion of MMPs, which negatively affects cartilage structure, function and regeneration following injury (Jeon et al., 2017). Indeed, transplanting senescent cells into young, healthy mice is sufficient to induce an osteoarthritis-like condition (Xu et al., 2016) as well as transfer of senescence to host tissues resulting in persistent physical dysfunction and shortened lifespan (Xu et al., 2018).

In tumorigenesis, SASP factors promote malignant cell growth both in culture and in xenografts (Krtolica et al., 2001, Wang et al., 2006, Coppé et al., 2006), for example through secretion of mitogens including HGF (Liu and Hornsby 2007). The SASP can also induce cancer stem cells (Cahu et al., 2012) and cause tissue damage through MMP functions, thus creating a permissive environment for tumour progression, for example increasing the permeability of tumour capillaries (Liu and Hornsby, 2007), and promoting epithelial-mesenchymal transition (EMT) resulting in increased metastatic capacity (Canino et al., 2012, Coppé et al., 2008, Laberge et al., 2012, Parrinello et al., 2005) whilst MMP1 secretion also results in collagen breakdown and skin ageing (Quan et al., 2013). Furthermore, accumulating senescent cells may also have deleterious impacts on stem cell populations with advanced age. For example, pharmacological clearance of senescent cells using ABT263 was shown to rejuvenate hematopoietic stem cells in normally aged mice (Chang et al., 2017).

1.3.7. Senescence-based therapies to promote healthy ageing

Following the compelling demonstration that senescent cells promote pathological ageing (Baker et al., 2011, Baker et al., 2016), there has been considerable interest in developing 'senolytic' agents that induce apoptosis selectively in senescent cells (Figure 1.5). These include inhibitors of the pro-survival BCL-2 protein family (BCL-2, BCL-XL, BCL-W), thereby activating BAX and BAK to trigger mitochondrial outer membrane permeabilization (MOMP) and cytochrome c release for programmed cell death. BCL-2 family inhibitors include ABT263 (also known as navitoclax, Zhu et al., 2016) and ABT-737 (Yosef et al., 2016). Further senolytics include combined treatment with dasatinib and quercetin (D+Q, Zhu et al., 2015) which inhibit tyrosine kinases and PI3K respectively, UBX0101 which stabilises p53 through inhibiting its interaction with the E3 ligase MDM2 (Jeon et al., 2017), natural products such as piperlongumine with multiple targets (including OXR1, Zhang et al., 2018) and fisetin (including mTOR, Yousefzadeh et al., 2018), 17-DMAG which targets HSP90 (Fuhrmann-Stroissnigg et al., 2017) and DRI-FOXO4, a D-retro-inverse peptide sequence of the binding domain of FOXO4 for p53. Inhibiting the FOXO4-p53 interaction prevents sequestration of p53 in the nucleus, permitting translocation to the mitochondria for induction of apoptosis (Baar et al., 2017, Figure 1.5). Excitingly, recent data has provided the first evidence that senolytic treatment (D+Q) successfully reduces the senescent cell burden in elderly patients (Hickson et al., 2019). Notably however, while natural products and derivatives with anti-cancer properties such as quercetin and fisetin may selectively kill senescent vs. proliferating cells *in vitro* and *in vivo*, they may act on many pathways, meaning that the physiological effects observed from such treatments should be interpreted with caution, as these may not result exclusively from senescent cell removal.

Senolytics are a promising area of drug development, but as senescent cells are highly heterogenous both in terms of cell type and senescence inducer, different populations can require different senolytic mechanisms, due to reliance on different anti-apoptotic

pathways. Also, in certain contexts, cellular senescence is highly beneficial (section 1.3.5). Indeed, depending on the tissue type and patient condition, a substantial proportion of cells may be senescent and thus targeted by senolysis (Biran et al., 2017); while certain tissues with a low senescent cell load or a high regenerative capacity may be able to cope with senolysis, using senolytic agents to treat non-proliferative tissues (e.g. in neurodegeneration) may be another matter. Furthermore, the current range of senolytic agents includes a number repurposed chemotherapeutic agents with high levels of off-target effects, though some targeting specific protein-protein interactions (e.g. DRI-FOXO4) may have enhanced specificity. In addition, anti-apoptotic factors upregulated in senescent cells are also highly expressed in other cell types including red blood cells (Sarvothaman et al., 2015), raising the issue of how selective such drugs truly are. However, there is scope for increased senescent cell selectivity using specialised delivery systems (Muñoz-Espín, 2019). Furthermore, there is no risk of escape from senescence after senolysis, and inducing senolysis also prevents deleterious SASP secretion. Senolysis may also be a useful tool in cancer therapy as well as in tackling age-related diseases, for example promising data has been obtained using gene therapy with a suicide gene under a senescence-specific promoter (Oisin Biotechnologies, Rodier et al., 2018). Pre-clinical data and early clinical trials have so far shown promising results in tackling age-related diseases through selective elimination of senescent cells (see Table 1.1).

Age-related condition	Evidence for senescence in disease aetiology and/or senolytic efficacy in preclinical or clinical models
Atherosclerosis	Foamy macrophages with senescent markers accumulate at disease onset and are implicated in driving pathology through secretion of inflammatory cytokines and chemokines. In

	advanced lesions, senescent cells promote plaque instability through production of metalloproteases. Genetic (p16-3MR mice) and pharmacological (ABT263) removal of senescent cells is beneficial in atherosclerosis treatment (Childs et al., 2016).
Liver steatosis	Accumulating senescent cells are implicated in hepatic fat accumulation and liver steatosis. Removal of senescent cells (genetic (INK-ATTAC) or pharmacological (D+Q)) reduces steatosis. Induction of hepatocyte senescence is sufficient to drive fat accumulation. Senescence-associated mitochondrial dysfunction is implicated in disease pathogenesis through failure to efficiently metabolize fatty acids (Ogrodnik et al., 2017).
Osteoarthritis (OA)	Senescent cells accumulate in the articular cartilage and synovium in OA and are causally implicated in disease development as their removal (p16-3MR mice and UBX0101) delays pathology (Jeon et al., 2017). Further, local transplantation of senescent cells is sufficient to induce an OA-like condition in young mice (Xu et al., 2017). Small clinical trial results (Unity, UBX0101) have reported promising results.
Diabetes	In type I diabetes (TID), a subset of beta cells become senescent and secrete SASP factors. Elimination of these senescent beta cells prevents immune-mediated beta cell destruction, suggesting that beta cell senescence drives TID pathogenesis by stimulating immune-mediated beta cell destruction (Thompson et al., 2019). In type II diabetes (TIID), insulin resistance accelerates beta cell senescence, leading to a loss of function and cell identity, coincident with metabolic decline. Senolysis using INK-ATTAC or ABT-263 improves glucose tolerance and beta cell function both in an ageing mouse model and in a pharmacological/high fat diet insulin resistance model (Aguayo-Mazzucato et al., 2019). Furthermore, in progeroid INK-ATTAC mice, senolysis prevents lipodystrophy, increases insulin sensitivity and enhances adipogenesis (adipose atrophy linked to ageing and senescence, Xu et al., 2015).
Idiopathic pulmonary fibrosis (IPF)	Senescent markers and cells accumulate in IPF lungs, and pro-inflammatory SASP secretion has pro-fibrogenic effects. In a bleomycin-injury IPF model, senescent cell ablation (INK-ATTAC and D+Q) improves pulmonary function, but lung fibrosis is unaltered (Schafer et al., 2017). In a human pilot study,

	participants with IPF were treated with intermittent D+Q for 3 weeks (n=14) but results were not as promising as preclinical evidence (Justice et al., 2019).
Osteoporosis	Removal of senescent cells (using INK-ATTAC mice or D+Q) improves bone mass and strength with age, lowering bone resorption while maintaining or improving bone formation. *In vitro* data shows that conditioned media (CM) from senescent cells impairs osteoblast mineralization and enhances osteoclast survival, promoting osteoclastogenesis, suggesting that senescence promotes bone loss with ageing through promoting bone resorption (Farr et al., 2017).
Vertebral disc degeneration	Senescent cells accumulate in SA-β-gal positive clusters within degenerating discs (Roberts et al., 2006). Transgenic mice (p16-3MR) show reduced disc degeneration on senescent cell removal (Patil et al., 2019). Senolytic treatment selectively kills senescent disc cells taken from patients during surgery (curcumin and o-Vanillin, Cherif et al., 2019).
Age-related blindness	Retinal pigment epithelial cell senescence is associated with age-related macular degeneration (AMD, Zhu et al., 2009). *BubR1*$^{H/H}$ INK-ATTAC progeroid mice show delayed incidence of cataracts following senescent cell removal (Baker et al., 2011). Bcl-2 inhibitor UBX1967 currently being evaluated in age-related diseases of the eye including AMD (Unity).
Alopecia	Senescent cells persist in the epidermis of p14-inducible mice, whilst their removal using ABT-727 leads to increased hair follicle stem cell proliferation (Yosef et al., 2016).
Cardiac dysfunction	Endothelial cell senescence is implicated in driving heart failure and is coincident with inflammation and cardiac dysfunction in senescence-accelerated mice (Gevaert et al., 2017).
Neurodegeneration	In a mouse model of tau-dependent neurodegenerative disease, p16^{+} astrocytes and microglia accumulate. Clearance of these cells using INK-ATTAC mice prevents disease phenotypes and cognitive decline (Bussian et al., 2018).

Table 1.1 Age-related diseases attenuated by senescent cell removal

A number of further interventions targeting senescent cells with ageing are also being explored. For example, it may be possible to increase senescent cell clearance through enhancing immune surveillance mechanisms: while senescent cell accumulation with age may arise as a consequence of long-term acquisition of cell stress or damage, inefficient immune surveillance or immune evasion through loss of markers for immune detection may also contribute. Indeed, decoy receptors such as DCR2 upregulated by cancer cells to evade immunity through neutralizing NK cell activity may be increased on senescence (Sagiv et al., 2013). This highlights an intriguing potential avenue for senescent cell therapies: by analogy to cancer immunotherapy targeting cancer epitopes, patient-derived cytotoxic T cells with chimeric antigen receptors (CAR-T) could be trained to recognise senescent-specific cell surface markers for senescent cell elimination (Childs et al., 2017, Kloss et al., 2013).

A further strategy to promote healthy ageing through targeting senescent cells involves cellular reprogramming, where terminally differentiated senescent cells are converted into induced pluripotent stem cells (iPSCs) through expression of the OSKM transcription factors (OCT4, SOX2, KLF4, MYC). This approach has produced promising results *in vitro*, where reprogramming abolishes several features of senescence including restoration of nuclear morphology and chromatin structure, which persist even after re-differentiation (Lapasset et al., 2011). However, certain features including DNA methylation status and mutations resulting from DNA damage can persist, and telomere extension is observed (Lapasset et al., 2011). This approach has also been used in WS patient-derived cells, which proliferate well until differentiation into mesenchymal lineage (Cheung et al., 2014). However, *in vivo* work-up in wild-type has revealed the risk of cancer progression alongside rejuvenation (Abad et al., 2013), though teratoma formation was abrogated during a 'partial' reprogramming strategy (Ocampo et al., 2016). The observed rejuvenation may result from enhanced tissue regenerative capacity, stem cell function, or dilution of dysfunctional cells through proliferation of healthy counterparts.

Alternative strategies to target senescent cells in pathological ageing include suppressing the deleterious effects of senescent cells, notably through suppressing the SASP. While the SASP is highly heterogeneous, depending on the mode of senescence, cell type, duration and which signalling pathways are activated (Basisty et al., 2019), it constitutes an important target to reduce the circulating levels of pro-inflammatory and pro-tumorigenic factors within ageing tissues, and after genotoxic chemotherapy. There are several opportunities for suppressing the SASP: to block secretion (e.g. protein post-translational modification required for secretion or exosome release), to inhibit the activity of individual components post-secretion (e.g. monoclonal antibodies against IL-6 (siltuximab) or IL-6R (tocilizumab)), or to target the underlying signalling pathways driving SASP expression, such as mTOR (Laberge et al., 2015, Herranz et al., 2015) or MAPK signalling (Alimbetov et al., 2016). Indeed, targeting nutrient sensing pathways including mTOR, IGF1 and AMPK with dietary restriction (DR) mimetics such as rapamycin and metformin is promising in terms of extending lifespan and healthspan, and delaying age-related disease; genetic or pharmacological mTOR inhibition extends lifespan in mice (e.g. Harrison et al., 2009, section 1.4.3.). Furthermore, caloric or dietary restriction reliably extends longevity in a range of small model organisms; though initial reports in rhesus macaques appeared conflicting (Colman et al., 2009, Cox, 2009, Cox and Mattison, 2009, Mattison et al., 2012, Mattison et al., 2017). Due to the important drawbacks of current senolytic treatments (see above), the exciting research into tackling age-related disease through DR-mimetics such as rapamycin, and the intriguing data suggesting mTOR signalling as a critical regulator of cellular senescence and ageing (section 1.4), I chose to primarily investigate mTOR signalling in cellular senescence in this thesis.

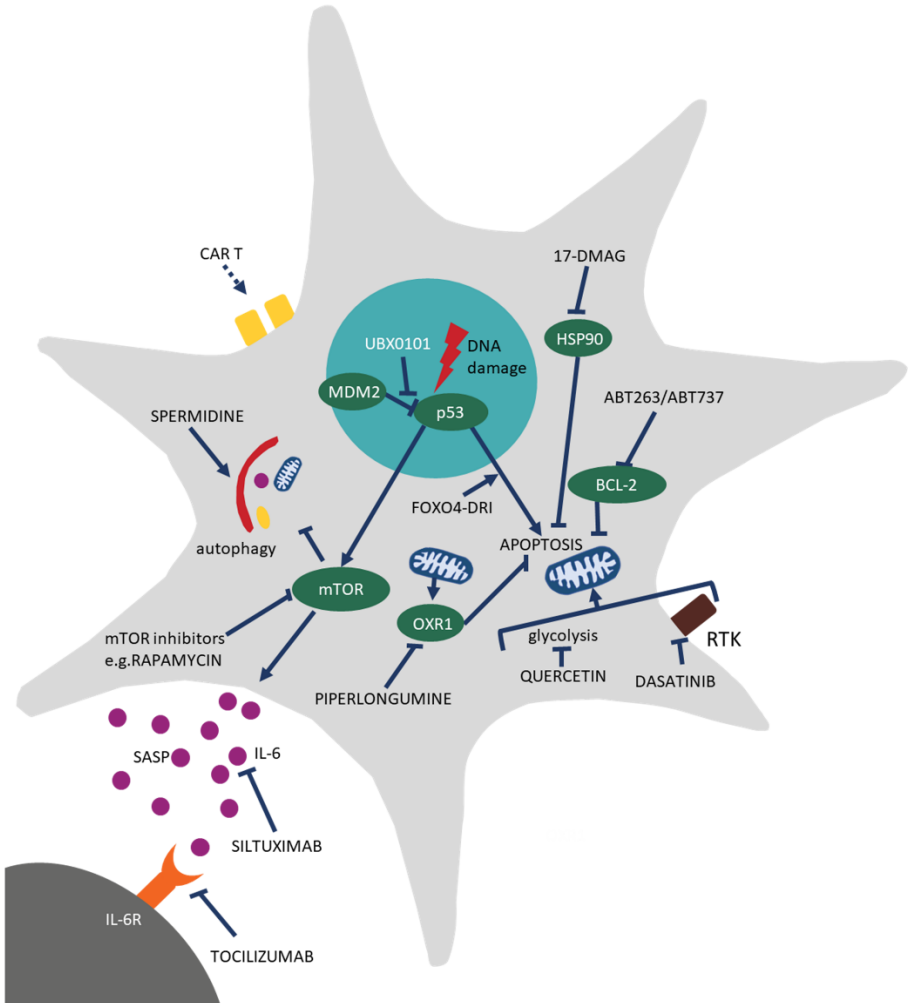


Figure 1.5. Possible therapeutic targets in senescence

Schematic representation of a senescent cell with target molecules, organelles and processes together with current treatment options to modulate, induce apoptosis or promote clearance of senescent cells. Drugs including rapamycin, which acts through mTOR inhibition, suppress the secretion of pleiotropic pro-inflammatory mediators (SASP) from senescent cells, while targeted therapies such as siltuximab (IL-6) and tocilizumab (IL-6R) interfere with these mediators or their receptors post-secretion. Spermidine acts to increase cellular autophagy. Therapies based on CAR-T may facilitate improved immunosurveillance of senescent cells by training immune cells to recognise specific senescent cell surface markers. Senolytic treatments interfere with various pathways regulating apoptosis in senescent cells; quercetin blocks glycolysis and dasatinib inhibits receptor tyrosine kinases (RTK), and combination (D+Q) treatment results in senolysis. The natural product piperlongumine has many targets, including OXR1 (oxidation resistance 1) which upregulates anti-oxidant proteins in response to oxidative stress to prevent induction of apoptosis. 17-DMAG inhibits HSP90, which itself acts to inhibit apoptosis in senescent cells. The peptidomimetic drug FOXO4-DRI induces mitochondrial translocation of p53 for apoptosis induction by inhibiting its nuclear sequestration by FOXO4, while UBX0101 blocks the MDM2-mediated ubiquitination and degradation of p53, and thus induces apoptosis. ABT263 directly inhibits the pro-survival factor BCL-2, resulting in senolysis.

1.4. mTOR in senescence and ageing

1.4.1. mTOR signalling

The serine/threonine kinase mTOR is a major regulatory nexus that integrates signals including levels of glucose, amino acids, oxygen, growth factors and hormones to direct cell growth and proliferation under suitable conditions. mTOR is the functional enzyme within two distinct complexes (mTORC1 and mTORC2) where it associates with several other proteins that are either distinct to each complex (e.g. Raptor/Rictor) or present in both (e.g. Deptor, mLST8, Figure 1.6). To drive cell growth and proliferation, mTORC1 regulates a number of anabolic pathways including autophagy and protein and nucleotide synthesis (Buj et al., 2019), whilst mTORC2 has a role in regulating actin organization as well as in metabolic control (Huang and Fingar, 2014). mTORC1 is negatively regulated by the tuberous sclerosis (TSC1/2) complex, but activated by Rheb on recruitment to the lysosome through the action of Rag GTPases and regulators, such as LAMTOR/Ragulator. mTORC2 is ribosomally associated on activation by insulin signalling; this activation is mediated through IGFR and IRS1/2 (Huang and Fingar, 2014), though localisation at mitochondria, the plasma membrane, ER, and lysosomes has also been reported (Ebner et al., 2017). There is significant cross-talk between mTORC1 and mTORC2 through feedback loops, in particular through Akt/PKB, and possibly through competition for FKBP subunits (Xie and Proud, 2014).

1.4.2. mTOR in senescence

Notably, the proliferative arrest that characterizes cellular senescence is not accompanied by a down-regulation of growth signalling. In fact, mTOR signalling is constitutively active in many models of senescence including replicative senescence and oncogene-induced senescence (Carroll et al., 2017). Rather than being dramatically increased in protein levels however, mTOR signalling may instead be dysregulated in senescence; mTORC1 activity persists despite the removal of serum and amino acids in senescent but not proliferating

fibroblasts, indicating constitutive activation that may be attributable to depolarization of the plasma membrane in senescence (Carroll et al., 2017). The mechanisms behind healthspan and lifespan extension afforded by mTOR inhibition (see 1.4.3) and the roles of mTOR signalling in senescence are both likely to be multi-factorial, as mTOR regulates a multitude of downstream signalling events (Figure 1.6).

Protein translation is regulated by mTORC1, through regulation of ribosome biogenesis (via kinase S6K) as well as translation initiation (via 4E-BP1 and S6K) and elongation (via eEF2). 4E-BP1 binds and inhibits eIF4E, a DEAD-box helicase which unwinds secondary structures at the 5' end of transcripts and is a critical factor in recruiting 40S ribosomal subunits for cap-dependent translation initiation: this inhibition is removed upon mTORC1-mediated 4E-BP1 phosphorylation (Gingras et al., 1999). By contrast, S6K is activated on mTORC1-mediated phosphorylation (Huang and Fingar, 2014), and can subsequently phosphorylate S6, a structural component of the 40S ribosomal subunit, as well as acting in ribosome biogenesis (Iadevaia et al., 2014) and regulating 5'TOP (terminal oligopyrimidine tract) mRNA translation through LARP1 (Hong et al., 2017), also regulated (in certain contexts) through 4E-BP-mediated regulation of eIF4E (Thoreen et al., 2012, Miloslavski et al., 2014). Further, mTORC1-dependent phosphorylation and activation of eEF2 promotes translocation of the ribosome along the mRNA, enhancing protein synthesis (Browne and Proud, 2004). While promotion of protein synthesis has largely been attributed to mTORC1, mTORC2 can also be activated by direct ribosomal association, and may play a role in co-translational processing of nascent polypeptides (Oh et al., 2010). mTOR-dependent upregulation of protein synthesis may be crucial in controlling senescence. For example, mTOR-dependent feedback loops involving IL1A translation coordinate establishment of pro-inflammatory secretion (Laberge et al., 2015). More generally, excess translation driven through constitutively active mTOR predisposes to ER stress, which can lead to induction of senescence (section

1.3.3.2.3). Furthermore, the hypertrophy exhibited by senescent cells is consistent with accumulation of biomass through activation of cellular growth pathways.

mTOR activity can also influence gene expression through interaction with transcription factors, particularly those involved in stress responses including HIF-1α in hypoxia (Majumder et al., 2004, Nakamura et al., 2005), NRF2 in oxidative stress (Lerner et al., 2013), HSF1 following heat shock (Santagata et al., 2013) and NFAT5 on osmotic stress (Ortells et al., 2012). mTORC is also phosphorylated and activated by the DNA damage responsive ATM/ATR kinases, resulting in Chk1 phosphorylation and proliferation arrest (Selvarajah et al., 2015). p38 MAPK also phosphorylates components of the mTOR/S6K axis following DNA damage, and p53 transcriptional targets such as TSC2, AMPK and REDD1 can further modulate mTOR activity in response to stress (Feng et al., 2007). However, mTOR itself can indirectly modulate p53-dependent transcription, for example by activating p53 through S6K and MDM2, or by enhancing its translation (Lee et al., 2007, Lai et al., 2010). mTOR activity may also regulate p53-dependent transcription of p21, an important molecular player in cell cycle control (Astle et al., 2012). Hence, chronic hyperactivation of mTOR in response to stress can drive growth without cell cycle progression.

mTOR activity also provides a critical link between the energy balance of the cell and mitochondrial load, regulating both mitochondrial biogenesis and mitophagy. Biogenesis is controlled through several mechanisms including PGC-1β-dependent mitochondrial biogenesis and preferential translation of nuclear-encoded mitochondrial-related mRNAs via the relief of 4E-BP inhibition (Morita et al., 2013), with mitochondrial oxidative function controlled through the YY1-PGC-1α transcriptional complex (Cunningham et al., 2007). Therefore, mTOR kinase is a critical regulatory hub controlling cell growth, proliferation and response to environmental stress, which may be dysregulated in senescence.

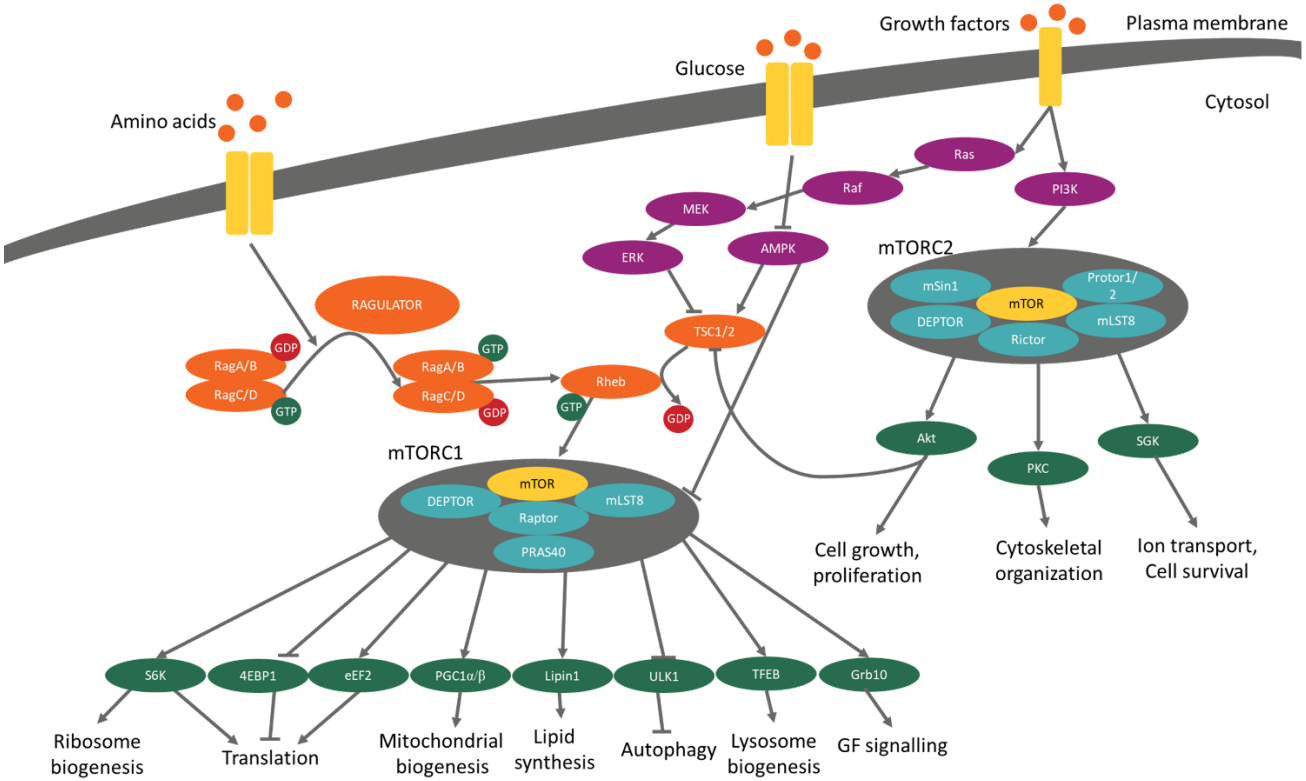


Figure 1.6. mTORC1 and mTORC2 regulation, crosstalk and downstream signalling consequences.

Schematic diagram showing upstream regulators and downstream targets of mTORC1 and mTORC2 with consequences for the cell. mTOR is the catalytic component of two Ser/Thr kinase complexes (mTORC1 and mTORC2) with some shared subunits (mLST8, DEPTOR) and other distinct components (mTORC1: Raptor, PRAS40; mTORC2: Rictor, mSin1, Protor1/2). mTORC1 is positively regulated by nutrient availability (amino acids, glucose) while both complexes are activated by growth factor signalling. mTORC1 is inhibited by TSC1/2 or activated by Rheb at the lysosome, through action of Rag GTPases and regulatory proteins (Ragulator). mTORC1 phosphorylates many substrates (green) with a range of biological outcomes. mTORC2 is less well-studied however its known substrates (green) have roles in cytoskeletal organization, cell growth and survival, and ion transport. Further, mTORC2 phosphorylation of Akt results in mTORC1 activation via inhibition of its inhibitor TSC1/2, highlighting cross-talk between the complexes.

1.4.3. mTOR in ageing

The involvement of mTORC signalling in ageing is supported by a large body of experimental evidence. Loss-of-function mutations in TOR have been shown to increase the lifespan of yeast (Kaeberlein et al., 2005), *C. elegans* (Vellai et al., 2003, Jia and Levine, 2007, Hansen et al., 2007), and *Drosophila* (Kapahi et al., 2004). Furthermore, deletion of S6K1, a downstream target of mTOR, increases lifespan in female mice (Selman et al., 2009). Reduced mTOR signalling increases lifespan and reduces age-related pathologies, including motor dysfunction and loss of insulin sensitivity (Selman et al., 2009). Notably, such findings contrast with other reports that chronic mTORC inhibition induces diabetes (Gyurus et al., 2011), which has been attributed to differential effects on mTORC1 versus mTORC2, though in some cases loss of mTORC2 signalling also increases lifespan and improves health. For instance, in the nematode worm, reduction in mTORC2 signalling by RNAi depletion of Rictor can increase lifespan under conditions of stress (high temperature) or high-quality food (i.e. the opposite of caloric restriction and akin to a high fat diet in mice), whereas the opposite is seen at lower temperatures and on a less rich food source (Mizunuma et al., 2014).

1.4.4. mTOR inhibitors

Rapamycin is a natural macrolide antibiotic lactone produced by *Streptomyces hydroscopius*, discovered in soil samples from Easter Island, and initially noted for inhibiting the proliferation of yeast (Vézina et al., 1975). At high doses (e.g. ≥ 5mg/day), rapamycin has immunosuppressive effects, and is FDA approved for prevention of transplant rejection (Dominguez et al., 2000). It is also in clinical use or in trials for a large number of cancers where mTORC signalling appears to be a key factor in promoting and/or sustaining oncogenic transformation (Grabiner et al., 2014). Reported side-effects of chronic high-dose administration include ulceration of mucosal tissues, haematological abnormalities, induction of insulin insensitivity, obesity and diabetes, though these adverse effects may be largely dose-dependent.

As discovered through *S. cerevisiae* genetic screens (Heitman et al., 1991), rapamycin mechanistically acts by binding the immunophilin/prolyly isomerase FKBP12, producing a complex that can bind the FRB region of mTOR and partially occlude the active site of mTOR kinase in the mTORC1 complex (Caron et al., 2010). This induces cellular effects including a decrease in protein synthesis, increase in autophagy and inhibition of cell growth. Rapamycin does not inhibit the phosphorylation of all mTORC1 substrates equally, however: it completely inhibits S6K phosphorylation, while only partially blocking 4E-BP phosphorylation (Choo et al., 2008). A crystal structure of mTOR with rapamycin and FKBP12 (Yang et al., 2013) suggests that this may be due to differential substrate access to the kinase active site, controlled by the mTOR FRB domain, through differential substrate quality could also be important (Stanfel et al., 2009). Structural and functional analogues of rapamycin (rapalogues) that also act by allosterically modulating the enzyme have been developed to improve bioavailability and pharmacokinetics, including drugs such as everolimus (RAD001) and deforolimus. These agents also act by recruiting FKBP12 to mTORC1.

By contrast to mTORC1, mTORC2 is not particularly sensitive to inhibition by rapamycin or rapalogues, though chronic administration does impact mTORC2 signalling (Sarbassov et al., 2006), either through feedback via the Akt/insulin signalling pathway, and/or through competition for key subunits FKBP12, 51 and 52, which may set different thresholds for rapamycin sensitivity between the two complexes (Schreiber et al., 2015). mTORC2 inhibition is implicated in impaired glucose homeostasis, insulin insensitivity and diabetes (Gyurus et al., 2011), though it may be beneficial in the context of stress (Mizunuma et al., 2014). It is important to note that studies of mTORC2 often rely on phosphorylation of Akt on S473 as a readout of mTORC2 activity, but this site on Akt may also be targeted by kinases IKKε, TBK1 (Joung et al., 2011) and DNA-PK (Toulany et al., 2011), potentially skewing the interpretation of mTORC2-specific effects.

A number of second-generation mTOR inhibitors have been developed primarily as chemotherapeutic agents to target mTOR hyperactivity observed in many cancers (Kim et al., 2017). These drugs compete with ATP for the active site of the mTOR kinase (Chresta et al., 2010), and hence are effective in inhibiting both mTORC1 and mTORC2. Some agents have extremely high specificity and selectivity for the mTOR kinase. For example, AZD8055 has 1000-fold greater inhibitory effect on mTOR than on other PI3 kinases (Chresta et al., 2010), whereas others (e.g. BEZ235) have dual inhibitory effects on both mTOR and PI3K (Maira et al., 2008), with a 3-5 fold higher K_d for damage response kinase ATR (Toledo et al., 2011). While these ATP-competitive inhibitors exhibit more potent apoptotic effects *in vitro* compared with rapalogues, and a number of such agents have been tested in clinical trials for safety, larger scale clinical trials for various cancers have not yet demonstrated greater efficacy than current best treatment regimens. Therefore, drugs such as AZD8055, AZD2014, AZD3147 and WYE354 have not yet received FDA approval and have been placed on back-catalogue by their developers, making them available through open discovery platforms.

1.4.5. mTOR inhibitors as therapeutics for age-related diseases

A landmark study from 2009 in which rapamycin was fed to middle-aged mice provided the first evidence that a small molecule drug, taken orally, could significantly extend both the mean and maximum lifespan in mammals (Harrison et al., 2009). In this multi-centre, large cohort study of genetically heterogeneous (UM-HET3) mice, rapamycin delayed the ageing of 20-month old male and female mice. Further studies have not only validated these results, but have demonstrated that rapamycin improves health, in terms of lower incidence or decreased severity of age-related disease, as well as prolonging life (Wilkinson et al., 2012).

Excitingly, there is a growing body of evidence that mTOR inhibitors could constitute beneficial treatments for a wide range of age-related conditions, highlighting mTOR

signalling as a commonality in the aetiology of age-related disease progression and pathological ageing (Table 1.2, Walters and Cox 2018). While rapamycin is already clinically licensed, its side effects and perception of action in immunosuppression (though this is only observed at very high doses) call into question its use as a treatment for less severe conditions. However, recent clinical trials of mTOR inhibitors in immunosenescence using low doses of the rapalogue RAD001 (0.5 mg daily/5mg weekly or 20 mg weekly, Mannick et al., 2014) or in combination with BEZ235 (daily doses of 0.1 mg RAD001/0.5 mg RAD001/10 mg BEZ235/0.1 mg RAD001+10 mg BEZ235, Mannick et al., 2018) reported minimal side effects in elderly humans, as well as improved immune responses to influenza vaccination (Mannick et al., 2014). Excitingly, 6-week dosage protected treated individuals from respiratory tract infections for a year following treatment, suggesting immune system rejuvenation (Mannick et al., 2018). Phase III clinical trials are now ongoing in patients with COPD and in individuals >85 years old with multimorbidities (resTORbio).

Further, in a small, short-term trial, middle-aged dogs treated with low doses of rapamycin exhibited a substantial benefit to cardiac health (n=24, 10-week trial, Urfer et al., 2017). Following these promising results, a larger trial involving 500 dogs is currently being performed, where the animals will be treated with rapamycin for 5 years, as part of a larger project examining genetic and environmental factors controlling longevity and health in dogs (10,000 dogs, Dog Aging Project; Savage, 2017). Using pet dogs for this research puts rapamycin to the test in human-oriented conditions, as pet animals share their owners' environment and receive a high standard of veterinary care. Further, researchers are able to follow the animals from birth to death within around a decade. By studying rapamycin treatment in middle-aged dogs over 5 years, their data may be able to distinguish whether rapamycin treatment extends the lifespan and healthspan of these dogs significantly.

Age-related condition	Evidence for role of mTOR signalling in disease aetiology	Therapeutic potential of mTORC inhibition
Immunosenescence (functional decline of immune system with age)	Mouse models show increased immune activity against pathogens on mild mTOR inhibition (Hurez et al., 2015)	Multiple placebo-controlled trials in elderly humans have reported improved vaccine responses (Mannick et al., 2014) and improved infection control (Mannick et al., 2018) following a short course of low dose mTORC inhibitor treatment (RAD001 ± BEZ235) without serious side-effects
Neurodegeneration (Alzheimer's disease, AD)	mTOR activity is upregulated in AD brains compared to age-matched controls (An et al., 2003), and is implicated in the development of tau pathology (Pei et al., 2008). Control of protein translation and autophagy is critically important in neurodegenerative diseases characterized by proteinaceous aggregates (autophagy decreases in neurons with age (Cuervo, 2008))	Rapamycin prevents cognitive decline in AD-Tg mouse model (Caccamo et al., 2010, Spilman et al., 2010, Majumder et al., 2011) and can reverse mild memory deficits (Lin et al., 2013), correlating with reduction of Aβ plaques and tau tangles, and increased localization of Aβ into lysosomes suggestive of appropriate processing
Age-related macular degeneration (AMD)	In senescence-accelerated OXYS rats, rapamycin administration decreased incidence and severity of AMD-like retinopathy (Kolosova et al., 2012); VEGF (SASP factor) implicated in AMD pathology	Several small clinical trials have produced conflicting results – possible dosing issues (Wong et al., 2013)
Osteoarthritis (OA)	Senescent cells are detected in osteoarthritis joints and are sufficient for disease progression (Xu et al., 2016); SASP secretion	Intraperitoneal administration of rapamycin reduces cartilage destruction and synovitis in experimentally-induced

	(regulated by mTOR, Laberge et al., 2015, Herranz et al., 2016) of metalloproteases is likely to impact on joint integrity	osteoarthritis in mice (Caramés et al., 2012)
Cardiovascular disease (CVD)	Age-related sterile inflammation in the heart reduced on rapamycin treatment (Wang et al., 2010), alongside increasing expression of glycolytic enzymes and mitochondrial protein expression (Dai et al., 2014)	Rapamycin improves cardiac health in aged mice (Flynn et al., 2013, Dai et al., 2014) and in aged companion dogs (Urfer et al., 2017; large scale dog trials now recruiting)
Diabetic nephropathy (DN)	In diabetes, hyperglycaemia increases mTOR activity through activation of Akt and inhibition of AMPK, with consequences for podocyte development (cells critical in production of the renal filtration barrier). Experimentally increasing mTORC1 activity in mouse podocytes induces DN phenotypes, podocyte loss and Nephrin mis-localization (cell surface protein important for barrier production).	Rapamycin and everolimus treatments are beneficial for DN in animal models e.g. in rats with STZ-induced diabetes (Lloberas et al., 2006, Yang et al., 2007, Sakaguchi et al., 2006, Mori et al., 2009, Cheng et al., 2011)
Cancer	Many oncogenic mutations activate mTOR signalling, consistent with a central role in cell growth, proliferation and angiogenesis (Grabiner et al., 2014); mTOR-regulated SASP has pro-tumorigenic consequences (Coppé et al., 2008), thought to underlie the increased occurrence of secondary tumours as a side effect of chemotherapy, and increase in tumour incidence with age.	mTOR inhibitors have limited and varied potential as monotherapies against cancers. Promising potential to prevent induction of therapy-induced, secondary or age-related cancers; rapamycin treatment can prevent the stimulation of prostate tumour growth by senescent fibroblasts in mice (Laberge et al., 2015)

Table 1.2. mTORC inhibitors as broad-spectrum therapeutics for age-related disease (adapted from Walters and Cox, 2018).

1.5. Aims of research

In this thesis, I set out to use pharmacological modulation and comparative proteomics to investigate the molecular processes driving cellular senescence. Firstly, I set out to fill a gap in the field by developing a novel, experimentally-amenable model of senescence through modulation of an ageing-associated molecular pathway. Subsequently, due to research implicating both in pathological ageing, I sought to investigate the role of mTOR signalling in senescence, an important nutrient sensing pathway which acts as a central coordinator of cell growth and proliferation, aiming to improve our mechanistic understanding of how mTOR inhibition extends lifespan and prevents or delays age-related diseases. Finally, I set out to use unbiased comparative proteomics to identify important molecular processes in senescence, and possible therapeutic targets.

2. Materials and methods

2.1. Cell Culture

2.1.1. Routine subculture of primary human cell lines

The cell lines used in this thesis and the appropriate media, supplements and suppliers are detailed in Table 2.1. For routine sub-culture, cells were harvested when assessed as ≥ 70% confluent using a digital EVOS microscope (Thermo Fisher). Cells were washed in PBS (Sigma) and then detached by incubation with Tryple Express Trypsin (Thermo Fisher), incubated for 3-5 minutes before gentle tapping. Cells were then diluted and gently triturated in complete media (see Table 2.1). A 20 µl aliquot of this suspension was taken for automated cell counting, viability and diameter analysis using a T4 Cellometer (Nexelcom). The number of population doublings (PD) undergone during culture was then calculated using the formula:

$$PD = \frac{log(\text{no. cells harvested/no.cells seeded})}{log(2)}$$

Cumulative population doublings (CPD) were subsequently calculated as a sum of total population doublings, whilst proliferation rate was calculated as a ratio of population doublings over time in culture (PD/day). Cells were then seeded at 4-8x10^3 cells/cm^2 in a filter-capped flask (T25/T75/T175 flasks or multi-well plates, Greiner) with cell line-appropriate media (see Table 2.1) and incubated in a humidified incubator at 37°C in 5% CO_2 and 20% O_2. For multi-well plate experiments, seeding densities were calculated to take into account experiment duration and proliferation rate in order to achieve optimal cell density at the point of analysis. For cryopreservation, cells were harvested as above and then pelleted in a Beckman GS-15R centrifuge (RT, 3 kRPM (equivalent to 2300xg, rotor S4180), 3 minutes) before gentle resuspension of the cell pellet in Synthafreeze to 6x10^5 cells/ml

(Thermo Fisher) and storage at -80°C or in vapour phase liquid nitrogen. Frozen cells were thawed by rapid warming in a water bath at 37°C before cell counting and immediate transfer into a flask with pre-warmed media at 37°C. After the cells had bedded down (2-24 hours), media was changed to remove Synthafreeze from the culture medium. Cells were always sub-cultured routinely at least once before use in experiments for recovery from freeze/thaw. Cells were routinely inspected by phase contrast microscopy for cell health and possible contamination, and tested for mycoplasma contamination by PCR according to Uphoff and Drexler (2002, 2004).

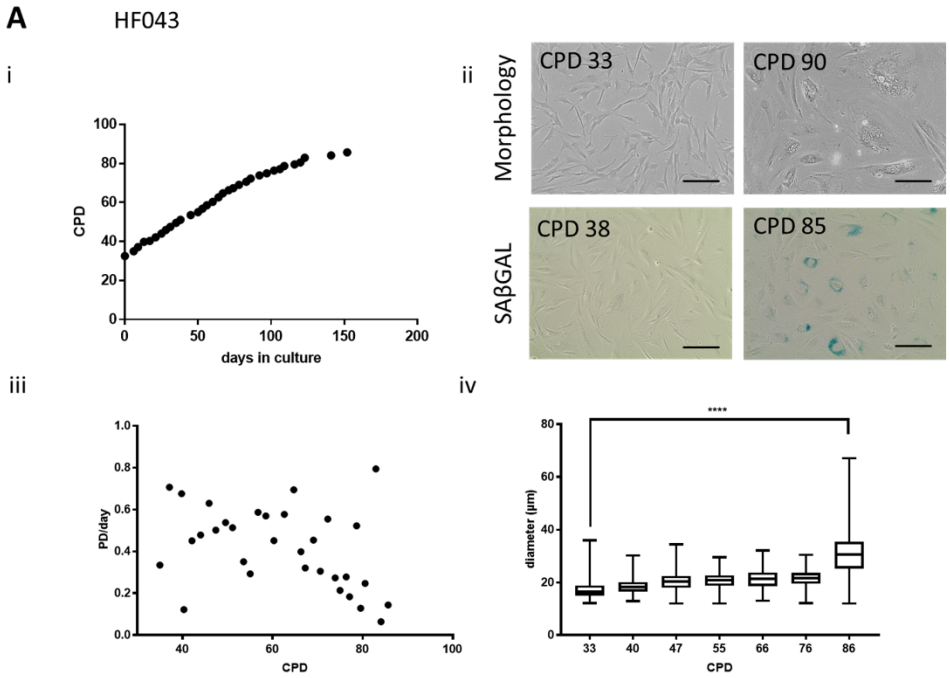
Cell line	Source	Donor age	Donor gender	Donor ethnicity	Donor condition	Cell type	DMEM supplements	Max. CPD
HF043	Dundee CELL products	Neonatal	Male	Caucasian	Wild-type	Foreskin fibroblast	10% FBS	90
AG09602	Gift (Dr. Terence Davis, University of Cardiff)	92	Female	Caucasian	Wild-type	Skin fibroblast	10% FBS	39
AG03141/WS3141	"	30	Female	Caucasian	Werner syndrome	Skin fibroblast	20 % FBS	<10
MRC5	ATCC	14 weeks foetus	Male	Caucasian	Wild-type	Lung fibroblast	10 % FBS	50
IMR90 ER:Ras	Gift (Prof. Peter Adams, Uni. Glasgow, SBP)	16 weeks foetus	Female	Caucasian	Wild-type	Lung fibroblast	20% FBS, 1 mM sodium pyruvate	N/A
HeLa (mCherry-Histone H2B, EGFP-α tubulin)	Gift (Prof. Francis Barr, Uni. Oxford)	31	Female	African American	Cancer	Cervical epithelial cells (adenocarcinoma)	10% FBS	N/A
HEK-Blue IL6	InvivoGen	Foetus	Female	Caucasian	Cancer	Embryonic kidney cells (carcinoma)	10 % FBS, penicillin, streptomycin, normocin	N/A

Table 2.1: Details of the cell lines used in this thesis and appropriate media supplements (DMEM D5796 (high glucose with L-glutamine), Sigma; FBS (heat-inactivated) Gibco; sodium pyruvate, Sigma; penicillin, streptomycin and normocin; InvivoGen). Note HF043 fibroblasts were checked by short tandem repeat analysis (Porton Down) and found to be primary diploid fibroblasts and uncomtaminated with any known lab cell line (data not shown).

2.1.2. Induction of senescence

2.1.2.1. Replicative senescence

The primary human cell lines HF043, MRC5 and AG09602 were each grown in continuous culture until replicative exhaustion. At each harvest, cell morphology, diameter and proliferation rate were measured and recorded. Cells were determined to be replicatively senescent when populations failed to increase in cell number within >2 weeks, and by SA-β-gal staining. Graphs showing the proliferative course, alterations in diameter, morphology and proliferation rate, as well as verification of senescence by SA-β-gal at maximum CPD are shown for each cell line (Figure 2.1).



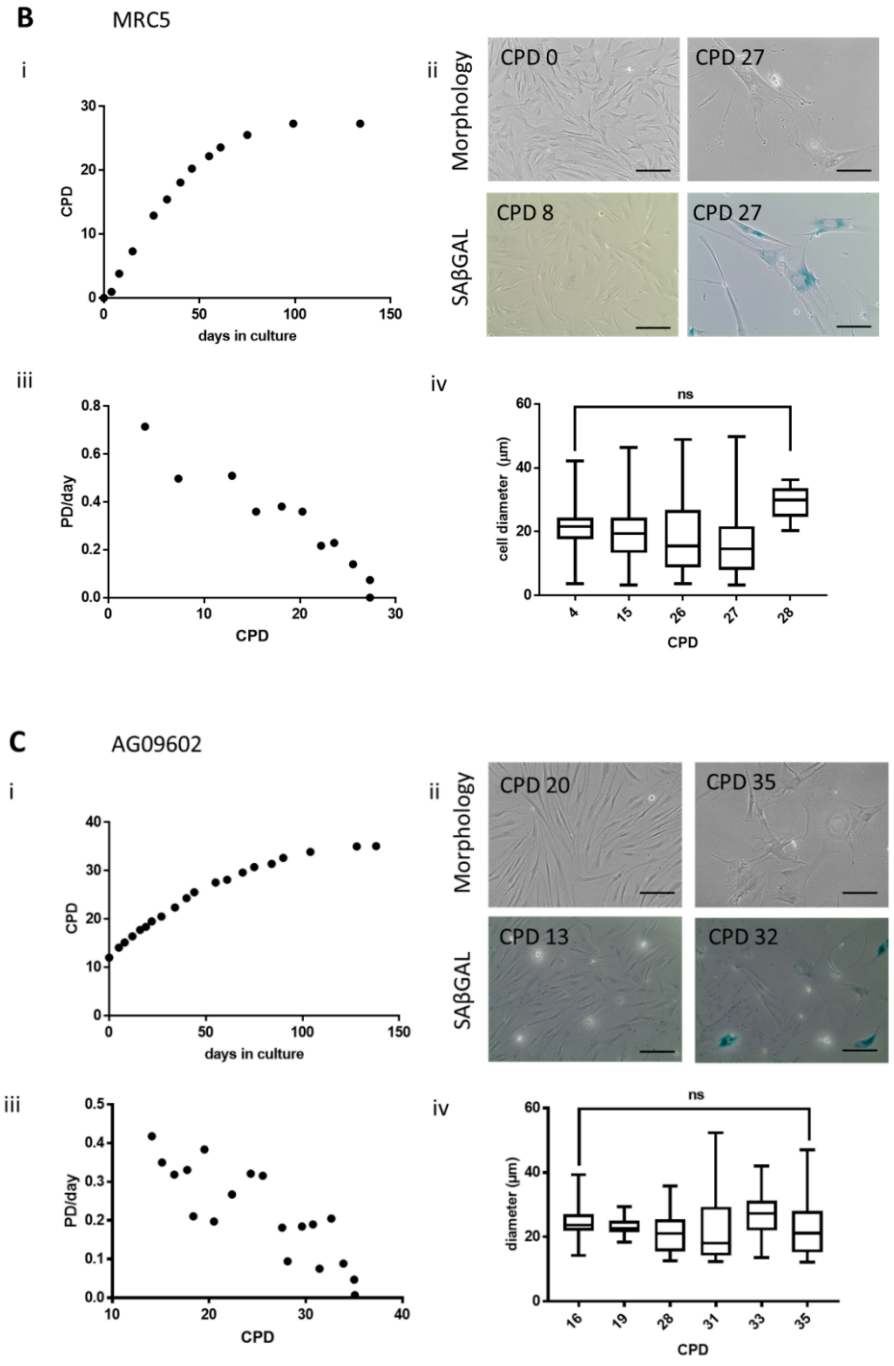


Figure 2.1 Induction of replicative senescence
HF043 (A), MRC5 (B) and AG09602 (C) cell lines (see Table 2.1) were cultured as stated in 2.1.1 continually in cell culture until replicative exhaustion. Replicative age (CPD, i), proliferation rate (PD/day, iii) and cell diameters (iv) were measured at each harvest using a cellometer. Morphology was routinely inspected by phase contrast microscopy; proliferating controls and replicatively senescent cells imaged using phase contrast microscopy live and following SA-β-gal staining are shown for verification of senescence (ii, n>3). Continuous passaging from low CPD was performed for HF043 and MRC5 ≥3 times, and continuous passaging for AG09602 was performed once, but the replicative profile produced was highly consistent with data from the Kipling lab (Uni. Cardiff) who kindly donated the cells. Scale bar 100 μm. Note MRC5 were cultured from 'passage 21' (i.e. not previously subject to cell counting thus CPD was initially designated as 0).

2.1.2.2. DNA damage induced senescence

To model DNA damage-induced senescence (DDIS), the topoisomerase inhibitor etoposide was used at 20 μM to treat HF043 fibroblasts (γH2AX immunofluorescence revealed DDR foci in >90% cells following 24 hour treatment, data not shown). After 7 days treatment, cells were verified as senescent by SA-β-gal staining and morphological assessment, as well as failure to re-proliferate. Cells at low CPD (<50) were always used for etoposide treatment to avoid confounding effects of replicative senescence (Figure 2.2A).

2.1.2.3. Oncogene-induced senescence

To model oncogene-induced senescence (OIS), IMR90 cells stably transfected with a tamoxifen (4-OHT)-inducible constitutively active Ras were used (ER:Ras). Cells were treated with 4-OHT at 1 μM for 7 days and assessed for senescence induction by SA-β-gal staining, morphological assessment and failure to re-proliferate (Figure 2.2B).

2.1.3. Drug treatments

Small molecules and doses used routinely in this work are listed in Table 2.2 (unless dose otherwise specified elsewhere in the text or figure legends). Compounds were dissolved and stored as directed by supplier (usually in DMSO at -20°C in the dark). For drug treatment, cells were seeded into flasks or multi-well plates the day before drug treatment and left to bed down overnight. Media was then removed and replaced with fresh media supplemented with the drug. Optimum concentrations and dosing periods were (unless otherwise specified) determined empirically from literature-informed pilot experiments or from previous studies in the host lab (L. Cox, personal communication).

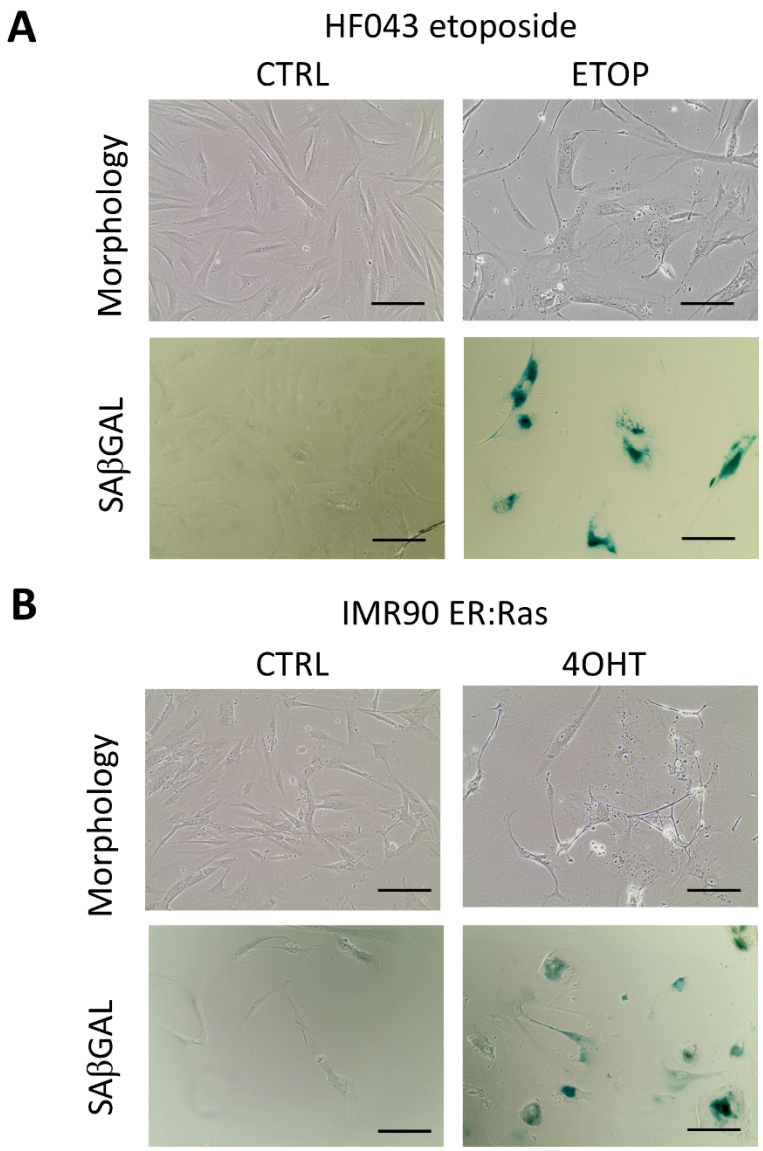


Figure 2.2 Induction of DNA damage and oncogene-induced senescence

A: HF043 fibroblasts were treated with 20 μM etoposide, B: IMR90 ER:Ras fibroblasts were treated with 1 μM 4-OHT, both for 7 days in culture with vehicle only controls (CTRL). Morphology was then inspected live using phase contrast microscopy and cells were imaged following SA-β-gal staining for verification of senescence induction. Scale bar 100 μm.

Compound	Cellular Target (I, inhibitor; A, activator)	Standard dose used	Supplier
Tenovin-6	SIRT1/SIRT2 (I)	2 µM	Cayman Chemical
Resveratrol	SIRT1 (A)	50 µM	Enzo (Fluor de Lys)
Trichostatin A	HDAC (I)	1 µM	Enzo (Fluor de Lys)
Rapamycin	mTORC1/FKBP12 (I)	70 nM	Selleckchem
Deforolimus	mTORC1/FKBP12 (I)	70 nM	Selleckchem
AZD8055	mTOR (I)	70 nM	Selleckchem
AZD3147	mTOR (I)	70 nM	Selleckchem
WYE354	mTOR (I)	1 µM	Selleckchem
Bafilomycin A1	V-ATPase (I)	10 nM	Sigma-Aldrich
Casin	Cdc42 (I)	1 µM	Sigma-Aldrich
PF-3758309	PAK4 (I)	1 µM	Sigma-Aldrich
Y-27632	ROCK1/2 (I)	1 µM	Sigma-Aldrich
Auranofin	Redox enzymes (I)	0.5 µM	Santa-Cruz
Etoposide	TOPO1/2 (I)	20 µM	Sigma-Aldrich
4-OHT	ER:Ras (IMR90, A)	1 µM	Sigma-Aldrich

Table 2.2: Drugs used in this thesis. For storage, all compounds were dissolved in DMSO and stored at -20^{o}C, apart from 4-OHT, which was dissolved in absolute ethanol and stored at 4^{o}C.

2.2. Commercial cell culture-based assays

2.2.1. alamarBlue metabolic activity assay

The alamarBlue assay for reducing capacity (a proxy for cell metabolic capacity and viability) was performed according to manufacturer's instructions (Thermo Fisher), adding the 10x stock at 1:10 dilution (volume/volume, v/v) to obtain 1x final concentration in complete media and assessing fluorescence (Ex570, Em585) after 4 hours incubation using a BMG Pherastar FS platereader. Control cell-free wells with 1x alamarBlue were included in every experiment for subtraction of background fluorescence.

2.2.2. Sulforhodamine B biomass assay

The SRB biomass assay was performed according to the protocol of Vichai and Kirtikara (2006) with addition of 10 mM Tris base (pH 10.5) for dye solubilisation; quantification was carried out using a Pherastar FS platereader (BMG) reading absorbance at 510 nm. For microscopy, cells were imaged prior to solubilisation of the dye.

2.2.3. Click-iT EdU proliferation assay

For detection for cell proliferation, progression through S phase was determined using Click-iT EdU analysis according to manufacturer's instructions (Invitrogen, C10337). Following seeding and/or treatment (2.1.3) cells were incubated with 10 μM EdU for 18 hours for continuous label incorporation of EdU into replicating DNA. Cells were then fixed in 3.7% formaldehyde in PBS (v/v, both Sigma), washed twice in 3% BSA in PBS (weight for volume, w/v Sigma, PBS-BSA) and permeabilized in 0.5% Triton X-100 in PBS (v/v) for 20 minutes, followed by two more washes in PBS-BSA. Cells were then incubated with freshly made Click-iT reaction cocktail (reaction buffer, $CuSO_4$, AlexaFluor azide and buffer additive) according to manufacturer's instructions (30 minutes, RT, in the dark) and washed in PBS-BSA. DNA was then counter-stained using Hoechst 33342 in PBS (2 μg/ml, 30 minutes, in the dark, RT) before imaging analysis (2.7.2).

2.2.4. Fluor de Lys® HDAC assay

For analysis of cellular deacetylase activity, the Fluor de Lys HDAC fluorometric cellular activity assay kit was used according to manufacturer's instructions (Enzo, BML-AK503). In brief, cells were seeded into 96-well plates and left to bed down before incubation with 50 μl complete media supplemented with 200 μM Fluor de Lys substrate with treatment or mock control (2 hours, 37°C). For assay termination, the supplied developer concentrate was diluted in cold cell lysis buffer (also supplied, to 1x) with the HDAC inhibitor TSA at 2 μM, and 50 μl of this solution was added per well and mixed by pipetting. A 'time zero' control sample was included where 50 μl complete media with 200 μM substrate was added to an

empty well with 50 µl lysis solution at the time of cell lysis, for subtraction of background substrate fluorescence. Plates were incubated at 37°C for 15 minutes following lysis and fluorescence readings were taken using a Pherastar FS platereader (BMG, Ex.360 nm, Em.460 nm).

2.2.5. Autophagy (CYTO-ID)

For detection of autophagy, the CYTO-ID kit (ENZ-51031) was used according to manufacturer's instructions (Enzo). In brief, cells were seeded into 96-well plates, left to bed down and treated (2.1.3). Cells were then washed twice with 1X Assay Buffer (supplied) containing 5% FBS (v/v). Cells were then incubated with 100 µl/well Dual Detection Reagent (2 µl CYTO-ID Green Detection Reagent and 1 µl Hoechst 33342 per 1 ml 1X Assay Buffer with 5% FBS) for 30 minutes at 37°C, then re-washed with 1X Assay Buffer with 5% FBS, before fluorescence imaging (2.7.2) in fresh complete media. Positive (rapamycin) and negative (DMSO) controls were included in all experiments. For validation of autophagic flux, cells were sequentially treated with bafilomycin A1, an inhibitor of autophagosome-lysosome fusion (Table 2.2).

2.2.6. Cell cycle stage determination (Cell Cycle Clock)

For cell cycle stage determination, cells were seeded and treated in 24-well plates and then harvested by trypsinization with TrypleExpress and quenched with complete media. Cells were then pelleted in a minifuge (30s, 6kRPM (equivalent to ~4000xg)), before resuspension of the pellet in 1:3 Cell Cycle Clock™ Reagent (v/v, Biocolor) in complete media, and incubation for 15 minutes (RT). The suspension was then re-pelleted, resuspended in 250 µl complete media, placed into wells of a fresh 12-well plate then imaged immediately using a digital EVOS microscope with brightfield and illumination. The photomicrographs were analysed by FIJI thresholding according to manufacturer's instructions (Biocolor). Assays

were only conducted on sub-confluent cells to avoid confounding effects of cell cycle exit due to contact inhibition inducing quiescence.

2.3. IL-6 detection

IL-6 secretion was detected by two independent assays using samples of 24-hour conditioned media (CM). For CM collection, cells were grown in multi-well plates and media changed 24 hours prior to the end of the experiment duration; this media was termed 24 hour CM.

2.3.1. IL-6 ELISA

0.5-1.0 ml samples of CM were snap-frozen in pre-chilled eppendorfs on dry-ice and kept at -80^{o}C before testing for IL-6 concentration by ELISA according to manufacturer's instructions (Human IL-6 Quantikine ELISA, R&D systems), with a standard curve generated for every experiment using purified recombinant IL-6, and absorbance (A450 - A540) read using a BMG Pherastar platereader. Data were normalized according to cell number as determined by direct cell counting, to calculate amount of IL-6 secreted per cell.

2.3.2. HEK-BLUE IL6 reporter cell assay

IL-6 detection using a reporter cell line was performed according to Rolt et al (2019). In brief, HEK-BLUE IL-6 cells were seeded into 384-well plates, and incubated with a sample of 24 hour CM, or a dilution range of recombinant IL-6 (for standard curve generation) for 24 hours. Secretion of SEAP (in response to IL-6 in CM) was assessed by incubation of HEK-CM with QuantiBlue (InvivoGen) in a fresh 384-well plate for 1-4 hours before absorbance was read using a BMG Pherastar platereader.

2.4. Western blotting

Western blotting analysis was performed as in Walters and Cox (2019). In brief, cells grown in T25 flasks were harvested by trypsinization (2.1.1), pelleted in a microfuge (6 kRPM/4000xg, 1 minute) then washed in 1 ml PBS, re-centrifuged and the buffer aspirated. The resulting pellet was resuspended in 30 µl RIPA (radioimmunoprecipitation assay) buffer (Thermo Scientific) supplemented with 1:100 (v/v) protease/phosphatase inhibitor cocktail (Cell Signalling). Lysates containing equal numbers of cells were then heated for 5 minutes (95^{o}C) in 1X NuPAGE LDS buffer (Novagen) containing 100 mM diothiothreitol and benzonase nuclease (Sigma Aldrich, 1:200 v/v) then proteins were separated on 10% Bis-Tris NuPage gels (Invitrogen). Transfer to nitrocellulose was performed using a BioRad Trans-Blot Turbo system (7 minutes, 1.3A, 17V). Blots were blocked in 5% BSA (w/v) in PBS-T (PBS with 0.1% Tween v/v, PBS-T-BSA) for $\geq$ 1 hour, washed twice in PBS, then probed with primary antibody in PBS-T-BSA ($\geq$ 1 hour, RT). Following five washes (two minutes per wash) in PBS-T, blots were probed with HRP-conjugated secondary antibodies in PBS-T-BSA ($\geq$1 hour, RT). Subsequently, blots were washed four times in PBS-T then once in PBS. The EZ-ECL kit (Biological Industries) was used according to manufacturer's instructions with Hyperfilm MP X-ray film (Amersham) and Xograph compact X4 automatic processor (Xograph, UK). Antibodies used are listed in Table 2.3. For statistical analysis, signal intensity (quantified by FIJI) was normalized against a loading control and compared between $\geq$3 biological replicates.

2.5. Telomere analysis

2.5.1. Southern blotting (TeloTAGGG)

Pellets of >1x10^{6} cells were harvested according to 2.1.1 and stored at -80^{o}C. Genomic DNA (gDNA) was then extracted using PureLink gDNA extraction kit (Qiagen) according to

manufacturer's instructions and quantified (A2680/280, Nanodrop^{1000} spectrophotometer). gDNA integrity was assessed by gel electrophoresis for quality control (10 ng DNA resolved as a high molecular weight band (i.e. no degradation) on a 1% (w/v) agarose gel; 200V, 60 minutes). 1 μg gDNA was then digested by incubation with restriction enzymes Hinf I and Rsa I (2 hours, 37^{o}C, both Sigma Aldrich) and used to perform the TeloTAGGG assay according to manufacturer's instructions (12209136001, Sigma Aldrich). In brief, digestion reactions were terminated by addition of gel electrophoresis loading buffer, and digests were run on a 0.8% Hi-Res agarose gel at 5 V/cm (1X TAE, 4 hours). DIG molecular weight markers were run to enable telomere restriction fragment (TRF) length measurement, and control DNA (from an immortalized cell line) was run on each gel. Following electrophoresis, the gel was treated with HCl (0.25M, 5-10 minutes, RT), denaturation solution (0.5M NaOH, 1.5M NaCl; 2x15 minutes, RT) and then neutralization solution (0.5M Tris-HCl, 3M NaCl pH 7.5; 2x15 minutes, RT). The digested DNA was then transferred onto a positively charged nylon membrane (Sigma Aldrich) by capillary Southern transfer (overnight, RT) using 20XSSC (3 M NaCl, 0.3 M sodium citrate, pH 7.0) as a transfer buffer. After transfer, DNA was fixed onto the membrane by UV crosslinking (Stratalinker, auto-crosslink programme), then washed (2x5 minutes, 2XSSC) and incubated with pre-hybridization solution (DIG Easy Hybridization solution (1 hour, 42^{o}C) with gentle agitation. The membrane was then incubated with hybridization solution containing diluted telomere probe and DIG Hybridization solution (1 μl probe per 5 ml solution, 3 hours, 42^{o}C, gentle agitation). The membrane was then thoroughly washed and blocked as directed, and TRFs were detected using detection buffer (supplied), with luminescence assessed by exposure to X-ray film as in 2.4. Average TRF length was calculated by densitometry analysis using FIJI according to manufacturer's instructions against supplied size markers run on each gel.

2.5.2. TeloFISH

TeloFISH was performed essentially according to Rossiello et al (2013). In brief, cells were seeded onto poly-L-lysine-coated glass coverslips (13 mm, Corning) in 24-well plates. Following bedding down, cells were exposed to treatment or mock control, then washed in PBS and fixed in 3.7% formaldehyde (Sigma) in PBS, re-washed three times in PBS and permeabilized in 0.2% Triton X-100 in PBS for 10 minutes, then re-washed three times in PBS. Coverslips were then incubated with 10 mM glycine in molecular biology grade H_2O (30 mins RT), washed three times in PBS, then incubated on glass slides maintained at 80^oC on a hot block for 5 minutes, on a 20 μl drop of hybridization mixture (70% formamide, blocking reagent, 10 mM Tris-HCl pH 7.4 and 0.5 μM telomeric and centromeric probes), followed by incubation in a humidified chamber (2 hours, RT). The centromere and telomere FISH PNA probes used were TAMRA-labelled C-rich telomere probe (PN-TC030-005) and FAM-labelled centromere probe (PN-CN001-005, both Eurogentec). The coverslips were then washed thoroughly in PBS and mounted in anti-fade mounting media with Hoechst 33342 (Vector Labs) and sealed around the edges using colourless nail varnish. Cells were then analysed by fluorescence microscopy immediately (2.7.2). The area positive for telomere foci within each nucleus was quantified by FIJI and normalized by the area of each nucleus.

2.6. Cell staining

2.6.1. Immunofluorescence

Cells were fixed in 3.7% formaldehyde (10 minutes, RT), washed in PBS, blocked in 5% donkey serum (Dako) in PBS and incubated with primary antibody diluted in PBS containing 0.3% Triton X-100 v/v and 1% BSA, w/v, at 4 °C overnight in a humidified chamber. Cells were then washed twice in PBS and incubated with secondary antibody (1-2 hours, RT in the dark, dilution buffer as for primary antibody). Cells were washed twice in PBS and DNA

counter-stained as detailed in section 2.6.7 before imaging. Antibodies used and dilutions are indicated in Table 2.3.

2.6.2. Mitochondria

For live imaging, mitochondria were labelled by incubation with Mitotracker Green FM or Mitotracker Red (1:1000 v/v dilution of 1 mM stock) according to manufacturer's instructions (Invitrogen Molecular Probes), for 30 minutes in complete media, at 37°C in the dark. Media was replaced before imaging. Alternatively, mitochondria were fluorescently labelled using a GFP-BacMam for mitochondria (GFP expressed fused to the leader sequence of E1 α pyruvate dehydrogenase) according to manufacturer's instructions; reagent was incubated with cells overnight, with concentration determined according to cell number as detailed in manufacturer's protocol (CellLight, Invitrogen). For analysis of fixed samples, mitochondria were stained by immunofluorescence (against TFAM; 2.6.1).

2.6.3. Lysosomes

For live lysosomal staining, cells were incubated in complete media containing 50 nM Lysotracker Red for 30 minutes at 37°C in the dark (Invitrogen Molecular Probes). Media was replaced with fresh complete media prior to live fluorescence microscopy analysis (see 2.7.2). For SA-β-gal staining, a commercial SA-β-gal kit was used (Cell Signalling, 9860); in brief, cells were fixed, washed and then incubated overnight with staining solution (all reagents supplied) at pH 6.0 containing the X-gal substrate for chromogenic detection of β-galactosidase activity. Cells were imaged after 16 hours incubation in PBS at 37°C in a non-humified incubator on a digital EVOS microscope.

2.6.4. Actin

For actin staining, cells were washed in PBS then fixed in 3.7.% formaldehyde in PBS (v/v, 10 minutes RT) before washing in PBS and permeabilization (0.1% Triton-X100 in PBS v/v, 10 minutes RT). For filamentous actin staining, cells were incubated for 40 minutes with

rhodamine- or FITC-phalloidin (6.6 nM in PBS), and for globular actin staining, cells were incubated for 20 minutes in DNaseI-AlexaFluor594 (300 nM in PBS, Molecular Probes, Thermo Fisher). Cells were then washed in PBS and imaged (2.7.2).

2.6.5. Tubulin

For live tubulin staining, cells were incubated with Tubulin Tracker Green diluted in complete media according to manufacturer's instructions (30 minutes, 37^{o}C, Thermo Fisher), media was replaced, and cells were imaged live.

2.6.6. Plasma membrane

Plasma membranes were labelled by incubating cells with 1:250 wheat germ agglutinin (WGA, v/v) conjugated with the fluorophores FITC or rhodamine (Vector Labs), either live in complete media or after 3.7% formaldehyde fixation in PBS (without permeabilization). Live cells were imaged immediately in fresh media after staining due to the toxicity of WGA.

2.6.7. DNA

DNA was stained using NucBlue Live (Hoechst 33342) according to manufacturer's instructions (20 minutes, 1 drop/ml, RT, Thermo Fisher) or using Hoechst 33342 within mounting dye (VECTACHSIELD, Vector Labs) for fixed cells, with 1 drop of mounting medium used for coverslip mounting as in 2.5.2. Images of nuclei stained with NucBlue Live and obtained by fluorescence microscopy (BioRad ZOE cell imager) were processed using thresholding in FIJI to select nuclei, with nuclear numbers and areas calculated and normalized according to the ZOE-generated scale bar. Cells with cytoplasmic chromatin fragments (CCFs) were manually counted from representative images; at least 50 cells were examined per replicate and data was expressed as % cells harbouring CCFs.

2.6.8. ROS

Cellular ROS was visualized by incubating PBS-washed cells live with Mitotracker CMX ROS (Thermo Fisher) according to manufacturer's instructions or by incubating with DCFDA (20 µM in PBS, Sigma, both incubated for 30 minutes in the dark at 37^{o}C). Cells were then re-

washed and imaged live in fresh complete media. A positive H_2O_2-treated control (to induce ROS, 20 μM, 1 hour) was included in each experiment.

	Target protein	Species raised in	Dilution	Supplier
Western blotting				
Primary antibodies	p21	Rabbit	1:1000	Abcam Ab109199
	γ-tubulin	Rabbit	1:1000	Sigma-Aldrich T5192
	Phospho 4E-BP1	Rabbit	1:1000	Cell Signalling 236B4
	TFAM	Mouse	1:1000	Abnova B01P
	GAPDH	Mouse	1:1000	Sigma-Aldrich G8795
Secondary antibodies	α-rabbit HRP-conjugated IgG	Goat	1:1000	Dako P0448
	α-mouse HRP-conjugated IgG	Goat	1:1000	Dako P0447
Immunofluorescence				
Primary antibodies	p21	Rabbit	1:200	Abcam Ab109199
	γH2AX	Rabbit	1:200	Cell Signalling 20E3
	TOM20	Mouse	1:200	Santa Cruz sc-6341
	LC3	Rabbit	1:500	MBL PM036
	TFAM	Mouse	1:200	Abnova B01P
Secondary antibodies	α-rabbit IgG AlexaFluor 488	Donkey	1:500	Invitrogen A-21206
	α-mouse IgG AlexaFluor 488	Donkey	1:500	Invitrogen A-21202
	α-rabbit IgG AlexaFluor 488	Goat	1:500	Invitrogen A-11008
	α-mouse IgG AlexaFluor 546	Goat	1:200	Invitrogen A-11003

Table 2.3: antibodies used in Western blotting and immunofluorescence

2.7. Microscopy

All microscopy images shown in this thesis are labelled with a 100 μm scale bar. Fluorescence images where red and green channels have both been used in image acquisition have been artificially re-coloured using FIJI (red – magenta).

2.7.1. Phase contrast microscopy

Phase contrast microscopy was performed using a digital EVOS AMG microscope (Thermo Fisher), with scale bars added to images using a graticule. Phase contrast microscopy was used for routine assessment of cells to determine % confluence before subculturing, as well as for morphological analysis, SRB analysis and SA-β-gal image acquisition (all images in this thesis taken using a 20X lens).

2.7.2. Fluorescence microscopy

Fluorescence microscopy was performed using a ZOE fluorescent cell imager (BioRad), with scale bars added automatically. For time-lapse imaging, the field of view was locked and images taken at specified intervals (see figure legends) according to a stopwatch.

2.7.3. High-content imaging

High content imaging was performed in collaboration with E. Dombi and Prof. J. Poulton (NDWRH, University of Oxford) according to Diot et al (2015), using an INCELL 1000 analyser to quantify mitochondrial co-localization with LC3-II positive autophagosomes. Antibodies used and staining conditions are listed in Table 2.3.

2.8. Quantitative comparative proteomics

Quantitative comparative proteomics was performed in collaboration with the Advanced Proteomics Facility (Department of Biochemistry, University of Oxford - Prof. S. Mohammed and Mrs S. Hester). In brief, T25 flasks of cells at the specified CPD were treated for 7 days with DMSO (vehicle control) or 70 nM AZD8055. Cells were harvested according to standard protocols (2.1.1), counted and then collected by brief centrifugation (30 s, minifuge at 6kRPM/4000xg). The cell pellet was washed in PBS and re-pelleted before lysis in RIPA buffer with 1:100 protease/phosphatase inhibitor cocktail (v/v). Samples were then prepared by the proteomics facility by Trypsin FASP digest for label-free Orbitrap LC-MS/MS. Protein

identification and label-free quantitation (LFQ) was performed using Mascot software according to default parameters. LFQ intensities were imported into Perseus (Tyanova and Cox, 2018); proteins identified only by site, reverse and contaminants were removed, then expression values were transformed (log_2). To compare expression of proteins between samples, t-tests were performed with a p-value threshold of <0.01 (used for Volcano plot generation). IPA™ software (Qiagen) was used for pathway analysis and gene ontology (GO) analysis (PANTHER) and Metascape online tools were also used for data interpretation (Mi et al., 2019, Consortium, 2019, Ashburner et al., 2000).

2.9. Statistical analysis

The GraphPad prism statistical analysis package was used to perform statistical tests and to interpolate data from standard curves. For comparative analysis between two populations, unpaired two-tailed Student's t-tests were performed. For comparisons between >2 samples, ANOVAs (analysis of variance) were performed with Tukey tests to compare the means of each sample. All graphs show mean values with standard deviations (as error bars), calculated from $n \geq 3$ independent experiments or from technical triplicates from representative experiments of $n \geq 3$ unless otherwise stated.

3. Generation of a novel model of primary human cell senescence through Tenovin-6 mediated inhibition of sirtuins

3.1. Introduction

Cellular senescence is an essentially irreversible proliferation arrest mechanism induced by various stress signals, such as telomere attrition or oncogene activation (section 1.3.1), and is causally linked to ageing and the development of age-related diseases (section 1.3.6, Table 1.1, Baker et al., 2016, Xu et al., 2016). While a multitude of signalling pathways can induce senescence, p53 is often a crucial mediator, driving upregulation of $p21^{CDNK1A}$ to induce proliferation arrest upon detection of stress (Muñoz-Espín and Serrano, 2014). By contrast, proteins of the evolutionarily conserved sirtuin family of histone and protein deacetylases have been reported to inhibit senescence (Hayakawa et al., 2015). First discovered in *S. cerevisiae*, the budding yeast Sir2 was shown to act as a histone deacetylase (HDAC), promoting tighter chromatin packing and reduced transcription at target loci including telomeric sequences, HM (mating type) loci and the rDNA locus RDN1 (Aparicio et al., 1991, Fritze et al., 1997). Importantly, suppression of histone acetylation (H4K16) around telomeres was shown to affect lifespan in yeast, linking histone modifications through Sir2 to ageing (Dang et al., 2009).

Overexpression of Sir2 has been shown to increase lifespan in yeast by 50% (Kaeberlein et al., 1999), possibly through inhibition of rDNA circle formation which may drive yeast replicative ageing (Sinclair and Guarente, 1997), or by mimicking the effects of caloric restriction (Chen and Guarente, 2007). Consistent with an anti-ageing effect of Sir2, deletion in yeast causes a lifespan reduction (Kaeberlein et al., 1999). Mice overexpressing SIRT1 in the brain have extended lifespan (Satoh et al., 2013), and small molecule SIRT1 activators SRT2104 and SRT1720 also extend lifespan in mice (Mercken et al., 2014, Mitchell et al., 2014). The phytoalexin resveratrol is a purported activator of SIRT1 and may also enhance the binding of SIRT1 to its activator lamin A (Liu et al., 2012), a protein closely tied to lifespan regulation since a splice site LMNA mutation results in Hutchinson-Gilford progeria

(Eriksson et al., 2003, section 1.3.3.5). However, no positive effect on longevity was detected on resveratrol feeding to mice in the highly powered multi-site Interventions Testing Program (Miller et al., 2011).

Seven mammalian sirtuins have now been identified, all of which share a highly conserved NAD^+ binding domain together with a catalytic domain, but they vary by intracellular localization and function (Dang, 2014). Sirtuins provide a direct link between cellular metabolism and protein post-translational modifications due to their requirement for NAD^+ for deacetylation, with the NAD^+/NADH ratio determined by the nutritional state of the cell (Dang, 2014). Of the mammalian sirtuins, SIRT1 has been the most extensively studied, acting mainly in the nucleus and deacetylating known longevity-associated targets including WRN, p53, mTORC1, NFκB, FOXO1,3,4, and PGC1α, as well as several histones (Dang, 2014); several of these known targets such as p53, mTORC1 and NFκB are crucial regulators of senescence (sections 1.3.2, 1.4 and 1.3.3.3.1 respectively). mTORC drives geroconversion and hypertrophy in senescence (Chapters 4 and 5, Leontieva and Blagosklonny, 2016) while both mTORC and NFκB regulate the pro-inflammatory SASP of senescent cells (Herranz et al., 2015, Laberge et al., 2015), whereby cytokines, chemokines and matrix-remodelling enzymes are secreted with pleiotropic and pro-tumorigenic consequences (Rodier et al., 2009). Consistent with possible regulation by sirtuins, the SASP has been shown to be suppressed on resveratrol treatment (Pitozzi et al., 2013).

SIRT2 is mainly cytoplasmic and deacetylates some targets shared with SIRT1 (e.g. FOXO1&3, PCG1α), as well as tubulin, PAR-3 and Cdc20 (Dang, 2014). Sirtuins are clinically important as they have been reported to play a role in retaining pluripotency of stem cells by interfering with differentiation; for example, knockdown or chemical inhibition of SIRT1 promotes neurogenesis from neural stem cells (Kim et al., 2016). In addition, sirtuin overexpression has also been linked to a number of different cancer types from leukaemia and lymphoma to

solid tumours including prostate, hepatocellular and colorectal cancer (Choi et al., 2013). Therefore, strategies to boost healthy ageing by activating sirtuins through NAD supplementation must be cautious to avoid promoting cancer progression.

Various small molecule inhibitors of sirtuins have been developed, predominantly to address the effect of sirtuin overexpression in cancer (Choi et al., 2013). Of these, tenovin-6 (TnV6), a drug initially developed in a forward chemical genetics screen to find activators of p53 was shown to be an inhibitor of SIRT1/2 by haploinsufficiency profiling in yeast (Lain et al., 2008) and by fluorescence and NMR-based assays (Pirrie et al., 2012). TnV6 showed anti-tumour effects in gastric cancer cells *in vitro* (Hirai et al., 2014) and in chronic myeloid leukaemia (CML) mouse models (Yuan et al., 2012), without apparent genotoxicity. Interestingly, TnV6 is reported to induce p21 expression, through a mechanism that requires SIRT2 but is independent of p53 (McCarthy et al., 2013); this induction of p21 may account for the proliferation arrest induced by TnV6 in cancer cells (van Leeuwen et al., 2012) accompanied by only low levels of apoptosis (Sunami et al., 2013).

Obtaining large numbers of replicatively senescent cells is experimentally laborious, while other models of senescence are also problematic: oncogene induced senescence (OIS) is an acute response to high levels of activated oncogene expression (usually Ras or BRAF), while senescence induced by DNA damaging agents such as etoposide or IR intrinsically incurs a high burden of DNA damage that will impact on gene expression patterns. However, experimentally manipulating a biologically relevant p21-dependent, non-genotoxic pathway as a means to obtaining large numbers of cells that have entered senescence may be highly experimentally useful both for biochemical analysis and potentially for screening of compounds that may modify senescent cell phenotypes.

3.2. Chapter aims

In this chapter, I set out to address the following questions:

1. Does Tenovin-6 treatment result in sirtuin inhibition in cells?
2. Is sirtuin inhibition toxic to primary and cancer cells in culture?
3. Does sirtuin inhibition through Tenovin-6 induce senescence in primary cells?
4. If so, what is the phenotypic basis of this senescence?

To address these questions, I used the SIRT1/2 inhibitor Tenovin-6 (TnV6) in human primary fibroblasts (HF043) and cancer cells (HeLa), with a range of assays to assess deacetylase activity *in vitro*, cell viability and phenotypes of senescence.

3.3. Results

3.3.1. TnV6 suppresses deacetylase activity

The drug TnV6 was originally described as an activator of p53 and developed for use as an anticancer agent; it was only subsequently found to act in a p53-independent manner as an inhibitor of SIRT1/2 (Lain et al., 2008). To verify this activity, I employed a commercial deacetylase activity assay (Fluor de Lys, Enzo), in which substrate deacetylation occurs within living cells, which is then assayed in cell lysates as the deacetylated substrate interacts with a developer to produce a quantifiable fluorescent signal (Figure 3.1A).

Proliferating primary human skin fibroblasts (HF043) and HeLa cells were incubated with TnV6 at 2 μM. Evolution of a fluorescent signal from TnV6-treated cells was compared with cells treated with resveratrol (RSV), an SIRT1 activator, vehicle only (DMSO) negative controls and cells treated with the HDAC inhibitor trichostatin A (TSA, NB sirtuins are insensitive to trichostatin A, Borra and Denu, 2003). Treatment with resveratrol led to

increased substrate deacetylation in this assay, which was especially notable in HeLa cells (Fig. 3.1B), while the non-specific HDAC inhibitor TSA only led to a small decrease in deacetylation in HF043 cells at the recommended dose (1 μM). However, I observed a complete ablation of deacetylation upon treatment of either primary HF043 fibroblasts or transformed HeLa epithelial cells with 2 μM TnV6, indicative of very strong inhibition of deacetylase activity. Hence, TnV6 acts as an inhibitor of deacetylation, presumably acting on HDACs; given its earlier identification as a SIRT1/2 inhibitor together with this data on inhibition of deacetylation, it is likely that TnV6 acts at least in part through inhibition of SIRT1/2 in human cells.

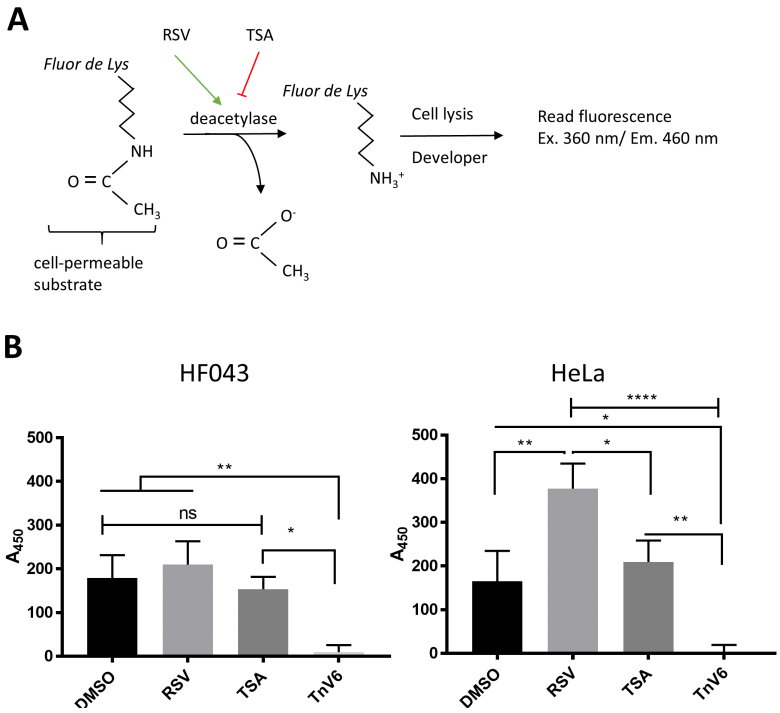


Figure 3.1 TnV6 strongly suppresses deacetylase activity in both primary and cancer cells

A: schematic depicting Fluor de Lys fluorometric cellular activity assay procedure, in which deacetylase activity is measured using the deacetylation of a Fluor de Lys substrate to generate a fluorescent product. B: transformed HeLa or primary HF043 cells were seeded in triplicate wells of 96-well plates, and subsequently treated with DMSO (vehicle control), resveratrol (RSV, 50 μM), trichostatin A (TSA, 1 μM) or TnV6 (2 μM). HF043 and HeLa experiments were performed on different days (n=2 independent experiments, each performed with technical triplicates, data from one representative experiment per cell line shown, one way ANOVA with Tukey test for multiple comparisons; **** $p<0.0001$, ** $p<0.01$, * $p<0.05$, ns not significant).

3.3.2. Low dose TnV6 treatment is cytostatic for primary cells and less toxic to cancer cells

TnV6 has been reported to halt tumour cell proliferation through inducing expression of the CKI p21 (Jin et al., 2015). To examine whether TnV6 also blocks primary cell proliferation, primary HF043 human fibroblasts at low CPD (<50) were treated with a range of concentrations of TnV6 from 100 nM to 5 μM; control cells were treated with the equivalent % of DMSO (≤0.05%). Cell viability was then examined by inspection of overall appearance, and by two independent assays: (i) alamarBlue (resazurin) reduction, and (ii) sulforhodamine B staining to quantify cellular biomass (Vichai and Kirtikara, 2006). A strong cytotoxic effect of 5 μM TnV6 was observed for primary HF043 skin fibroblasts within only 24 hours treatment; cells became detached from the substrate, rounding up and losing viability (Fig. 3.2A). Longer treatment for 72 hours was highly toxic as shown by both alamarBlue and SRB measurement (Fig. 3.2 B, C). Cell numbers observed microscopically after 24 hours treatment with 2 μM TnV6 were decreased compared with controls (Fig. 3.2A), and treated cells did not exhibit the high mitotic index observed in control populations (Fig. 3.2A). Following 72 hours treatment with 2 μM TnV6, there was a reduction both in alamarBlue and SRB signals to ~60% of control values (Fig. 3.2 B, C). Combined with the microscopy findings (Fig. 3.2A), I hypothesized that this may reflect proliferation arrest rather than cell death during the treatment period.

To determine whether cancer cells were equally sensitive to TnV6, HeLa cells were treated with a concentration range of TnV6 for 72 hours before viability analysis by alamarBlue due to its superior sensitivity over SRB analysis (Fig. 3.2 D). I observed that a higher dose of TnV6 was required for complete cytotoxicity of HeLa cells compared with HF043 fibroblasts (10 vs. 5 μM TnV6) suggesting that primary fibroblasts may be highly sensitive to TnV6 treatment compared to cancer cells, though these effects could also be cell-type specific.

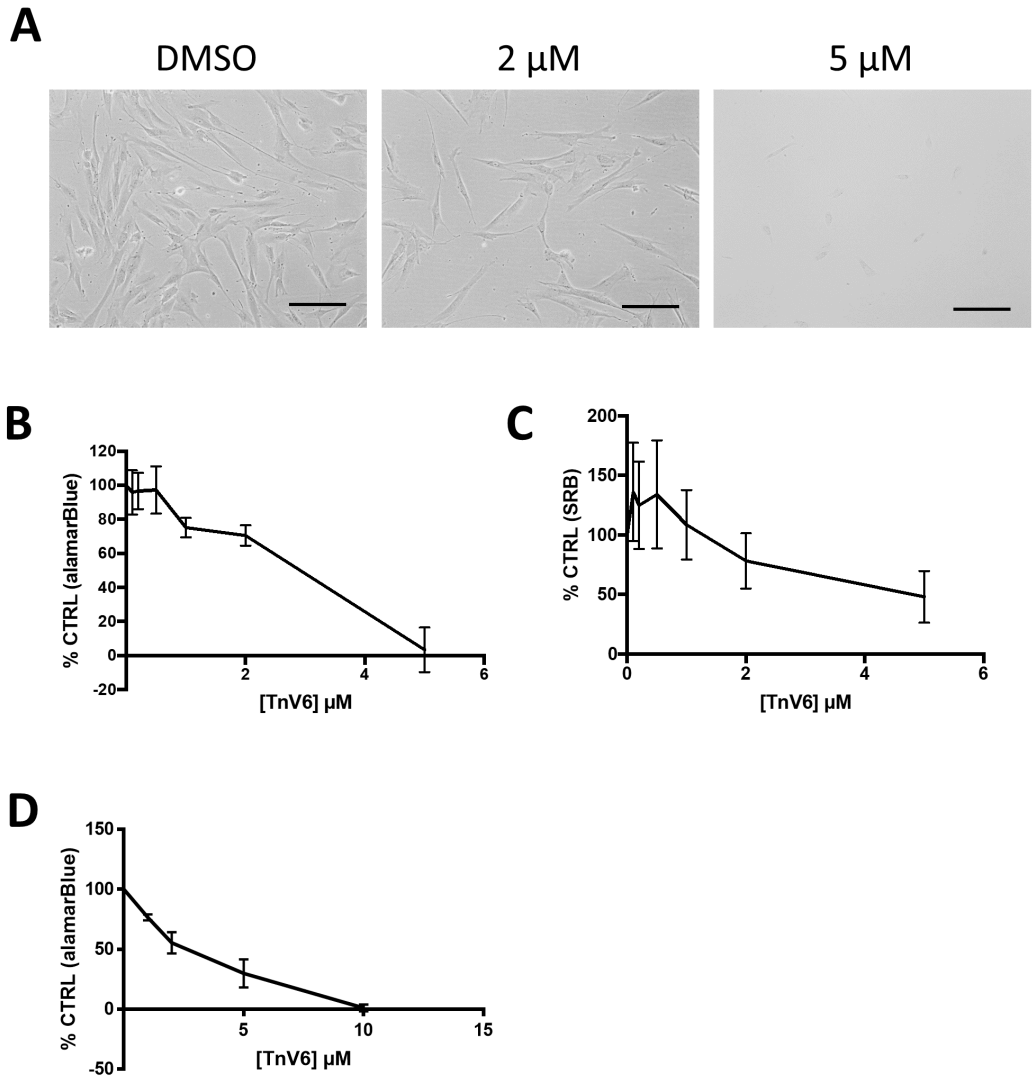


Figure 3.2 TnV6 exhibits dose-dependent toxicity in primary and transformed cells

A: Phase contrast microscopy images of HF043 fibroblasts (at low CPD <50) treated with DMSO, 2 µM or 5 µM Tnv6 for 24 hours (n>3 independent experiments, representative images shown). B: Analysis of reducing capacity, taken as a proxy for cell viability, using the alamarBlue vital dye, following treatment of HF043 fibroblasts with TnV6 concentrations ranging from 0.1 µM to 5 µM for 72 hours. C: Total cell biomass was measured by staining with sulforhodamine B (SRB) on cells treated as in (B). D: HeLa cells were treated with a range of concentrations of TnV6 for 72 hours before viability analysis using alamarBlue as in (C). (For B, C and D n=3, mean ± SD shown.) Scale bar 100 µm.

The possible cytostatic effect on low dose TnV6 in primary fibroblasts was further assessed by treating cells continuously for 7 days with 2 µM TnV6 (or DMSO control) then directly counting cell numbers. While control populations had proliferated at a rate of ~0.6 populations doublings/day, the number of cells harvested after 7 days TnV6 treatment was comparable to the number of cells seeded, again suggesting a cytostatic effect of TnV6 treatment at this dose (Figure 3.3A). These findings were also recapitulated in another primary human fibroblast cell line (HCA2, data not shown).

To determine whether the proliferative arrest induced by TnV6 treatment was permanent, HF043 cells were again treated for 7 days with 2 µM TnV6 (or DMSO control), before directly counting cell numbers. Cells were then re-seeded without TnV6 treatment and incubated for a further 7 days, before counting to determine the rate of proliferation within the incubation window. As shown in Figure 3.3B, the proliferation arrest induced by 7 day treatment with TnV6 was sustained even after treatment removal.

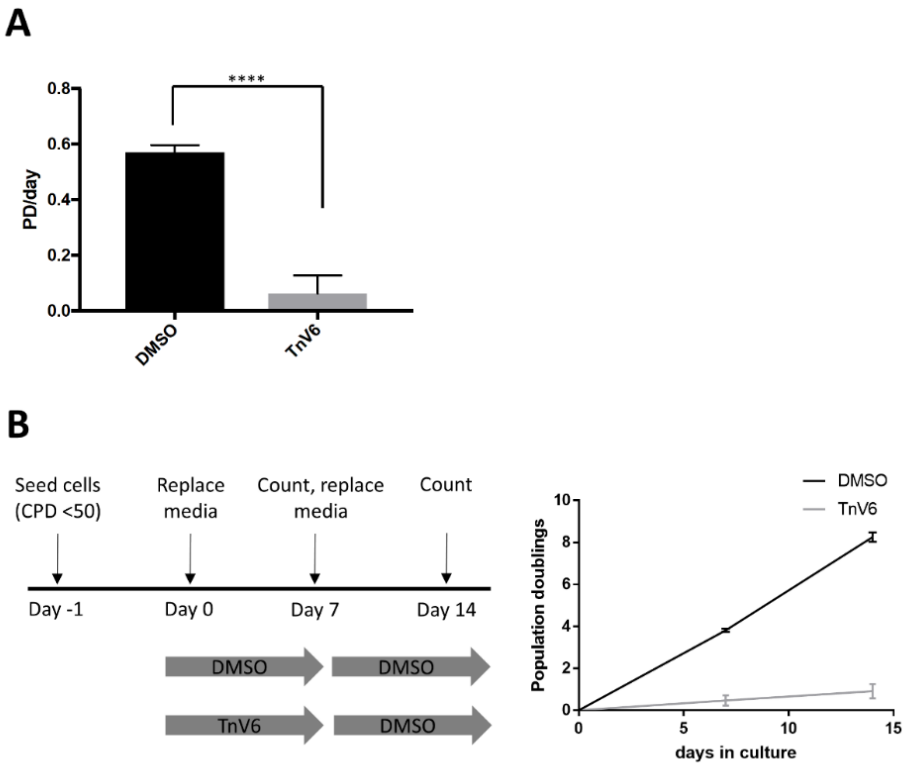


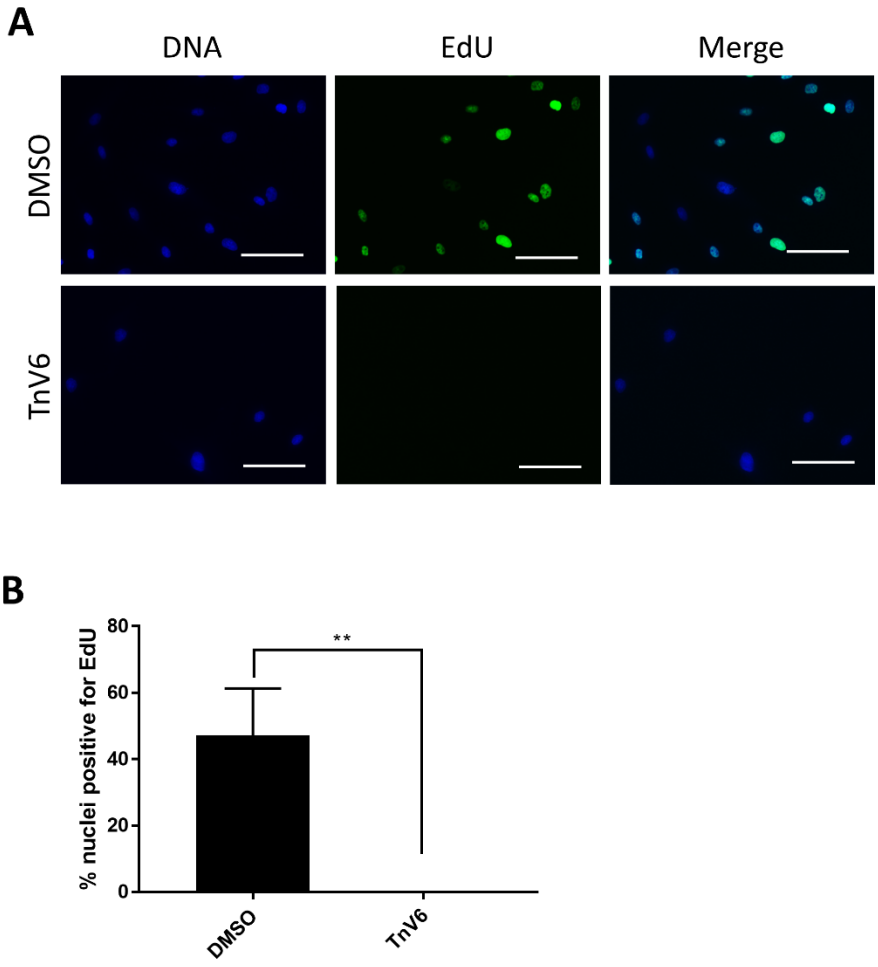
Figure 3.3 Low dose TnV6 induces sustained proliferation arrest in primary human fibroblasts

Proliferation rate measured as population doublings (PD) per day for HF043 fibroblasts cultured with either DMSO or 2 μM TnV6. A: PD per day was calculated after 7 days incubation using a Cellometer T4 (n= 3). 2-tailed unpaired t-test *** $p < 0.0002$. B: number of population doublings over a 14-day period was measured, as in (A) with control cells treated with DMSO throughout, and TnV6 cells treated with 2 μM TnV6 for the first 7 days, and DMSO for days 7–14 (n=3).

To further probe the possible cytostatic effect observed on 2 μM TnV6 treatment, I next assessed whether treatment was inhibiting cell cycle progression, using the nucleotide analogue EdU to label proliferating cells undergoing S phase. Following 72 hours treatment with 2 μM TnV6 (or DMSO control), cells were then incubated for 18 hours with 10 μM EdU, before fixation and staining for EdU incorporation. Nuclear EdU staining was detected in almost half of the control cells (Fig. 3.4, DMSO), consistent with their observed proliferation rates in routine sub-culture (Fig. 3.3A, ~0.6 PD/day for control fibroblasts). In stark contrast, none of the TnV6 treated cells showed any EdU incorporation (Fig. 3.4, TnV6), strongly suggesting that they had arrested in the cell division cycle without undergoing S phase (DNA synthesis).

Figure 3.4 Ablation of DNA replication in primary human fibroblasts on low dose TnV6 treatment

A, B: DNA replication was assessed in HF043 fibroblasts treated for 72 hours with either DMSO or 2 μM TnV6, before incubation with 10 μM EdU for 18 hours, fixation and staining using Click-IT chemistry for incorporated EdU. A: Cells were then imaged on a ZOE fluorescence imager with gain and contrast settings kept identical between wells and images. B: FIJI software was used for quantification. 2-tailed unpaired t-test used to compare means of technical triplicates (at least 50 cells analysed per well) from each of 3 independent experiments ** $p = 0.0043$. Scale bar 100 μm.



3.3.3. Primary cells arrest in G1 on TnV6 treatment

These data on cell proliferation (Figure 3.3) and DNA replication (Figure 3.4) strongly suggest that TnV6 treatment induced cell cycle arrest. I therefore assessed cell cycle phase distribution of fibroblasts treated with TnV6 (2 µM) or DMSO as control. Primary HF043 fibroblasts at low CPD were again incubated with 2 µM TnV6 (or DMSO) for 72 hours before cell cycle stage was assessed using the proprietary dye Cell Cycle Clock™ (Biocolor, Figure 3.5A for example staining). Approximately 48% of the control cells (DMSO) were found to be in G1 phase, with 37% in S, and 15% in G2/M (Fig. 3.5). By contrast, very few TnV6-treated cells were in either G2/M or S phase; instead the vast majority (91%) of cells were in G1, suggesting a G1 phase cell cycle arrest upon low dose TnV6 treatment.

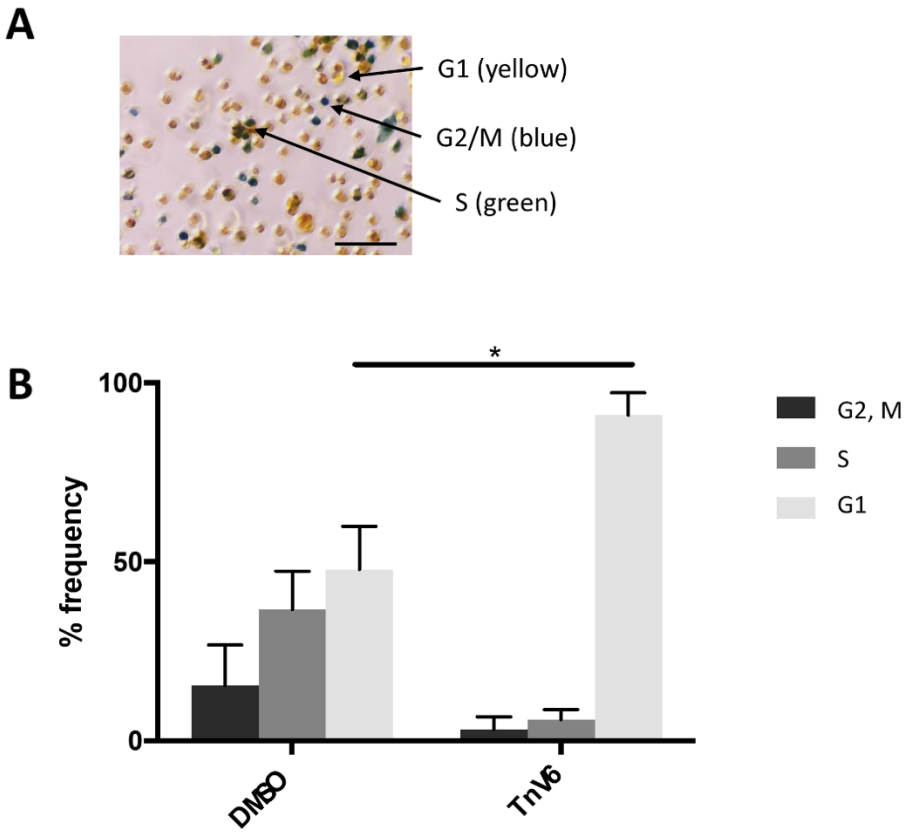


Figure 3.5 G1 phase arrest in primary human fibroblasts treated with TnV6

A, B: cell cycle stage was assessed in HF043 fibroblasts treated with DMSO or 2 µM Tnv6 in triplicate for 72 hours using the Cell Cycle Clock dye reagent. Images of stained cells (control image shown in A) were then analysed (B) by FIJI (n=3, 50 cells per well analysed, data from one representative experiment shown). * $p < 0.05$.

To determine the basis of this G1 arrest, I then probed treated cells for the presence of the cyclin kinase inhibitor p21. Cell lysates were probed by Western blotting for p21 (Figure 3.6A), and levels quantified by densitometry, with normalisation against the loading control γ-tubulin (Figure 3.6B). A marked increase in p21 was detected following 7-day exposure of cells to TnV6. Similarly, immunofluorescence of HF043 fibroblasts treated for 7 days showed strong nuclear staining for p21 after TnV6 treatment that was not detected in the vehicle-only controls (Figure 3.6C). Interestingly, I noted the presence of extra-nuclear DAPI-staining in a subset of TnV6-treated cells suggestive of cytoplasmic chromatin fragments (CCFs) that are characteristic of senescent cells (Ivanov et al., 2013).

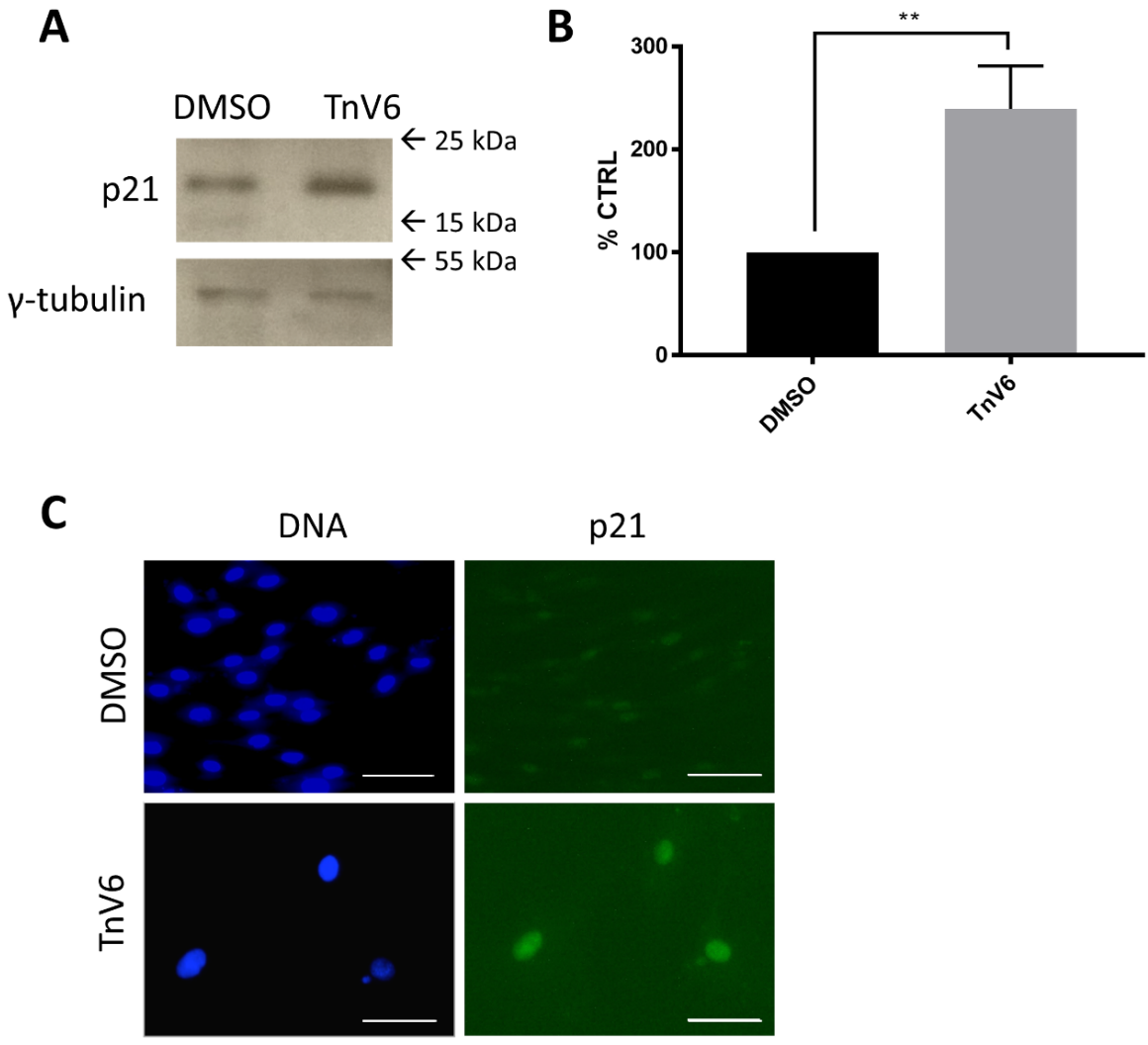


Figure 3.6 TnV6 induces p21 upregulation in primary human fibroblasts

A: Western blot of lysates of HF043 fibroblasts treated with either DMSO (control) or 2 µM TnV6 for 7 days, probed with anti-p21 antibody (upper panel) or anti- γ-tubulin antibody (lower panel). Marker sizes shown by arrows on right. B: bands on the blots were quantified by densitometry using FIJI software and then the p21 signal was normalised against the tubulin loading control (n=3, unpaired t-test; ** p=0.0044). C: immunofluorescence of HF043 fibroblasts treated with DMSO or 2 µM TnV6 for 7 days then probed with anti-p21 antibody and Alexafluor-488 secondary antibody, with DNA counterstained with NucBlue live (representative images shown from n=3 experiments).

3.3.4. Extended TnV6 treatment leads to increased cell size and senescent morphology in primary fibroblasts

Since elevated p21 together with lack of proliferation are features of both transiently arrested and senescent cells, I next assessed whether extended exposure to TnV6 would

lead to morphological changes associated with cell senescence. I treated cells continuously for 7 days with 2 μM TnV6 prior to analysis for phenotypes of senescence, since morphological changes on induction of senescence by experimental DNA damage or oncogene activation only fully manifest about 1 week after induction (data not shown). Phase contrast microscopy revealed that control cells (DMSO only) maintained classic fibroblast spindle morphology throughout the experiments, whereas TnV6-treated cells became dramatically enlarged and showed granular inclusions (Fig. 3.7A); these morphological differences were especially apparent after staining with SRB, with TnV6-treated cells also appearing flattened (Fig. 3.7B). To quantify this increase in cell size, I harvested the cells and measured their diameter in suspension, in order to overcome possible issues of flattening and spreading which indicate area only and may give an over-estimate of overall cell size/volume. I observed a statistically significant increase in cell diameter in suspension following TnV6 treatment. Further, consistent with the increased heterogeneity associated with biological ageing and senescence, there was greater variation in the cell size distribution compared with control cells (Fig. 3.7C).

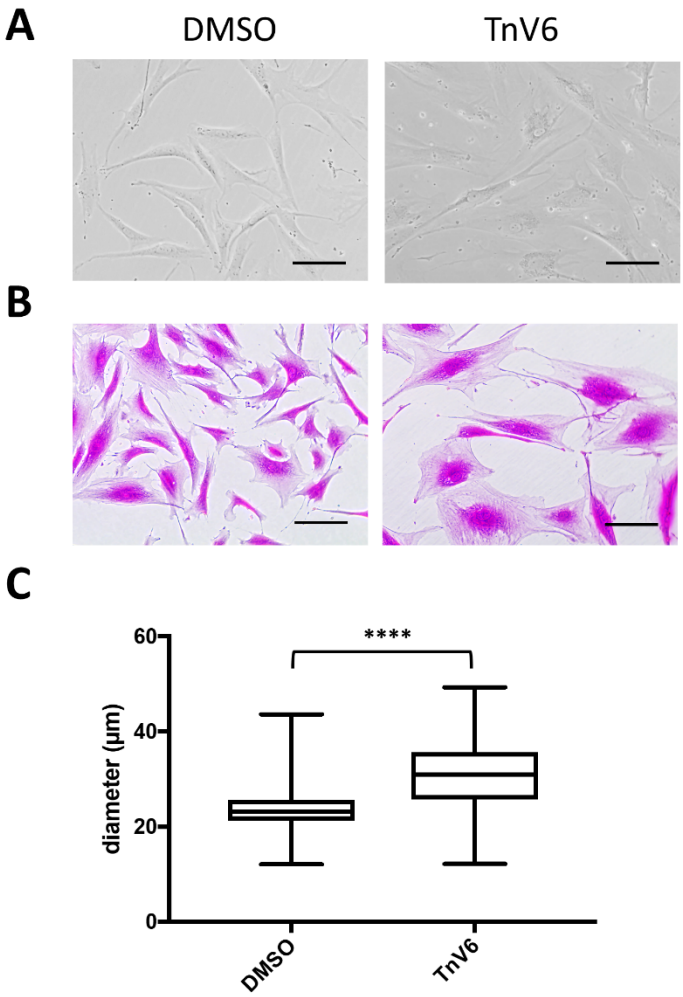


Figure 3.7 Extended TnV6 treatment induces senescent morphology

A: phase contrast microscopy of HF043 fibroblasts treated with DMSO or 2 µM TnV6 for 7 days (n>3). B: cells as in (A) were fixed and stained with sulforhodamine B then imaged using phase contrast microscopy (n>3). C: cell diameter was analysed for cells treated as above, with >30 cells counted per sample (n>3 biological replicates, results from one representative experiment shown). Box shows 25th and 75th percentiles with median line; bars show maximum and minimum, **** $p < 0.001$. Scale bar 100 µm.

3.3.5. Markers of cell senescence are elevated on TnV6 treatment

The observed increases in cell size and granularity, together with cell cycle arrest and p21 elevation were suggestive that TnV6 treatment might be driving cells into senescence. I next examined the lysosomal content of treated and untreated cells using Lysotracker Red (a pH-

dependent lysosomal fluorescent stain) alongside the canonical marker of senescence, lysosomal β-galactosidase activity at pH 6.0 (Dimri et al., 1995). I found that treated cells had dramatic increases in both SA-β-gal (Fig. 3.8A) and Lysotracker staining (Fig. 3.8B), compared to the controls (DMSO). These changes are indicative of lysosomal stress and induction of senescence.

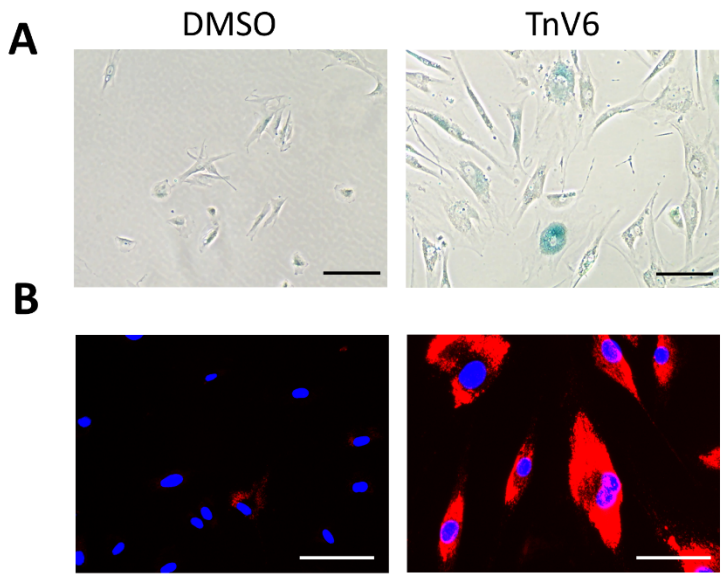


Figure 3.8 Extended TnV6 treatment induces senescence-associated lysosomal dysfunction

A: SA-β-gal staining of HF043 fibroblasts treated for 7 days with DMSO or 2 μM TnV6. B: Lysosomal analysis by Lysotracker Red staining of HF043 fibroblasts treated for 72 hours with DMSO or 2 μM TnV6; DNA was counterstained with NucBlue Live. Images were acquired in living cells on a ZOE fluorescence imager with gain and contrast settings constant throughout. Scale bar 100 μm.

Notably, I also observed a statistically significant increase in mean nuclear area from 200 μM^2 in control cells to 245 μM^2 which occurred within 72 hours TnV6 treatment (Fig. 3.9). Simplistically, this finding is consistent with chromatin decompaction, a likely consequence of TnV6 inhibition of sirtuin-mediated histone deacetylation, but is also consistent with nuclear enlargement upon induction of senescence. Since this nuclear enlargement occurs

within just 72 hours of treatment i.e. before the onset of other senescence-associated morphological changes, it is possible that a changing chromatin landscape may drive alterations in gene expression that result in senescence-specific changes.

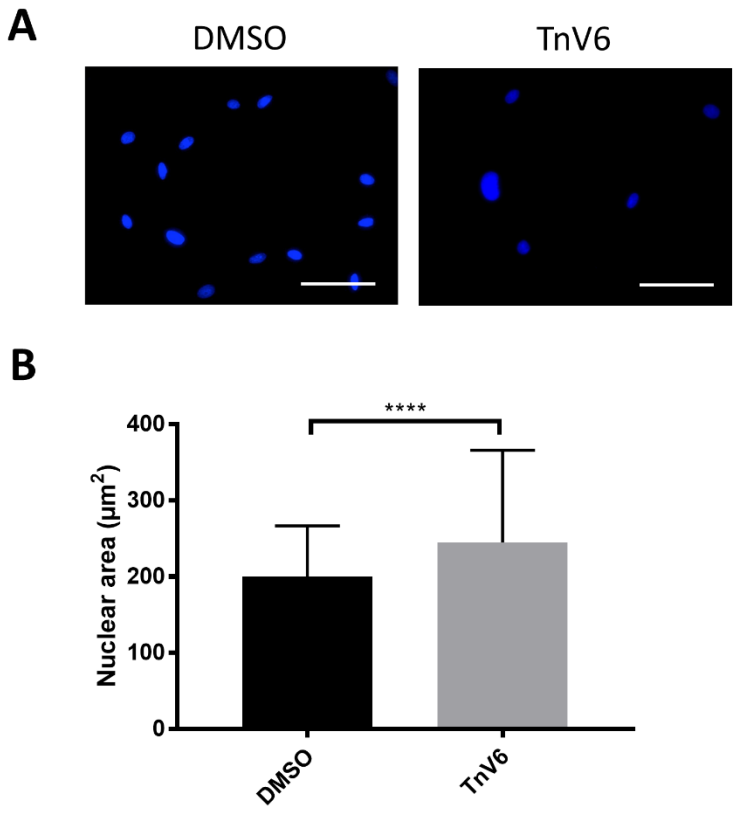


Figure 3.9 TnV6 treatment results in nuclear area increase

Nuclear area was analysed from fluorescence microscopy images (A) of cells treated for 72 hours with TnV6 at 2 μM (or DMSO control) stained with NucBlue Live and quantified (B) by FIJI (n>3, >50 nuclei counted per sample, data from one representative experiment shown, 2- tailed unpaired t-test **** $p < 0.001$). Scale bar 100 μm.

Cellular mitochondrial load is known to increase in senescence, either as a compensatory mechanism for increasingly inefficient mitochondrial activity, or playing a causative role in driving senescence (Correia-Melo et al., 2016). I therefore assessed mitochondrial load in treated and untreated living cells using Mitotracker Green. I observed a dramatically increased and highly reticular mitochondrial load following TnV6 treatment, compared to

control proliferating fibroblasts (DMSO alone) which exhibited a low mitochondrial load, with the majority of control cells showing a perinuclear distribution of mitochondria (Fig. 3.10A).

A further biomarker of senescence is the presence of filamentous actin stress fibres. I therefore used rhodamine-phalloidin to visualize cellular actin after prolonged exposure to TnV6. A marked increase in senescent-like actin stress fibres was observed in cells treated with TnV6 compared with vehicle-only control cells, which showed more diffuse actin patterns characteristic of proliferating cells (Fig. 3.10B).

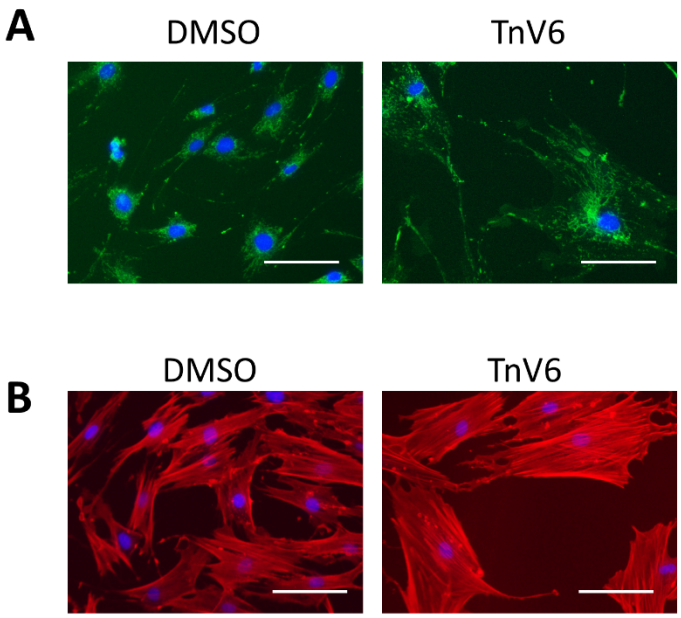


Figure 3.10 Extended TnV6 treatment results in mitochondrial accumulation and actin stress fibres

A: Mitochondrial staining of HF043 fibroblasts after 7 day treatment with DMSO or 2 µM TnV6 using Mitotracker Green and imaged live (n=3). B: Rhodamine-phalloidin staining for actin in HF043 fibroblasts fixed and stained after 7-day treatment with DMSO or 2 µM TnV6. DNA was counterstained with NucBlue Live (n=3). Scale bar 100 µm.

3.3.6. Extended TnV6 treatment induces SASP secretion from primary fibroblasts

Senescent cells secrete a broad profile of pro-inflammatory cytokines, chemokines, matrix-remodelling enzymes and growth factors (the SASP, section 1.3.3.3.1), which has pleiotropic signalling consequences; as well as alerting the immune system to the presence of senescent cells for clearance, the SASP can induce senescence in neighbouring cells, and have pro-tumorigenic signalling effects including promoting epithelial to mesenchymal transition (EMT, Laberge et al., 2012). The SASP may therefore underlie many of the deleterious effects of senescent cell accumulation *in vivo* (Baker et al., 2016; Xu et al., 2016). To test whether extended TnV6 treatment could induce SASP secretion, I chose to use IL-6 as a marker for the SASP, both because IL-6 is known to be a consistent and robustly secreted component of a highly heterogeneous SASP, and because IL-6 itself is implicated in pro-tumorigenic SASP signalling (Ortiz-Montero et al., 2017). Cells were treated with 2 μM TnV6 for 6 days, medium replaced (supplemented with TnV6) and after a further 24 hours, levels of IL-6 in 24 hour conditioned media (CM) taken from treated and control cells were measured by ELISA (Figure 3.11A). Results were quantified using a standard curve generated using purified recombinant human IL-6 protein (Figure 3.11B), and absolute values in terms of IL-6 secreted per cell were calculated by dividing interpolated IL-6 concentrations by total cell numbers, which were determined by performing direct cell counting after harvesting of conditioned medium (Fig. 3.11C). While little IL-6 was detectable in the medium of proliferating fibroblasts (DMSO controls), I observed a ~3.5-fold elevation in IL-6 secreted by cells treated for 1 week with low dose (2 μM) TnV6, indicative of significant upregulation of the SASP on TnV6 treatment (consistent with the levels of IL-6 upregulation observed upon replicative senescence in these fibroblasts, data not shown).

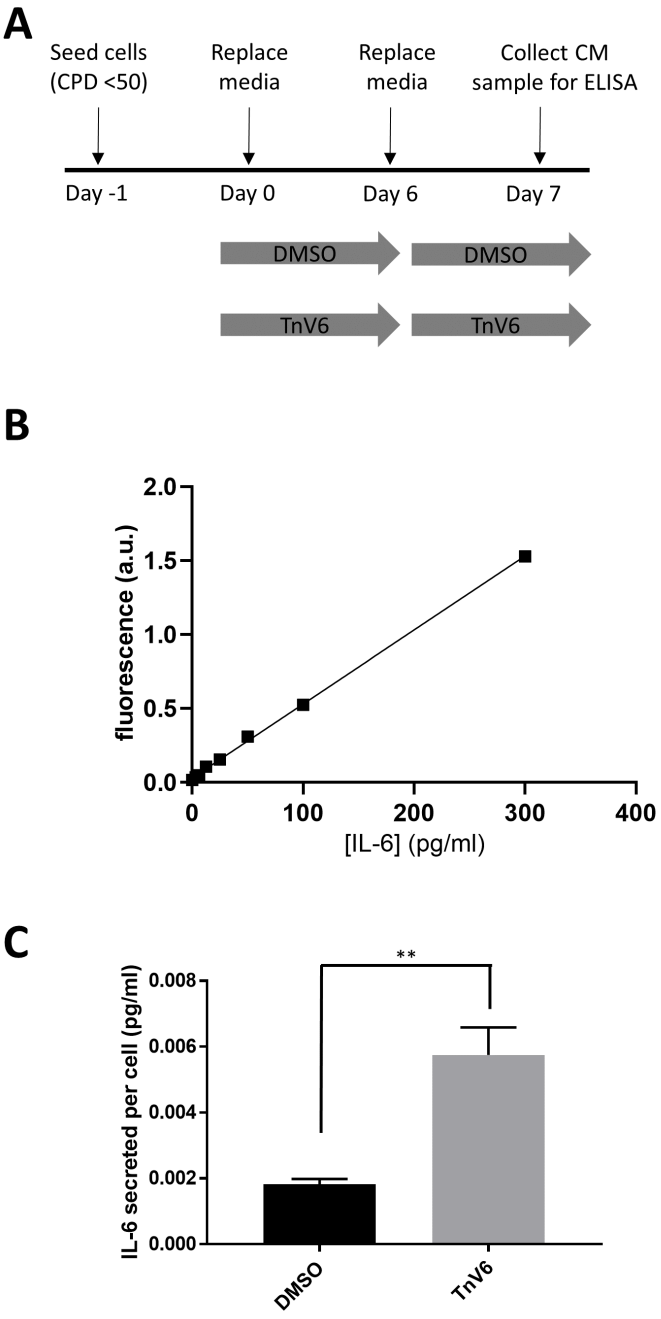


Figure 3.11 IL-6 is upregulated in TnV6-treated cells

A: schematic depicting experimental design, where ELISA was used to measure IL-6 secreted into 24-hour conditioned medium by HF043 fibroblasts treated with 2 µM TnV6 or DMSO for 7 days in total. B: recombinant human IL-6 was used to generate a standard curve for determination of IL-6 amounts. C: IL-6/cell (pg/ml) was calculated following cell counting. n=3, mean ± S.D. are shown, 2- tailed unpaired t-test p = 0.0059.

3.3.7. Unexpected DNA damage following TnV6 treatment of primary cells

TnV6 has been reported to have no genotoxic effects in transformed cancer cell lines (MacCallum et al., 2013). However, my data show that it induces senescence in primary fibroblasts including secretion of IL-6, a canonical marker of the SASP, together with senescence markers such as lysosomal dysfunction and increased mitochondrial load. While no mechanism is known for TnV6 to induce DNA damage directly, autocrine feedback loops that reinforce senescence are activated by SASP signalling upon senescence induction that can induce DNA damage through release of mitochondrial ROS (Passos et al., 2010), and senescent cells display a chronic DNA damage response (Fumagalli et al., 2014), which can both initiate and maintain the growth arrest. Alternatively, chromatin decompaction may lead to accumulation of DNA breaks, as shown for the HDAC inhibitor TSA in Werner syndrome cells (Turaga et al., 2007). I therefore examined levels of the DNA damage marker γH2AX by immunofluorescence in HF043 fibroblasts after 7 days exposure to TnV6. While only 20% of control cells showed γH2AX positive staining, which was of low intensity and not localised to specific subnuclear foci, the vast majority (~85%) of TnV6-treated cells were positive for γH2AX, with multiple foci per nucleus (Fig. 3.12). Hence treatment of primary cells with TnV6 for as little as 7 days results in a persistent DNA damage signal, in contrast with previous data suggesting TnV6 is not directly genotoxic.

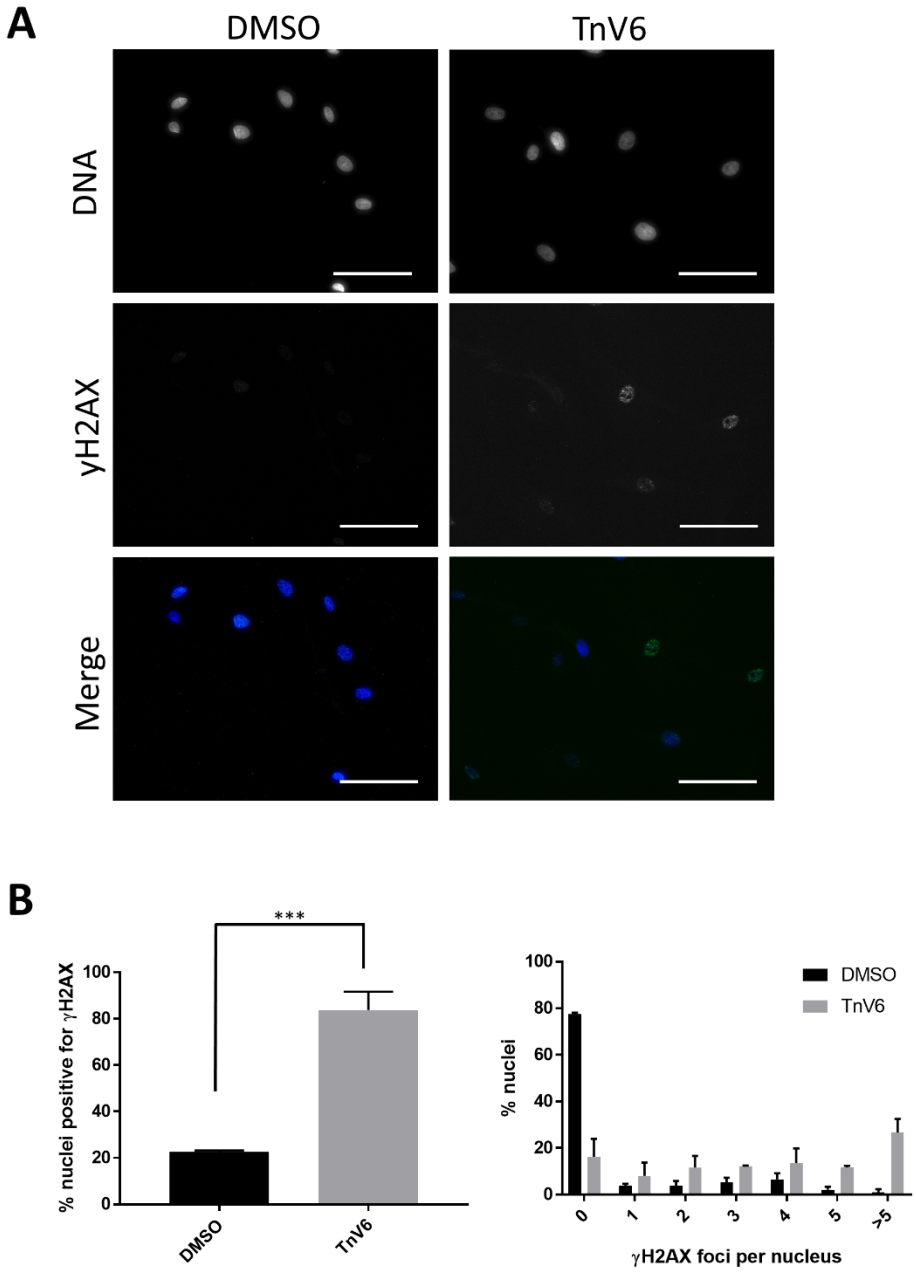


Figure 3.12 Extended TnV6 treatment induces DNA damage

A: analysis of DNA damage by immunofluorescence for γH2AX in HF043 fibroblasts treated for 7 days with 2 µM TnV6 or DMSO, with DNA counterstained by NucBlue Live. B: quantitation of % nuclei with γH2AX staining (2- tailed unpaired t-test p = 0.0002) and number of γH2AX foci per nucleus. Mean ± S.D. shown of n=3 biological replicates. Scale bar 100 µm.

3.4. Discussion

In this chapter, I have demonstrated that pharmacological inactivation of SIRT1/2 by low dose treatment with the drug Tenovin-6 results in onset of cellular senescence in primary human skin fibroblasts. The role of sirtuins in ageing has for some years been controversial. While Sir2 overexpression increases yeast lifespan and mutation decreases lifespan (Kaeberlein et al., 1999), and studies in worms and flies suggest that sirtuins act as pro-longevity factors (Wood et al., 2004), it has also been argued that such studies are dependent on factors other than the sirtuins (Burnett et al., 2011). For example, metabolic activators and/or downstream components of sirtuin activity (e.g. nicotinamide mononucleotide) have been reported to improve muscle strength and improve certain ageing phenotypes in mice (Imai and Guarente, 2016). However, the mechanistic basis of the impact of a deacetylase on ageing has not been clearly elucidated. In this chapter I have provided evidence that sirtuins may be active in protecting against ageing by delaying the onset of cellular senescence, as their inhibition promotes premature senescence.

My results underline a link between sirtuin signalling and senescence, and although these findings are consistent with previous data showing TnV6 upregulation of p21 (Lain et al., 2008), exactly how the sirtuins regulate cell proliferation is not yet clear. Both SIRT1 and SIRT2 are pleiotropic in terms of cellular targets: SIRT1 deacetylates nuclear proteins including p53, mTORC1, PI3K, FOXO1,3,4, PCG1a, HSF1 and NFκB, as well as several histones, while SIRT2 also targets some of these proteins in the cytoplasm, as well as tubulin, PAR-3 and Cdc20 (Dang, 2014). A large proportion of these targets have well-documented roles in senescence, for example mTOR is a biochemical nexus for senescence signalling, inhibition of which reverses phenotypes of senescence (Leontieva and Blagosklonny, 2016, Walters et al., 2016; see Chapter 4). Moreover, mTORC1 and NFκB both regulate the SASP (Herranz et al., 2015, Laberge et al., 2015); this signalling axis may be responsible for the upregulation of IL-

6 that I observed following prolonged TnV6 treatment. Further, p53 is a critical regulator of proliferation, senescence and apoptosis, and its interaction with another SIRT1 target (FOXO4) may regulate entry into senescence (Baar et al., 2017). Over-active p53 promotes ageing (Rodier et al., 2007), while deacetylation, possibly by sirtuins, may damp down p53's pro-ageing activity; TnV6 may block this deacetylation to promote senescence onset. Indeed, I demonstrated in a fluorometric assay that TnV6 treatment of cells leads to reduced deacetylation of an assay substrate. However, it remains possible that TnV6 may also inhibit the activity of non-sirtuin deacetylases. This could be further explored experimentally by investigating any antagonism of NAD^+ supplementation on TnV6-mediated sirtuin inhibition, as SIRT1 and SIRT2 are NAD^+-dependent deacetylases. It will also be important to investigate the relative contributions of SIRT1 and 2 in preventing premature senescence, through genetic manipulation or direct targeting using inhibitors such as the SIRT2-specific Tenovin-D3, shown to upregulate p21 in a p53-independent manner (McCarthy et al., 2013).

The observation of γH2AX foci, and by inference, sites of DNA damage and a persistent DNA damage response (DDR) in TnV6-treated cells is intriguing. It is well documented that senescent cells exhibit a chronic DDR responsible for establishing and maintaining senescence (Fumagalli et al., 2014). Furthermore, retrograde signalling by TGFβ as a component of the SASP increases cellular ROS, causing a DDR that reinforces the state of senescence (Passos et al., 2010). I observed increased IL-6 secretion upon extended treatment with TnV6 and an increased mitochondrial load, suggestive of an active SASP and possibly of increased ROS. This could constitute a possible mechanism for the observed DNA damage caused by a supposedly non-genotoxic agent (Lain et al., 2008). However, SIRT1 may also have a role in DNA repair, promoting homologous recombination (Palacios et al., 2010), meaning that SIRT1 inhibition could compromise cellular DNA repair capacity. Interestingly, SIRT1-mediated homologous recombination may require WRN, a helicase and exonuclease mutated in the premature ageing Werner syndrome (section 1.3.3.4.3). Replication stress

resulting from WRN mutation (Pichierri et al., 2001; Rodríguez-López et al., 2002) may itself drive cellular senescence by triggering a DNA damage response, and highly premature senescence is characteristic of Werner syndrome patient-derived cells. Interestingly, a link between upregulation of WRN and SIRT1 was observed in calorically restricted rats, with *in vitro* investigation suggesting that sirtuin-mediated deacetylation may stabilize WRN levels (Kahyo et al., 2008).

Cellular senescence is also accompanied by marked changes in chromatin, such as epigenetic changes including CpG methylation and histone modifications (e.g. Cruickshanks et al., 2013, section 1.3.3.5). Acting as histone deacetylases, the sirtuins broadly promote closer chromatin packing (Dang, 2014). I observed a significant increase in nuclear area after only 72 hours treatment with TnV6; as I observed that TnV6 induces a G1 phase arrest, this increase in nuclear area is not simply due to a higher proportion of nuclei with a 4N (replicated) DNA complement. Simplistically, this nuclear enlargement is consistent with the concept that blockade of sirtuin-mediated histone deacetylation allows chromatin decompaction, which is likely to be accompanied by changes in gene expression patterns. However changes to chromatin and nuclear structure may instead occur downstream of senescence-associated pathways, as significant alterations in nuclear size, lamina structure (Lenain et al., 2017), and chromosome localization (Bridger et al., 2000) occur in senescence. Of note, other HDAC inhibitors may also induce p21-driven senescence, including TSA (Okamoto et al., 2006).

Intriguingly, results from other labs have suggested that sirtuin suppression is associated with telomere dysfunction and premature ageing. Indeed, the *S. cerevisiae* homologue of SIRT1, Sir2, maintains a silent chromatin environment at telomeres, but is re-distributed from telomeres during ageing or following DNA damage, possibly to promote DNA repair (Guarente, 2000). A similar sirtuin re-distribution on response to DNA damage has been

reported in mice (Oberdoerffer et al., 2008). Furthermore, SIRT6 directly binds telomeres, and its loss results in increased DNA damage foci at telomeres and chromosome end-to-end fusions, suggesting a role for SIRT6 in telomere integrity (Tennen and Chua, 2011). Furthermore, telomere dysfunction and sirtuin repression are also both associated with predisposition to age-related diseases including liver disease. In patients with the telomere-maintenance disorder dyskeratosis congenita (DKC), as well as compromising the regenerative capacity of highly proliferative tissues such as skin, intestine and the hematopoietic system, telomere shortening induces liver fibrosis, probably resulting from insufficient telomerase activity in proliferating hepatocytes (Vulliamy et al., 2001, Calado et al., 2009). On the other hand, overexpressing or pharmacologically activating SIRT1 protects against fatty liver disease, while decreasing its activity increases hepatic steatosis (Purushotam et al., 2009). Crucially, recent results have provided a mechanistic link between sirtuin repression and telomere dysfunction in liver disease; in late-generation (G4) telomerase knockout mice exhibiting phenotypes of premature ageing such as shortened lifespan and stem cell compromise, downregulation of all 7 sirtuins and telomere dysfunction were both observed in the liver, which were rescued following telomerase re-introduction *in vitro* (Amano et al., 2019). Further analysis concluded that telomere dysfunction leads to the repression of sirtuins through p53-dependent mechanisms. Indeed, following DNA damage, NAD^+ levels fall in cells with dysfunctional telomeres. Furthermore, boosting NAD^+ levels contributes to telomere maintenance in a partially SIRT1-dependent manner, which counteracts telomere-dependent disease (Amano et al., 2019).

TnV6 has been developed as a promising anticancer agent, toxic at micromolar concentrations in tumour cell lines (Hirai et al., 2014; Jin et al., 2015). However, I observed toxicity in primary cells at doses to which cancer cells were less sensitive (Figure 3.2). Even low doses, which did not appreciably impact on cancer cells, were cytostatic for primary cells. Furthermore, my novel finding that TnV6 induces cellular senescence in primary

human fibroblasts has significant implications for clinical use of this drug in cancer chemotherapy— inducing senescence in healthy neighbouring cells could drive premature ageing, secondary cancer formation and promote metastasis through the SASP. Indeed, the HIV protease inhibitors used in HAART treatment have been shown to induce senescence in primary cells (Hernandez-Vallejo et al., 2013), and may have thus caused premature ageing in patients through induction of senescence (Torres and Lewis, 2014). It is therefore necessary to be cautious with novel cancer therapies that modulate biochemical pathways implicated in cell and organismal ageing.

However, although senescence has become synonymous with pathological ageing, it is important to remember that it also has beneficial physiological roles in development, wound healing and regeneration, as well as providing a barrier to tumorigenesis. Therefore, in certain contexts, agents that induce senescence may be therapeutically useful. For example, and crucially only if delivery could be targeted to avoid healthy neighbouring cells, TnV6 could be used to induce senescence in tumour cells (possibly in combination with a senolytic agent to subsequently induce apoptosis in such cells), or to induce senescence and promote regeneration in liver, cardiac and renal fibrosis, in skin wound healing or to prevent development of atherosclerotic plaques (Muñoz-Espín and Serrano, 2014). Hence, Tenovin-6 may retain some clinical utility by exploiting its ability to induce senescence.

3.5. Evaluation of TnV6-induced senescence as an experimental system

As demonstrated above, induction of senescence through pharmacological inhibition of SIRT1/2 is a reliable and experimentally-amenable system which recapitulates every typical characteristic of senescence so far tested. Notably, 7 day TnV6 treatment at 2 μM also induced permanent proliferative arrest and phenotypes of senescence in a second primary

human fibroblast line (HCA2, data not shown) showing that induction of senescence is not specific to the one cell line shown above (HF043). For experiments where large numbers of senescent cells are required in a short time frame, this system may therefore be highly useful. However, care must be taken to avoid over-interpreting biological conclusions from this artificial system. Therefore, for the rest of this thesis, I will use a range of models of senescence to investigate its molecular basis. As we learn more about the primary causes of senescence *in vivo*, it will be important for the research community to thoroughly evaluate our current experimental systems and adjust them accordingly to generate physiologically-relevant biological insights.

4. Reversal of phenotypes of cellular senescence by pan-mTOR inhibition

4.1. Introduction

Cellular senescence is a hallmark of ageing and senescent cells accumulate with age *in vivo* in mammals; this is thought to drive aging by limiting tissue replicative capacity, causing tissue dysfunction and through the pleiotropic effects of the pro-inflammatory SASP (Campisi, 2013). Senescent cells can be characterized by significant alterations in cellular phenotypes: they exhibit a large, flat, vacuolated and granular morphology with accumulation of lipid droplets and visible stress fibres, together with increased lysosomal content, filamentous actin stress fibres, mitochondrial accumulation and pro-inflammatory secretion (see 1.3.3). Developing strategies to remove or modulate senescent cells may therefore provide a route to prevent a range of age-related diseases. Targeting senescence as a means to combat ageing and age-related diseases is however challenging due to its antagonistically pleiotropic nature; any treatment needs to limit the deleterious impacts of senescent cells without impacting the barrier they provide against tumorigenesis.

While caloric restriction has been reported to reliably extend healthspan in many model organisms including rhesus monkeys, one of the most promising candidates for a longevity therapeutic in mammals is rapamycin (Harrison et al., 2009). Rapamycin is a macrolide antibiotic produced by *Streptomyces hygroscopius*, discovered in the soil of Easter Island (Vézina et al., 1975). It is clinically licensed for immunosuppression in kidney transplant patients and for renal cell carcinoma treatment, due to its broad inhibitory effects on cell growth and proliferation. As discovered through *S. cerevisiae* genetic screens, rapamycin mechanistically acts by binding the protein FKBP12, producing a complex which can bind and inhibit mTOR, a conserved eukaryotic Ser/Thr kinase (Heitman et al., 1991). mTOR constitutes the point at which diverse environmental signals are coordinated into a cellular response, regulating pathways including cell growth, proliferation, survival, motility and protein synthesis. mTOR is present in two complexes in metazoa, mTORC1 and mTORC2,

which have different components and functions (Huang and Fingar, 2014, section 1.4). Rapamycin inhibits mTORC1, but chronic treatment may also disrupt mTORC2. Rapamycin does not inhibit the phosphorylation of all mTORC1 substrates equally: it completely inhibits phosphorylation of S6K1 while only partially blocking the phosphorylation of 4E-BP1. A crystal structure of mTOR, rapamycin and FKBP12 suggests that this may be due to differential substrate access to the kinase active site (Yang et al., 2013). However, the second-generation ATP-mimetic pan-mTOR inhibitor AZD8055 has IC_{50} of 0.8 nmol/L for mTOR, with ~1000- fold selectivity for mTOR over other PI3K family members and no significant activity against a large panel of other cellular kinases (Chresta et al., 2010). AZD8055 has anti-proliferative effects similar to those of rapamycin and has been taken forward into clinical trials against various forms of cancer (Naing et al., 2011, Banerji et al., 2011). Indeed, mTOR inhibition extends lifespan in mice even when administered late in life (Harrison et al., 2009). As cellular senescence also limits the healthy lifespan of mice (Baker et al., 2016) it is possible that mTOR may be a critical signalling nexus in cellular senescence.

4.2. Chapter aims

In this chapter, I set out to address the following questions:

1. Does AZD8055 inhibit mTOR activity in human primary fibroblasts *in vitro*?
2. Does acute pan-mTOR inhibition alter features of senescence, such as enlarged morphology, actin stress fibres, lysosomal and mitochondrial dysfunction, alteration of nuclear morphology and pro-inflammatory secretion?
3. Is mTOR signalling chronically active in senescence?
4. Is mTORC1-selective or pan-mTOR inhibition more effective in modulating features of senescence?

To address these questions, I used a panel of inhibitors to disrupt mTOR signalling in a range of models of senescence, initially focusing on AZD8055 in replicatively senescent human primary fibroblasts. I employed a range of microscopy and molecular biology assays to assess phenotypes of senescence and their possible regulation through mTOR signalling.

4.3. Results

4.3.1. Nanomolar dose AZD8055 is non-toxic and inhibits mTOR-dependent phosphorylation events

To establish appropriate inhibitor doses to investigate the role of mTOR signalling in senescence, I first set out to determine a non-toxic dose range of AZD8055 in proliferating and senescent human primary fibroblasts (HF043). Replicatively senescent fibroblasts were obtained by serial passaging in the absence of any drug treatment (see 2.1.2.1). To measure AZD8055 toxicity, I implemented the alamarBlue assay, which measures cellular reducing capacity as a proxy for cell viability. Over a treatment period of 48 hours, I observed only a mild loss of cell viability in either proliferating or senescent cells on exposure to up to 100 nM AZD8055, though higher doses resulted in more severe toxicity (Figure 4.1A). Further, proliferating cells were marginally more sensitive to AZD8055 (Figure 4.1A). It is likely that this reflects a reduction of cell division during the treatment window, as mTOR signalling is critically important in directing cell growth and proliferation. Based on these results, I took forward a sub-toxic concentration range of 0-100 nM AZD8055 into future experiments.

To ensure that non-toxic nanomolar doses of AZD8055 were sufficient to inhibit mTOR activity, I used 4E-BP1 phosphorylation as a readout of mTOR activity, by Western blotting of control or treated cells, with GAPDH used as loading control. 4E-BP1 is hierarchically phosphorylated on multiple sites by mTOR, and in cells treated with 70 nM AZD8055 for 24

hours in culture, the intense bands reflecting higher order phosphorylation of 4E-BP1 were diminished, indicating mTOR inhibition by a non-toxic dose of AZD8055 (Figure 4.1B).

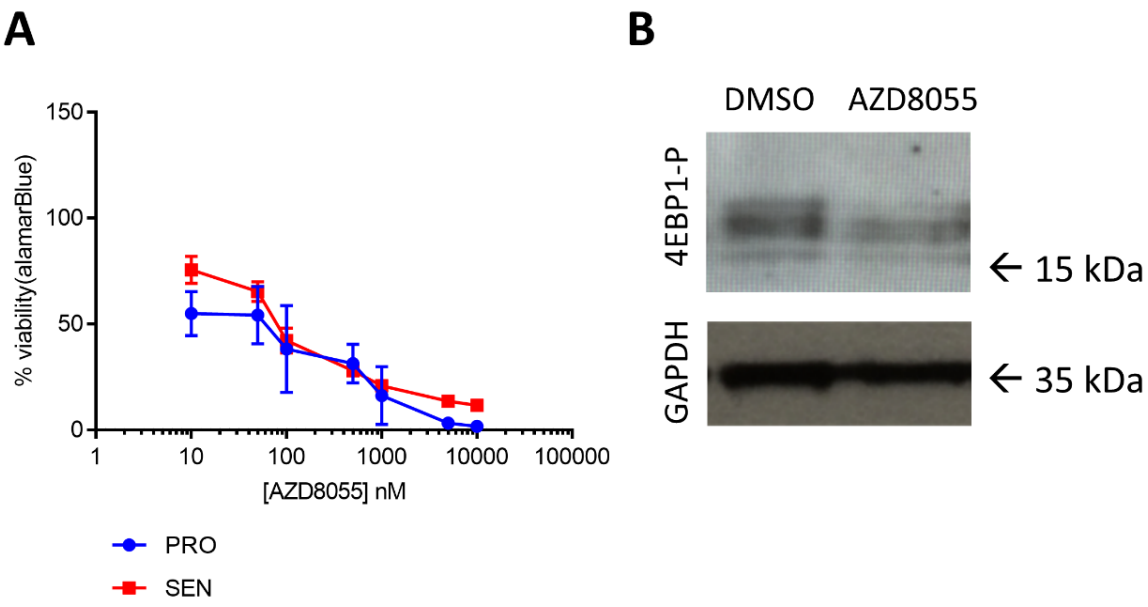


Figure 4.1: A non-toxic dose of AZD8055 inhibits mTOR activity

A: Proliferating (CPD <50) and replicatively senescent (CPD ~90) HF043 fibroblasts were seeded into a 96-well plate and treated with a dose range of AZD8055 (0-10 μM) for 48 hours. Cell viability was then assessed using the alamarBlue assay (mean ± SD of three independent experiments shown). B: HF043 fibroblasts were seeded into a T25 flask, left to bed down and then treated with 70 nM AZD8055 or DMSO control for 24 hours in culture. Cells were then harvested, lysed and used for Western blotting for 4E-BP1 and GAPDH (loading control). Representative data from n>3 biological replicates shown.

4.3.2. Morphological rejuvenation of senescent cells by acute pan-mTOR inhibition

To establish the role of mTOR signalling in senescence, I set out to determine whether AZD8055 treatment impacted on important biomarkers of senescence, such as senescent cell morphology. To this end, I treated replicatively senescent and proliferating control fibroblasts with DMSO (vehicle only control), or 70 nM AZD8055 for 7 days in culture. I then inspected cellular morphology by phase contrast microscopy. As expected, control

proliferating fibroblasts exhibited classic spindle morphology, characteristic of proliferating fibroblasts at low CPD. Furthermore, acute AZD8055 treatment did not alter this spindle morphology. Control replicatively senescent fibroblasts exhibited a dramatically enlarged, vacuolized and granular morphology, typical of senescent cells. By contrast, one week's acute treatment with AZD8055 led to marked alteration in senescent cell morphology, with treated cells re-acquiring the classical spindle morphology characteristic of proliferating fibroblasts at low CPD (Figure 4.2A).

To further investigate these morphological differences, I fixed and stained cells with the dye sulforhodamine B; this dye is utilized for cytotoxicity screening and biomass measurements (Vichai and Kirtikara, 2006) but it is also very informative for morphological analysis of cells. As consistently observed, AZD8055 treatment produced a notable decrease in senescent cell size compared with control cells, with treated senescent cells showing re-acquisition of fibroblastic morphology (Figure 4.2B).

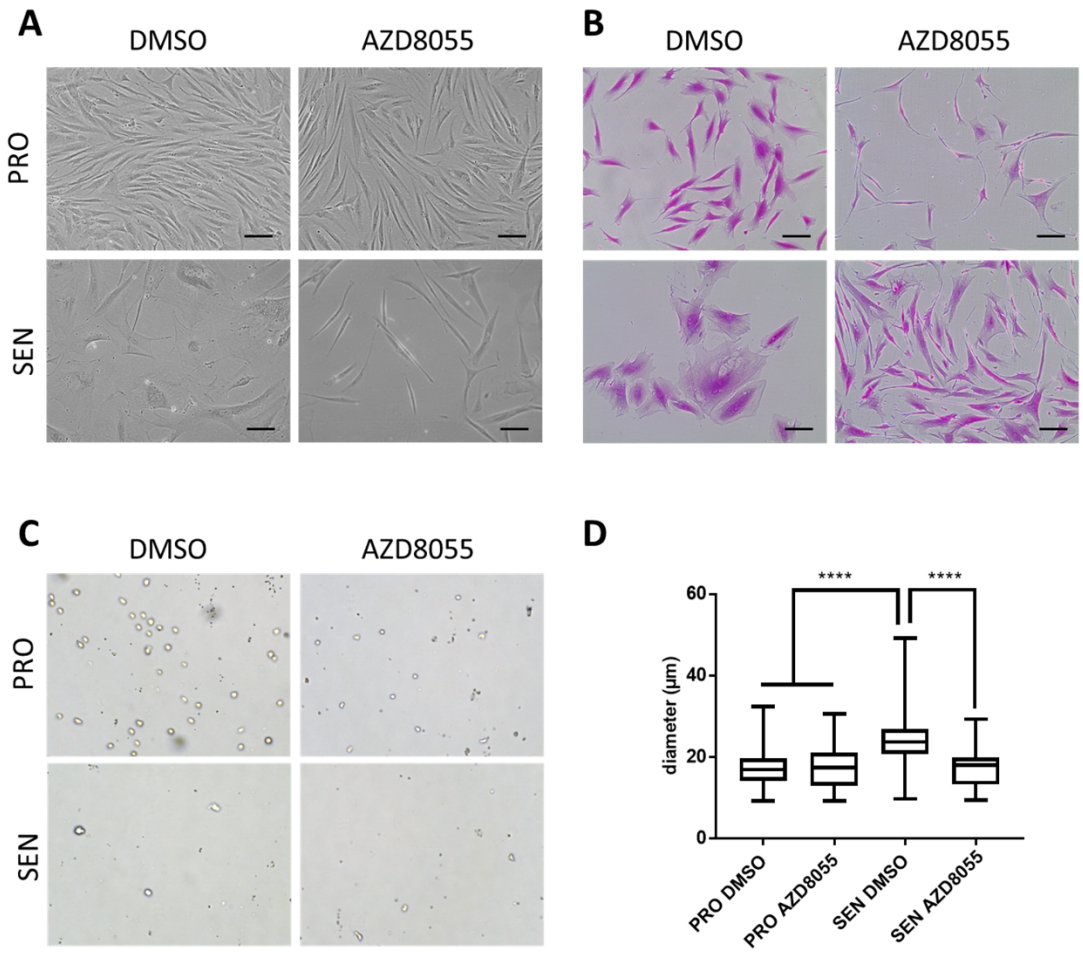


Figure 4.2: AZD8055 rejuvenates senescent cell morphology

A, B: Proliferating (CPD 42, PRO) and replicatively senescent (CPD 87, SEN) HF043 fibroblasts were treated with 70 nM AZD8055 or DMSO control for 7 days, then cell morphology was analysed live (A) or following fixation and SRB staining (B) using a digital EVOS microscope. C, D: Proliferating (CPD 35) and senescent (CPD 87) HF043 fibroblasts were treated with 70 nM AZD8055 or DMSO for 7 days. Cells were harvested and then cell diameter was analysed using a Cellometer T4 (C: representative images and D: quantification). Data was analysed by a one way ANOVA with means from each group compared by Tukey tests (**** $p < 0.0001$, all n>3 biological replicates, representative data shown). Scale bar 100 µm.

To determine whether these apparent cell size changes were quantifiably different following AZD8055 treatment, I harvested both proliferating and senescent fibroblasts, (either AZD0855-treated or DMSO control) by gentle trypsinization so that the cells detach from the substrate and round up to ovoid/spherical shapes. Cell diameters in these harvested

populations were then measured using a Cellometer T4 (section 2.1). Consistent with the differences observed between proliferating and senescent cells by phase contrast microscopy, I found a highly significant increase in cell diameter ($p<0.0001$) in senescent control cells (mean diameter 23.8 μm) compared to proliferating controls (17.1 μm). Notably, AZD8055 treatment of senescent cells led to a highly significant decrease in cell size (mean 17.2 μm), a cell diameter highly similar to that of low CPD untreated cells, consistent with cell morphology changes revealed by phase contrast microscopy (Figure 4.2C). While these diameter changes are highly significant, they appear more marginal than the dramatic reduction in cell size observed by microscopy, however a small change in the diameter of a sphere corresponds to a much larger change in cell volume ($volume = \frac{4}{3}\pi r^3$, i.e. a 6.6 μm reduction in mean senescent cell diameter following AZD8055 treatment actually corresponds to a decrease in mean cell volume from >7000 μm^3 to <3000 μm^3).

4.3.3. Effects of pan-mTOR inhibition on lysosomal dysfunction

The cellular lysosomal content increases dramatically on senescence, and lysosomal dysfunction as measured by SA-β-gal is commonly used as a senescence biomarker (Dimri et al., 1995). To assess the effect of mTORC inhibition on lysosomal dysfunction, I treated replicatively senescent and control proliferating fibroblasts with AZD8055 or DMSO for 7 days and stained cells for SA-β-gal. As anticipated, a high proportion of control senescent cells stained positive for SA-β-gal (~90%), compared to a significantly lower staining index for proliferating controls (~10%, Figure 4.3). Further, acute AZD8055 treatment significantly reduced the proportion of senescent cells that stained positive for SA-β-gal (~15%, Figure 4.3). This marker of senescence is therefore greatly diminished on AZD8055 treatment, suggesting a reversal of specific cellular metabolic features associated with senescence.

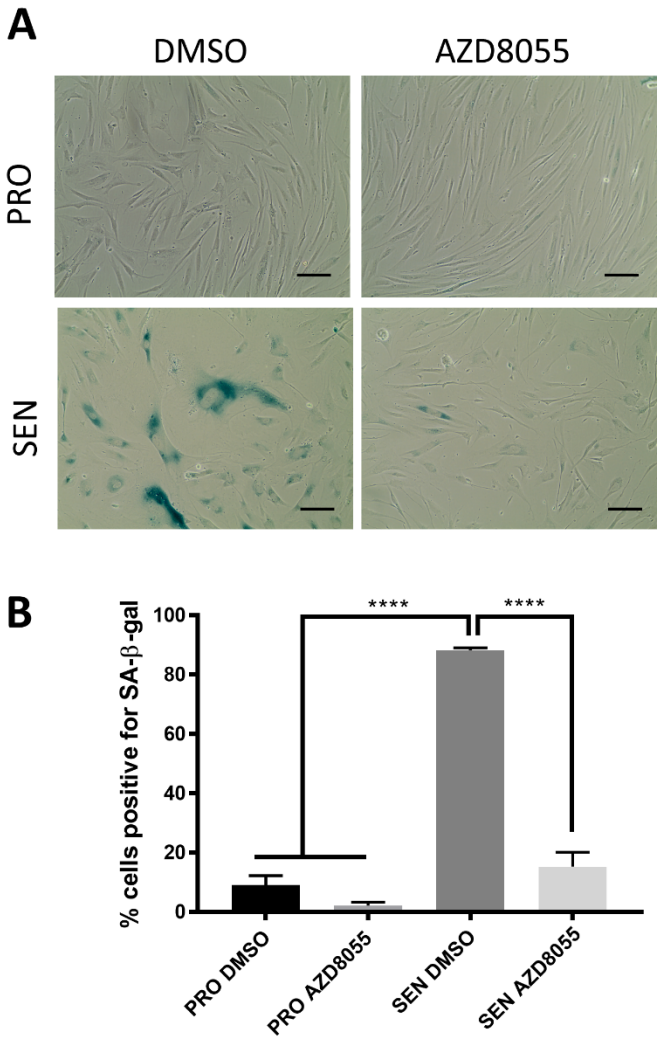


Figure 4.3: AZD8055 treatment reduces lysosomal dysfunction

Proliferating (PRO) and replicatively senescent (SEN) HF043 fibroblasts were treated with 70 nM AZD8055 or DMSO control for 7 days. A: cells were subsequently fixed and stained for SA-β-gal then imaged on a digital EVOS microscope. The proportion of cells staining positive for SA-β-gal was manually counted and quantified (B), with results analysed by one way ANOVA with Tukey test for multiple comparisons (**** $p<0.0001$; error bars represent standard deviation between 3 technical replicates, results from one representative experiment shown of $n>3$). Scale bar 100 μm.

4.3.4. Major rearrangement of the actin cytoskeleton accompanies reversal of other senescent biomarkers

As observed in Figure 4.2, untreated senescent cells have a distinct, enlarged morphology that is altered on acute treatment with AZD8055. As cell size and shape is controlled by the cytoskeleton, I investigated whether actin organization is altered in senescence. Actin stress fibres are associated with senescence (Nishio and Inoue, 2005); these are composed of bundles of actin filaments made up of actin monomers. Furthermore, previous data has shown that actin organization is regulated by mTORC2-dependent regulation of Rho GTPases (Liu et al., ,2010). To investigate mTOR-dependent regulation of actin organization in senescence, I fixed, permeabilized and stained both treated and control fibroblasts with two actin-specific fluorescent dyes: FITC-phalloidin which binds filamentous actin, and Rhodamine-DNase I which stains globular actin (Cramer et al., 2002; Figure 4.4, note rhodamine-DNase I has been re-coloured magenta using FIJI). Large filamentous actin stress fibres were clearly visible in control replicatively senescent fibroblasts (Figure 4.4), but after 7 days of AZD8055 treatment such fibres became much less prominent and actin instead appeared more centrally distributed, accompanied by a shift from filamentous to globular conformation as evidenced by a shift from green (FITC) to magenta (rhodamine) staining, more reminiscent of the actin distribution shown in proliferating controls where few stress fibres are visible, and a high proportion of globular actin is perinuclearly distributed (Figure 4.4). AZD8055 treatment did not appreciably alter actin distribution in proliferating cells. Using scratch assays monitored by live cell imaging, I investigated whether this reorganization of the actin pool was accompanied by an increase in cell motility, however no substantial or consistent effects were observed (data not shown).

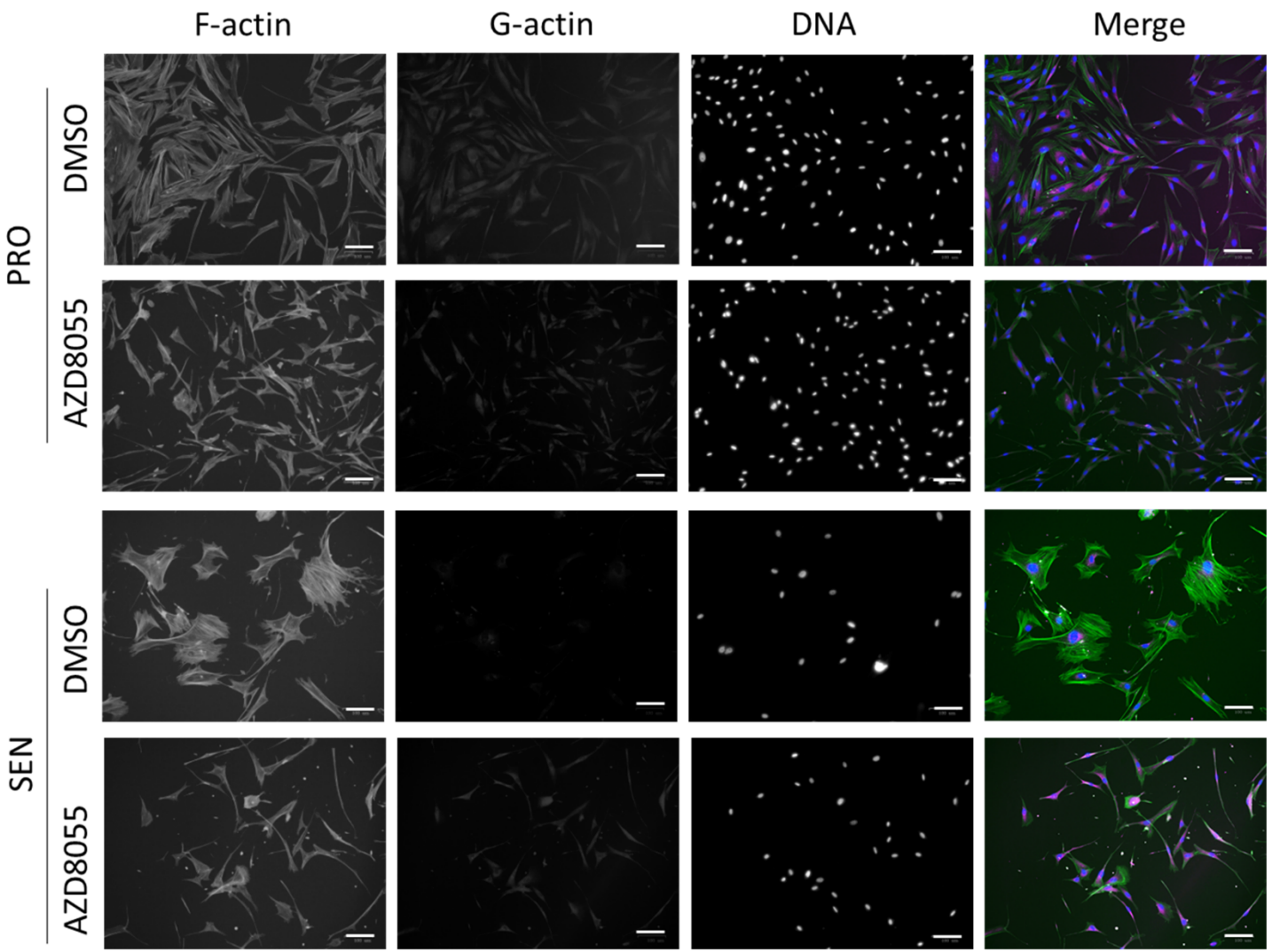


Figure 4.4: AZD8055 treatment disrupts actin stress fibres in senescent fibroblasts

Proliferating and replicatively senescent (PRO CPD <50, SEN CPD ~90) HF043 fibroblasts were treated with 70 nM AZD8055 or DMSO control for 7 days. Cells were then fixed, permeabilized and stained for filamentous actin (FITC-phalloidin) and globular actin (Rhodamine-DNase I, re-coloured magenta in merge). Representative data from n>3 experiments shown. Scale bar 100 μm.

4.3.5. Loss of dysfunctional mitochondrial on pan-mTOR inhibition

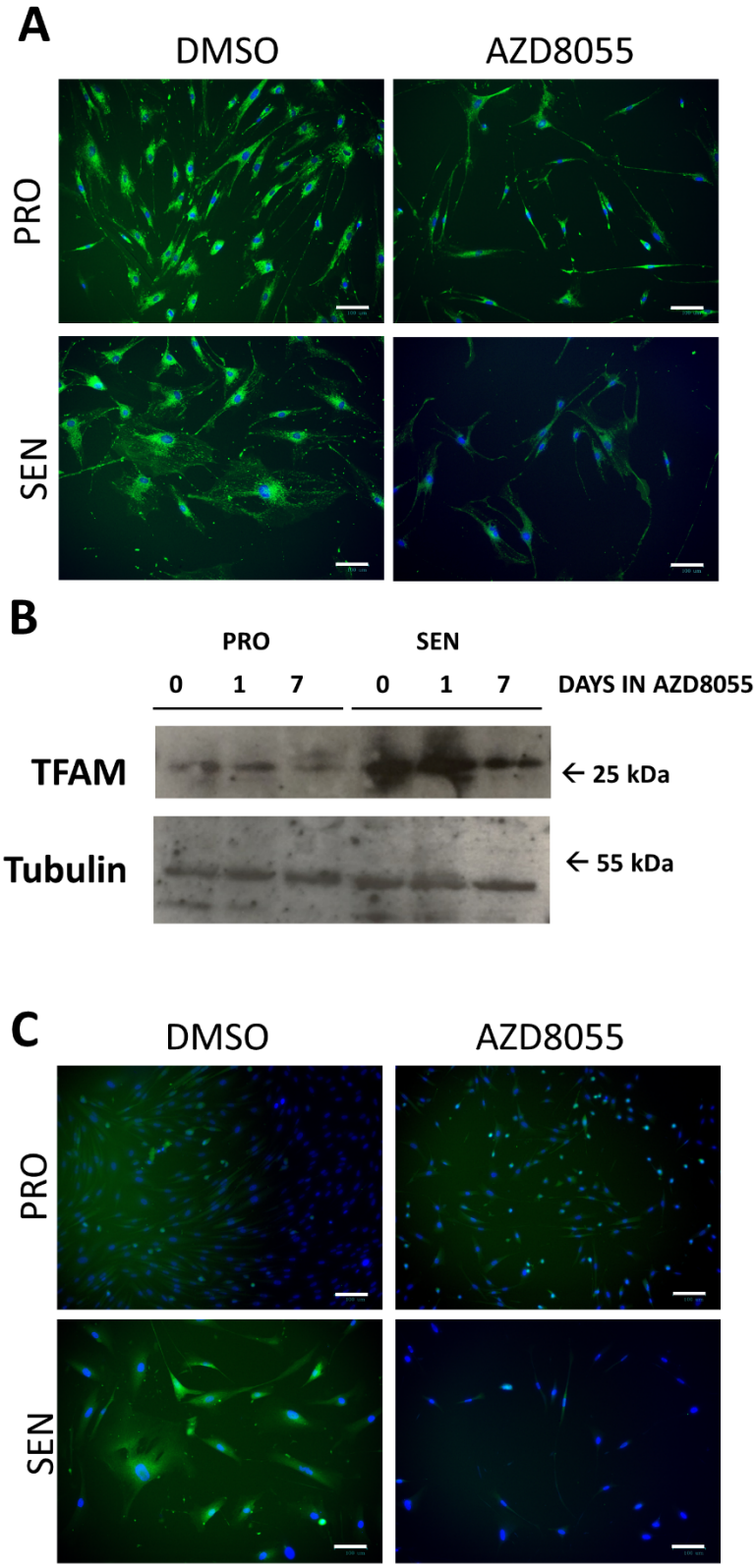
Mitochondrial biomass is dramatically increased in senescence, possibly due to increased mitochondrial biogenesis, altered fission/fusion dynamics, and failure of mitochondrial recycling (mitophagy, section 1.3.3.2.1). I therefore used a mitochondria-specific probe, Mitotracker Green FM, to label mitochondria in proliferating and replicatively senescent fibroblasts following acute pan-mTOR inhibition using 70 nM AZD8055 for 7 days (Figure 4.5A). Using fluorescence microscopy, mitochondria were detected as reticular networks throughout the fibroblasts, though in proliferating fibroblasts, the cellular mitochondrial load was comparatively low both without and with AZD8055 exposure. By contrast, a high Mitotracker signal was observed in control senescent cells (Figure 4.5A), suggesting a dramatically increased mitochondrial network. This was reduced on acute AZD8055 treatment, to levels similar to those detected in cells early in their proliferative lifespan (Figure 4.5A).

To assess whether this apparent increase in mitochondrial load on senescence and decrease in senescent fibroblasts following pan-mTOR inhibition was simply due to the effects of cell spreading in highly flattened senescent cells, proliferating and senescent cells treated with a time course of AZD8055 for 0, 1 and 7 days and lysed for analysis by Western blotting. Antibodies against the mitochondrial protein TFAM (which stoichiometrically associates with mitochondrial DNA and thus reflects mitochondrial load), and γ-tubulin (loading control) were used to probe the blot (Figure 4.5B). Proliferating fibroblasts showed a weak TFAM band at ~25 kDa irrespective of pan-mTOR inhibition, corresponding to a low mitochondrial load per cell, while the TFAM signal was much stronger in senescent fibroblasts but gradually reduced over time with AZD8055 treatment; observations highly consistent with the Mitotracker results (Figure 4.5A).

It has been reported that the increase in mitochondrial load in senescent cells reflects mitochondrial dysfunction (Passos et al., 2007, Dalle Pezze et al., 2014). To test the effect of AZD8055 on mitochondrial dysfunction, I used cellular ROS levels as a proxy for mitochondrial dysfunction, using DCFDA to stain cells for fluorescence microscopy analysis. After diffusing into cells, the DCFDA reagent is deacetylated by cellular esterases to a non-fluorescent compound, which is subsequently oxidized by ROS into the highly fluorescent product DCF, which can be visualized using fluorescence microscopy (FITC channel). As anticipated, control senescent fibroblasts (Figure 4.5C) showed strong positive staining for ROS in comparison with proliferating cell controls, which was again reversed in senescent cells on acute pan-mTOR inhibition (Figure 4.5C). Taken together, these results indicate that pan-mTOR inhibition in senescent cells reduces the mitochondrial load and cellular ROS, suggestive that dysfunctional mitochondria may be removed during treatment.

Figure 4.5: AZD8055 treatment reduces dysfunctional mitochondrial accumulation in senescent fibroblasts

Proliferating and replicatively senescent HF043 fibroblasts (CPD <50 and ~90 respectively) were treated with 70 nM AZD8055 or DMSO control for 7 days. A: cells were stained with Mitotracker Green and NucBlue Live (DNA) and imaged live in fresh media. B: proliferating and senescent fibroblasts were treated with DMSO control or AZD8055 for 1 or 7 days in culture then lysed and analysed by Western blotting for the mitochondrial protein TFAM with a γ-tubulin loading control. C: cells were stained with DCFDA and NucBlue Live and imaged in fresh media for ROS staining. For all, representative data shown from n≥3 biological replicates. Scale bar 100 μm.


A
DMSO
AZD8055
PRO
SEN
B
PRO
SEN
0
1
7
0
1
7
DAYS IN AZD8055
TFAM
← 25 kDa
Tubulin
← 55 kDa
C
DMSO
AZD8055
PRO
SEN

4.3.6. Increase of autophagy and mitophagy on pan-mTOR inhibition in senescent fibroblasts

To determine whether the loss of dysfunctional mitochondria observed above in senescent fibroblasts on acute pan-mTOR inhibitor treatment (Figure 4.5) could be due to increased mitophagy, I first set out to detect whether AZD8055 treatment was indeed inducing autophagy. To this end, I used CYTO-ID staining, where a selective proprietary dye labels autophagosomes in live cells (see 2.2.5). However, as autophagy is not only regulated at the level of autophagosome formation, I also used the V-ATPase inhibitor Bafilomycin A1 to block flux through the system in sequential treatment with AZD8055 as a control (Figure 4.6A). After only 5 hours drug treatment, I observed that 70 nM AZD8055 treatment did indeed induce autophagosome formation, which was stabilized following bafilomycin A1 addition (final hour treatment), indicating that autophagic flux was increased on pan-mTOR inhibition (Figure 4.6B).

I next set out to determine whether pan-mTOR inhibitor treatment induced selective recycling of mitochondria in senescent cells. To this end, I treated senescent fibroblasts with AZD8055, and in collaboration with Eszter Dombi (Prof. Jo Poulton lab, NDWRH, University of Oxford), performed high content imaging (HCI) on cells stained using immunofluorescence for LC3-II (autophagosomes) and TOM20 (mitochondria) over a time course. Analysis of these results using algorithms produced by the collaborating lab (Diot et al., 2015) indicated that over a time-course of AZD8055 treatment, mitochondria/autophagosome co-localization increased, suggesting that pan-mTOR inhibition stimulated selective recycling of mitochondria (mitophagy) in senescent cells (Figure 4.6C, D).

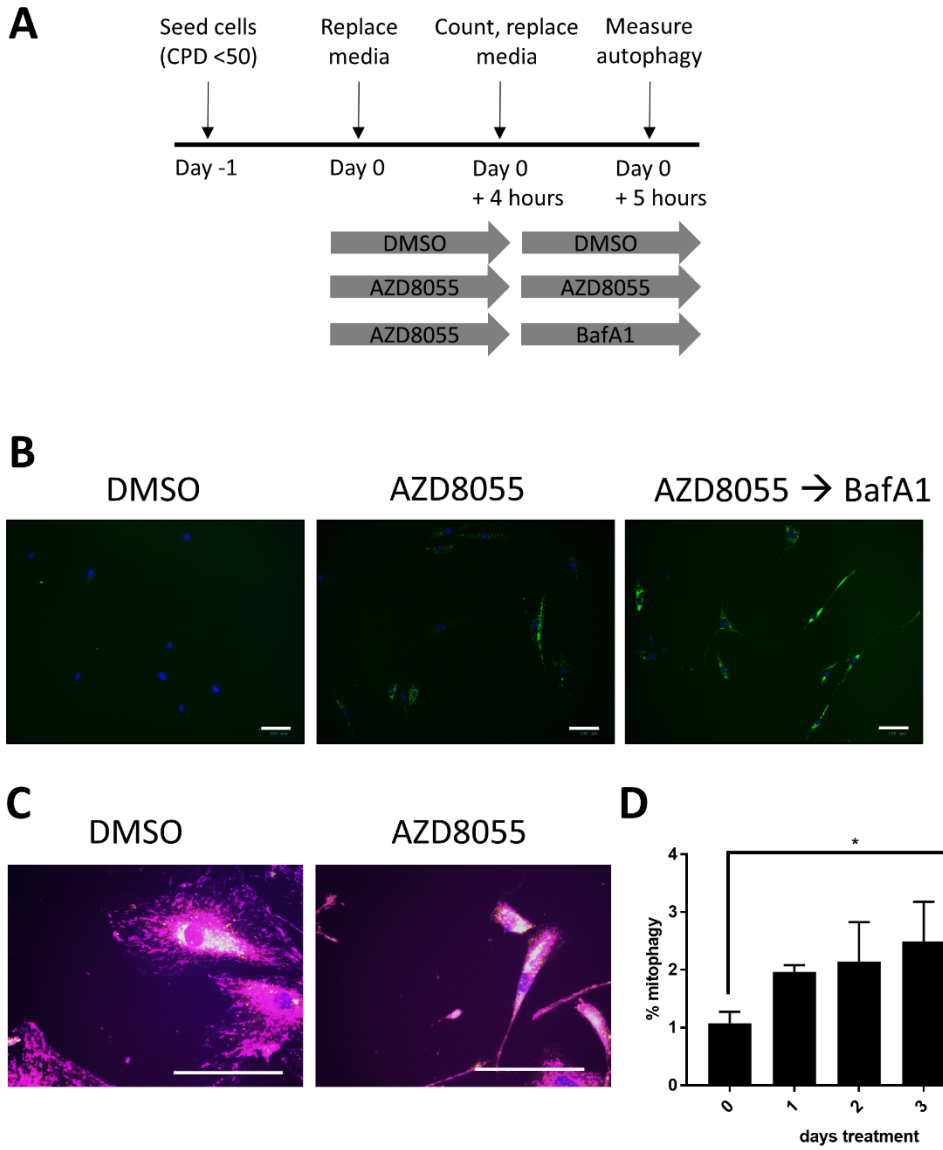


Figure 4.6: AZD8055 treatment induces autophagy and mitophagy

A: schematic depicting design of autophagy experiment. HF043 fibroblasts were treated with DMSO, 70 nM AZD8055 (4 hours) or 70 nM AZD8055 (4 hours) and then Bafilomycin A1 (10 nM, 1 hour), then autophagosome number was analyzed by CYTO-ID staining (B, n>3). DMSO – BafA1 control treatments were also used in every experiment. C: Mitophagy was analyzed in senescent fibroblasts by high content imaging analysis (InCell1000) of TOM20 and LC3 II co-localization over a time-course of 70 nM AZD8055 treatment and quantified (D) according to Diot et al (2015). Error bars are standard deviation from 3 technical replicates of representative data from n>3 experiments. Scale bar 100 μm.

4.3.7. Reduced nuclear area and improved nuclear integrity on pan-mTOR inhibition

Due to profound changes in the expression and localization of a number of proteins which regulate nuclear architecture in cell senescence (e.g. lamin B, HMGB1&2, discussed in 1.3.3.5), senescent cells exhibit nuclear enlargement. Indeed, recent single cell analysis has suggested that in a highly heterogeneous population of senescent cells, those with extremely large nuclei may be responsible for high levels of pro-inflammatory secretion, due to the pronounced nuclear loss of regulators of nuclear architecture such as HMBG1, which also acts as an alarmin (Sofiadis et al., 2019). Therefore, as a number of other biomarkers of senescence were reversed by pan-mTOR inhibition, I investigated the impact of AZD8055 treatment on nuclear enlargement. Proliferating and replicatively senescent fibroblasts were again treated with DMSO or AZD8055 (70 nM) for 7 days, DNA was labelled using the live DNA (Hoechst 33342) dye NucBlue Live, cells were imaged using a fluorescent cell imager and nuclear area was subsequently measured in images using FIJI software. As anticipated, I observed enlarged and highly heterogeneous nuclei within the senescent cell population, with a mean nuclear size of ~420 nm^2 (Figure 4.7 A, B). However, on acute AZD8055 treatment, I observed a dramatic decrease in nuclear area, to sizes highly similar to those of control proliferating fibroblasts (proliferating DMSO mean ~230 nm^2, senescent AZD8055 mean ~200 nm^2). While this decrease in nuclear area could be caused simply by a reduction in cell size or cytoskeletal organization, it is possible that pan-mTOR inhibition may restore nuclear integrity.

Furthermore, cytoplasmic chromatin fragments (CCFs) have recently been observed in senescent cells (Ivanov et al., 2013), where portions of chromatin are lost from the nucleus and activate intracellular DNA sensing immune pathways (cGAS – STING, Dou et al., 2017, Glück et al., 2017). These fragments may eventually be removed by autophagy (Ivanov et al., 2013). As I had observed increased autophagy (Figure 4.6) and a possible restoration of

nuclear integrity on pan-mTOR inhibition in senescent fibroblasts (Figure 4.7), I investigated whether pan-mTOR inhibition affected levels of CCFs in replicatively senescent fibroblasts. I used fluorescence microscopy to detect CCFs within senescent and proliferating populations, with and without AZD8055 treatment (70 nM, 7 days). Following manual observation, I noted a proportion of control senescent fibroblasts exhibiting CCFs consistent with previous published data (Figure 4.7C, D controls ~25%, Ivanov et al., 2013). However, I also observed a statistically significant decrease in the proportion of cells that contained CCFs following acute pan-mTOR inhibition (Figure 4.7 C, D ~25% controls vs ~5% in treated cells). This reduction in CCFs on AZD8055 treatment could possibly occur through decreased formation resulting from improved nuclear integrity, by recycling through enhanced autophagy or indeed through secretion of CCFs and hence elimination from the cell. Indeed, nuclear-origin DNA has been identified within secreted extracellular vesicles and proposed as a homeostatic mechanism (Takahashi et al., 2017).

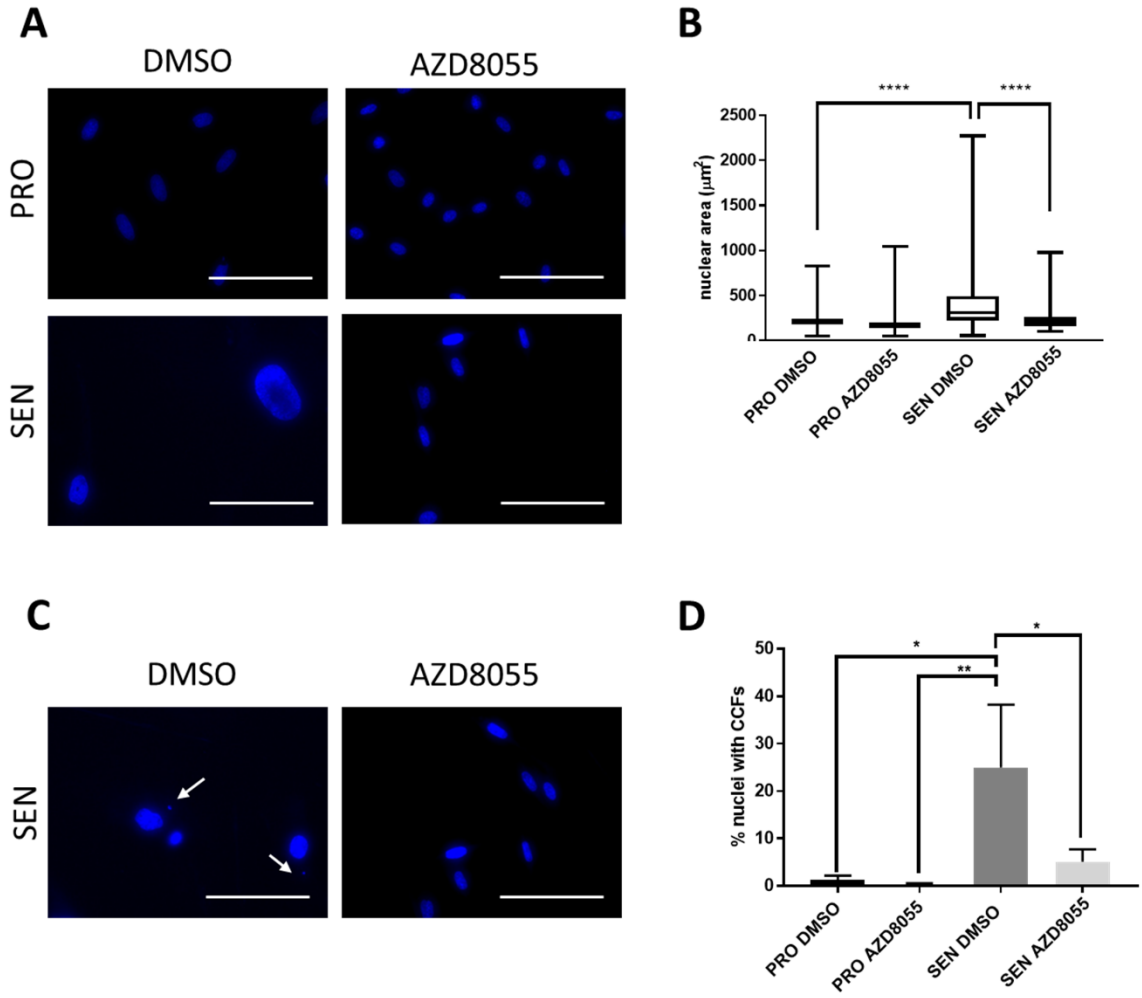


Figure 4.7. Pan-mTOR inhibition reduces nuclear size and improves nuclear integrity in senescent fibroblasts

Nuclear area and CCF incidence were analysed in live proliferating (CPD >50 PRO) or senescent (CPD ~90, SEN) cells treated with DMSO or 70 nM AZD8055 for 7 days then stained with NucBlue Live. Nuclear area was then analysed in images using FIJI (B) and CCF incidence (C) manually quantified as % cells harbouring one or more CCF (D). Over 50 nuclei analysed per technical replicate; representative data shown from n>3 independent experiments for B and D. Data was analysed by a one way ANOVA with means from each group compared by Tukey tests (*** $p < 0.001$, ** $P < 0.01$, * $P < 0.05$). Scale bar 100 μm.

4.3.8. Pan-mTOR inhibition reduces pro-inflammatory secretion

As I had observed reduced nuclear size and decreased CCF incidence in senescent cells following AZD8055 treatment (Figure 4.7), which are both implicated in pro-inflammatory secretion, I next investigated whether pan-mTOR inhibition reduced the secretion of the pro-inflammatory cytokine IL-6, using IL-6 levels as a marker of the SASP. Not only is IL-6 consistently and strongly upregulated despite considerable heterogeneity within SASP factors of different senescent cell types, but it is also implicated in paracrine pro-tumorigenic signalling (Coppé et al., 2008). I employed two separate assays to measure IL-6 levels secreted over a 24 hour period by treated and untreated senescent cells (see Figure 4.8A for experimental design): IL-6 ELISA, and a cell-based reporter assay where binding of IL-6 (present within conditioned media) to IL-6R expressed on the reporter cells results in SEAP production, which can be quantified colorimetrically (HEK-SASP, Rolt et al., 2019). Both assays revealed higher IL-6 levels in conditioned media from control senescent fibroblasts compared to proliferating controls (Figure 4.8 B, C). Notably, a dose-dependent decrease in IL-6 levels was observed in both assay systems following 7 day AZD8055 treatment of senescent cells. These results are highly consistent with published data showing that mTOR signalling has a crucial role in SASP secretion (Laberge et al., 2015, Herranz et al., 2015).

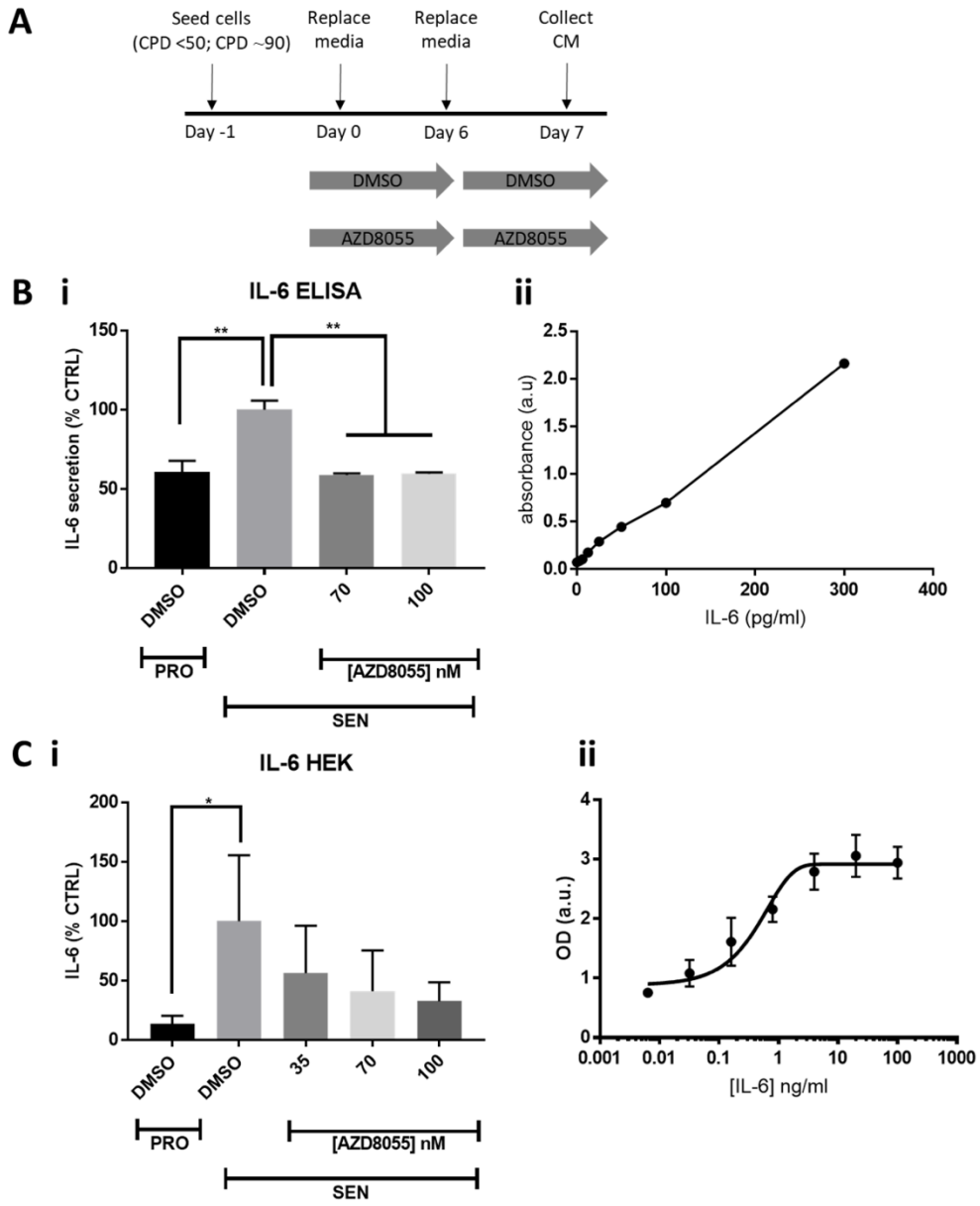


Figure 4.8: AZD8055 treatment reduces IL-6 secretion from senescent fibroblasts
A: Proliferating control or replicatively senescent HF043 fibroblasts were seeded and subsequently treated with DMSO control or a dose range of AZD8055 for 6 days in culture. Media was then replaced and incubated for 24 hours before conditioned media (CM) samples were taken for analysis of IL-6 secretion. B: CM samples were snap-frozen and subsequently analysed by B: IL-6 ELISA or C: HEK-SASP reporter cell assay, where IL-6 present in CM binds IL6R expressed on reporter cells, ultimately resulting in quantifiable SEAP production. For ELISA and HEK-SASP assays, data were normalised according to recombinant IL-6 standards (standard curves shown in Bii and Cii and interpolated results in Bi and Ci respectively; n=3 for both assays, representative data shown). One way ANOVAs were performed for each respective test for statistical analysis, *; $p<0.05$, **;$p<0.01$. Note control experiment performed to test if AZD8055 in CM interfered with SEAP production in HEK cells; no effect seen (Rolt et al., 2019).

4.3.9. Removal of treatment results in re-acquisition of senescent phenotypes

Cell senescence constitutes an important barrier to tumorigenesis by halting proliferation of potentially compromised cells and recruiting the immune system for clearance and remodelling (Sagiv et al., 2013, Lumjambio et al., 2013). As shown above (Figures 4.2-4.8), a number of deleterious phenotypes of senescence were reversed on acute (7 day) pan-mTOR inhibition. In rodent cells, it has been reported that short term rapamycin treatment induces permanent release from senescence, such that cells proliferate indefinitely (Demidenko et al., 2009), which could risk compromising the cell-autonomous tumour suppression associated with senescence.

To investigate the duration of the AZD8055 effects, I assessed cell morphology and the senescence marker SA-β-gal upon removal of AZD8055 after 7 day treatment, or with continuous dosing for 14 days (see Figure 4.9A for experimental design). Untreated (DMSO) senescent fibroblasts exhibited enlarged, flattened and granular morphology together with strong SA-β-gal staining (Figure 4.9B, C). By contrast, senescent cells treated continuously (14 days) with 70 nM AZD8055 showed spindle-like cell morphology and weak SA-β-gal staining, highly reminiscent of untreated proliferating controls (Figure 4.9B, C). However, senescent cells initially treated with AZD8055 reacquired the enlarged, granular morphology and SA-β-gal staining characteristic of senescence following removal of drug (Figure 4.9B, C), suggesting that pan-mTOR inhibition does not permanently alter these core phenotypes of senescence in primary human fibroblasts. This re-acquisition of senescent phenotypes following cessation of treatment further suggests that mTOR is constitutively active in these senescent fibroblasts, as following release of inhibition, mTORC-regulated phenotypes are re-established.

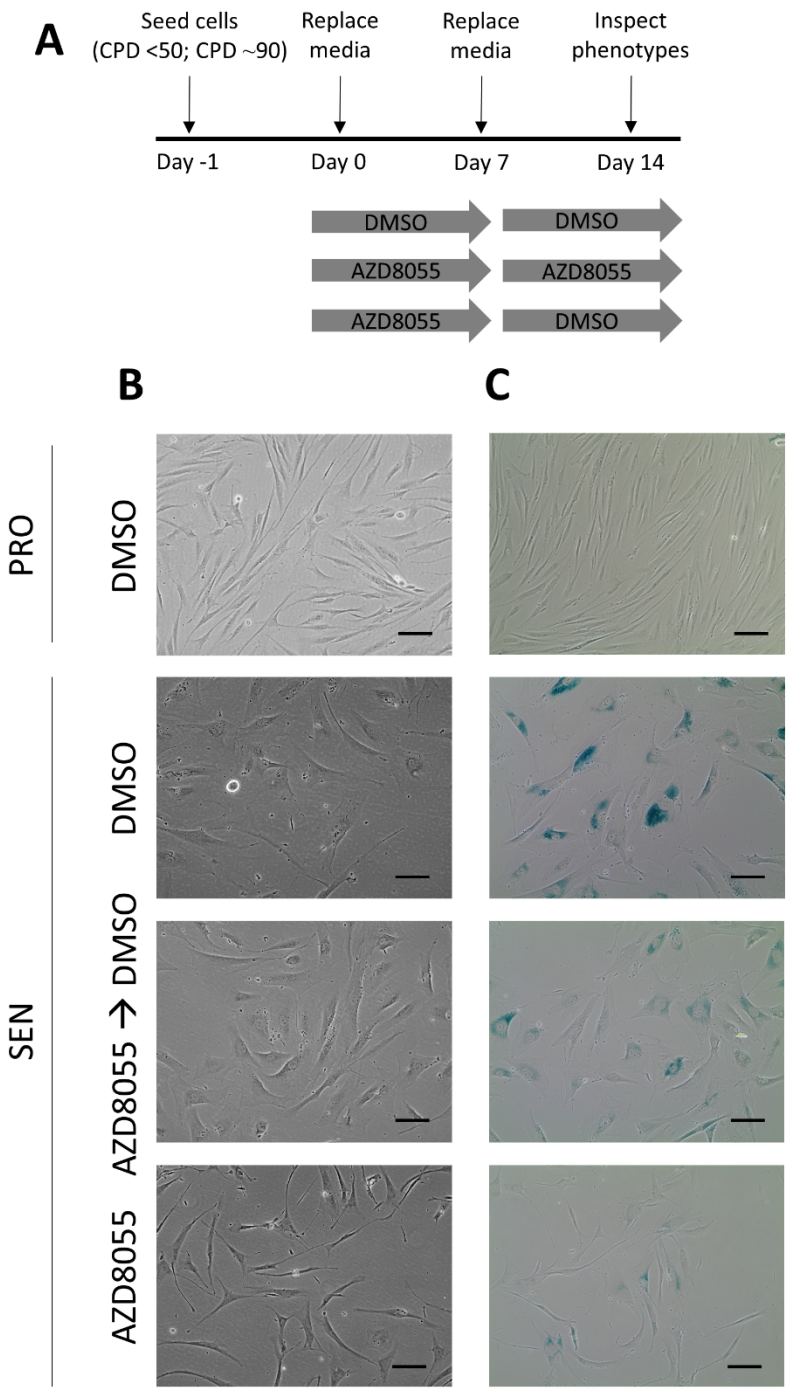


Figure 4.9: Senescent phenotypes re-appear following AZD8055 treatment removal

A: schematic depicting experimental design in which replicatively senescent (SEN) fibroblasts were seeded and subsequently treated with control DMSO (vehicle control) or 70 nM AZD8055 for 14 days, or AZD8055 for 7 days and fresh media (DMSO only) for the following 7 days, alongside untreated proliferating controls at low CPD (PRO) for comparison. B: cell morphology was then analysed and C: cells were fixed and stained for SA-β-gal. Scale bar 100 μm.

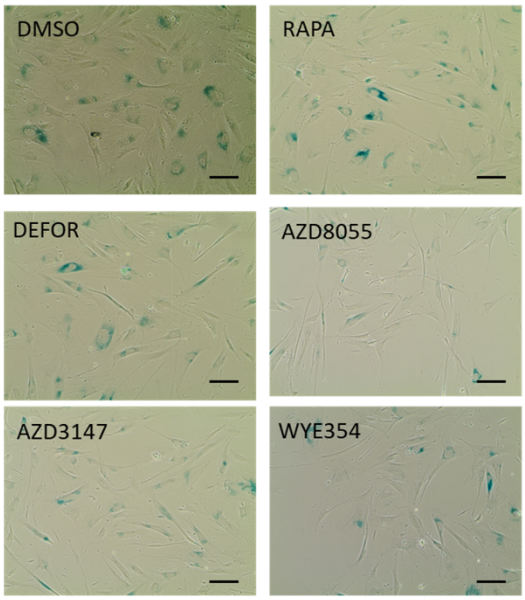
4.3.10. Reversal of phenotypes of cell senescence using a panel of mTOR inhibitors

AZD8055 is an ATP-competitive pan-mTOR inhibitor, known to be highly selective (>1000 fold) for mTOR over other highly related PI3-like kinases (Chresta et al., 2010). However, it is not possible to rule out that the observed effects of AZD8055 on senescent fibroblasts could occur through off-target effects. I therefore tested the effect of a panel of mTOR inhibitors with different modes of action (Figure 4.10A), including mTORC-1 selective inhibitors (rapamycin and its analogue deforolimus), and further pan-mTOR inhibitors (AZD3147, WYE354). Several phenotypes of senescence were examined in control (DMSO) and drug-treated fibroblasts, including SA-β-gal (Figure 4.10B), morphology (SRB staining – Figure 4.10C), mitochondrial accumulation (Mitotracker Green, Figure 4.10D), actin organization (rhodamine-phalloidin, Figure 4.10E) and pro-inflammatory secretion (IL-6 by reporter-cell assay HEK-SASP, Figure 4.10F). The orally bioavailable pan-mTOR inhibitor WYE354 appeared less potent in my initial screening experiments (data not shown) and was therefore used at a higher dose range than the other agents (Figure 4.10A). While mTOR inhibition reduced cell size and IL-6 secretion in all cases, the pan-mTOR inhibitors appeared particularly effective in reducing SA-β-gal staining, mitochondrial accumulation and actin reorganization compared with mTORC1-selective drugs.

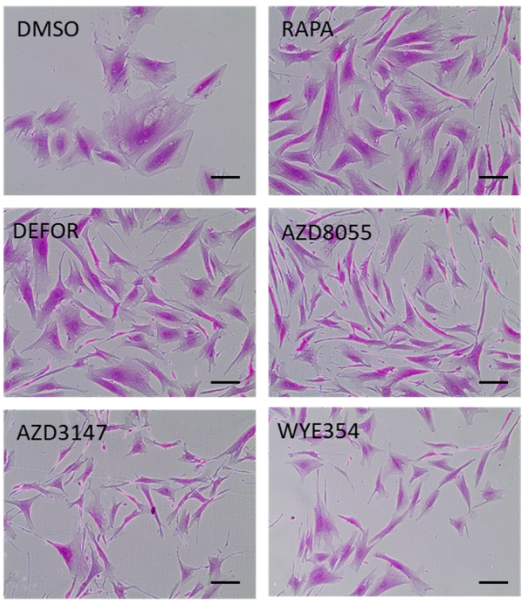
A

Compound	Molecular target	Effective dose
Rapamycin	mTORC1	70 nM
Deforolimus		
AZD8055	mTORC1 and mTORC2	
AZD3147		
WYE-354		1 µM

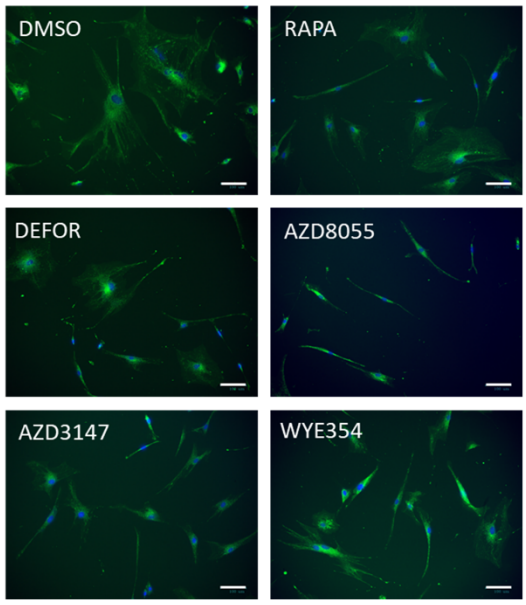
B



C



D



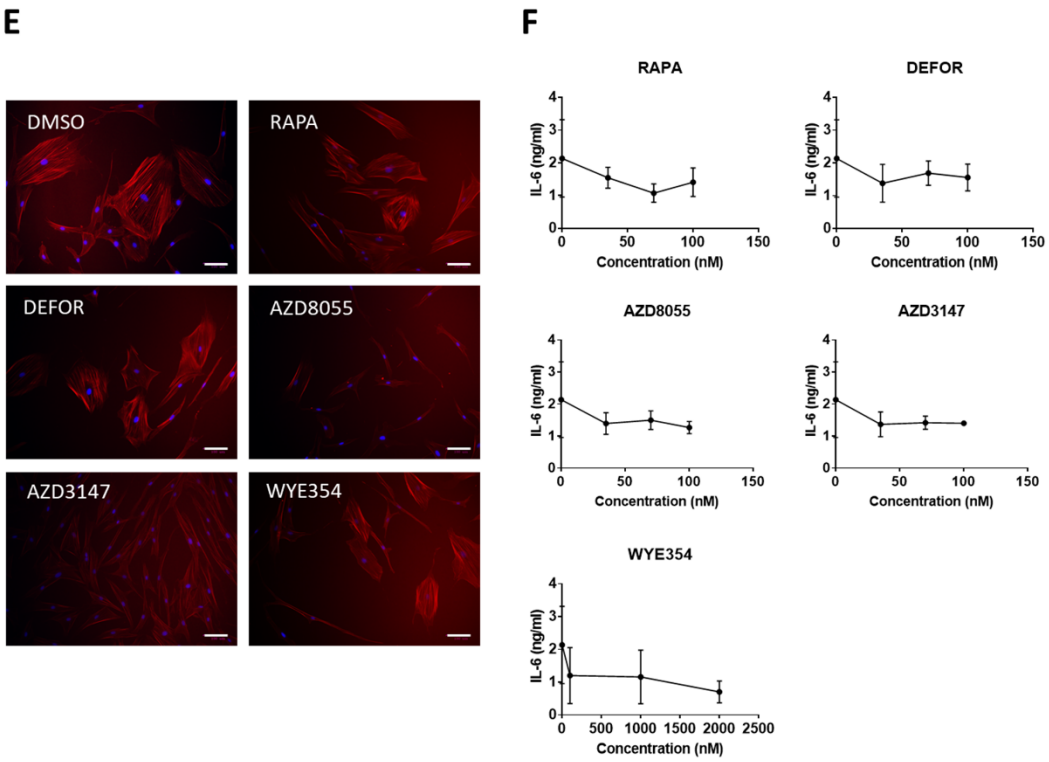


Figure 4.10: Rapalogue treatment reverses phenotypes of senescence including lysosomal dysfunction, enlarged morphology, mitochondrial accumulation, actin stress fibres and IL-6 secretion

Replicatively senescent HF043 fibroblasts were treated with optimal doses of mTOR inhibitors for 7 days in culture (A) and then analysed for phenotypes of senescence. B: Treated fibroblasts were fixed and stained for SA-β-gal, C: cells were fixed and stained with SRB, D: cells were stained with Mitotracker green and NucBlue Live (DNA), E: cells were fixed, permeabilised and stained with rhodamine-phalloidin to label actin and NucBlue Live (DNA), before imaging. F: 24-hour conditioned media was taken for IL-6 secretion analysis using the HEK-SASP assay (Rolt et al., 2019, error bars are SD from n=3 technical replicates, n>3 independent experiments, representative data shown). Scale bar 100 μm.

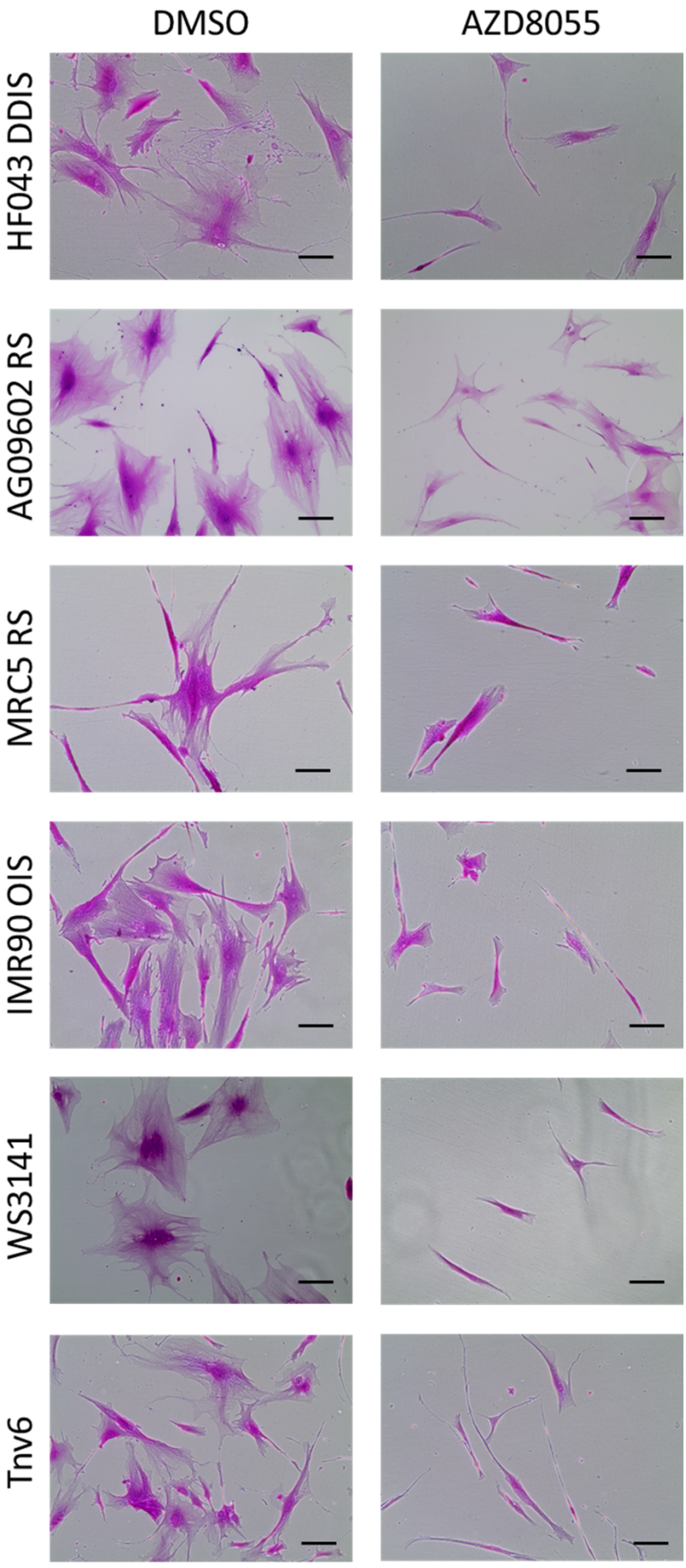
4.3.11. Reversal of phenotypes of cell senescence in other models of senescence

Senescence is a highly heterogenous proliferation arrest programme, and a range of different signals can induce senescence through a number of different pathways, and in different cell types. To investigate whether mTOR inhibitor-induced reversal of phenotypes

of senescence was specific to replicative senescence, or to the cell line so far tested (primary neonatal foreskin fibroblasts, HF043), I repeated these experiments in a number of different models of senescence, including DNA damage induced senescence (DDIS; 20 μM etoposide treatment for 7 days, see 2.1.2.2) and TnV6-induced senescence (TIS; 2 μM TnV6, 7 days) within the same HF043 cell line, as well as oncogene-induced senescence using inducible Ras in lung fibroblasts (IMR90, Ras-OIS), and replicative senescence in different cell lines, including different cell lineages (MRC5; lung embryonic fibroblasts) and from different age/gender donors (AG09602; female skin fibroblasts from 92 year old donor) and in premature senescence in Werner syndrome patient-derived skin fibroblasts (WS3141). For all models and in all phenotypes tested (morphology, SA-β-gal staining, mitochondrial accumulation and actin stress fibres), I observed results comparable with those seen in replicatively senescent HF043 fibroblasts above (Figure 4.11, only SRB morphology images shown for clarity). The panel of mTOR inhibitors in 4.10 was also tested on the range of senescence models in Figure 4.11 and the increased efficacy of pan-mTOR vs. mTORC1-specific inhibition was consistently observed. These results therefore indicate that acute pan-mTOR inhibition by treatment with AZD8055 at 70 nM for 7 days is sufficient to reverse several features of senescence including the enlarged, granular morphology characteristic of senescence, regardless of the model of senescence, or the specific pharmacological agent.

Figure 4.11: AZD8055 treatment rejuvenates morphology in a range of models of senescence

To model DNA damage induced senescence (DDIS), HF043 fibroblasts were treated with 20μM etoposide for 7 days. For oncogene-induced senescence (OIS), IMR90:ER-Ras fibroblasts were treated for 7 days with 1 μM 4-OHT to drive oncogenic Ras expression. For sirtuin inhibition induced senescence, HF043 fibroblasts were treated with 2 μM TnV6 for 7 days. To model replicative senescence in cells from multiple donors and cell lineages, AG09602 fibroblasts (skin fibroblasts, 92 year old female donor) and MRC5 fibroblasts (male fetal lung fibroblasts) were continuously cultured to replicative senescence. Finally, premature senescence was modelled using Werner Syndrome patient-derived fibroblasts (WS3141). Subsequently, senescent fibroblasts were treated with DMSO or 70 nM AZD8055 for 7 days, then fixed and stained for SRB and imaged using a digital EVOS microscope (n>3, representative data shown). Scale bar 100 μm.


DMSO
AZD8055
HF043 DDIS
AG09602 RS
MRC5 RS
IMR90 OIS
WS3141
Tnv6

4.4. Discussion

In this chapter, I have shown that short-term administration of AZD8055 can reverse morphological and biochemical phenotypes of senescence in human fibroblasts, including reduction in cell size and granularity accompanied by actin cytoskeleton reorganization, loss of SA-β-gal staining, loss of dysfunctional mitochondria and induction of mitophagy, reduction in nuclear enlargement and CCF incidence and reduction of pro-inflammatory secretion. These findings were validated in a range of models of senescence (i.e. different inducers) and in different cell types, and by using a panel of mTOR inhibitors. The universality of these findings suggest that these potentially deleterious phenotypes of senescence are consistently under mTORC control in senescence, underlining a crucial role for mTOR signalling in regulating cellular senescence. Such effects are likely to be thanks to inhibition of both mTORC1 and mTORC2, as mTORC1-selective inhibitors showed lesser effects. Importantly, cessation of treatment resulted in re-acquisition of such phenotypes, meaning that acute treatment does not permanently reverse senescence per se and is unlikely to overcome the barrier to tumorigenesis imposed by senescence. These findings also suggest that mTOR is constitutively active in senescent cells.

As important recent work has demonstrated a causal role for cellular senescence in the pathogenesis of age-related diseases (section 1.3.6), pharmacologic strategies to modulate the deleterious aspects of cell senescence, especially pro-inflammatory secretion, are likely to have beneficial consequences for organismal health during ageing. Results from several other laboratories have also shown that mTOR inhibition in senescent cells results in suppression of pro-inflammatory secretion, implicating IL1A and MAPKAPK2 translation as mechanistic targets for mTORC regulation of the SASP (Laberge et al., 2015, Herranz et al., 2015). My results are highly consistent with these data and provide further insight into the phenotypic consequences of mTORC1&2 inhibition in senescent cells.

The data presented in this chapter show that acute administration of mTOR inhibitors markedly altered senescent phenotypes in primary human fibroblasts. Importantly, levels of SA-β-gal, a marker of cellular senescence (Dimri et al., 1995) markedly dropped, on mTORC1 inhibition and even more so on pan-mTOR inhibition, suggesting that lysosomal metabolism shifted away from that characteristic of senescent cells. It may be possible that mTOR inhibition in senescent cells allows the re-acidification of lysosomes, and hence degradation of accumulated intra-lysosomal components. In addition, I observed a reduction in nuclear area and in CCF incidence following acute pan-mTOR inhibition in replicatively senescent fibroblasts. Recent research has suggested that CCFs can be recycled through autophagy (Ivanov et al., 2013) – indeed, I observed activation of autophagy upon AZD8055 treatment. It would be interesting to investigate whether the reduction in CCF incidence therefore results from improved nuclear structure (i.e. reduction in CCF formation) or through recycling (or possibly secretion) of cytoplasmic DNA. Recently, an intriguing link has been investigated between mTOR signaling and recognition of cytoplasmic DNA for activation of innate immune responses. Using Adenovirus infection to activate the cytosolic DNA sensor cGAS, it has been shown that the mTOR target S6K (especially the S6K1 isoform) is required for activation of the downstream transcription factor IRF3. Further, S6K1 physically interacts with activated STING, forming a S6K1-STING-TBK1 complex. Hence, S6K appears to be important for the induction of innate immune signaling following cytosolic DNA detection (Wang et al., 2016).

Furthermore, I found a very robust reversal of morphological phenotypes of senescence, from enlarged, flattened, amorphous cells to an elongated spindle morphology characteristic of low CPD proliferating skin fibroblasts, which was especially notable on pan-mTOR vs mTORC1 inhibition. The cell sizes observed following AZD8055 administration were entirely consistent with those reported for normal fibroblasts at low CPD and appear to be cell-intrinsic in both low CPD fibroblasts and senescent drug-treated cells, suggesting that pan-

mTOR inhibition may reset endogenous cell size regulation. Coincident with this marked alteration in size and shape, I observed a significant change in the organisation of the cytoskeleton, with loss of filamentous structures together with rearrangement of actin monomers from prominent stress fibres in control senescent cells to a central diffuse distribution with a higher proportion of globular actin upon treatment.

While pan-mTOR inhibition induced a marked reorganization of the actin cytoskeleton, mTORC1 inhibition (rapamycin, deforolimus, Figure 4.10) was less effective in reducing the incidence of actin stress fibres in senescent cells. Rapamycin and its analogues ('rapalogues') act allosterically through binding to the FKBP12 protein, which then associates with mTOR kinase and partially occludes the active site in mTORC1 (Caron et al., 2010). This results in biased inhibition of mTORC1 signalling, with strong inhibition through S6K, and only weak inhibition of other targets such as 4E-BP1. Prolonged treatment also results in indirect mTORC2 inhibition through cross-talk feedback with Akt (Figure 1.5). Second generation mTOR inhibitors such as AZD8055 have been designed instead to act as reversible ATP-competitive inhibitors that are highly specific for mTOR above other PI3K-family kinases and all other cellular kinases (Chresta et al., 2010), without affecting substrate preference. Indeed, while mTORC1 regulates a number of different pathways including protein translation and mitochondrial biogenesis (see 1.4.2, Figure 1.5), mTORC2 has an important role in regulating actin organization. Abrogation of mTORC2 activity leads to loss of phosphorylation of Rac/Cdc42 and downstream PAK; resulting in relief of inhibition of cofilin and causing a shift in the equilibrium of filamentous to globular actin (Sarbassov et al., 2004, Jacinto et al., 2004). However, it has been suggested that F-actin polymerisation, under the regulation of mTORC2, is critical for both short-term memory and long-term potentiation in the brain, raising the worrying prospect that long-term AZD8055 administration may impact on cognitive function (Huang et al., 2013). However, rapamycin (which on long-term treatment also induces mTORC2 inhibition through feedback loops) actually improves

learning and memory in older mice (Majumder et al., 2012). It remains to be seen whether AZD8055 is similarly beneficial to cognitive function, but it is already in clinical trials as an anti-cancer therapeutic, where any adverse side effects will have been noted. Therefore, my findings overall suggest that inhibition of both mTORC1 and mTORC2 may be necessary to elicit maximal cellular changes necessary to reverse senescent phenotypes, possibly through influencing cellular actin organization in conjunction with autophagy and control of transcription and translation. However, mTORC2 indirectly regulates mTORC1 activity through Akt, and rapamycin and deforolimus exert only partial mTORC1 inhibition. Therefore, due to the interplay between mTORC1 and mTORC2 complex activity and the multitude of downstream signalling components, a careful genetic analysis (e.g. using CRIPSR) may be required to dissect the roles of each complex in senescent phenotypes. My very preliminary experiments in this area suggested that knockout of Rictor (i.e. selective mTORC2 suppression) had effects similar to AZD8055 treatment in terms of rejuvenating senescent cell morphology, whereas Raptor knockout (mTORC1 suppression) showed little immediate morphological effect. However, this experiment was conducted only once (data not shown).

Cell viability in proliferating fibroblasts treated with AZD8055 for 48 hours was marginally diminished compared with controls, though no signs of toxicity were observed, suggesting a reduction in cell proliferation (supported by further cell counting data, not shown). This is likely to be a consequence, at least in part, of AZD8055 inhibition of protein synthesis, as its inhibition of mTORC1 then prevents both relief of translational inhibition by downstream target 4E-BP-1, as well as phosphorylation and activation of S6K, usually required for efficient translation. Indeed, AZD8055 treatment has been reported to alter the profile of translated mRNAs in the cell. In particular, a subset of mRNAs with a 5' terminal oligopyrimidine (TOP) tract are affected, such mRNAs include those encoding a host of ribosomal proteins together with cell cycle factors such as the replicative MCM helicases and

the sliding clamp PCNA (Jefferies et al., 1994). Hence factors required for increasing cellular mass through ribosomal biogenesis, and those directly involved in critical cell cycle processes such as DNA replication, are likely to be maintained at lower levels in mTORC-inhibited cells. This is explored in greater depth in Chapter 6. Consistent with this, I found significant alteration in phospho-4E-BP-1 isoforms on AZD8055 treatment that correlate with the decreased growth rates of treated cells (Figure 4.1). Previous work has implicated control of protein translation in establishment of senescence, as sub-toxic doses of the translation inhibitor cycloheximide were reported to increase the replicative capacity of primary human fibroblasts (Takauji et al., 2016). However, I found that acute treatment with sub-toxic doses of cycloheximide was insufficient to reverse the range of senescent phenotypes associated with mTORC inhibition (data not shown) suggesting that the effects of mTOR inhibition are mediated not only via direct effects on translation but also through further regulatory pathways.

Autophagy has been suggested as a potential mechanism by which mTORC1 inhibitors exert putative anti-ageing effects, as mTORC1 phosphorylates and inactivates the autophagy-initiating kinase ULK1 (Figure 1.3). Other approaches that stimulate autophagy can also improve health outcomes on ageing, such as spermidine suppression of immunosenescence in mice (Puleston et al., 2014). Furthermore, I observed induction of autophagy on pan-mTOR inhibition, together with increased co-localization of mitochondria with autophagosomes (Figure 4.6), suggesting activation of mitophagy. To validate activation of autophagy using the CYTO-ID assay, I used the lysosomal H^+ ATPase inhibitor Bafilomycin A1 to block autophagic flux, observing stabilization of autophagosomes following AZD8055 treatment. However, this control was not incorporated into the high content imaging mitophagy analysis and it is possible that the reduction in mitochondria observed was instead due to suppression of mitochondrial biogenesis on mTOR inhibition. Further, pan-mTOR inhibition appeared to decrease cell flattening in senescent fibroblasts (Figure 4.2);

therefore, z-stacking should also be incorporated into the analysis to check that the observed co-localization of mitochondria and LC3 puncta is due to mitophagy, rather than as a result of cell rounding. However, in accordance with the possible importance of autophagy in these data, I investigated whether stimulation of autophagy could be responsible for the rejuvenated phenotypes seen upon AZD8055 treatment of senescent cells. However, activation of autophagy by spermidine was insufficient to reverse the phenotypes of senescence analysed here (data not shown).

mTORC inhibition provides a highly promising route to improving the healthspan of older mammals: as well as increasing overall lifespan of mice (Harrison et al., 2009), many measures of health are improved on administration of the mTORC1 inhibitor rapamycin or other similar compounds to mice or humans (Mannick et al., 2014, 2018, Urfer et al., 2017, Majumder et al., 2012). Given the huge projected increase in age-related dementias with demographic change in Western populations, it is of particular importance that rapamycin increases brain blood flow, reduces amyloid tangles and plaques and improves cognitive function in mouse models of Alzheimer's disease (Spilman et al., 2010, Caccamo et al., 2010); it also shows promise in Parkinson's disease, other neurodegenerative disorders and potentially age-related decline in cognitive function distinct from disease (reviewed in Walters and Cox, 2018). Far from its original role as an immunosuppressant (at high dose), rapamycin actually improves immune function in response to antigenic challenges when used at lower doses; indeed, an orally-available derivative, RAD001, has good bioavailability and has shown promise in stimulating anti-viral immunity in older people on challenge with influenza vaccine (Mannick et al., 2014).

My work presented in this chapter adds to our understanding at the cellular level of how mTORC inhibition may be a useful strategy in combatting age-related diseases. Notably, I found that pan-mTOR inhibitors may be more potent and have more wide-reaching effects

on senescent phenotypes than the partial (S6K-biased) mTORC1 inhibition produced by rapamycin treatment. Excitingly, a study investigating everolimus treatment in combination with the pan-mTOR (and PI3K) inhibitor BEZ235 on immune function in elderly humans resulted in highly robust responses to vaccine challenge, with few side effects and improved infection control in the co-treated cohort lasting at least a year after treatment (Mannick et al., 2018). However, while BEZ235 has shown clinical benefit in combination treatment in this small cohort study and in larger phase III clinical trials for respiratory tract infections, I suggest that caution should be taken when progressing it further in the clinic, as its promiscuous inhibitory activity is not only effective against mTOR and PI3K, but also against important DNA damage sensor kinases such as ATR, which are critically important in responding to damage and potential oncogenic transformation. Hence this anti-ageing effect carries the risk of enhancing tumorigenesis.

5. Pan-mTOR inhibition delays but does not reverse replicative, DNA damage and sirtuin inhibition induced senescence

5.1. Introduction

Cellular senescence is a proliferation arrest programme characterized by marked phenotypic alterations and induction of pro-inflammatory secretion (the SASP - section 1.3). Senescence can be induced by a range of stimuli including oncogene activation, exhaustive telomere attrition (Figure 1.2), and TnV6-mediated sirtuin inhibition, as revealed in Chapter 3. Senescence can also be induced by proximity to other senescent cells through a bystander mechanism mediated through the pleiotropic paracrine effects of the senescent pro-inflammatory phenotype (Nelson et al., 2012, Acosta et al., 2013) as well as through juxtacrine mechanisms (Hoare et al., 2016). Furthermore, loss or mutation of critical DDR components, such as the WRN helicase/exonuclease, predispose to premature cellular senescence *in vitro* and premature ageing phenotypes *in vivo* (Werner syndrome, WS, section 1.3.3.4.3). WRN is implicated in dissociating complex structures such as Holliday junctions that arise as products of homologous recombination (Saintigny et al., 2002), in repairing stalled DNA replication forks (Pichierri et al., 2001, Rodríguez-López et al., 2002) and in telomere maintenance (Crabbe et al., 2004, Reddy et al., 2010), promoting replication through complex DNA structures such as the T/D loops and G-quartets through its helicase activity (Opresko et al., 2005, Ahn et al, 2009), whilst suppressing recombination between highly repetitive sequences.

Cell senescence provides a crucial barrier to tumorigenesis, firstly as a proliferation arrest mechanism activated upon recognition of cellular stress or damage (Campisi, 2013) and secondly through releasing pro-inflammatory cytokines and chemokines, thus contributing to tumour immunosurveillance (Kang et al., 2011). However, failure to clear senescent cells results in a state of chronic inflammation, and the SASP exerts pleiotropic, paracrine pro-tumorigenic effects (see 1.3.6). Indeed, cancer cells employ strategies to circumvent senescence (Hanahan and Weinberg, 2000; 2011). For example, telomere attrition and thus

replicative senescence can be counteracted by expression of telomerase or through the ALT (alternative lengthening of telomeres) pathway, which relies on homology-directed telomere extension (Bodnar et al., 1998). Furthermore, depletion of factors involved in orchestrating the proliferation arrest such as p53, Rb and p16 result in prevention of senescence (Beauséjour et al., 2003). Accordingly, these senescence-promoting factors serve important roles as tumour suppressor genes (TSG).

In Chapter 4, I demonstrated that acute pan-mTOR inhibition resulted in reversal of morphological enlargement, mitochondrial accumulation, stress fibre production, pro-inflammatory secretion and lysosomal dysfunction in senescent fibroblasts (Walters et al., 2016). Release from pan-mTOR inhibitor treatment resulted in re-acquisition of senescent phenotypes, suggesting that mTOR is chronically active in senescent cells, driving hypertrophic phenotypes in the absence of proliferation (Figure 4.9). Furthermore, previous work has suggested that mTOR signalling may be required for induction of proliferation arrest in cellular senescence (Kolesnichenko et al., 2012, Lerner et al., 2013, Leontieva and Blagosklonny, 2016). However, many of these experiments have reported only mild effects of delaying senescence on mTOR inhibition and have largely focused on rapamycin treatment; notably, I found the mTORC1 inhibitors rapamycin and deforolimus less effective in reversing senescent phenotypes than AZD8055, which targets both mTORC1 and mTORC2 (Figure 4.10). Further, several reports have used artificial systems, such as highly aggressive cancer cell lines where p21 upregulation is driven by addition of IPTG to enforce cell cycle arrest (Leontieva and Blagosklonny, 2016). It could be argued that such systems do not sufficiently recapitulate senescence induction in primary cells *in vivo*. Further, testing compounds such as mTOR inhibitors which interfere with protein translation is not scientifically valid in model systems reliant on upregulation of translation to enforce senescence.

Cellular senescence is antagonistically pleiotropic: the induction of proliferation arrest in response to genotoxic or other damaging stimuli is an important tumour suppressor mechanism (Sharpless et al., 2002), but the deleterious aspects of senescent cells which accumulate *in vivo* drive pathological ageing (Baker et al., 2016). Any therapeutic intervention to promote healthy ageing through targeting senescent cells should therefore blunt the deleterious aspects of senescence without compromising its tumour suppressor functions. While pan-mTOR inhibitor treatment is promising in terms of reversing a range of features of senescence (Chapter 4), in order to serve as a useful potential therapeutic, it must not carry significant pro-tumorigenic risk, particularly by permitting re-proliferation of cells that have entered 'deep' senescence.

5.2. Chapter aims

In this chapter I set out to address the following questions:

1. Does mTOR inhibition permit senescent cells to re-enter the cell cycle?
2. Does mTOR inhibition prevent or delay entry into senescence?
3. If so, can mTOR inhibition delay entry into premature senescence in models of premature ageing?

To answer these questions, I used a number of models of cell senescence in primary human fibroblasts and the pan-mTOR inhibitor AZD8055, which is highly selective for mTOR over other PI3K family kinases (Chresta et al., 2010).

5.3. Results

5.3.1. Deeply senescent cells do not re-start proliferation on extended pan-mTOR inhibition

As cellular senescence constitutes an important barrier to tumorigenesis by preventing the propagation of potentially compromised cells, I investigated whether pan-mTOR inhibition could result in re-entry into the cell cycle in cells that had already undergone replicative or DNA damage-induced senescence (DDIS) i.e. primary human fibroblasts (HF043) that were deeply replicatively senescent. For RS, I defined this as cells at very high CPD which had failed to proliferate for >1 month in culture, and for DDIS as previously proliferative HF043 that had been induced to undergo DDIS by 7 day treatment with 20 μM etoposide (section 2.1.2) followed by a further week without drug to ensure 'deep' senescence.

These 'deeply' senescent fibroblasts were seeded into 96-well plates, and subsequently treated with the pan-mTOR inhibitor AZD8055 (0-100 nM) for 28 days in continuous culture (doses chosen according to my previous optimisation/toxicity studies, Chapter 4). Cells were re-fed with complete medium supplemented with fresh drug or DMSO (vehicle control) every 7 days and monitored by microscopy throughout the experiment duration (Figure 5.1A). To assess proliferation, cells were incubated with the resazurin dye, alamarBlue, which measures reducing capacity (Figure 5.1B, C); this can be used as a proxy for cell number/viability. Rather than any increase in reducing capacity, which would have indicated increased cell number and hence re-proliferation, I instead observed that extended treatment of deeply replicatively or DNA damage-induced senescent primary fibroblasts with AZD8055 actually induced a mild dose-dependent reduction in alamarBlue staining and hence viability. These data indicate that pan-mTOR inhibition, at least within this dose range, is not sufficient to compromise proliferation arrest in deeply senescent primary fibroblasts and therefore, does not 'reverse' senescence.

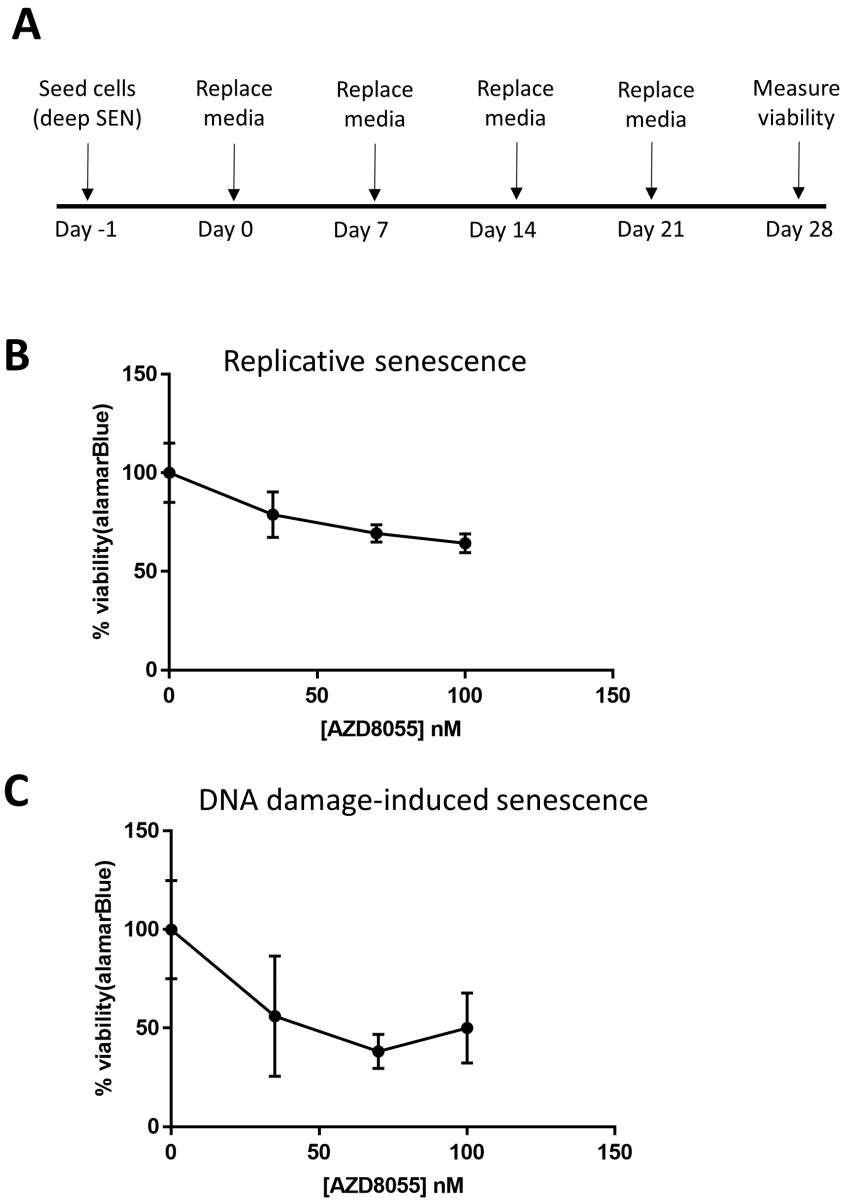


Figure 5.1 Pan-mTOR inhibition does not compromise proliferation arrest in deeply senescent fibroblasts

A: schematic depicting experimental design in which deeply replicatively senescent HF043 fibroblasts (failed to proliferate for > 1 month in culture) and DNA damage-induced senescent fibroblasts (7 days 20 μM etoposide followed by an additional 7 day incubation in drug-free media) were seeded into 96-well plates and treated with a dose range of AZD8055 for 28 days (0-100 nM; fresh media with DMSO or drug treatment supplemented every 7 days). B, C: cell viability was assessed following extended treatment in the replicatively senescent fibroblasts (B) and DDIS fibroblasts (C) by the alamarBlue assay (error bars represent SD between 4 technical replicates from representative experiment of n=3).

While the reduction in metabolic capacity measured following AZD8055 treatment could be indicative of a senolytic effect, it may also reflect the reduction in cell size (and therefore metabolic capacity per cell) induced on pan-mTOR inhibition, as observed previously (see Chapter 4). Indeed, SRB staining and manual inspection by microscopy did not reveal evidence of cytotoxicity in deeply senescent fibroblasts following extended AZD8055 treatment (data not shown).

5.3.2. Extension of primary human fibroblast replicative capacity on continuous or pulsed pan-mTOR inhibition

As I had observed that pan-mTOR inhibition was insufficient to reverse proliferative arrest in deeply senescent fibroblasts, I next investigated whether AZD8055 could instead prevent cells from entering senescence. This work had already begun in the host lab, which showed that control fibroblasts (DMSO) proliferated rapidly at low CPD, before gradually slowing and reaching replicative senescence at CPD ~90 after ~200 days of continuous culture (Figure 5.2A). In addition, treatment with 35 nM AZD8055 led to slower rates of proliferation (consistent with the negative impact of mTOR inhibition on protein synthesis and hence proliferation rates (see also Figure 4.1)), but while proliferation rates did gradually decrease further, fibroblasts treated continuously with AZD8055 did not undergo replicative senescence at CPD 90 like the control DMSO populations however, but instead slowly continued proliferating for a number of further divisions. Indeed, AZD8055-treated fibroblasts reached >CPD 110 before the experiment was terminated, corresponding to over 20 additional population doublings compared to the control populations (Figure 5.2A, data courtesy of Prof. Lynne Cox, University of Oxford). Hence AZD8055 appeared to prevent entry into senescence.

However, the additional 20 population doublings afforded by AZD8055 treatment occurred at extremely slow rates, requiring nearly 300 days of continuous tissue culture (Figure 5.2A).

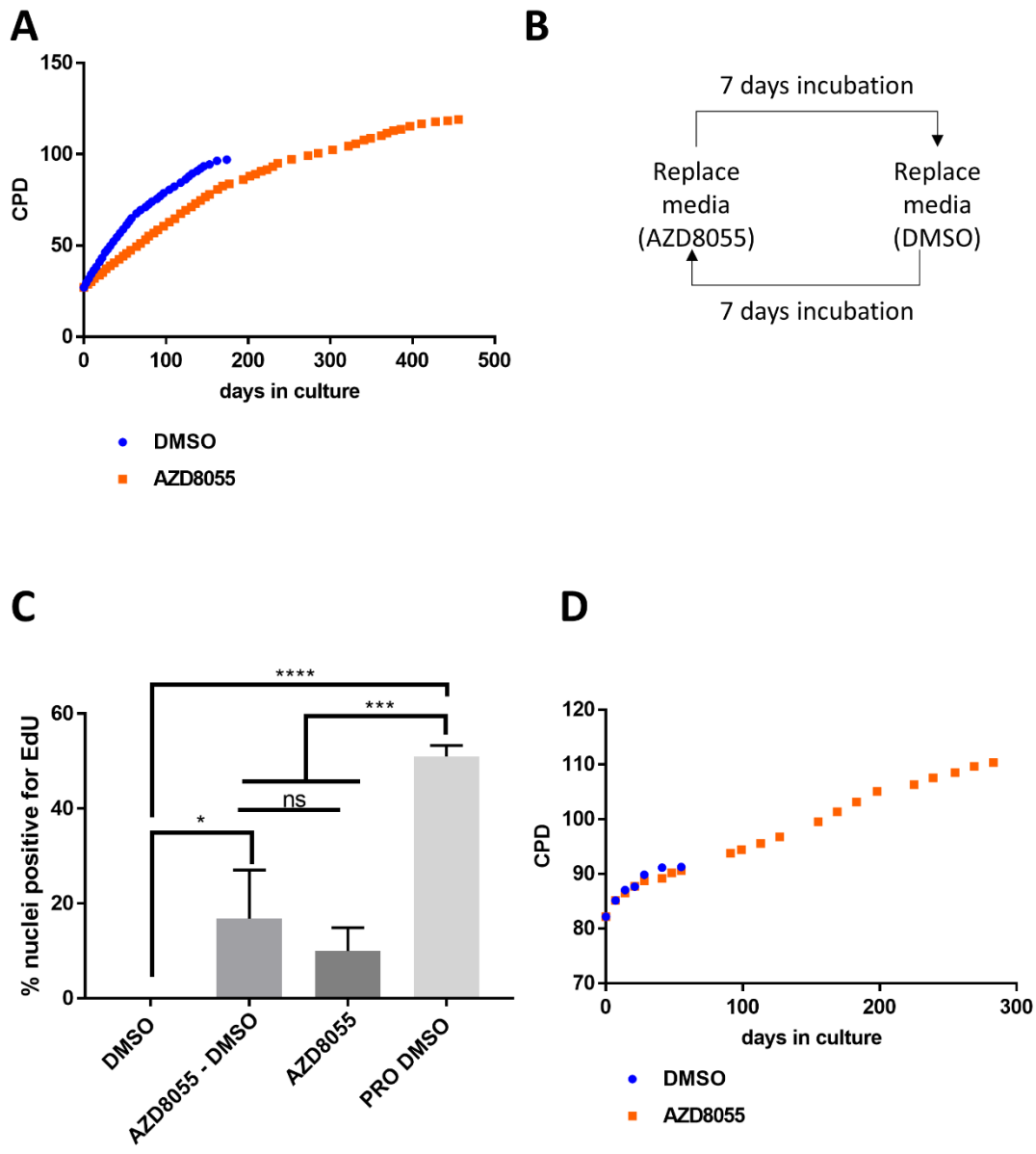
I hypothesized that due to the inhibitory effect of mTOR inhibition on cell cycle progression (Figure 4.1, Figure 5.2A), pulse-dosing of AZD8055 would increase cell cycle progression even in fibroblasts at high CPD. Indeed, pulse-dosing *in vitro* may better approximate intermittent treatment in the clinic (i.e. dosing less than once daily), which is associated with increased treatment adherence due to reduced side effects and improved convenience (Kruk and Schwalbe, 2006).

To this end, I developed a pulse-dosing regimen where fibroblasts at high CPD (>80) were treated with AZD8055 for 7 days, followed by a 7 day drug-free 'recovery' period (DMSO only, Figure 5.2B). To analyse whether pulse-dosing improved cell cycle progression, I measured the proportion of cells undergoing S phase over an 18 hour labelling window using Click-iT EdU staining, in pulse-dosed and control fibroblasts at extremely high CPD, alongside DMSO-only treated controls at low CPD. Indeed, I observed EdU incorporation in ~50% of the nuclei of untreated fibroblasts at low CPD (Figure 5.2C), consistent with previously observed proliferation rates (e.g. ~0.6 PD/day, Figure 3.3). Untreated fibroblasts at extremely high CPD exhibited very little EdU incorporation, but during AZD8055 pulse-dosing (analysed at 7 days AZD8055), EdU incorporation was significantly increased (Figure 5.2C). Further, I observed that upon release from drug treatment (analysed following 1 day release from AZD8055 treatment, (AZD8055-DMSO, Figure 5.2C), EdU incorporation was increased yet further, albeit not in a statistically significant manner, possibly due to the low proliferation rates in treated fibroblasts at high CPD. These data therefore suggested that pulse-dosed AZD8055 treatment increases cell cycle progression in high CPD fibroblasts (Figure 5.2C).

While the above data (Figure 5.2A) revealed that AZD8055 treatment extended the proliferative capacity of cells treated continuously from low CPD, any potential use of AZD8055 for ageing indications would require use in elderly populations, with cells presumably at later CPD (according to leukocyte telomere length analysis, (Sanders and Newman, 2013), though the source of senescent cells in elderly patients is still yet to be fully understood). Therefore, I performed a longitudinal culture study starting with primary cells at high CPD, with weekly pulse dosing to test whether the enhanced cell cycle progression observed on pulse-dosing at high CPD (Figure 5.2C) reflected greater overall proliferative capacity on mTOR inhibition. Consistent with the previous longitudinal experiment (Figure 5.2A), control (DMSO) fibroblasts grown in culture from high CPD completed several population doublings before undergoing replicative senescence at just over CPD 90 (Figure 5.2D). However, when AZD8055 pulse-dosing was performed from high CPD, cells continued to proliferate beyond CPD 90, with primary fibroblasts again undergoing ~20 additional population doublings (Figure 5.2D). These additional 20 population doublings occurred within ~200 further days, indicating an increase in overall proliferation rates, even at extremely high CPD, compared to on continuous drug treatment (Figure 5.2).

Figure 5.2. Pan-mTOR inhibition extends replicative capacity of human primary fibroblasts

A: data collected by Professor Lynne Cox. HF043 fibroblasts were passaged continuously from low CPD (<30) in the presence of either DMSO (blue) or 35 nM AZD8055 (orange) in complete media. At every passage, CPD was calculated and recorded against time in culture. Representative data from n=3 experiments shown. B: schematic depicting pulse-dosing regimen, where fibroblasts were treated with AZD8055 for 7 days before 7 days incubation with vehicle only (DMSO) media. C: HF043 fibroblasts at high (>80) and low (<50) CPD were treated with either vehicle only DMSO, or pulse-dosed with AZD8055 according to B. Cells were analysed by Click-iT EdU incorporation (18 hour labelling window) at high CPD (~90) following 7 day AZD8055 treatment, 7 day AZD8055 + 1 day DMSO (pulsed) or vehicle only control (over 50 nuclei analysed per technical replicate (n=3), representative data shown from one of three independent experiments shown). One-way ANOVA and Tukey test used to compare means between each group used for statistical analysis (* $p<0.05$, *** $p < 0.001$, **** $p < 0.0001$, ns not significant). D: HF043 fibroblasts from high CPD (>80) were passaged continuously in culture, either in the presence of DMSO or pulse-dosed according to B. Data from one representative experiment shown (n=3).



These data therefore indicate that although pan-mTOR inhibition does not reverse proliferation arrest in deeply senescent fibroblasts (Figure 5.1), AZD8055 treatment – either continuously or on pulse-dosing – can delay the induction of senescence, even when treatment is initiated close to the replicative limit. Further, these data are consistent between two experimental designs and researchers. Importantly, if the pulse-dosing regimen was terminated in fibroblasts at CPD >90 (i.e. >7 days DMSO-only media) cells failed to proliferate further, indicating that delaying induction of replicative senescence was

dependent on near-continuous AZD8055 treatment (data not shown) and does not reflect a switch to an unregulated pro-proliferative phenotype.

Since I had revealed that acute AZD8055 treatment disrupts a range of features of senescence, I therefore investigated whether pulse-dosing also delayed the induction of senescence phenotypes. AZD8055-treated cells and DMSO vehicle control fibroblasts at extremely high CPD (~90) were assessed for morphological enlargement and SA-β-gal staining, two robust features of senescence. As anticipated, control (DMSO only) fibroblasts exhibited enlarged, granular morphology characteristic of senescence, together with strong SA-β-gal staining (Figure 5.3). However, pulse-dosed fibroblasts during treatment with 70 nM AZD8055 remained spindle-shaped and did not stain positively for SA-β-gal; features that are reminiscent of untreated fibroblasts at low CPD (Figure 5.3). Therefore, these data suggest that AZD8055 treatment not only delays the induction of replicative senescence of primary fibroblasts, but also prevents the induction of canonical phenotypes of senescence even at extremely high CPD, though notably, such phenotypes were marginally re-acquired in DMSO-only media in pulse-dosing (data not shown).

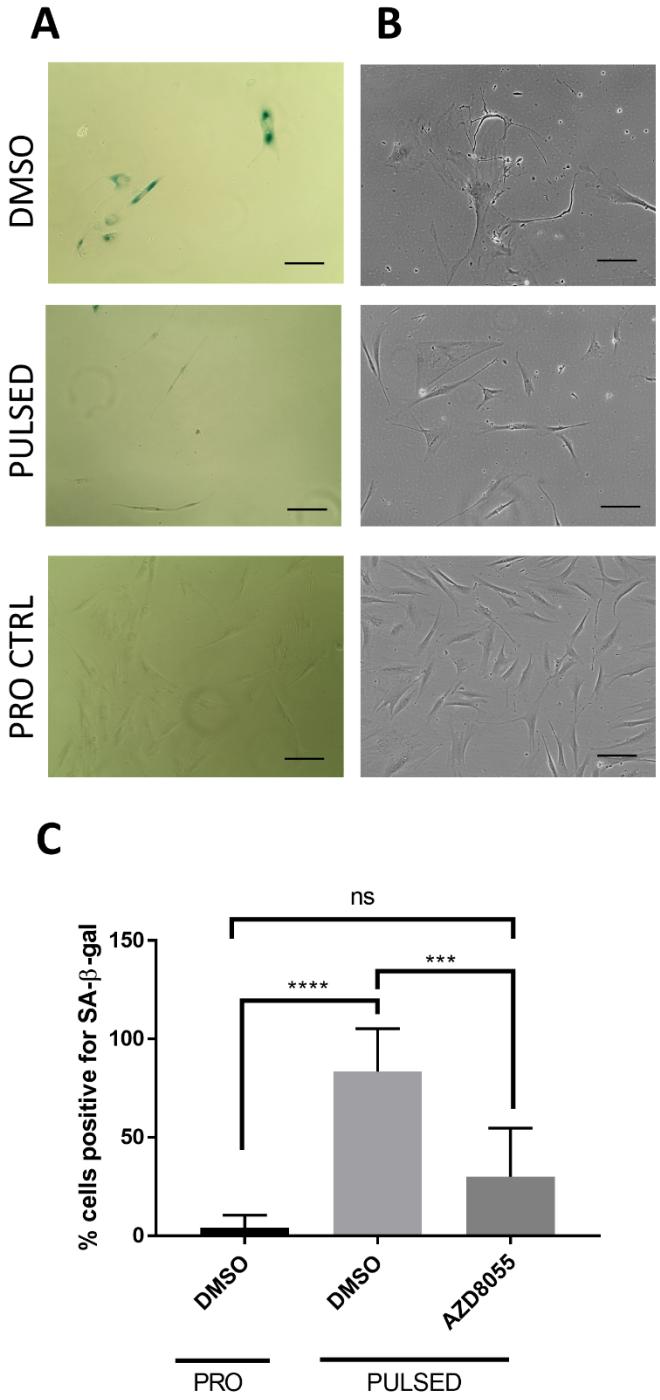


Figure 5.3 Pan-mTOR inhibition prevents induction of senescence phenotypes

Untreated proliferating fibroblasts as well as pulse-dosed (examined following 7 days AZD8055 treatment at 70 nM) and vehicle only HF043 fibroblasts at CPD $\geq$ 90 were A: stained for SA-β-gal (with quantification in C) and B: examined live for morphology by phase contrast microscopy. C: statistical analysis was performed using one way ANOVA with Tukey test for multiple comparisons, ****; $p<0.0001$, ***; $p<0.001$, ns; not significant. Representative data shown from n>3 experiments. Scale bar 100 μm.

5.3.3. Pan-mTOR inhibition does not result in dramatic telomere elongation despite extension of replicative capacity

Replicative senescence has been attributed to exhaustive telomere attrition (Bodnar et al., 1998), yet I observed that pan-mTOR inhibition substantially increased the replicative capacity of primary fibroblasts *in vitro*. I therefore hypothesized that the molecular basis for this increase might involve either telomere extension or a delay in telomere attrition. To investigate this hypothesis, I employed two different techniques for telomere analysis: teloFISH and Southern blotting. In teloFISH, PNA probes complementary to telomeric ends are used to stain telomeric DNA in fixed cells, with either an internal centromere PNA probe or total DNA (Hoechst 33342) used as a normalization control (Rossiello et al., 2013). TeloFISH therefore allows analysis of telomere length at the single cell (and even single telomere) level. Following fixation and FISH staining, telomeres and centromeres of individual chromosomes appear as foci within interphase nuclei (Figure 5.4D) and signal intensity can be quantified using FIJI image analysis software (Figure 5.4 A-C).

Telomere analysis by Southern blotting requires purification of a substantial amount ($\geq$ 1 µg) of genomic DNA for digestion with restriction endonucleases (Rsa I, Hinf I) that selectively digest non-telomeric gDNA. The remaining DNA (i.e. telomeric) is run on a high-resolution agarose gel, and then transferred to a nylon membrane by Southern blotting. The DNA fragments can then be hybridized to a digoxigenin (DIG)-labelled probe specific for telomeres, and then incubated with a DIG-specific antibody covalently attached to alkaline phosphatase, for chemiluminescence detection. The resulting smear of signal indicates the location of the immobilized telomere probe, corresponding to the TRF (telomere restriction fragment) length, determined by reference to specific molecular weight markers and again quantified using FIJI (Kimura et al., 2010, Figure 5.5). While Southern blotting is more experimentally laborious and requires a large number of cells for analysis, analysis is not

dependent on nuclear/centromeric morphology which may be disrupted upon senescence (Lenain et al., 2015, Hédouin et al., 2017).

Firstly, I used both assays to investigate whether telomere attrition occurred during continuous passaging of HF043 fibroblasts in the absence of AZD8055 treatment (Figure 5.4A, 5.5A). Indeed, teloFISH staining showed a reduction in the size of telomeric foci with increased CPD (images shown in Figure 5.4D), with the fraction of nuclear area positive for telomeric foci falling from a mean per nucleus of ~0.5 at low CPD (CPD 49) to <0.1 at replicative senescence (CPD 93, Figure 5.4A). Southern blotting also revealed a reduction in TRF length and signal intensity at high CPD (CPD 85 and CPD 90, Figure 5.5A) in comparison with control immortalized cells (Figure 5.5A 'CTRL') or primary fibroblasts at low CPD (Figure 5.5A CPD 40, CPD 50). Densitometry-based quantification showed the mean TRF length at CPD 40 was 3.19 kb, in comparison with 2.08 kb at CPD 90 (Figure 5.5A).

To test whether AZD8055 treatment impacts on telomere length, I compared acute (7 day) and long-term (pulse-dose) treatment. Unsurprisingly, no significant change in the size of telomere foci or TRF length was observed on acute AZD8055 treatment, irrespective of CPD of the cells treated as assessed using both Southern blotting and teloFISH (Figure 5.4B, 5.5B). Hence short-term AZD8055 treatment does not induce detectable changes in telomere length. Telomere attrition *in vivo* is a gradual process occurring over multiple cell cycles, hence I examined whether the observed extension of primary fibroblast replicative capacity (Figure 5.2D) on long-term pulse-dosing with AZD8055 could be accounted for by amelioration of telomere attrition at high CPD. Using teloFISH, I observed no significant difference in telomere foci (indicative of length) between control (DMSO) fibroblasts at replicative senescence (~CPD 90) and AZD8055 pulse-dosed fibroblasts (CPD >90), with telomeres from both populations appearing as very small foci; this finding was consistent over three biological replicates (Figure 5.4C). By Southern blotting however, I observed a

weak signal corresponding to an extremely short average TRF length for control cells at replicative senescence (TRF = 1.97kb, Figure 5.5C) while the TRF signal for AZD8055 pulse-dosed cells appeared stronger in intensity and at marginally higher molecular weight, again consistent over three separate biological replicates (TRF = 2.39 kb, Figure 5.5C). However, the TRF signal observed from pulse-dosed fibroblasts (CPD >90) was still substantially shorter and weaker in signal intensity than the signal from hTERT-immortalized control DNA (Figure 5.5C), which was comparable in length and intensity to primary fibroblasts at low CPD ('CTRL' and CPD 40; Figure 5.5A).

While these findings indicate that AZD8055 treatment does not increase telomere length in cells very close to senescence, extended treatment may stabilize telomere length at extremely high CPD. These findings are consistent with the slow rates of proliferation observed upon extended AZD8055 treatment at extremely high CPD (Figure 5.2A, D) rather than the proliferation kinetics (and long telomeres) associated with immortalized cells, and with the observation that treatment cessation results in progression into senescence (Walters et al., 2016 and data not shown). However, these findings were inconsistent with teloFISH analysis, perhaps as the normalization of telomere signal in FISH relies on internal standards (nuclear or centromere staining) which are themselves altered upon entry into senescence (Lenain et al., 2015, Hédouin et al., 2017). Importantly, these data do not show that telomerase is necessarily activated upon AZD8055 treatment; alternatively, the potential protection in telomere length observed could be accounted for by selection pressure for cells yet to undergo exhaustive telomere attrition. Alternatively, AZD8055 treatment, which slows the cell cycle and promotes autophagy, may also promote repair of DNA damage and hence protect telomeric integrity, consistent with my preliminary data on reduction in DNA damage markers on AZD8055 treatment (see Figure 5.11 below). Future analysis should include TRAP assays for telomerase enzyme activity as well as co-immunofluorescence for markers of the DNA damage within the telomeres.

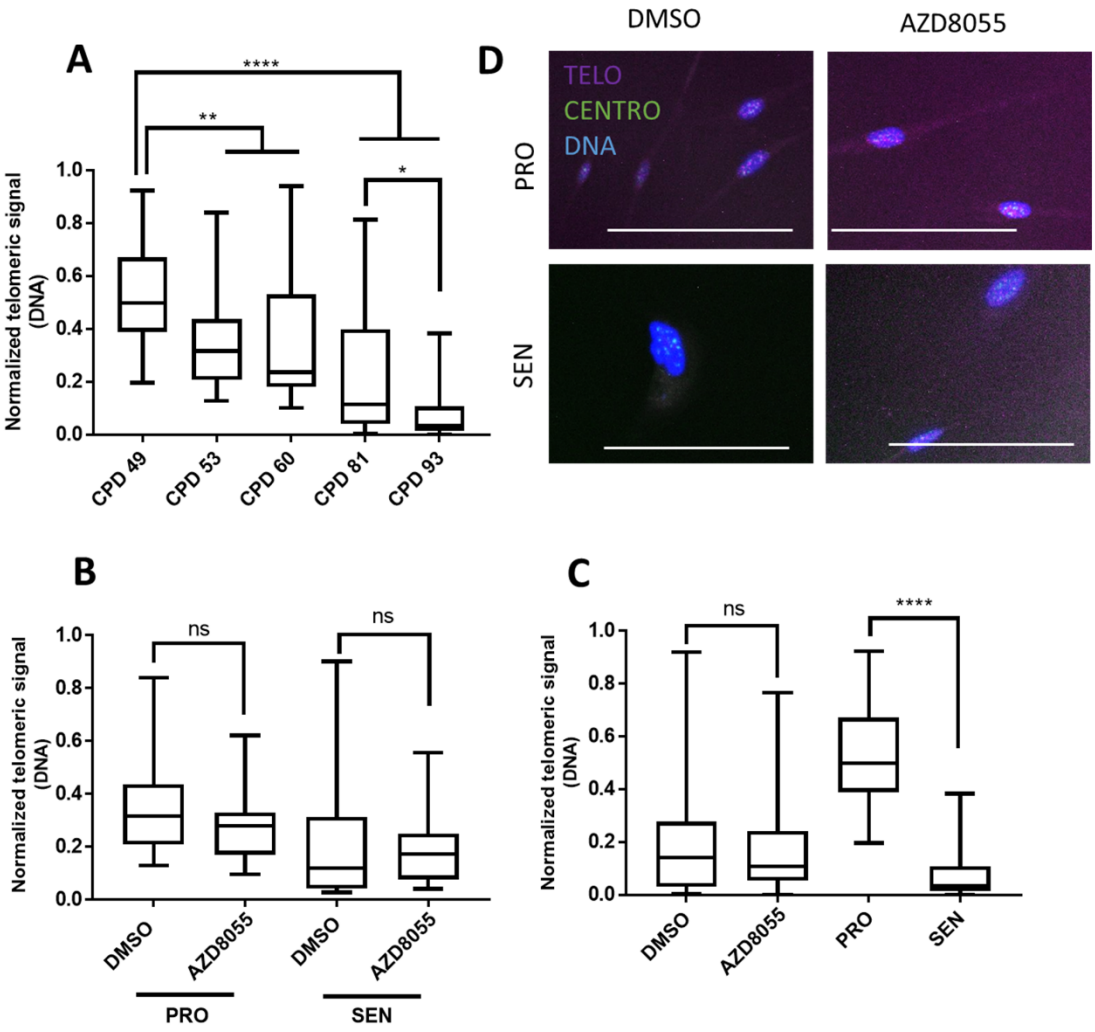


Figure 5.4: Telomere assessment over continuous passaging with and without AZD8055 treatment by TeloFISH

A-D: HF043 fibroblasts at indicated CPD and treatment were seeded onto poly-L-lysine coverslips before fixation and staining, with PNA FISH probes against telomeric (magenta) and centromeric (green) DNA, and Hoechst 33342 for DNA (blue). Nuclei were imaged using a ZOE fluorescent cell imager and telomeric signal intensity per nucleus was quantified using FIJI (A, B, C: quantification, D: representative images). One-way ANOVA with Tukey test for multiple comparisons were used for statistical analysis (*p<0.05, ** p<0.001, **** p< 0.0001, ns not significant). At least 30 nuclei were analysed per sample. A-C one representative dataset shown from B. Representative data shown from C: n=3 and A: n=2 independent experiments. Scale bar 100 μm.

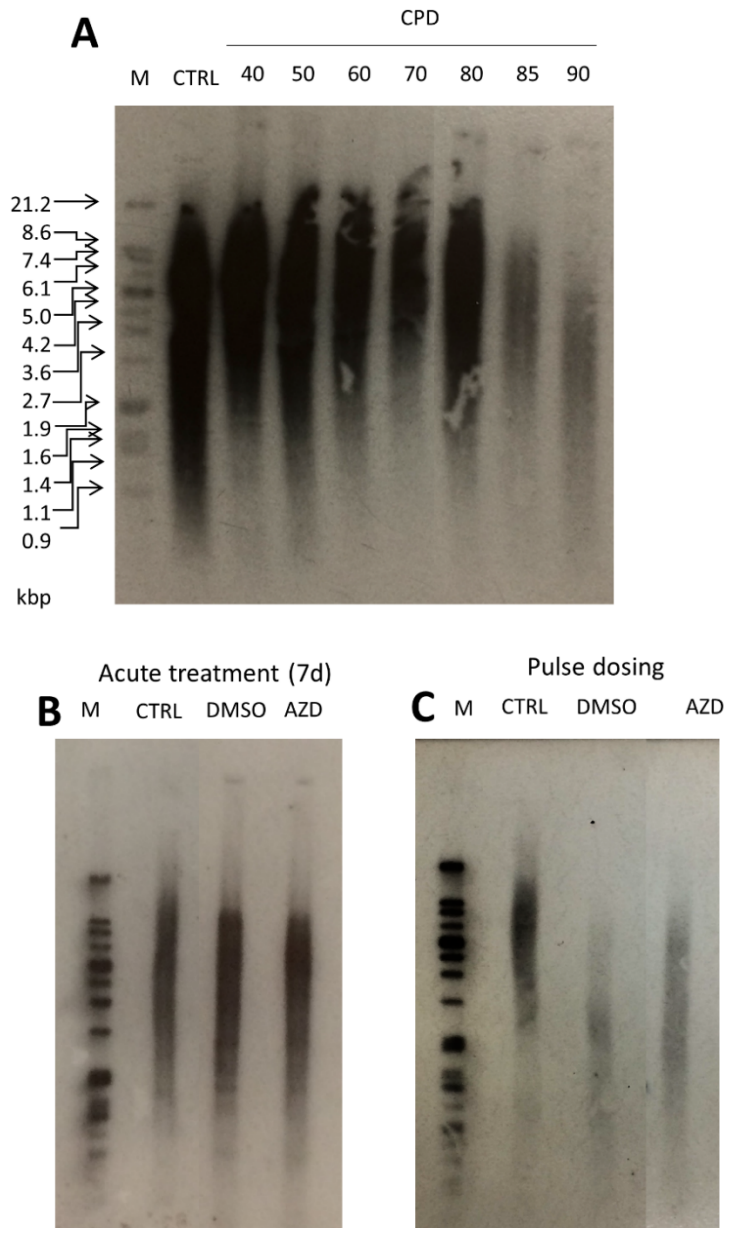


Figure 5.5: Telomere assessment over continuous passaging with and without AZD8055 treatment by Southern blotting

For Southern blotting, genomic DNA was harvested from cells at indicated CPD and treatment, digested to TRF fragments and run on an agarose gel for telomere probing using α-DIG AP, with molecular weight markers of indicated length and control gDNA taken from an hTERT-immortalized cell line ('CTRL'). FIJI was used to quantify TRF length according to manufacturer's instructions; A: CPD 40 3.19 kb; CPD 50 2.90 kb; CPD 60 3.50 kb; CPD 70 4.41 kb; CPD 80 3.39 kb; CPD 85 2.77 kb; CPD 90 2.08 kb; B: DMSO 3.20 kb; AZD8055 3.18 kb; C: DMSO 1.97 kb; AZD8055 2.39 kb. n=3, paired student t-test showed no significant difference between signal in B or C over n=3 independent experiments (mean increase in TRF length on pulse-dosing 1.35-fold, p=0.1662). Note that C shows parts of the same blot cropped together to show the relevant drug-treated and control populations alongside each other.

To further investigate the molecular basis of the delay to entering replicative senescence observed on pan-mTOR inhibition, I next analysed expression of the CKI p21, which is upregulated to enforce cell cycle arrest following detection of DNA damage and p53 activation (Figure 1.2). Cells at high CPD (>CPD 85) and low CPD controls (<CPD 50) were treated for 24 hours with 70 nM AZD8055 or vehicle control (DMSO), before analysis by Western blotting for p21, with GAPDH used as an internal loading control. I observed that p21 levels were increased in control fibroblasts at high CPD compared with untreated fibroblasts at low CPD (Figure 5.6). However, 24 hour treatment with AZD8055 attenuated the upregulation of p21 in fibroblasts at high CPD. These data suggest that mTOR may delay entry into replicative senescence through regulating the expression of the cyclin kinase inhibitor p21 as well as through stabilization of telomere length.

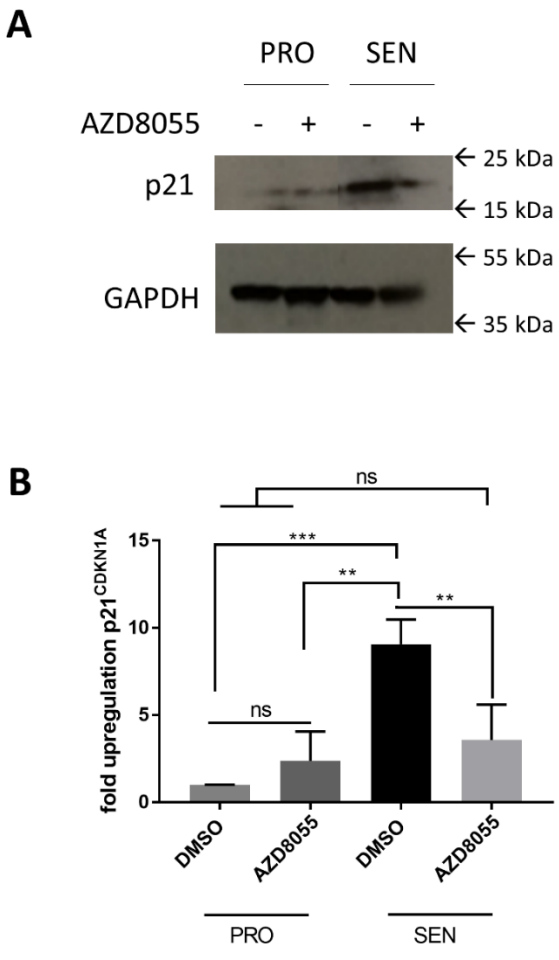


Figure 5.6 AZD8055 treatment prevents p21 upregulation in high CPD fibroblasts

High CPD (>85, 'SEN') and low CPD (<50, 'PRO') HF043 fibroblasts were treated with AZD8055 (70 nM) DMSO control for 24 hours in culture, then cells were lysed for Western blotting against $p21^{CDKN1A}$ with GAPDH loading control (representative data shown in A and quantification of 3 independent biological repeats in B, *** p<0.001, **p<0.01, ns not significant, one way ANOVA with Tukey test for multiple comparisons). Note that in A, two parts of the same blot have been cropped together to show the relevant lanes.

5.3.4. Premature senescence in Werner syndrome fibroblasts is attenuated by pan-mTOR inhibition

The above data demonstrate that AZD8055 treatment cannot reverse senescence, but delays entry into replicative senescence in normal ('wild-type') primary human fibroblasts in culture, without dramatically extending telomere length, or immortalizing the fibroblasts. Premature cellular senescence *in vitro* due to loss or mutation of the WRN helicase/exonuclease WRN correlates with premature ageing *in vivo* in Werner syndrome, where an increased senescent cell load is likely to contribute to age-related disease susceptibility (reviewed in Cox and Faragher, 2007). I therefore investigated whether AZD8055 was sufficient to delay premature senescence in the Werner syndrome patient-derived fibroblast line AG03141 (hereafter referred to as WS3141 for clarity), derived from a patient with a nonsense mutation resulting in truncation of the WRN mRNA prior to the nuclear localization sequence coding region at the 3' end of the transcript. By Western blotting, WRN protein is barely detectable in these fibroblasts, indicating that nonsense-mediated decay of WRN mRNA may result in an essentially null phenotype (data not shown). While these patient-derived fibroblasts proliferate extremely slowly and undergo senescence prematurely in culture, we have previously observed that hTERT immortalization or SV40 transformation rescues these phenotypes and restores normal proliferation kinetics (S. Gover, personal communication).

Due to the extreme sensitivity and scarcity of these fibroblasts, it was not possible to source sufficient material to conduct a full battery of investigations. Instead, I decided to investigate whether continuous AZD8055 treatment was sufficient to delay induction of premature senescence (Figure 5.7A). As anticipated, control (DMSO) WS3141 fibroblasts proliferated very slowly, undergoing only a few doublings before ceasing proliferation at ~CPD 8, after >100 days in culture. Cells were then periodically re-fed and maintained *in vitro* for the full duration of the experiment, but failed to proliferate further. Untreated WS3141 fibroblasts also strongly stained for SA-β-gal and exhibited classic senescent morphology (Figure 5.8). However, upon continuous treatment with AZD8055 (35 nM or 70 nM) WS3141 cells initially proliferated more slowly (consistent with data from wild-type fibroblasts, Figure 5.2A) but continued to proliferate beyond the point at which controls had undergone senescence, reaching CPD >18. Indeed, continuous AZD8055 treatment substantially delayed entry into senescence, more than doubling the replicative capacity of DMSO-treated fibroblasts. Continuous proliferation on AZD8055 treatment but not in vehicle-only media beyond CPD 8 in WS3141 fibroblasts was confirmed by Click-iT EdU analysis (Figure 5.7A, B). Further, treated fibroblasts did not stain positively for SA-β-gal unlike DMSO controls, and exhibited spindle-like fibroblastic morphology throughout their replicative capacity (Figure 5.8) thus restoring wild-type, low CPD phenotypes to patient cells consistent with my previous observations from wild-type fibroblasts (Figure 4.11).

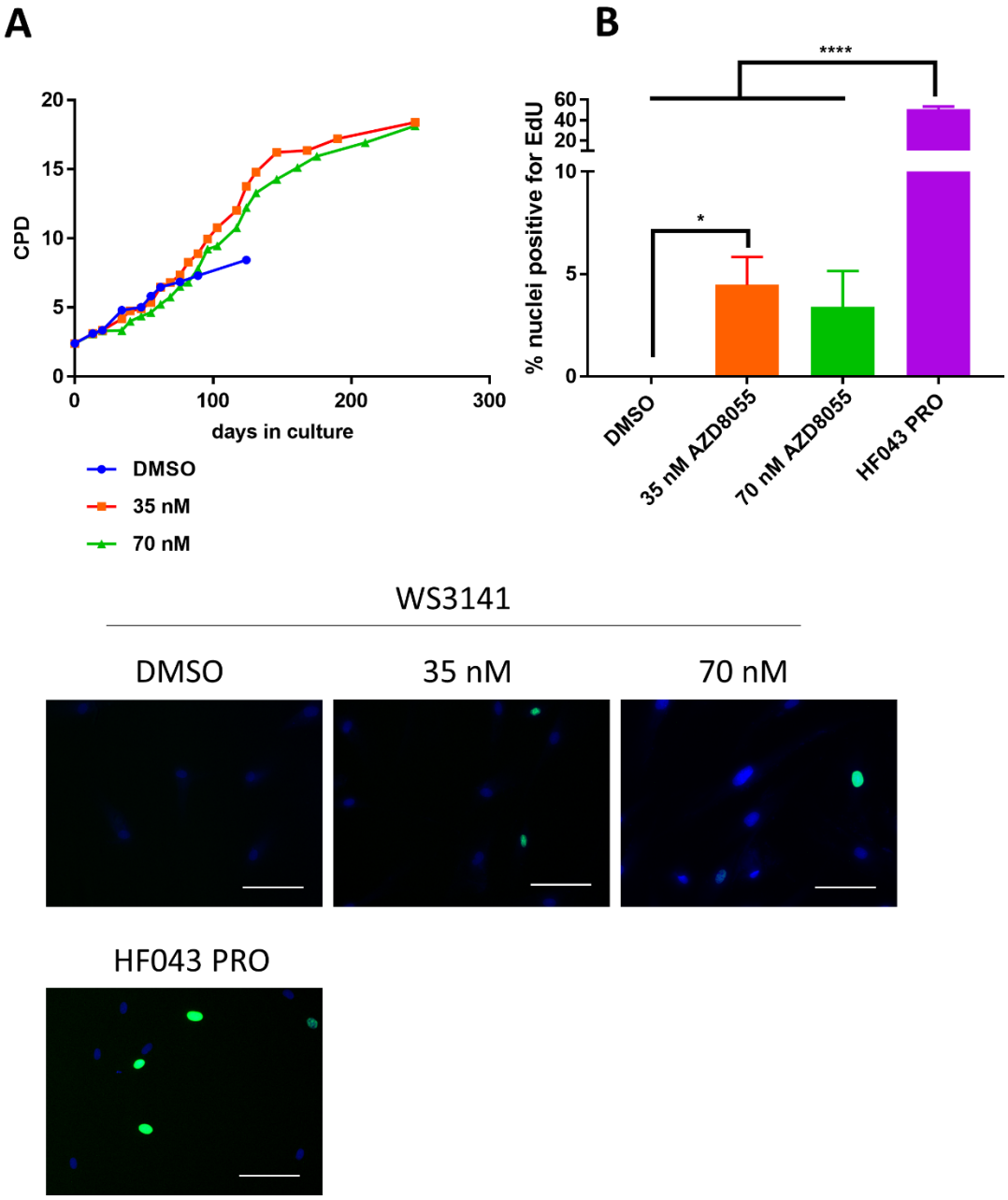


Figure 5.7: Pan-mTOR inhibition extends proliferative capacity of Werner Syndrome fibroblasts

A: AG03141 (WS3141) fibroblasts were continuously cultured according to standard protocols in complete medium with DMSO control or 35/70 nM AZD8055 until replicative exhaustion; CPDs were calculated at every passage according to automated cell counts (representative data shown of n=2 well-correlated replicates, due to scarcity of cells). B: WS3141 fibroblasts in DMSO control or AZD8055-treated media alongside HF043 proliferating controls (CPD <40) were stained for Click-iT EdU following 18 hour EdU incorporation. >30 cells analysed per replicate, error bars represent SD between 3 technical replicates from one representative experiment (of n=3) with one way ANOVA and Tukey test used for statistical analysis (* $p<0.05$, **** $p<0.0001$). Scale bar 100 μm.

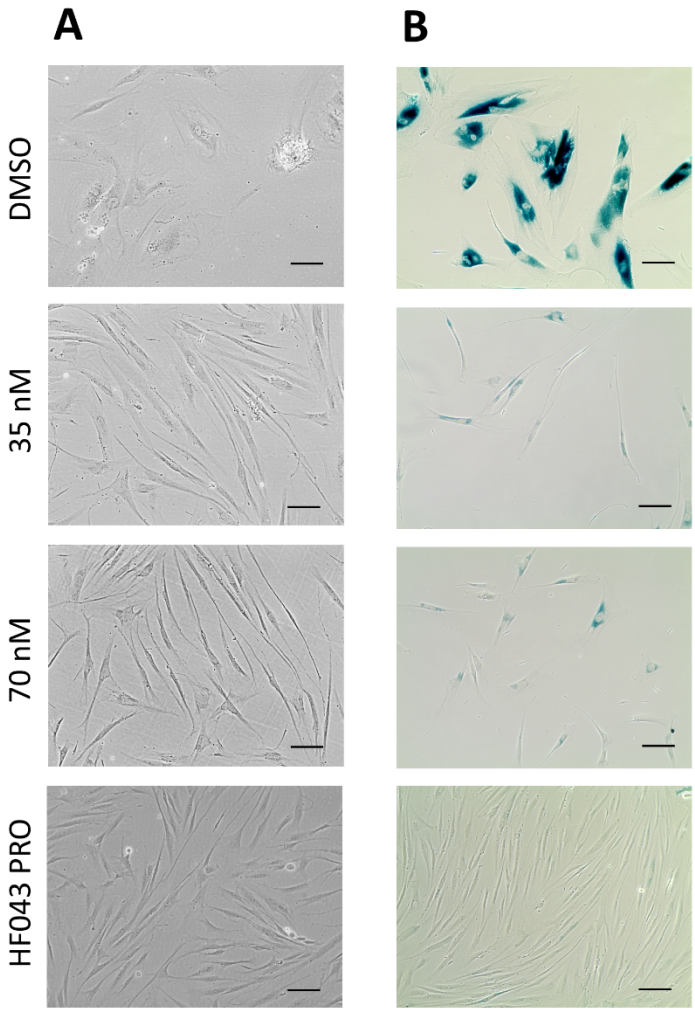


Figure 5.8 Pan-mTOR inhibition disrupts phenotypes of senescence in Werner Syndrome fibroblasts.

WS3141 fibroblasts in DMSO control or AZD8055-supplemented media alongside HF043 proliferating controls were examined for morphology using phase contrast microscopy or B: stained for SA-β-gal. (Representative data shown from n=3 experiments.) Scale bar 100 μm.

As well as playing important roles in DNA replication and repair, WRN is known to function in telomere maintenance (Reddy et al., 2010). Indeed, Werner syndrome patient-derived fibroblasts have been reported to exhibit extremely short telomere lengths (Ouellette et al., 2000). However, I had observed a substantial increase in the replicative capacity of WS fibroblasts on treatment with AZD8055, which in wild-type fibroblasts appeared to mildly

stabilize telomere length at extremely high CPD (Figure 5.5). To investigate whether telomere protection occurred during the extension of replicative capacity in WS-patient fibroblasts on AZD8055 treatment, I used teloFISH for telomere length analysis (Figure 5.9), as the extremely low rates of proliferation in patient-derived cells prevented thorough analysis by Southern blotting due to the large amount of gDNA required per sample.

Compared with wild-type HF043 proliferating controls, DMSO-treated WS patient cells showed very little telomeric FISH staining, comparable with untreated replicatively senescent HF043 fibroblasts that had undergone 90 population doublings. These findings of negligible telomeric staining in WS are consistent with previous reports (Ouellette et al., 2000) and the important role for WRN in telomere replication (Crabbe et al., 2006). However, a small yet significant increase in telomere FISH staining was observed in 35 nM AZD8055 treated WS cells, alongside a more marginal increase on 70 nM treatment, compared to vehicle-only controls. However, the telomere staining observed still corresponded to considerably shorter lengths than those typical of low CPD wild-type controls (Figure 5.9). These data indicate that AZD8055 treatment substantially increases the replicative capacity of Werner syndrome patient fibroblasts *in vitro*, while preventing the induction of senescent phenotypes and stabilizing telomere length. While such treated WS fibroblasts are not afforded an infinite replicative capacity or telomere extension to levels comparable to wild-type controls, more than doubling their replicative capacity may be sufficient to ameliorate at least some of the senescence-driven age-related diseases suffered prematurely by WS patients. These findings are shortly to be taken forward into animal models of WS by the host lab (L. Cox, personal communication).

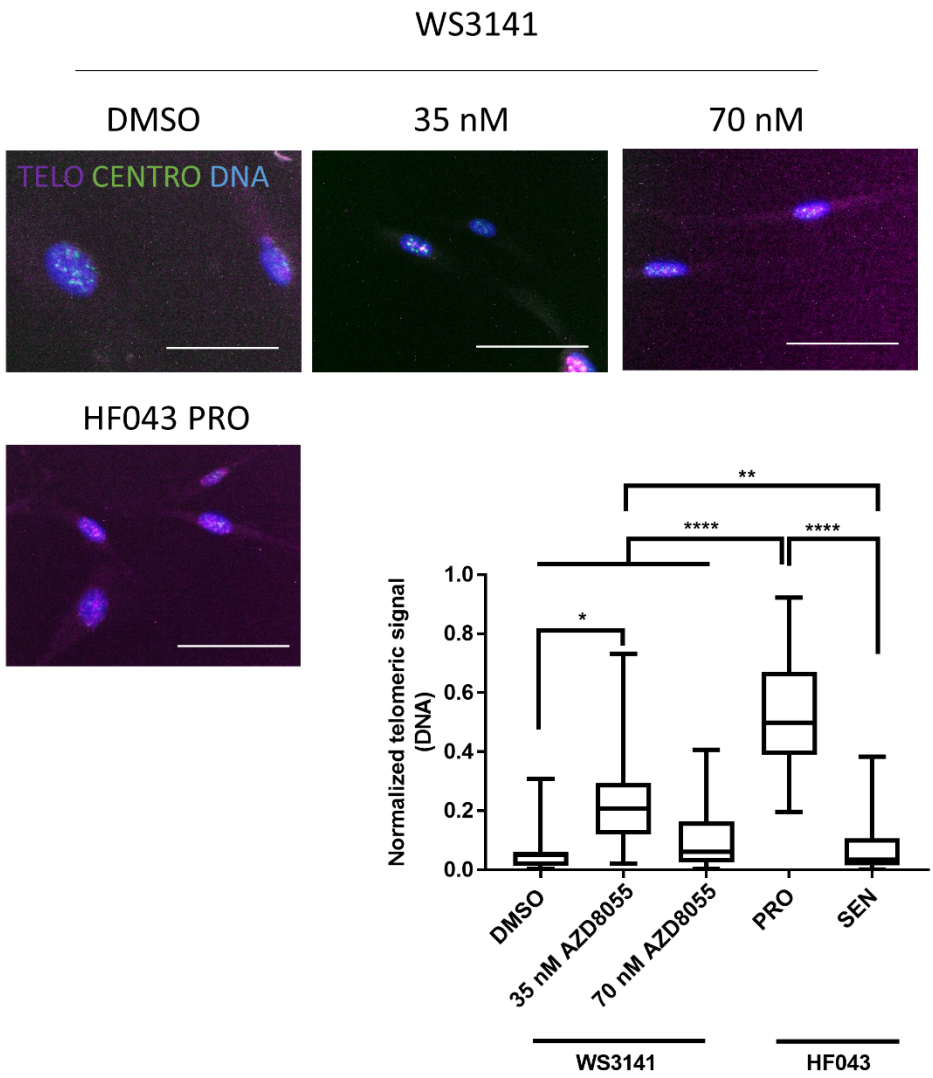


Figure 5.9 Telomere length is stabilized on pan-mTOR inhibition in Werner syndrome fibroblasts

WS3141 fibroblasts treated with DMSO control or AZD8055 alongside HF043 proliferating controls (<CPD 50) were stained by teloFISH for telomere analysis. >30 cells analysed per sample, n=3 biological replicates (representative data from one experiment shown). One way ANOVA with Tukey test for multiple comparisons used for statistical analysis (* $p<0.05$, ** $p<0.01$, **** $p<0.0001$). Scale bar 100 μm.

5.3.5. Pan-mTOR inhibition disrupts acutely-induced senescence

Induction of premature senescence in healthy bystander cells during genotoxic chemotherapy may predispose patients to the progression of secondary tumours (Campisi,

2005). As I had observed that pan-mTOR inhibition using AZD8055 could not reverse proliferation arrest in deeply senescent fibroblasts but could delay the induction of replicative senescence in wild-type fibroblasts and premature senescence in WS patient-derived fibroblasts, I next investigated whether AZD8055 treatment could disrupt the acute induction of senescence using a DNA damaging agent. To this end, I implemented my previously optimized protocol for induction of senescence using etoposide - a topoisomerase II inhibitor - where 7 days treatment with 20 μM etoposide induces senescent morphology, SA-β-gal staining and permanent proliferation arrest (section 2.1.2.2).

Firstly, I analysed whether AZD8055 treatment could interfere with induction of etoposide-induced DNA damage by performing immunofluorescence for γH2AX following 24 hours treatment with etoposide and AZD8055 (20 μM and 70 nM respectively) compared with single treatment and vehicle only controls. I found that a high proportion of cells (>90%) exhibited nuclear γH2AX foci following etoposide treatment, and that this was not affected by AZD8055 co-incubation (data not shown) indicating that AZD8055 does not affect initial induction of DNA damage upon etoposide treatment.

I then took HF043 fibroblasts at low CPD (<50) and co-treated them for 7 days with etoposide and AZD8055 (20 μM and 70 nM respectively), with single treatment and DMSO controls. I subsequently monitored proliferation rates at 7 day intervals by harvesting and counting cells to calculate population doublings. At each interval, cells were seeded into fresh media supplemented with either DMSO vehicle control or 70 nM AZD8055, and monitored for 21 days in total at which point cells were analysed for phenotypes of senescence (see Figure 5.10A for experimental design).

As anticipated, control fibroblasts treated only with DMSO proliferated quickly throughout the experiment, completing ~10 population doublings within 21 days (Figure 5.10B DMSO),

maintaining spindle morphology throughout the treatment window (Figure 5.11A). Similarly, AZD8055-only treated controls proliferated continuously, albeit more slowly (Figure 5.10B), again maintaining characteristic low CPD spindle morphology (Figure 5.11A). By contrast, cells treated with etoposide for the first 7 days and maintained in control (DMSO) media exhibited a stable proliferation arrest following etoposide treatment (Figure 5.10B ETOP-DMSO). At the end of the experiment, these cells exhibited classic senescent morphology (Figure 5.11A), with prominent γH2AX foci (Figure 5.11C) and SA-β-gal staining (Figure 5.11B). Treatment with AZD8055 (days 7-21) after initial etoposide treatment (days 1-7, Figure 5.10B ETOP – AZD) did not allow re-proliferation, consistent with previous findings (Figure 5.1) and did not prevent the occurrence of γH2AX foci (Figure 5.11C). However, these cells did appear spindle-shaped (Figure 5.11A) and did not stain positively for SA-β-gal (Figure 5.11C), indicating that whilst AZD8055 treatment did not reverse the established proliferation arrest, it disrupted phenotypes of senescence, consistent with earlier data (Figure 5.1 and Chapter 4).

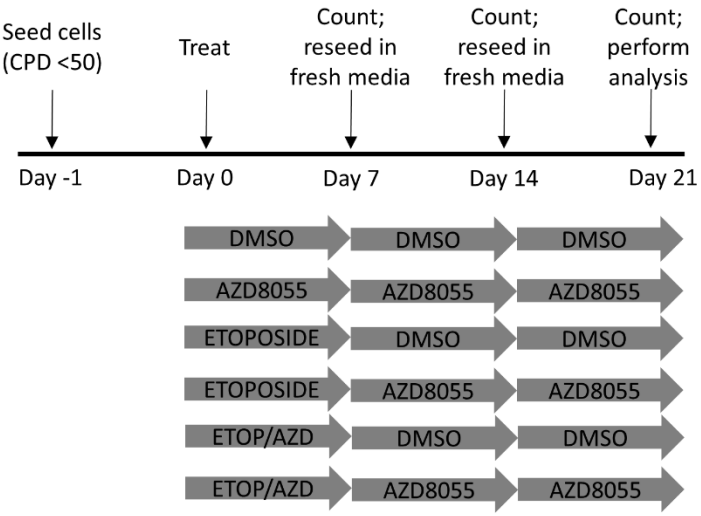
Cells co-treated with AZD8055 and etoposide in the first 7 days, and subsequently maintained in DMSO-only media (Figure 5.10B ETOP/AZD-DMSO) at first proliferated slowly (if at all), comparable with etoposide-only treated cells. However, in the final 7 days of treatment (during which the cells were maintained in vehicle only media), these cells re-proliferated substantially, completing >1.5 population doublings within 7 days (Figure 5.10B ETOP/AZD-DMSO), with re-entry into the cell cycle confirmed by Click-iT EdU incorporation in >50% of the fibroblasts during an 18-hour labelling window following the treatment period (Figure 5.10C). Indeed, at the end of the experiment (day 21), these cells appeared confluent, with spindle-like morphology (Figure 5.11A), failed to stain for SA-β-gal (Figure 5.11B, and exhibited little γH2AX staining, indicating resolution of DNA damage, perhaps at least within those cells that re-proliferated (Figure 5.11C). Similarly, cells co-treated with etoposide and AZD8055, and subsequently maintained in AZD8055 (Figure 5.10B ETOP/AZD-

AZD) appeared to gradually re-start proliferation after 21 days, as indicated by Click-iT EdU incorporation (Figure 5.10C), though at considerably lower rates than co-treated cells subsequently maintained in DMSO only, perhaps due to the reduction in proliferation rates associated with AZD8055 treatment. These cells also exhibited spindle morphology, failed to stain for SA-β-gal and lacked γH2AX foci (Figure 5.11A, B, C). Together, these data indicate that AZD8055 treatment blocks the establishment of DNA damage induced proliferative arrest and associated phenotypes of senescence.

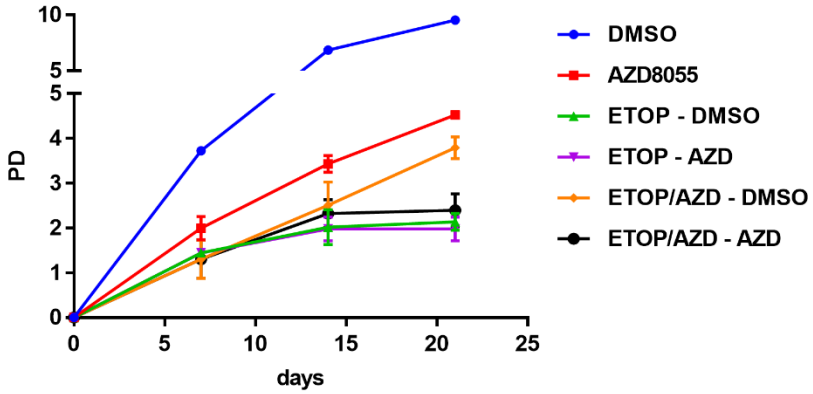
Figure 5.10: Pan-mTOR inhibition disrupts induction of DNA damage induced senescence

A: schematic depicting experimental design in which low CPD (<50) proliferating HF043 fibroblasts were seeded into 6-well plates and treated with DMSO, AZD8055 (70 nM), etoposide (20 μM) or AZD8055 and etoposide for 7 days, before cells were lifted and counted to calculate CPD. Cells were then re-seeded, and treated with either DMSO or AZD8055 for the following 14 days, and counted and re-seeded at day 14 and day 21. B: Population doublings (PD) within the treatment window were calculated by direct cell counting (n=4, error bars are SD between 4 independent biological replicates). C: at day 21, cells were re-seeded into 96-well plates and incubated with EdU for 18 hours without drug treatment, then stained for Click-iT EdU and quantified using ImageJ. A one-way ANOVA with Tukey test for multiple comparisons was used for statistical analysis (* $p<0.05$, **** $p<0.0001$, n=3).

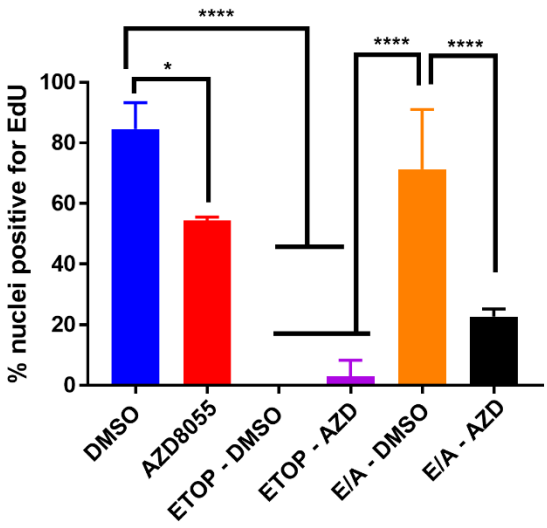
A


Seed cells (CPD <50)
Treat
Count; reseed in fresh media
Count; reseed in fresh media
Count; perform analysis
Day -1
Day 0
Day 7
Day 14
Day 21
DMSO
DMSO
DMSO
AZD8055
AZD8055
AZD8055
ETOPOSIDE
DMSO
DMSO
ETOPOSIDE
AZD8055
AZD8055
ETOP/AZD
DMSO
DMSO
ETOP/AZD
AZD8055
AZD8055

B


PD
days
DMSO
AZD8055
ETOP - DMSO
ETOP - AZD
ETOP/AZD - DMSO
ETOP/AZD - AZD

C


% nuclei positive for EdU
****
*
****
****
DMSO
AZD8055
ETOP - DMSO
ETOP - AZD
E/A - DMSO
E/A - AZD

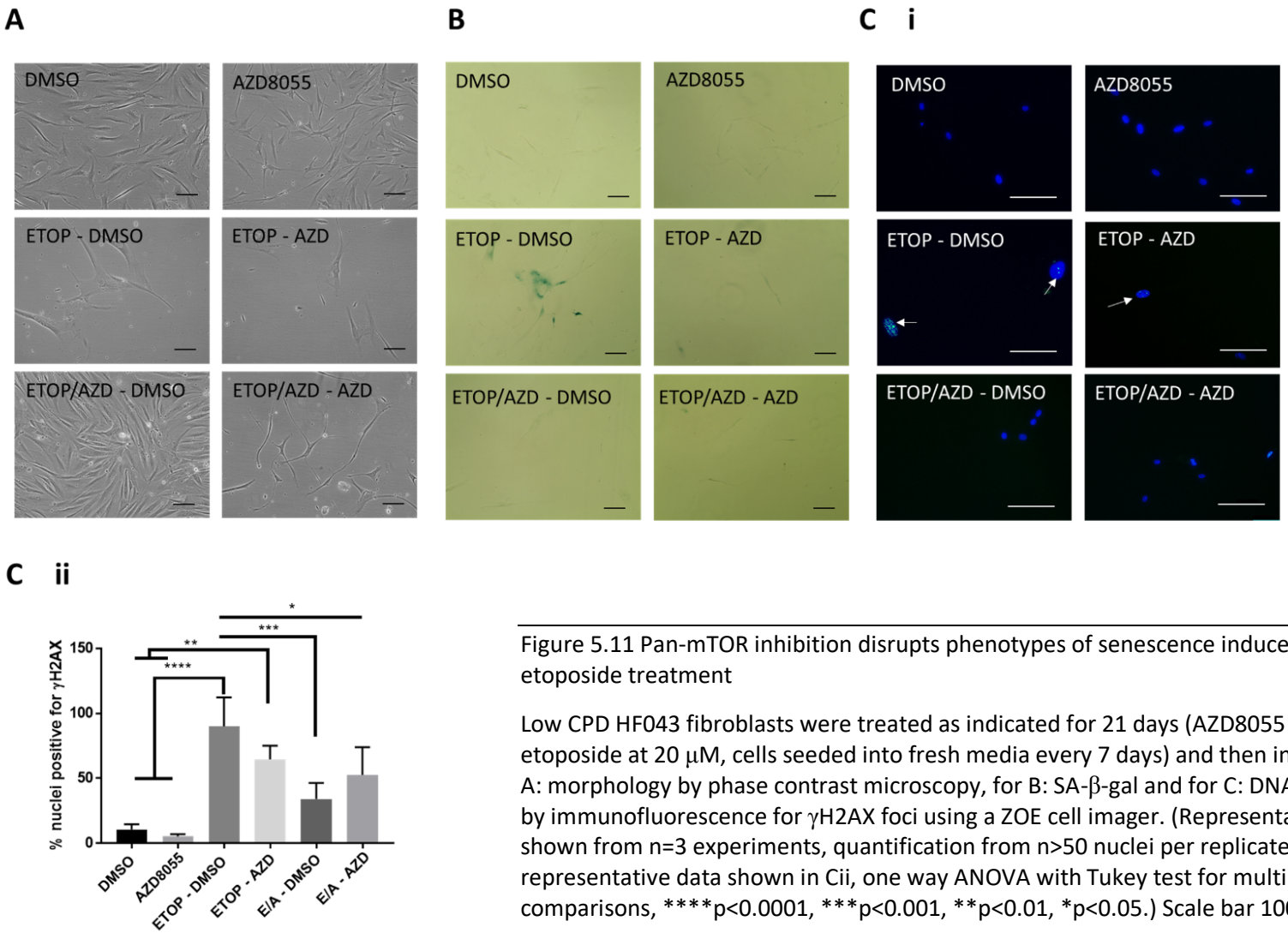
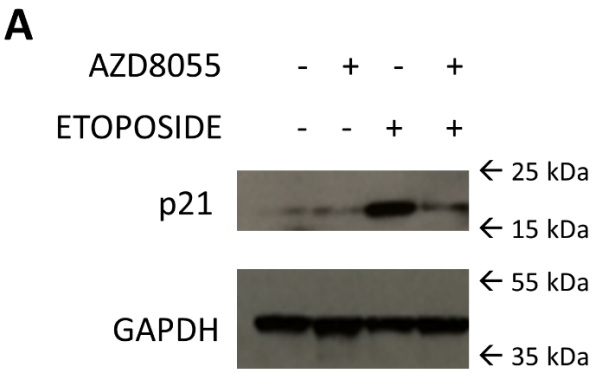


Figure 5.11 Pan-mTOR inhibition disrupts phenotypes of senescence induced by etoposide treatment

Low CPD HF043 fibroblasts were treated as indicated for 21 days (AZD8055 at 70 nM, etoposide at 20 μM, cells seeded into fresh media every 7 days) and then inspected for A: morphology by phase contrast microscopy, for B: SA-β-gal and for C: DNA damage by immunofluorescence for γH2AX foci using a ZOE cell imager. (Representative data shown from n=3 experiments, quantification from n>50 nuclei per replicate of representative data shown in Cii, one way ANOVA with Tukey test for multiple comparisons, ****p<0.0001, ***p<0.001, **p<0.01, *p<0.05.) Scale bar 100 μm.

To investigate the molecular basis of this arrest, I treated low CPD, proliferating HF043 fibroblasts with etoposide, AZD8055 (again at 20 μM and 70 nM respectively or DMSO control) alone or in combination, then lysed cells for Western blotting (Figure 5.12). I found that expression of the CKI p21 was upregulated following 24 hours etoposide treatment in proliferating cells compared to DMSO only treated controls, implicating p21 in enforcing proliferative arrest. However, co-treatment with AZD8055 significantly prevented etoposide-induced p21 upregulation in proliferating fibroblasts, suggesting that pan-mTOR inhibition interferes with CKI upregulation in response to DNA damage, resulting in preservation of proliferative capacity. These results are consistent with AZD8055 abrogating p21 upregulation in fibroblasts at high CPD (Figure 5.6).



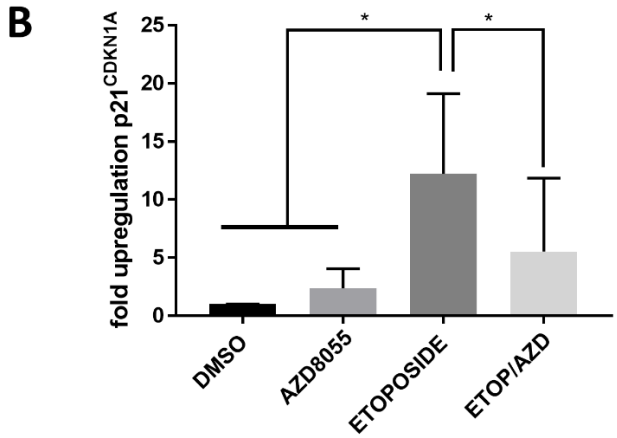
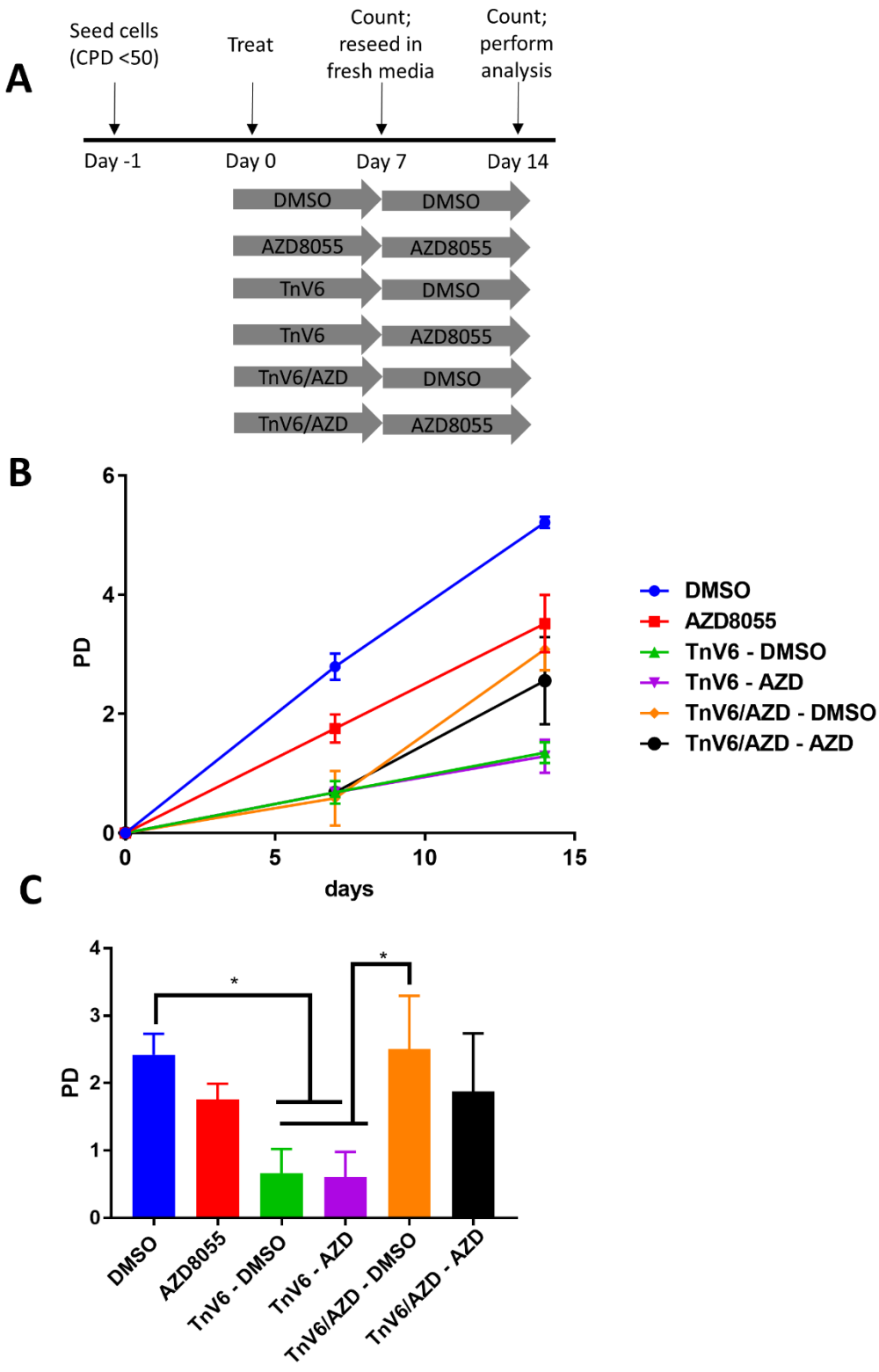


Figure 5.12 AZD8055 treatment prevents p21 upregulation on etoposide treatment

Proliferating (CPD > 50) HF043 fibroblasts were treated with AZD8055 (70 nM), etoposide (20 μM) or DMSO control for 24 hours in culture, then cells were lysed for Western blotting against $p21^{CDKN1A}$ with GAPDH loading control (representative data shown in A and quantification of 3 independent biological repeats in B; * $p<0.05$ by one way ANOVA with Tukey test to compare means of each group).

As I had previously shown that induction of acute senescence mediated through pharmacological SIRT1/2 inhibition was associated with upregulation of p21 (Chapter 3, Walters and Cox, 2019) I next investigated whether acutely-induced senescence on Tenovin-6 (TnV6) treatment could similarly be disrupted by pan-mTOR inhibition using the same experimental set-up as for etoposide treatment (Figure 5.13A). Again, DMSO-only treated fibroblasts proliferated quickly throughout the treatment window, and AZD8055-only treated fibroblasts proliferated continuously, but at a slower rate. Furthermore, cells treated with TnV6 for the first 7 days and subsequently maintained in DMSO-supplemented media completed ~1 population doubling within the first 7 days, and <1 in the second 7 days (Figure 5.13B), indicating a stable proliferation arrest (TnV6 – DMSO), consistent with previous findings (Chapter 3, Walters and Cox, 2019). TnV6-treated cells that were subsequently treated with AZD8055 (TnV6 – AZD) also failed to re-proliferate, though they showed rejuvenated morphology (Figure 5.13D). However, fibroblasts that were co-treated with AZD8055 and TnV6, then maintained in either DMSO or AZD8055 re-started proliferation after removal of TnV6 (Figure 5.13B, C), and showed spindle-like morphology (Figure 5.13D). Therefore, acutely induced senescence mediated by sirtuin inhibition is disrupted by pan-mTOR inhibition.


A
Seed cells (CPD <50)
Treat
Count; reseed in fresh media
Count; perform analysis
Day -1
Day 0
Day 7
Day 14
DMSO
DMSO
AZD8055
AZD8055
TnV6
DMSO
TnV6
AZD8055
TnV6/AZD
DMSO
TnV6/AZD
AZD8055
B
PD
days
DMSO
AZD8055
TnV6 - DMSO
TnV6 - AZD
TnV6/AZD - DMSO
TnV6/AZD - AZD
C
PD
DMSO
AZD8055
TnV6 - DMSO
TnV6 - AZD
TnV6/AZD - DMSO
TnV6/AZD - AZD

D

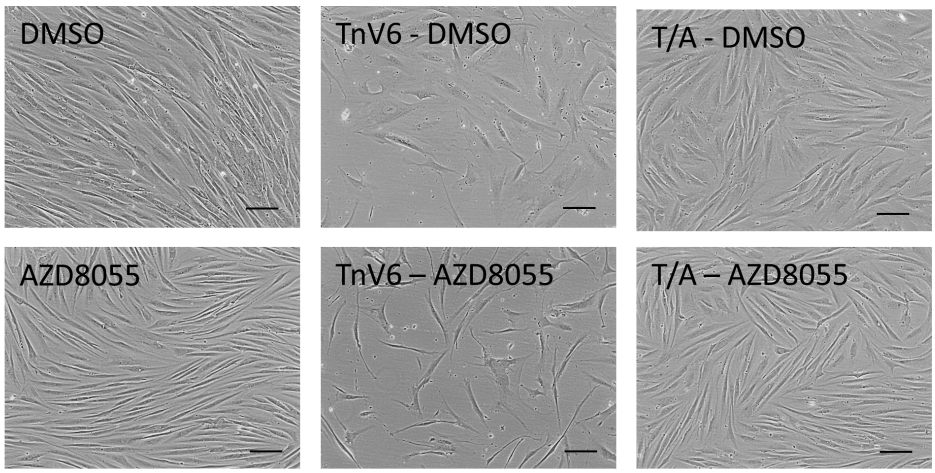


Figure 5.13: Pan-mTOR inhibition disrupts induction of TnV6-mediated senescence

A: Low CPD (<50) proliferating HF043 fibroblasts were seeded into 6-well plates and treated with DMSO, AZD8055 (70 nM), TnV6 (2 μM) or AZD8055 and TnV6 for 7 days, before cells were lifted and counted to calculate CPD. Cells were then re-seeded, and treated with either DMSO or AZD8055 for the following 7 days, and counted at day 14 to calculate CPD (n=3, error bars are SD between 3 independent biological replicates). B: population doublings between day 8-14 are shown, calculated by automated cell counting (n=3, error bars are SD between 3 independent biological replicates). Statistical analysis was performed by one-way ANOVA with Tukey test for multiple comparisons (*p<0.05). C: before counting on day 14, cells were imaged using phase contrast microscopy (n=3). Scale bar 100 μm.

5.4. Discussion

In this chapter, I have shown that while treatment with non-toxic doses of the pan-mTOR inhibitor AZD8055 is not sufficient to re-start proliferation in deeply senescent primary fibroblasts, continuous or pulse-dosed treatment during continuous passaging results in a failure to establish features of cellular senescence such as enlarged morphology, lysosomal dysfunction and proliferative arrest. Indeed, AZD8055 treatment resulted in a substantial delay to entry into replicative senescence, extending the replicative capacity of HF043 fibroblasts by over 20 population doublings, regardless of whether the treatment was

started early in the cellular replicative capacity (CPD ~30) or late (CPD ~80). However, cessation of treatment at extremely high CPD resulted in proliferative arrest, indicating that pan-mTOR inhibition did not immortalize primary fibroblasts. Using Southern blotting and teloFISH, I observed marked telomere erosion over continuous passaging in the absence of drug treatment, especially notable at high CPD. TeloFISH showed little effect of extended AZD8055 treatment on telomere length in primary fibroblasts at high CPD, but Southern blotting suggested a possible mild stabilization of telomeric length upon extended pulse-dosing. Furthermore, I noted stabilization of telomere length using teloFISH in Werner syndrome patient-derived fibroblasts treated continuously with AZD8055 (though not to lengths consistent with wild-type cells at low CPD), alongside a substantial increase in the replicative capacity of these cells in culture. Whilst treated fibroblasts still only reached CPD ~18 (compared to control CPD~8) and proliferated at a very slow rate, AZD8055 treatment also prevented the establishment of phenotypes of senescence such as enlarged morphology and SA-β-gal staining. Furthermore, co-treatment with AZD8055 during acute induction of senescence using etoposide (DNA damage) or TnV6 (sirtuin inhibition) also resulted in a disruption to senescence induction. Using Western blotting, I noted an upregulation of p21 in high CPD fibroblasts and in proliferating cells treated with etoposide, which was abrogated upon AZD8055 treatment, suggesting a molecular mechanism for disruption of proliferation arrest. Collectively, these data highlight an important role for mTOR in coordinating, though not maintaining, the senescent proliferative arrest.

5.4.1. Regulation of p21 and proliferation arrest by mTOR signalling

As highlighted above, I observed that pan-mTOR inhibition prevented p21 upregulation following etoposide treatment and in replicatively senescent fibroblasts (Figure 5.6, 5.12). Hence pan-mTOR inhibition may block induction of senescence through preventing sufficient accumulation of the CKI p21 to mediate proliferation arrest. Indeed, accumulating evidence suggests a multi-layered interaction network of crosstalk between p53 and mTOR may finely

regulate p21 levels in response to cellular stress at the levels of transcription, translation and protein stability.

Indeed, transcriptional upregulation of p21 is a major target of p53 activity: following DNA damage, p53 is phosphorylated at multiple sites including Ser-15, which causes p53 stabilization by impairing binding by its E3 ubiquitin ligase MDM2 which otherwise ubiquitinates p53, targeting it for proteasomal degradation (Chen et al., 1995, Chen et al., 1996). DNA damage response kinases including ATM, ATR and DNA-PK have been implicated in p53 Ser-15 phosphorylation and stabilization (reviewed in Cox and Lane, 1995). However, recent research has shown that both mTORC1 and mTORC2 complexes can directly phosphorylate p53 at Ser-15 during p53-dependent, PTEN-loss induced senescence, highlighting a previously undiscovered role for mTORC2 signalling in senescence (Jung et al., 2019). Furthermore, while MDM2 ubiquitinates and destabilizes p53 in the nucleus, MDM2 can itself be phosphorylated by a number of kinases, which promotes its cytoplasmic shuttling. Intriguingly, S6K1 (itself phosphorylated and activated by mTORC1) phosphorylates MDM2, inhibiting MDM2-mediated p53 ubiquitination, thus promoting activation of p53 (Lai et al., 2010). Therefore, mTOR inhibition may prevent p21 upregulation by impairing p53 stabilization and activity through directly and indirectly promoting MDM2-mediated p53 degradation.

Furthermore, mTOR activity plays an important role in promoting both protein translation (through S6K, 4E-BP1 and eEF2) and protein stability (through inhibition of autophagy-inducing kinase ULK1, Figures 1.3, 1.5), and also elicits finely-tuned control over the translation of a subset of mRNAs with a terminal oligopyrimidine track in their 5'UTR (5'TOP mRNAs, Jefferies et al., 1994). However, no TOP motif has been found in the 5'UTR of p21 (Llanos et al., 2016). Despite this, as a relatively short-lived protein, p21 may be particularly susceptible to global changes in protein translation and stability (Jascur et al., 2005). Indeed,

polysome profiling revealed a decrease in p21 translation in line with global translation decreases on mTOR inhibition by RAD001 (Beuvink et al., 2005) suggesting that while mTOR may not elicit specific control over p21 translation, its expression is markedly changed by mTOR activity in part due to the high rate of p21 turnover.

Recent evidence has also demonstrated that as well as regulating global translation and p53-dependent transcription of p21, mTOR may control p21 levels by regulating its degradation. Indeed, unphosphorylated 4E-BP1 directly interacts with p21, as shown in co-immunoprecipitation assays in cells treated with a pan-mTOR inhibitor (Torin-1) or using a unphosphorylated mutant 4E-BP1, and promotes p21 degradation (Llanos et al., 2016). Hence, mTORC1 activation may prevent p21 degradation mediated by unphosphorylated 4E-BP1. In contrast to Torin-1 treatment, rapamycin was less effective in limiting p21 upregulation; while both inhibit phosphorylation of S6K, rapamycin is less effective at inhibiting mTORC1-mediated 4E-BP1 phosphorylation compared to pan-mTOR inhibitors (Llanos et al., 2016). Together, these data indicate that mTOR regulates p21 expression at the transcriptional level through regulating p53 stability, p21 stability through 4E-BP1 and global translation levels (particularly affecting proteins such as p21 with a high turnover).

Though the experiments are not shown, we also performed continuous and pulse-dosing experiments on human primary fibroblasts using the mTORC1 inhibitors rapamycin and deforolimus. We found both treatments less effective in extending replicative capacity (at least within the dose range tested) than the pan-mTOR inhibitor AZD8055 (data not shown and personal communication, Lynne Cox). These findings are consistent with a more potent effect of pan-mTOR inhibition: p21 stability can be regulated through 4E-BP1 on pan-mTOR inhibition (but not rapamycin), both mTORC1 and mTORC2 can phosphorylate p53 at Ser-15, and mTORC2 also regulates mTORC1 activity in complex cross-talk through Akt (Figure 1.5). Previous work using shRNA against the partner proteins of mTOR in both complexes (Raptor

and Rictor) suggested that mTORC1 but not mTORC2 activity is important in establishing proliferation arrest (Kolesnichenko et al., 2012). However, it is possible that the knockdown was actually insufficient to see the effect of abrogating mTORC2 signalling; measuring mTORC2 activity is complicated by the numerous kinases and phosphatases that act on the Akt-S473 phosphorylation site often used as a readout of mTORC2 activity (e.g. TBK1: Joung et al., 2011 and DNA-PK: Toulany et al., 2011).

To further investigate the roles of each complex and the possibly multi-layered regulation of p21 expression by mTOR activity following replicative exhaustion or induction of DNA damage, experiments including shRNA knockdown of Rictor and Raptor, qPCR of p21 and Western blotting against p21, p53, MDM2 and p53/MDM2 phospho-variants, following treatment with inhibitors of translation (e.g. cycloheximide), autophagy (e.g. Bafilomycin A1) and proteasomal degradation (e.g. MG132) may be informative. However, it is likely that multiple layers of regulation occur simultaneously and possibly redundantly to ensure mTOR elicits exquisite control over p21 expression in response to cellular stress. Recent work has exemplified such multi-faceted regulation, showing multiple pathways through which mTOR controls SASP secretion from senescent cells (Laberge et al., 2015, Herranz et al., 2015).

5.4.2. Crosstalk between mTOR and telomerase

In 'wild-type' and WS human primary fibroblasts, I observed that pan-mTOR inhibition resulted in a significant delay to senescence onset; WS fibroblast replicative capacity more than doubled (Figure 5.7), and normal fibroblasts underwent over 20 additional population doublings (Figure 5.2). While my data do not suggest a significant extension of telomeres on pan-mTOR inhibition through telomerase re-activation or ALT activation (consistent with a sustained low rate of cell proliferation), I did observe possible mild telomeric stabilization in wild-type fibroblasts on extended pan-mTOR inhibition by Southern blotting, and increased telomere length in WS patient-derived cells by teloFISH. The data were however

inconclusive, as I obtained different results from FISH and Southern blotting (Figure 5.4, 5.5). However, I have previously shown that AZD8055 treatment counteracts the nuclear enlargement observed on senescence (Chapter 4) and as telomeric/nuclear area was used for quantification, it is possible that the normalization may be affected by the effects of senescence and pan-mTOR inhibition on overall nuclear area, resulting in biased quantification of FISH images. Using higher resolution microscopy and z-stacking could therefore be used to improve the quality of teloFISH analysis. However, if long-term pan-mTOR inhibition does indeed result in mild telomeric stabilization in wild-type fibroblasts, it is possible that this could be simply due to population effects, as cells retaining sufficient telomere length following stochastic attrition retain a proliferative advantage, while those with critically short telomeres are diluted from the population.

Alternatively, a mechanistic link could connect mTOR activity to telomeric protection. Indeed, previous research has shown that rapamycin treatment can influence telomerase activity. While the RNA-protein enzyme telomerase maintains telomere length in cells using its RNA template, its catalytic protein component TERT also functions to protect cells from oxidative stress, DNA damage and apoptosis through its mitochondrial functions (Saretzki, 2014). Indeed, short-term dietary restriction or rapamycin treatment has been shown to promote mitochondrial TERT accumulation in mice brains through its mitochondrial localization sequence, corresponding with lower levels of oxidative stress (Miwa et al., 2016). Interestingly, TERT and mTOR have been shown to form a complex (also including HSP90, Akt and S6K), providing compelling evidence in support of mTOR-dependent regulation of telomerase activity (Sundin and Hentosh 2012). Co-immunofluorescence for TERT and mTOR in treated and control fibroblasts during senescence and proliferation as well as assays for telomerase activation may therefore be informative in this area.

The WRN helicase/exonuclease is implicated in telomere maintenance: it interacts with the TRF1, TRF2 and POT1 components of the shelterin complex, and expression of hTERT rescues the short telomere length, premature senescence and slow proliferation phenotypes of WS fibroblasts (S. Gover, personal communication). Direct mTOR-dependent regulation of telomerase through complex formation or re-localization, or alternatively slowing cell cycle progression to allow for increased damage resolution on mTOR inhibition may therefore benefit efficient proliferation in WS fibroblasts on AZD8055 treatment. Again, co-immunofluorescence analysis or *in vitro* DNA replication assays in control or treated patient fibroblasts may be informative in examining these possibilities.

5.4.3. Regulation of paracrine senescence?

Coordination of proliferative arrest by mTOR activity should also be considered in the context of mTOR-dependent regulation of pro-inflammatory secretion from senescent cells, which can have pleiotropic effects on neighbouring cells, including promoting proliferation or conversely, inducing paracrine senescence and re-enforcing autocrine growth arrest (section 1.3.3.3.1). Indeed, I have demonstrated suppression of IL-6 secretion on AZD8055 treatment in HF043 fibroblasts (Chapter 4). Therefore, population effects could play crucial roles in the onset of senescence: in a population of cells experiencing a senescence-inducing stimulus, only a proportion may initially undergo senescence (for example due to stochastic telomere shortening or sufficient irreparable DNA damage load). Due to paracrine or juxtacrine signalling from these 'primary' senescent cells, the proliferative capacity of the remaining bystander cells could be hampered by paracrine pro-senescence (and possibly mTOR-dependent) signalling. Indeed, single cell RNA-seq has revealed distinct populations of primary and secondary senescent cells following induction of OIS (Teo et al., 2019). Thus, mTOR inhibition may decrease bystander senescence by reducing secretion of pro-senescent factors by pre-existing senescent cells (or by altering juxtacrine communication, see Chapter 7).

Indeed, following co-treatment of cells at low CPD with etoposide and AZD8055, there was a considerable lag of at least 7 days before re-proliferation was observed in cells subsequently maintained in drug-free media (Figure 5.10). Further, wild-type fibroblasts at extremely high CPD proliferated at very slow rates (Figure 5.2). These proliferation dynamics may be consistent with only a small proportion of cycling cells having repaired DNA damage or maintaining sufficient telomere length/integrity for continued proliferation. Indeed, I observed that fibroblasts induced to senesce by 7 day etoposide treatment exhibited persistent γH2AX foci when maintained in DMSO-only media following etoposide treatment (Figure 5.11). However, a smaller proportion of nuclei exhibited DNA damage foci following etoposide/AZD8055 co-treatment when maintained in DMSO-only media (Figure 5.11). Control experiments confirmed that AZD8055 treatment did not interfere with initial induction of DNA damage by etoposide (γH2AX staining after 24 hours treatment with etoposide or etoposide/AZD8055, >90% nuclei positive for DNA damage foci, data not shown). It is therefore possible that only cells that have resolved the incurred DNA damage may be allowed to re-enter the cell cycle following AZD8055/etoposide co-treatment, unhampered by paracrine pro-senescence signalling.

Furthermore, proliferation also re-started more rapidly following co-treatment with TnV6 and AZD8055 in comparison with etoposide and AZD8055 (TnV6 Figure 5.13; days 7-14 vs. etoposide Figure 5.10; days 14-21). While I have observed induction of DNA damage foci on extended TnV6 treatment (Figure 3.12, Walters and Cox, 2019), this effect may be indirect and therefore potentially slower to establish than the DNA damage induced by etoposide treatment. It is therefore possible that the delay in re-starting proliferation following etoposide/AZD8055 treatment in comparison with TnV6/AZD8055 is due to a delay to repair highly damaged DNA, or because a smaller proportion of cells are indeed able to correctly repair DNA to permit cell cycle progression, or indeed due to differences in the DDIS and TnV6-induced SASP profiles of pro-senescence factors.

To establish whether mTOR inhibition prevents the onset of senescence in damaged cells, cell fate analysis could be performed where proliferation events of individual cells are mapped over time, to analyse whether there are separate populations of cells that are proliferating or arrested, ideally in a DNA damage or shelterin component fluorescent-reporter cell line. Alternatively, single cell RNA-seq analysis could be performed for in-depth analysis of potentially distinct cell populations that result from a senescence-inducing stimulus, and how these populations are affected by pan-mTOR inhibition.

5.4.4. Therapeutic options for Werner syndrome and healthy ageing

The above results demonstrate that pan-mTOR inhibition delays premature senescence in WS patient-derived fibroblasts. Further experiments should be performed to analyse whether WRN protein levels are stabilized on pan-mTOR inhibition, but these results are promising and consistent with data from other labs suggesting mTOR as a target in WS. For example, hydrogen sulphide treatment (as NaHS) was shown to restore a normal morphological phenotype to WS fibroblasts, with hyperactive mTOR activity associated with WS fibroblasts blocked during restoration (Talaei et al., 2013). Furthermore, rapamycin treatment following WRN knockdown by shRNA in wild-type fibroblasts mitigated the loss of cellular proliferative capacity, though the effect size was small (Saha et al., 2014).

Indeed, Werner syndrome patients are highly vulnerable to the progression of both age-related diseases and to cancer, and standard DNA damage-inducing chemotherapies are inappropriate cancer treatments in WS, as patients are especially vulnerable to treatment side effects (Bird et al., 2012, Seiter et al., 2005). Furthermore, WS patients may have a dramatically high load of senescent cells, meaning that senolytic therapies should be approached with caution. Therefore, mTOR inhibitors or similar therapies to blunt the deleterious impacts of senescent cells, and potentially delay the onset of premature senescence *in vivo* may be viable therapeutic options. Indeed, p38 MAPK inhibitors such as

SB203580 can also increase the replicative capacity of WS fibroblasts (Davis et al., 2005, Tivey et al., 2013), though are associated with a severe side effect profile; newer MAPK inhibitors are currently in development (Davis et al., 2016).

Collectively, these data add to our mechanistic understanding of how mTOR inhibitors extend healthy mammalian lifespan and hold promise for a wide range of age-related diseases (Harrison et al., 2009, reviewed in Walters and Cox, 2018). Our finding that the pan-mTOR inhibitor AZD8055 is markedly more effective in disrupting senescence phenotypes and proliferation arrest than rapamycin warrants further investigation in whole animal models such as *C. elegans* or *Drosophila* and crucially, in cancer-prone model organisms to investigate the risks of disrupting senescence onset; while compromising the onset of cellular senescence (e.g. by telomerase re-activation) can mitigate tissue degeneration, it is also associated with an elevated risk of tumorigenesis (Jaskelioff et al., 2011). Importantly, previous data has shown that rapamycin treatment not only extends lifespan, but also reduces tumorigenesis in cancer-prone mice (Anisimov et al., 2010) and mTOR inhibitors are actually moderately effective anti-cancer therapeutics (discussed in Walters and Cox, 2018). Therefore, the current evidence suggests that while mTOR inhibition results in disruption of senescence *in vitro*, inhibiting mTOR signalling (at least using rapamycin) is not pro-tumorigenic *in vivo*. Indeed, mTOR inhibition did not reverse established senescent proliferation arrest, therefore is involved in the onset but not the maintenance of senescent proliferation arrest (Figure 5.1). Hence AZD8055 could indeed be a viable therapeutic option for age-related diseases or progeria, or following genotoxic chemotherapy to mitigate secondary tumour formation, provided that it does not compromise the anti-tumorigenic response of initial induction of senescence.

6. Comparative proteomic profiling of replicative senescence reveals proteome rejuvenation on pan-mTOR inhibition together with therapeutic candidates including actin reorganization

6.1. Introduction

As evidence for the deleterious role of senescence in pathological ageing increases (Baker et al., 2016, Table 1.1), an in-depth, unbiased analysis of the molecular underpinnings of senescence is increasingly required. In recent years, molecular analysis of biological systems has been markedly enhanced by advances in proteomics, which can now enable the detection and quantification of thousands of proteins within a sample based on mass spectrometry analysis of peptide fragments from lysed and trypsin-digested biological material (Deracinois et al., 2013). Proteomics has many applications, from informing our understanding of various cell states or disease models, to target identification or mechanism of action analysis in drug discovery. Currently the vast majority of biological research focuses on a small proportion of well-known genes and proteins (Stoeger et al., 2018). Similarly, ageing and senescence research is biased towards a small number of highly conserved pathways implicated in ageing from historical model organism studies (Kenyon, 2010). However, generating an unbiased profile of senescence using 'omics technology could generate novel biological insight and target identification within this complex cell state.

6.1.1. Proteomics principles and methodology

Traditional comparative proteomics approaches operate using high resolution, two-dimensional gel electrophoresis (2DGE) to separate proteins from lysed samples. Proteins that are differentially expressed are then selected and stained for identification using mass spectrometry. However, these approaches only resolve a small number of proteins within each sample and have therefore been surpassed by newer approaches, in which proteins isolated from lysed biological material are first subjected to Trypsin FASP (filter aided sample preparation) digest, for quantitative detection of peptides using LC-MS/MS, where samples are separated using chromatography to reduce sample complexity prior to detection and quantification using tandem mass spectrometry (Aslam et al., 2017). Sample quantification

can be performed in a label-free manner by sequential analysis of samples, where the number of peptides sequenced for a given protein based on spectral counting correlates to its abundance (label free quantification, LFQ), or by using a number of different labelling systems. Of these, SILAC (stable isotope labelling by amino acids in cell culture i.e. heavy ^{13}C vs light ^{12}C) and TMT (tandem mass tag, for simultaneous analysis of >2 samples) are two of the most popular. Of these approaches, SILAC produces the most reliable quantification as samples are labelled in parallel prior to collection, while TMT labelling is subject to variability in lysis or digestion yields prior to labelling, though samples are analysed in parallel by LC-MS/MS. LFQ is the least accurate in terms of quantification as it is dependent on very precise calibration. However, LFQ is quick, simple and inexpensive, and has no limit to the number of samples to be compared (Deracinois et al., 2013, Figure 6.1).

6.1.2. Applications of comparative proteomics

Using proteomics for therapeutic target identification can identify individual 'druggable' proteins with significant expression changes in the disease versus normal state. While target-based approaches can be effective, especially against pathogens or in single gene mutation diseases, they are associated with a substantial failure rate in targeting complex diseases underpinned by systems-level proteome changes, such as senescence and ageing (Swinney, 2012). Therefore sophisticated analysis at the pathway and network level is required to identify a target – or indeed multiple targets – within a complex system that when inhibited, do not allow network compensation through in-built redundancy (though alternatively, phenotypic screening bypasses the requirement for a target).

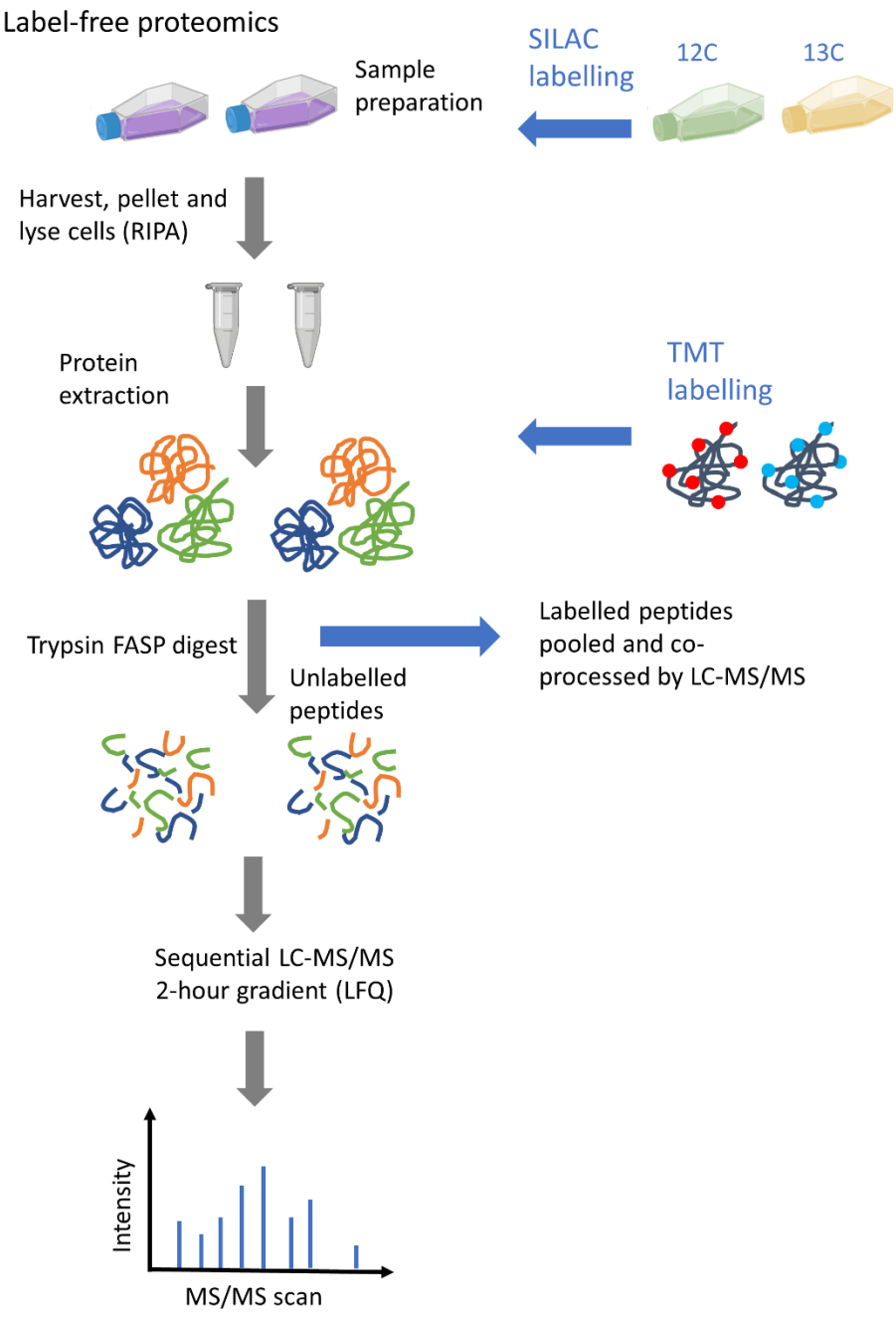


Figure 6.1 Comparative proteomics methodology

Schematic depicting the principles of comparative proteomics, in which samples are collected, proteins extracted and then lysed using Trypsin FASP digest before separation and quantification by LC-MS/MS for label-free quantification by sequential analysis. Alternatively, protein labelling using SILAC heavy/light isotopes can be performed prior to sample collection or using TMT during sample processing as alternative quantification strategies, but these approaches limit the number of samples to be compared and are more costly compared to LFQ. (Stock images of culture flask and eppendorf from BioRender.com).

Certainly, comparative proteomics is not the only technique that provides an in-depth, unbiased analysis of a biological system; RNA-seq also fulfils these requirements and actually allows the detection of a greater number of genes due to incorporation of an amplification stage. However, transcripts are subject to finely-tuned post-transcriptional regulation, with transcript half-life, translation efficiency and protein localization and stability not reflected in transcriptomics. Indeed, the transcriptome has often been noted to poorly reflect the proteome (Maier et al., 2009). Proteomics datasets do not capture data on protein localization or activity however, merely protein levels, and due to the detection limit are less useful for analysing low copy number proteins. However, proteomics can be effective in establishing strongly expressed, 'druggable' target proteins or pathways (Aslam et al., 2017).

Several datasets have already been published using comparative proteomics to analyse cellular senescence. For example, 2DGE has been used to compare stress-induced and replicative senescence (by number of ^{35}S-Met spots without protein identification; Dierick et al., 2002) and to investigate chemotherapy-induced senescence (2DGE with MALDI-TOF MS, identifying 5 differentially expressed proteins; Li et al., 2014), while in-gel Trypsin digestion has been used to profile replicative senescence (11 proteins detected as differentially expressed between proliferating and RS cells using LFQ; Tan et al., 2018). Notably, more sophisticated platforms have been used to create a proteomic profile of the SASP (Acosta et al., 2013, Basisty et al., 2019).

6.2. Chapter aims

In this chapter I set out to address the following questions:

1. What molecular changes occur at the protein and pathway level upon induction of replicative senescence?

2. What molecular changes are involved in blocking entry into senescence and reversing deleterious senescence phenotypes through pan-mTOR inhibition?

3. Can proteins and pathways markedly altered by the onset of replicative senescence be targeted pharmacologically for senescence therapies?

To answer these questions, I used label-free quantitative comparative proteomics to analyse the molecular changes occurring at the onset of replicative senescence, in the absence of treatment, or following acute treatment with the pan-mTOR inhibitor AZD8055.

6.3. Results

6.3.1. Comparative proteomic profile of replicative senescence

In order to create a proteomic profile of replicative senescence, I analysed human primary fibroblasts (HF043) at three stages in their replicative capacity during continuous culture to replicative exhaustion. I designated 'PRO' fibroblasts as those with a proliferation rate of over 0.6 PD/day, spindle-like morphology and lack of appreciable SA-β-gal staining (<CPD 40, Figure 6.2). 'PERI' (peri-senescent) fibroblasts were those that had started to show signs of senescence, including enlarged cell size under microscopy analysis and weak SA-β-gal staining, as well as a reduction in proliferation rate (~0.2 PD/day) without yet undergoing permanent cell cycle arrest (Figure 6.2, CPD 70-80). Finally, 'SEN' fibroblasts were replicatively senescent, as detected by a failure to proliferate in culture for > 1 month, a CPD of ≥90, strong SA-β-gal staining and senescent morphology including enlarged cell size and granularity (Figure 6.2). Importantly, including peri-senescent fibroblasts in the dataset enabled analysis of the early changes that occur towards replicative exhaustion, which could represent processes important in driving senescence and its phenotypes.

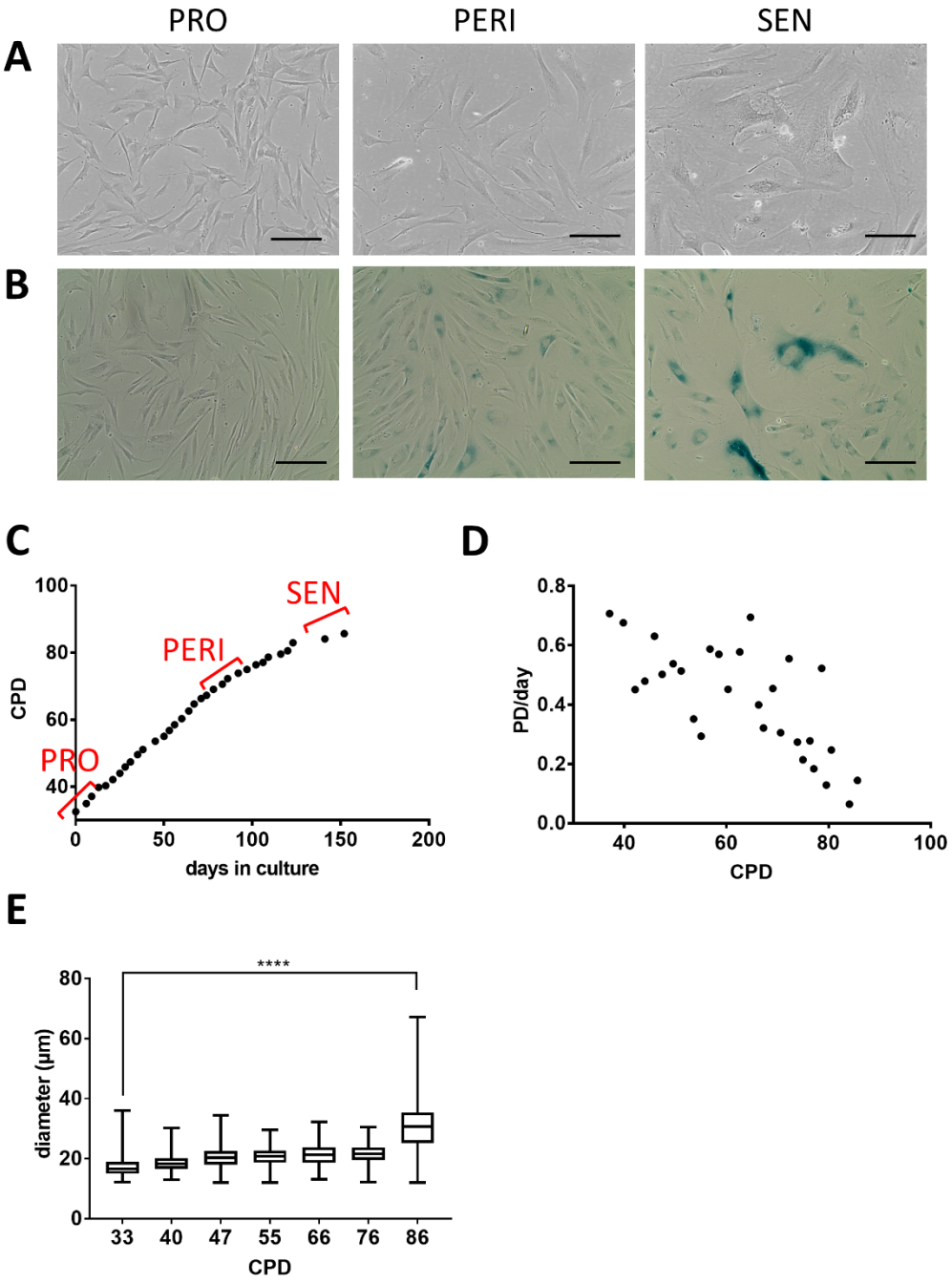


Figure 6.2 Analysis of phenotypes of senescence in proliferating, peri-senescent and replicatively senescent fibroblasts for comparative proteomic analysis.

HF043 fibroblasts were grown according to routine protocols until replicative exhaustion (see section 2.1). Representative images showing cell morphology (A) and SA-β-gal staining (B) for cells at low CPD ('PRO' <40), at peri-senescence ('PERI' CPD 70-80) and at replicative senescence ('SEN' CPD ≥ 90) are shown. At every harvest, cumulative population doublings (CPD, C), population rates (D) and cell diameters in suspension (E) were recorded. Scale bar 100 µm.

Cell populations were cultured in T25 flasks then harvested and counted following routine protocols (section 2.1), before cells were pelleted, washed and lysed in RIPA buffer with phosphatase and protease inhibitors (section 2.8). For quantitative comparative proteomics analysis, samples were subjected to trypsin FASP digestion, then peptides were detected by Orbitrap LC-MS/MS with a 2-hour gradient for deep coverage, with peptide/protein identification and label-free quantitation performed using Mascot software, by the Advanced Proteomics Facility (Department of Biochemistry, University of Oxford). Sample collection, preparation and quantification was performed independently for three separate biological replicates, with each independent experiment measuring at least 3000 proteins. LFQ intensities were imported into Perseus, where proteins only identified by site, reverse and contaminants were removed. Expression values were transformed to logarithmic scale with base 2. Data quality was inspected by means of Pearson correlations in multi-scatter plots.

Firstly, to gain a broad overview of the important molecular changes in senescence, I used Ingenuity Pathway Analysis software (IPA, Qiagen), which enables interpretation of 'omics data at the level of biological processes, disease associations, molecular pathways and individual proteins. I used the comparison analysis feature to determine the molecular pathways showing the greatest change between PRO, PERI and SEN samples in 3-way comparisons, with data visualized by plotting z-scores normalized by the mean values between samples for each pathway in heatmaps (Figure 6.3). Indeed, this analysis confirmed that pathways I had already linked to senescence in earlier work were affected by continuous culture: sirtuin signalling was decreased from PERI to SEN samples, consistent with my finding that pharmacological inhibition of SIRT1/2 induces senescence (Chapter 3). Furthermore, suggesting activation of mTOR signalling in senescence, signalling through the mTOR substrate p70S6K and regulation of eIF4 was increased in SEN samples (eIF4E is inhibited by the mTOR substrate 4E-BP1, Figure 6.3). However, PPARα activation (a

transcription factor which controls expression of fatty acid oxidation genes) and Nrf2-mediated oxidative stress response (both regulated through mTOR, Laplante and Sabatini, 2013) increased in PERI samples versus PRO, then fell in senescence, suggesting dysregulation of certain mTOR-regulated pathways upon induction of senescence (Figure 6.3).

Furthermore, I observed that a number of pathways already associated with senescence were also increased in senescent fibroblasts, such as integrin, telomerase, EIF2, IGF-1, oxidative stress and ERK/MAPK signalling (Figure 6.3). In addition, I noted a predominance of inflammatory pathways, with IL-6 and NFκB signalling both increased in senescence. Further, IL-1 and IL-9 signalling were increased in PERI vs PRO samples, possibly reflecting the role that IL-1 signalling plays in orchestrating secretion of the SASP, as an early change in senescence (Laberge et al., 2015). Similarly, interferon signalling was increased in PERI vs PRO fibroblasts but fell in SEN vs PERI fibroblasts. However, the IFN-I response has previously been shown to be a phenotype of late senescence, contributing to SASP maintenance following mobilisation of retrotransposable LINE-1 elements that re-localize to the cytoplasm (De Cecco et al., 2019); similarly induction of interferon is downstream of cytoplasmic DNA detection in senescence through cGAS-STING (Stimulator of Interferon Genes, Dou et al., 2017). My data therefore suggest that interferon signalling could also be triggered earlier in the progression towards senescence through an as yet unknown mechanism.

However, I also noted that inflammasome signalling progressively decreased with increasing cell population age, which contrasts with recent evidence revealing activation of the inflammasome in senescence orchestrates the SASP in oncogene-induced senescence (Acosta et al., 2013). While this could be due to heterogeneity between different types of senescence, this may warrant further investigation. Furthermore, I also noted an

upregulation of proteins implicated in cytoskeleton organization between PRO, PERI and SEN fibroblasts. Signalling through Rho family GTPases, in particular the GTPase Cdc42, together with its downstream activator PAK were both increased progressively towards senescence over the three sampling points (Figure 6.3).

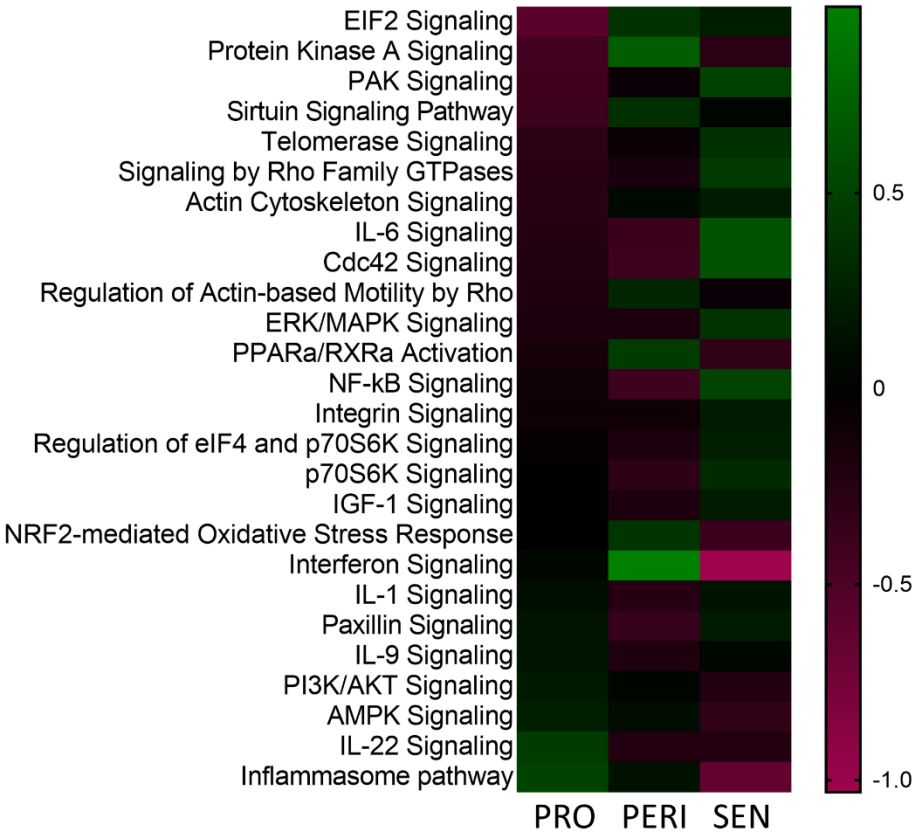


Figure 6.3 Pathway analysis of comparative proteomics reveals important molecular drivers of senescence

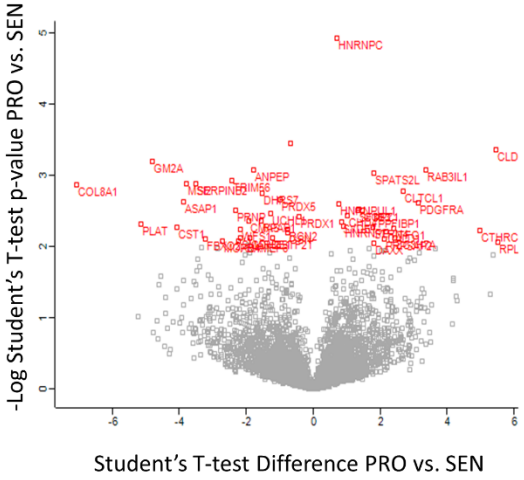
Entire proteomics datasets (log_2 expression values; representative data from n=3 independent experiments shown) were analysed using the comparison analysis feature of IPA™ pathway analysis software to identify statistically significant pathway changes over the replicative lifespan of HF043 primary fibroblasts (PRO vs. PERI vs. SEN). The heatmap shown represents z-scores for activation of each pathway for each of the samples, normalised by the mean z-score between samples.

To gain a deeper molecular insight into the data, I used Perseus software to identify 'hit' proteins that were significantly differentially expressed in PRO, PERI or SEN fibroblasts. The

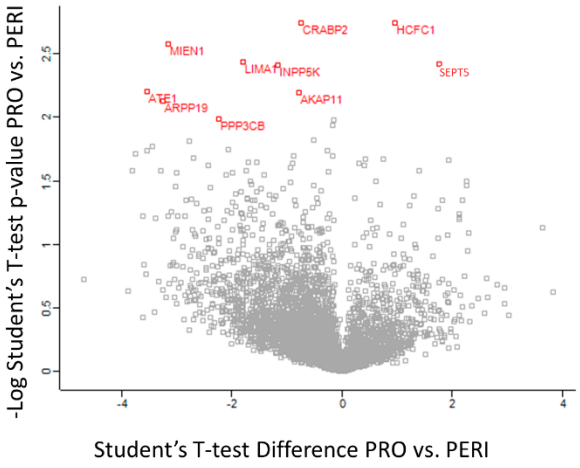
expression of proteins between 2 groups was compared using t-tests with p-value threshold set at <0.01 and plotted in Volcano plots (Figure 6.4 A-C, see supplementary Table S6.1 for full list of statistical hits; 93 differentially expressed proteins in total detected in pairwise comparisons). Gene ontology (GO) enrichment analysis (PANTHER v.14.0) in which ranked lists of statistically differentially expressed genes are analysed according to pre-assigned cellular processes then provided functional insights in pairwise comparisons analysing early, late and overall proteome changes occurring in replicative senescence, analysed by p-value based on the number of hit proteins implicated in the pathway (Figure 6.4 D-F; Ashburner et al., 2000, Gene Ontology Consortium, 2019, Mi et al., 2019).

I noted a substantial convergence of the GO enrichment with the IPA™ pathway analysis, verifying the importance of processes such as oxidative stress, cytoskeleton organization, protein synthesis and interferon, telomerase, MAPK and inflammatory signalling in senescence, despite using only the statistically significant hits for GO analysis (Figure 6.3, 6.4D-F). Indeed, this is not surprising as IPA™ includes all data prior to assignment of significance to avoid arbitrary cut-offs therefore identical trends in a large number of proteins all contributing to a biochemical pathway can provide a high level of significance for those pathways, even if each factor individually fails to reach significance. However, using GO enrichment, I observed further important changes between proliferating and senescent fibroblasts in processes such as mRNA splicing and plasma membrane organization, with early changes (PRO vs. PERI) affecting cell growth, cell cycle and cell division processes and late changes (PERI vs. SEN) including DNA repair, nucleus organization, RNA processing and regulation of mitochondrial fission (Figure 6.4D-F).

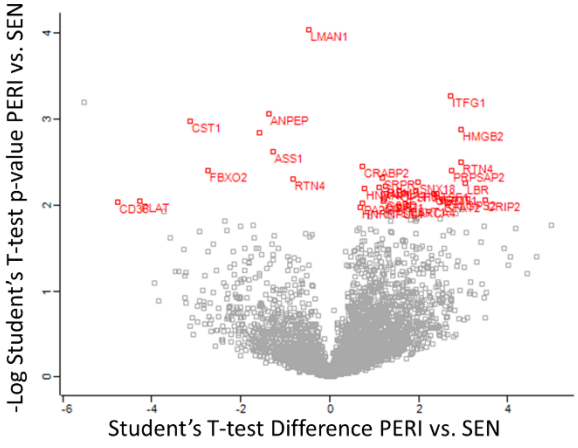
A


HNRNPC
CLD
GM2A
ANPEP
SPATS2L
RAB3IL1
COL8A1
CLTCL1
ASAP1
PDGFRA
PRDX5
PRDX1
PLAT
CST1
CTHRC
RPL
-Log Student's T-test p-value PRO vs. SEN
Student's T-test Difference PRO vs. SEN

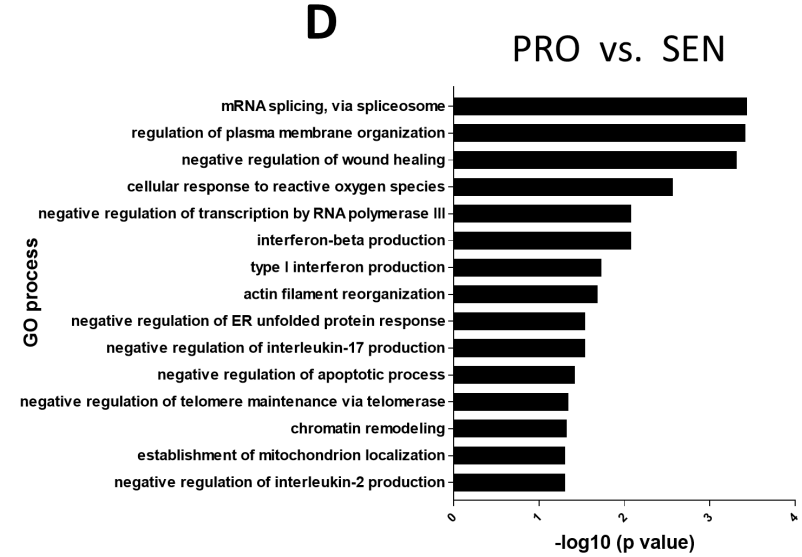
B


CRABP2
HCFC1
MIEN1
LIMA1
INPP5K
SEPT5
AKAP11
ARPP19
PPP3CB
-Log Student's T-test p-value PRO vs. PERI
Student's T-test Difference PRO vs. PERI

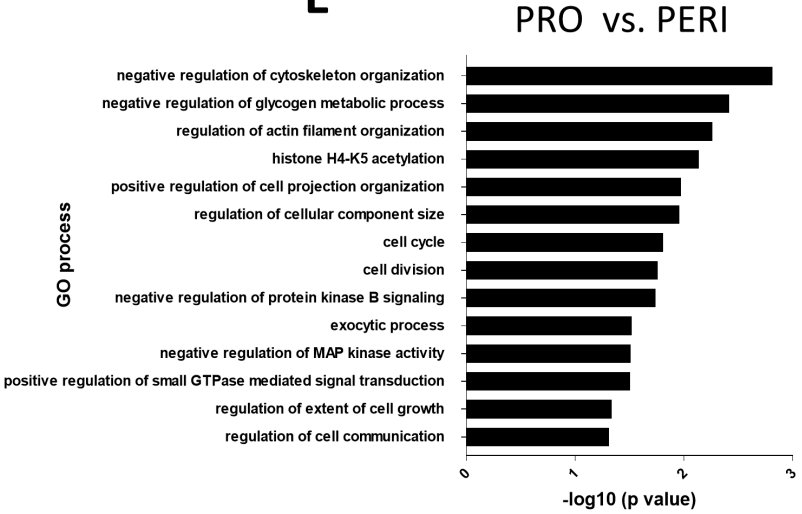
C


LMAN1
ITFG1
CST1
ANPEP
HMGB2
ASS1
FBXO2
CRABP2
RTN4
RTN4
PPSAP2
LBR
CD36
LAT
-Log Student's T-test p-value PERI vs. SEN
Student's T-test Difference PERI vs. SEN

D


PRO vs. SEN
mRNA splicing, via spliceosome
regulation of plasma membrane organization
negative regulation of wound healing
cellular response to reactive oxygen species
negative regulation of transcription by RNA polymerase III
interferon-beta production
type I interferon production
actin filament reorganization
negative regulation of ER unfolded protein response
negative regulation of interleukin-17 production
negative regulation of apoptotic process
negative regulation of telomere maintenance via telomerase
chromatin remodeling
establishment of mitochondrion localization
negative regulation of interleukin-2 production
GO process
0
1
2
3
4
-log10 (p value)

E


PRO vs. PERI
negative regulation of cytoskeleton organization
negative regulation of glycogen metabolic process
regulation of actin filament organization
histone H4-K5 acetylation
positive regulation of cell projection organization
regulation of cellular component size
cell cycle
cell division
negative regulation of protein kinase B signaling
exocytic process
negative regulation of MAP kinase activity
positive regulation of small GTPase mediated signal transduction
regulation of extent of cell growth
regulation of cell communication
GO process
0
1
2
3
-log10 (p value)

F

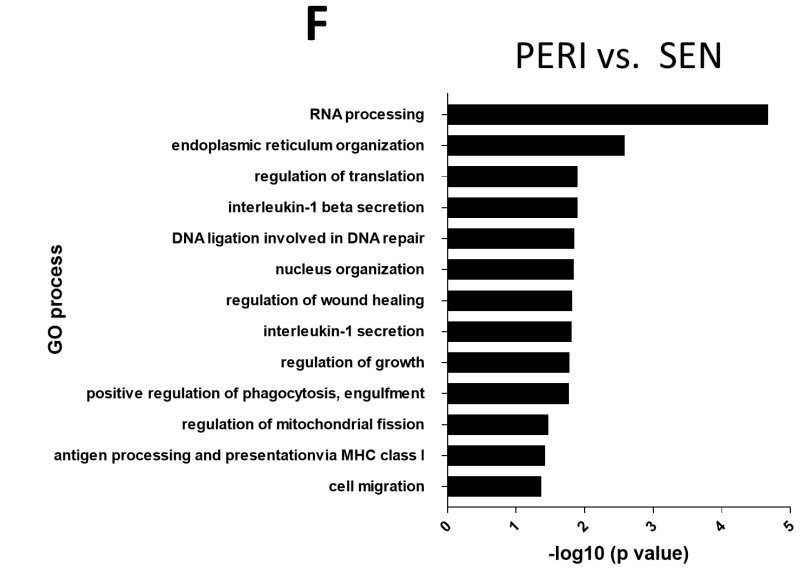

PERI vs. SEN
RNA processing
endoplasmic reticulum organization
regulation of translation
interleukin-1 beta secretion
DNA ligation involved in DNA repair
nucleus organization
regulation of wound healing
interleukin-1 secretion
regulation of growth
positive regulation of phagocytosis, engulfment
regulation of mitochondrial fission
antigen processing and presentationvia MHC class I
cell migration
GO process
0
1
2
3
4
5
-log10 (p value)

Figure 6.4 GO analysis of comparative proteomics highlights important processes altered by replicative senescence

Perseus software was used to perform t-tests using comparative proteomics datasets (log_2expression values between n=3 independent experiments) to produce a list of statistically significant expression changes in the annotated pairwise comparisons. The significantly altered candidate genes ('hits' p<0.01 cut-off in t-test) are shown in red in Volcano plots of pairwise comparisons (A-C). D-F: these hits were subsequently analysed as groups using GO term/PANTHER analysis to produce lists of molecular processes implicated by these expression changes, which were manually curated. The significance of each molecular process is shown as -log_{10}(p-value).

Expression of the individual candidate genes attributed to the GO terms was then assessed (Figure 6.5). In processes related to actin cytoskeletal organization, I observed upregulation in senescence of proteins including the regulator of actin filament assembly gelsolin (GSN), reticulon-4 (RTN4), implicated in cell migration, ER tubule formation and membrane trafficking, and plasminogen activator (PLAT) associated with cell migration and tissue remodelling (see Table S6.1 for p-values and t-test difference of 'hit' proteins). Proteins downregulated in senescence included the tyrosine kinase receptor PDGFRA, whose activity is context-dependent in processes including wound healing, chemotaxis and cell migration, proliferation and survival, the Rho GTPase activating protein SYDE1 which is highly expressed in the placenta, and CTHRC1, implicated in tissue remodelling (Figure 6.5). These differences in expression could indicate nuanced changes to the actin organization network in senescence; it is responsible for coordinating a multitude of different processes, possibly including inhibition of cell proliferation, migration and even apoptosis, as well as promoting transcription, translation, vesicle trafficking, wound healing and tissue remodelling.

Further, a number of GO processes that changed on replicative senescence were related to chromatin organization, RNA processing/splicing and protein translation. For example, I observed downregulation of the multifunctional DNA binding protein HMGB2 in SEN vs. PERI fibroblasts (Figure 6.5, Table S6.1). HMGB2 is associated with multiple DNA processes

including repair, recombination, transcription and chromatin remodelling. Furthermore, it has been implicated in orchestrating the SASP (Aird et al., 2016) and in senescence-associated transcriptional remodelling, by looping DNA at TAD boundaries, with its loss re-organizing CTCF-defined chromatin clustering (Zirkel et al., 2018). Furthermore, protein expression is intimately linked to senescence: continuous treatment with sub-toxic doses of the translational inhibitor cycloheximide delays replicative senescence (Takauji et al., 2016), nucleolar size (indicative of rRNA transcription and ribosome assembly) correlates with both senescence and ageing (Buchwalter and Hetzer, 2017, Tiku et al., 2017) and a subset of ribosomal genes identified through an siRNA screen have been shown to activate senescence in $p16^{+}$ breast cancer cells, showing increased nucleolar size and fragmentation in 'ribosomal stress-induced senescence' (Moore et al., 2018).

In the context of RNA processing, I observed downregulation of the splicing factors HNRNPC, HNRNPL and HNRNPUL1 as well as the polyadenylation regulator SF3B3 in SEN vs PRO fibroblasts (Figure 6.5, Table S6.1), suggesting aberrant regulation of splicing in senescence. Indeed, recent evidence has suggested that splicing factors are dysregulated both with ageing and in senescence of both endothelial cells and fibroblasts, and that cell cycle factors are major targets of differential splicing. However, a different molecular profile of significant expression changes was detected using microarray analysis and qPCR (Holly et al., 2013); this could highlight the importance of post-transcriptional regulation in controlling protein expression and these changes may also contribute to the increasing heterogeneity observed in senescence. Furthermore, treatment of senescent cells with analogues of resveratrol was shown to restore splicing factor expression (perhaps indirectly) and allow re-entry of apparently senescent cells into the cell cycle (Latorre et al., 2017). In addition, the alternative splicing mediator PTBP1 (polypyrimidine tract binding protein 1) was identified in an siRNA screen for genes which suppress the SASP without compromising proliferation arrest in senescence. Indeed, PTBP1 was shown to downregulate the SASP via controlling the

alternative splicing of EXOC7, which is involved in intracellular trafficking (Georgilis et al., 2018), highlighting a functional role for changes in regulation of splicing in senescence.

Interestingly, my data also suggest that the membrane protein and scavenger receptor CD36 is significantly upregulated in senescence (Figure 6.5, Table S6.1). CD36 coordinates intracellular import of fatty acids but is also implicated in RNA processing, plasma membrane organization and immune signalling. My observation that CD36 is upregulated in senescence is highly consistent with recent results: CD36 and further genes involved in lipid-related processes were shown to increase in replicative senescence of MRC5 and BJ fibroblasts by RNA-seq, with lipidomics analysis subsequently highlighting extensive membrane remodelling on senescence with an increase in phosphatidylcholines in senescent fibroblasts, with CD36 upregulation implicated in these changes (Saitou et al., 2018). Further data have suggested a role for CD36 upregulation in initiating the secretory phenotype, with ectopic CD36 expression sufficient to initiate SASP secretion via NFκB, while loss-of-function experiments revealed a requirement for CD36 in pro-inflammatory secretion (Chong et al., 2018). Intriguingly, *in vitro* data has shown that ezetimibe (the FDA-approved, off-patent treatment for high cholesterol) targets CD36 in pancreatic beta cells, thus protecting against glucotoxicity (Yoon et al., 2016). These findings warrant further investigation in the context of cellular senescence.

My comparative proteomics profile of replicative senescence also revealed that several ubiquitin-modifying enzymes were dysregulated in senescence. Firstly, levels of the ubiquitin E3 ligase TRIM56 are higher in PERI and SEN samples vs PRO fibroblasts (Figure 6.5); one target of its mono-ubiquitination is the cytosolic DNA sensor cGAS. TRIM56-mediated ubiquitination of cGAS induces its dimerization and activation (Seo et al., 2018); if it subsequently detects cytosolic DNA, it is then fully activated and converts ATP into GTP and the 2nd messenger cGAMP, which subsequently induces activation of STING, ultimately

resulting in expression of interferon, and driving pro-inflammatory secretion in senescence (Dou et al., 2017). Targeting TRIM56 to block cGAS activation may therefore present an alternative option to the STING inhibitors currently being explored in treating inflammation in senescence, cancer and a range of inflammatory diseases characterized by increased interferon signalling (Sheridan, 2019).

The deubiquitinating enzyme UCHL1 also appears to be elevated in senescence (Figure 6.5). This protein, which also has E3 ligase activity (Liu et al., 2002), has been implicated in the progression of both Alzheimer's and Parkinson's diseases; it may inhibit autophagy and has indeed been shown to interact with the E3 ligase Parkin, noted for its role in inducing degradation of dysfunctional mitochondria (Figure 1.4). Indeed, Parkin binds and ubiquitinates UCHL1 for degradation. The inhibitor LDN57444 has already been developed for UCHL1 (Liu et al., 2003), and should therefore be tested in senescent cells, particularly for regulation of autophagy and mitophagy, given the interaction between UCHL1 and Parkin. Finally, I also saw upregulation of the F-box protein family member FBXO2 in senescent fibroblasts, which comprises a subunit of SCF ubiquitin ligase complexes. In particular, FBXO2 has been linked with innate immune signalling and class I antigen processing and presentation, as well as the ERAD pathway activated in response to misfolded proteins in the ER, suggesting upregulation of FBXO2 could occur in response to cell stress, and mediate senescence – immune interplay.

In summary, this comparative proteomic profile of senescence analysed by pathway and GO analysis suggests a number of important changes in senescence, including regulation of gene expression, cytoskeletal organization and immune signalling, and highlighted a number of therapeutic candidate proteins and pathways for further investigation.

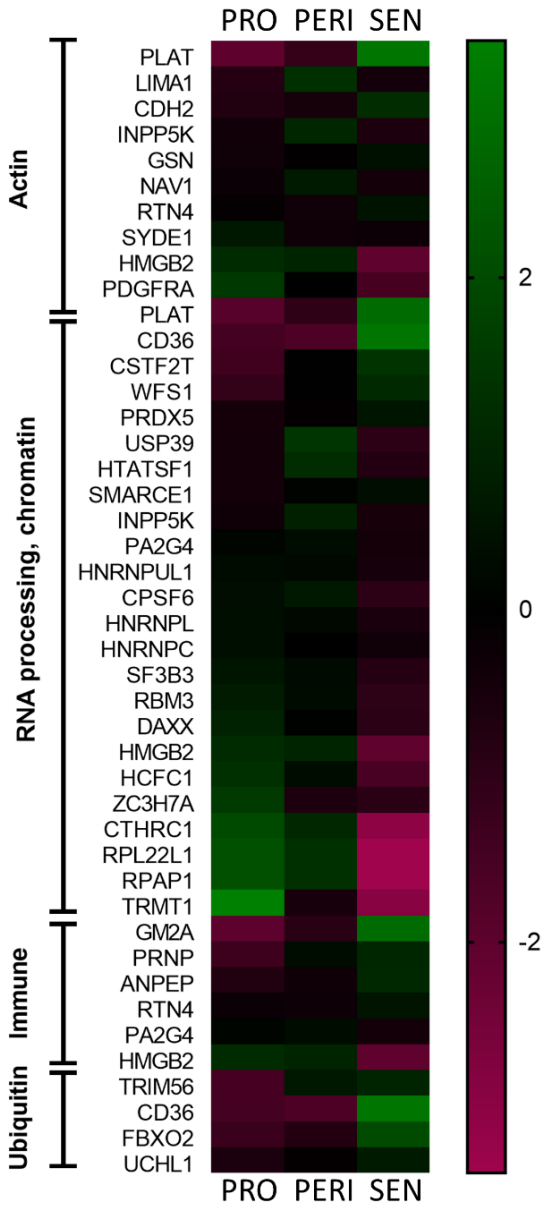


Figure 6.5 Important protein level changes in senescence

Proteins with significant expression changes (student t-test, $p<0.01$ cut-off, Figure 6.4A-C) implicated in important GO processes (Figure 6.4D-F) are listed by category, alongside expression (normalised intensity) as a heatmap averaged over n=3 independent experiments and then normalised by mean expression between samples (PRO, PERI and SEN). See Table S6.1 for full p-values and t-test differences of all differentially expressed protein hits.

6.3.2. Rejuvenation of the senescent proteome by acute pan-mTORC inhibition

My previous data suggested that short-term (7 day) treatment with AZD8055 can reverse phenotypes of senescence, and continuous or pulse-dosing treatment blocks entry into irreversible senescence (Chapter 4&5). To understand such changes at the molecular level, label-free comparative proteomics was conducted on HF043 fibroblasts following acute 7 day treatment with AZD8055 or vehicle control in PRO, PERI and SEN samples (as in Figure 6.2, n=3 independent experiments). Again, data quality was inspected by Pearson correlations and I subsequently interpreted the results using a combination of IPA™ and GO enrichment analysis to probe the biochemical pathways and individual proteins respectively (t-test, threshold for significance $p<0.01$, Figure 6.6 for Volcano plots and Table S6.2 for full list of statistical hits; 58 differentially expressed proteins detected in total on AZD8055 treatment).

IPA™ pathway analysis suggested that mTOR-associated pathways such as regulation of eIF4 and p70S6K signalling were strongly reduced on mTOR inhibition regardless of fibroblast replicative age, (Figure 6.6A) highly consistent with the known biochemical impact of AZD8055 as a pan-mTOR inhibitor (Chresta et al., 2010 and Figure 4.1). Interestingly, I noted that a number of pathways I had previously seen to increase on senescence, such as integrin, EIF2, IL-6, NFκB and MAPK signalling, were downregulated by AZD8055 treatment (Figure 6.6A). These results are highly consistent with decreased IL-6 secretion from AZD8055-treated senescent fibroblasts (Figure 4.8) and suggest potential proteomic rejuvenation by pan-mTOR inhibition. In addition, I noted that the increase in interferon signalling between PERI vs. PRO samples was rescued by mTOR inhibition, further emphasizing a role for mTOR signalling in regulating inflammation in senescence (Figure 6.6A). Intriguingly, TGFβ signalling was also dampened on AZD8055 treatment alongside telomerase signalling in

acutely treated senescent fibroblasts. These data are consistent with my observation that AZD8055 treatment does not immortalize fibroblasts or reverse senescence induction (Chapter 5) but also with my hypothesis that treatment could possibly impact paracrine pro-senescence signalling, in which TGFβ has been implicated. Furthermore, progressive increases in a number of actin reorganization pathways with increasing CPD were dampened by acute AZD8055 treatment including actin cytoskeleton, PAK and Rho GTPase signalling (Figure 6.6A). These findings are consistent my previous observations of dissolution of actin stress fibres and rejuvenation of senescent morphology on AZD8055 treatment of senescent fibroblasts (Chapter 4).

In addition, sirtuin signalling was also increased on AZD8055 treatment irrespective of sample replicative age, consistent with AZD8055 treatment preventing induction of senescence upon pharmacological SIRT1/2 inhibition (Chapter 5). Indeed, there may be important interplay between sirtuin and mTOR signalling; SIRT1 interacts with TSC1/2 to negatively regulate mTORC1 activity (Ghosh et al., 2010) but phosphorylation of SIRT1 by mTORC1 at Ser-46 inhibits its deacetylase activity. Furthermore, p70S6K activity is regulated by cross-talk in SIRT1/2-mediated deacetylation and mTOR-mediated phosphorylation (Hong et al., 2014, Igarashi and Guarente, 2016).

Significant changes in protein levels at each CPD upon acute AZD8055 treatment were analysed using Perseus software (Figure 6.6 B-D, Table S6.2), with GO enrichment analysis used to analyse the molecular processes implicated by these protein expression changes (Figure 6.6 E-G). In proliferating fibroblasts (PRO), I observed that AZD8055 treatment affected cell cycle pathways including regulation of the spindle assembly checkpoint and nuclear division, consistent with decreased rates of cell division observed in proliferating cells under AZD8055 treatment. I also noted that response to interferon and cytoskeletal organization were also impacted by AZD8055 treatment even in PRO samples, indicating a

role for mTOR signalling in regulating these processes independently of replicative senescence (Figure 6.6E).

In both PRO and PERI samples, GO processes relating to protein expression were prominently altered particularly by AZD8055 treatment. Such processes include regulation of translation initiation, ribosome assembly and RNA processing, highly consistent with a central role for mTOR signalling in regulating protein translation through 4EBP-1 and p70S6K. In terms of individual statistically significant hits (Figure 6.6H, Table S6.2 for p-values and t-test differences), the ATP-dependent RNA helicase DDX3X was significantly downregulated in PERI samples on AZD8055 treatment; DDX3X is involved in several stages of gene expression including transcription, RNA processing and translation initiation, particularly through cooperating with the eIF4F complex for translation of mRNAs carrying stem loop structures within the 5'UTR. Furthermore, DDX3X has anti-apoptotic activity and is also implicated in interferon production, and stress granule assembly – stress-induced cytosolic aggregations of proteins and stalled translation pre-initiation complexes that may be of importance in senescence (Shih et al., 2012). Downregulation of DDX3X after 7 day AZD8055 treatment could therefore indicate relief of proteotoxic stress.

Further prominent proteomic changes on AZD8055 treatment in PERI samples included regulation of mitochondrial fission, highly consistent with my data showing a decrease in mitochondrial load following AZD8055 treatment in senescent fibroblasts (Chapter 4). Indeed, STAT2, the regulator of mitochondrial fission which controls phosphorylation of the fission mediator DRP1 (Shahni et al., 2015), is downregulated by AZD8055 treatment in PERI samples vs vehicle only controls. Further, AZD8055 treatment also affected ROS processes at peri-senescence; acute treatment induced downregulation of proteins including catalase, which mediates decomposition of H_2O_2 to protect cells from ROS-induced oxidative damage, perhaps suggesting a lower level of oxidative stress following exposure to AZD8055.

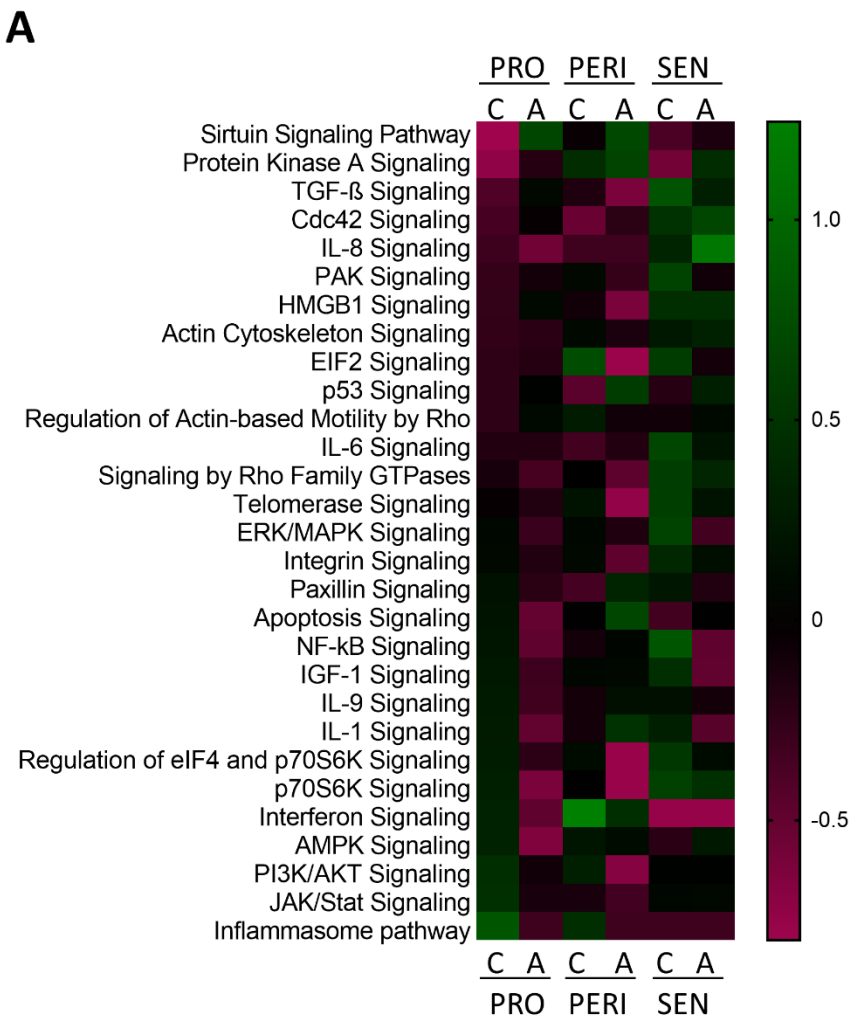
Furthermore, regulation of actin polymerization and the cytoskeleton were also affected by mTOR inhibition in PERI samples, highly consistent with pathway analysis (Figure 6.6A) and previous microscopy data (Chapter 4). In addition, AZD8055 treatment also affected regulation of nuclear size at peri-senescence, highly consistent with previous microscopy data showing AZD8055 treatment reduced senescent nuclear area (Chapter 4).

In senescent fibroblasts, a number of cytoskeletal processes were affected by AZD8055 treatment, including organization of cell projections, actin filaments and microtubules (Figure 6.6G). In particular, the actin nucleation factor WASL and motor protein KIF2A were downregulated on AZD8055 treatment, consistent with my observation of reduced actin filamentation on AZD8055 exposure (Table S6.2, Figure 6.6G, Figure 4.4). Further, the GO term apoptotic cell clearance was affected by mTOR inhibition in senescent fibroblasts, consistent with IPA™ analysis (Figure 6.6A,G) where apoptosis signalling was increased by AZD8055 treatment in both peri-senescent and senescent fibroblasts. This result warrants further investigation as to whether upon mTOR inhibition, senescent cells lose any inherent resistance to apoptosis (see section 8.2.2). Furthermore, I noted that a number of inflammatory pathways including antigen presentation and phagocytosis were also affected by mTOR inhibition in senescence (Figure 6.6G).

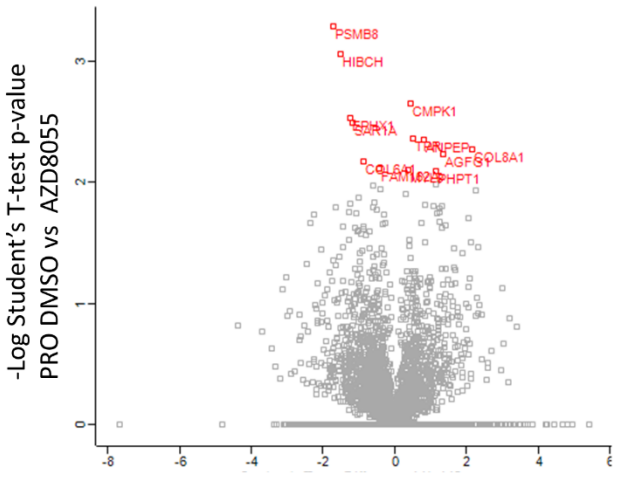
In summary, a number of important pathways and processes were reverted back to levels more consistent with PRO fibroblasts following AZD8055 treatment in peri-senescent and senescent fibroblasts, consistent with a degree of proteomic rejuvenation. In particular, cytoskeletal organization, protein synthesis, inflammatory signalling and processes including mitochondrial fission and apoptosis were markedly altered, highly consistent with my observations of reversal of phenotypes of senescence following pan-mTOR inhibitor treatment (Chapter 4).

Figure 6.6 Pan-mTOR inhibition causes proteomic changes over the replicative lifespan of primary fibroblasts

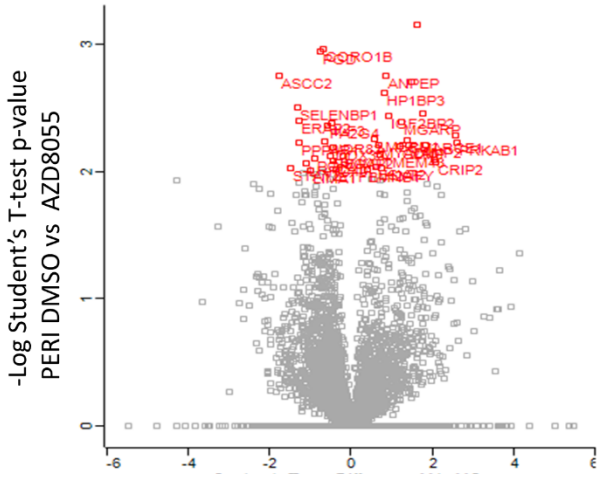
PRO, PERI and SEN fibroblasts as in Figure 6.2 were treated with DMSO vehicle control or 70 nM AZD8055 for 7 days before proteomic analysis. A: representative datasets from n=3 independent experiments were subsequently interpreted using IPA™ comparison analysis for important changes between samples, with the heatmap shown representing z-scores for activation of each pathway at each CPD with or without treatment, normalised by the mean z-score between samples. B-D: significantly altered proteins (red) on pan-mTOR inhibition at each replicative stage were calculated using student t-tests ($p<0.01$) and visualized in Volcano plots (see Table S6.2 for full list of 'hits'). E-G: statistical hits were subsequently analysed by GO term/PANTHER analysis and manually curated, with $-\log_{10}$ p-values shown indicating the significance of each affected process. H: proteins with significant expression changes (from B-D) implicated in important GO processes (in E-G) are listed by category, alongside expression averaged over n=3 independent experiments and normalized by mean intensity between samples, shown as a heatmap.



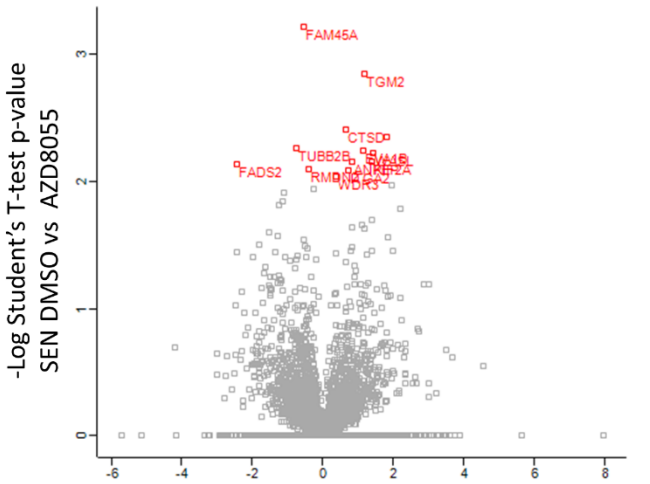
B


-Log Student's T-test p-value
PRO DMSO vs AZD8055
PSMB8
HIBCH
CMPK1
AGFG1
SOL8A1
PHPT1
Student's T-test Difference PRO DMSO vs AZD8055

C

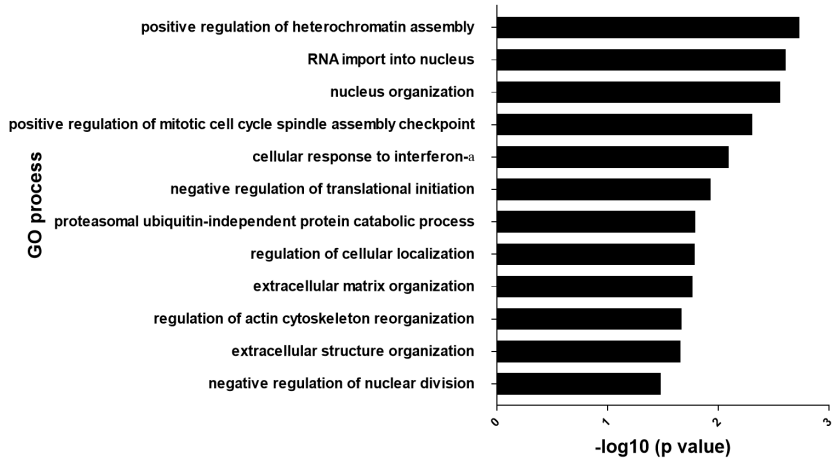

-Log Student's T-test p-value
PERI DMSO vs AZD8055
ASCC2
HP1BP3
SELENBP1
CRIP2
Student's T-test Difference PERI DMSO vs AZD8055

D


-Log Student's T-test p-value
SEN DMSO vs AZD8055
FAM45A
TGM2
CTSD
FADS2
Student's T-test Difference SEN DMSO vs AZD8055

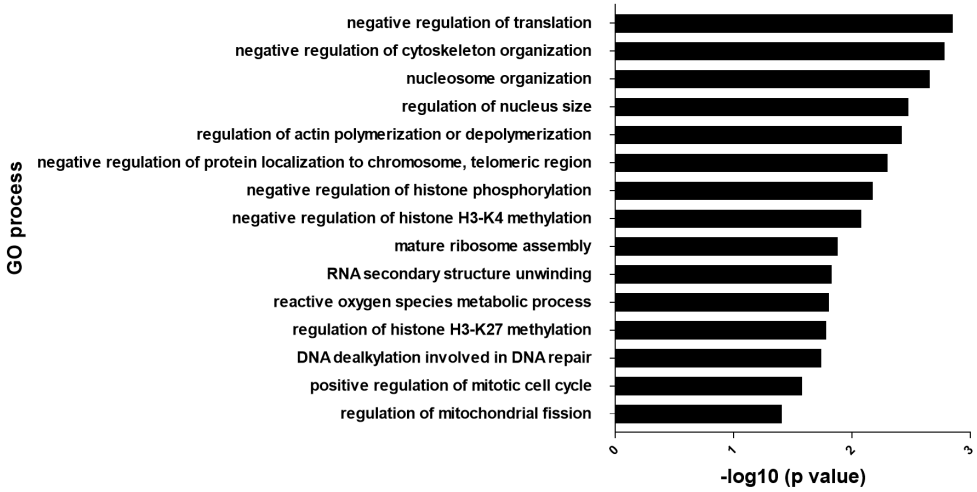
E

PRO ± AZD8055



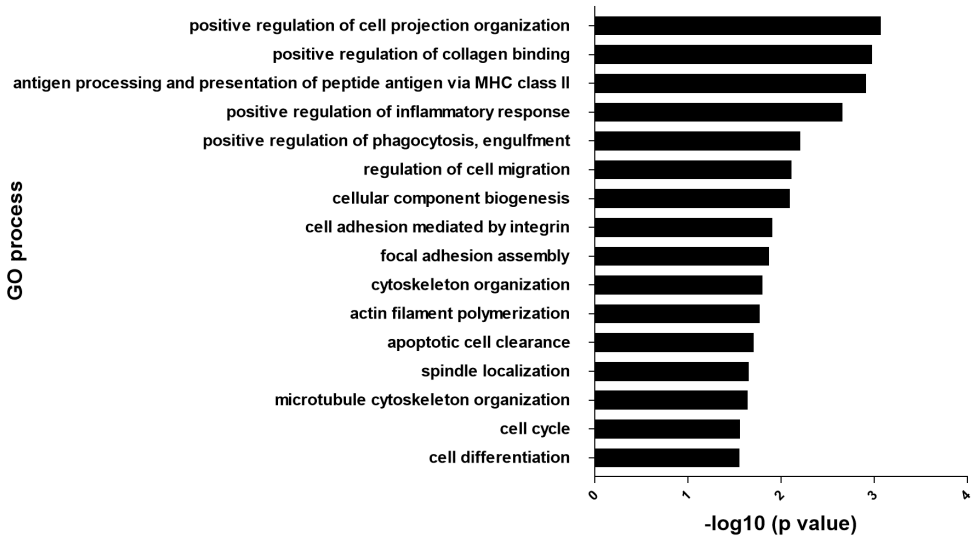
F

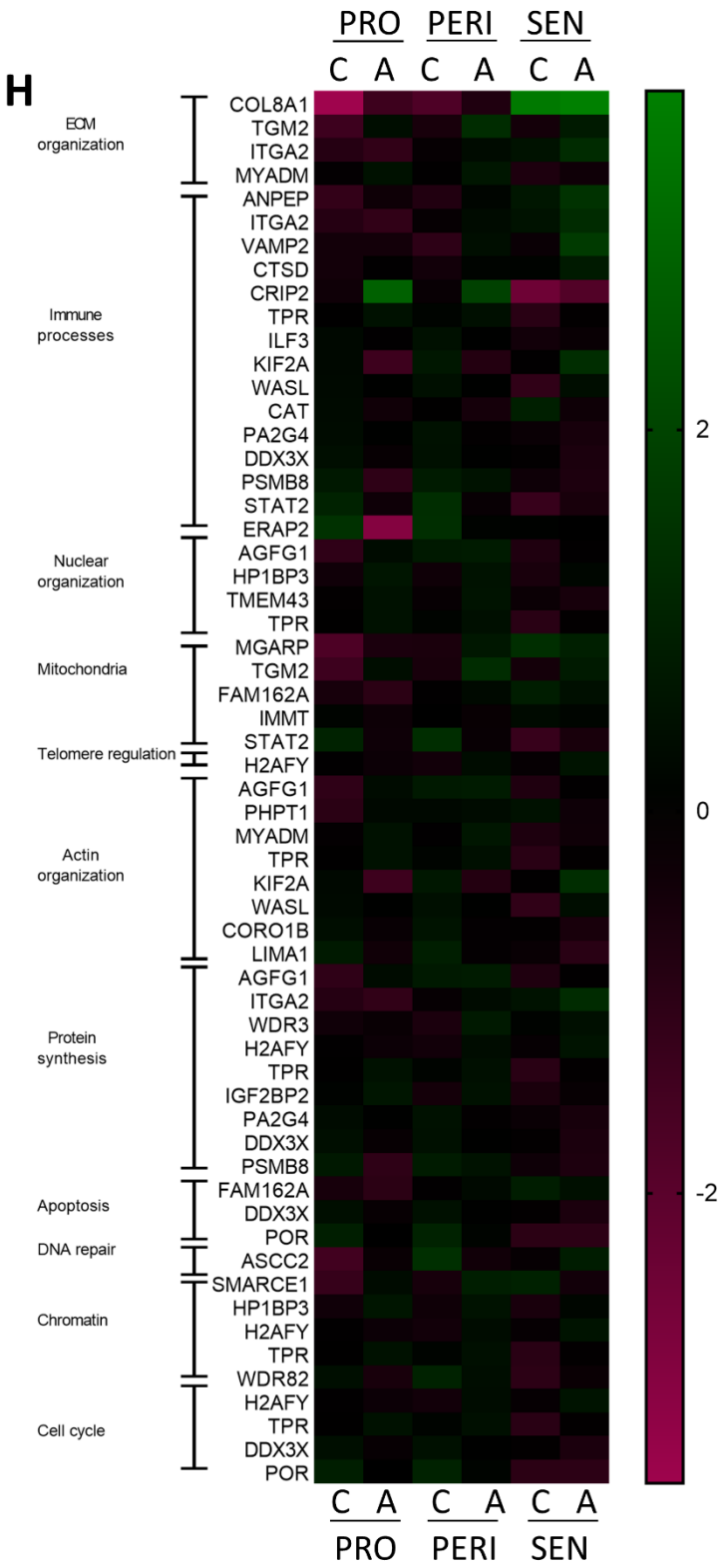
PERI ± AZD8055



G

SEN ± AZD8055




H
PRO PERI SEN
C A C A C A
ECM organization
COL8A1
TGM2
ITGA2
MYADM
Immune processes
ANPEP
ITGA2
VAMP2
CTSD
CRIP2
TPR
ILF3
KIF2A
WASL
CAT
PA2G4
DDX3X
PSMB8
STAT2
ERAP2
Nuclear organization
AGFG1
HP1BP3
TMEM43
TPR
Mitochondria
MGARP
TGM2
FAM162A
IMMT
Telomere regulation
STAT2
H2AFY
Actin organization
AGFG1
PHPT1
MYADM
TPR
KIF2A
WASL
CORO1B
LIMA1
Protein synthesis
AGFG1
ITGA2
WDR3
H2AFY
TPR
IGF2BP2
PA2G4
DDX3X
PSMB8
Apoptosis
FAM162A
DDX3X
DNA repair
POR
ASCC2
Chromatin
SMARCE1
HP1BP3
H2AFY
TPR
Cell cycle
WDR82
H2AFY
TPR
DDX3X
POR
2
0
-2
C A C A C A
PRO PERI SEN

6.3.3. Comparative proteomics analysis of replicative senescence identifies therapeutic candidate pathways and targets

6.3.3.1. Targeting actin reorganization

My comparative proteomic profiling of entry into replicative senescence in primary human fibroblasts, alongside analysis of how the senescent cellular proteome is rejuvenated on acute pan-mTOR inhibition, allowed me to identify pathways and proteins that may be viable therapeutic candidates to target in senescent cells. Such pathways or proteins should be significantly altered in senescence, and amenable to inhibition by existing commercially-available compounds, to assess whether these targets are valid and druggable, at least in senescent cells *in vitro*.

I first identified signalling pathways that my pathway analysis had shown to be significantly altered upon entry into senescence (Figure 6.3), which had not yet been fully explored for their therapeutic potential in senescence. Intriguingly, I observed that actin cytoskeleton signalling networks were substantially elevated with increasing CPD, as well as associated regulatory pathways including signalling through Rho GTPases such as Cdc42, or downstream effector kinases such as PAK (highlighted in Figure 6.7A). Following activation, Rho GTPases bind a variety of effectors including protein kinases and actin-binding proteins, to mediate the local assembly or disassembly of actin filaments and thus modulate cytoskeletal dynamics. For example, activated Cdc42 activates p21-activated kinases (PAKs) which in turn regulate actin reorganization (reviewed in Heasman and Ridley, 2008). ROCK kinases are also involved in regulating actin cytoskeletal organization and associated functions, as well as cell proliferation and motility. Indeed, through phosphorylating and activating MLC (myosin light chain) and inhibiting MLC-phosphatase through phosphorylation, ROCK1/2 activity has been linked with increased assembly and stability of actin stress fibres (Amano et al., 1996). Senescent cells exhibit highly filamentous actin

organization, with prominent stress fibres, which are reorganized upon pan-mTOR inhibition (Chapter 4). Therefore, I hypothesized that inhibiting effector proteins upregulated in senescence which act to induce actin filamentation would impact stress fibre assembly and possibly alter senescent morphology.

To test this hypothesis, I chose three commercially available pharmacological inhibitors of these cytoskeletal modulators: the Cdc42 inhibitor CASIN (Cdc42 Activity Specific Inhibitor, a specific and reversible inhibitor discovered in a high throughput screen, Liu et al., 2008), the PAK4 inhibitor PF-3758309 (a selective, ATP-competitive inhibitor developed from high throughput screen using structure-based design, Murray et al., 2010) and Y-27632, a selective kinase domain inhibitor of the ROCK family kinases 1/2 (Uehata et al., 1997) which are major downstream effectors of the small GTPase RhoA (Figure 6.7B).

Using this panel of inhibitors, I first determined non-toxic doses of each compound using the alamarBlue assay, which uses cellular reducing capacity measured through reduction of a resazurin compound as a proxy for cell viability. Doses of ≤1 μM of each compound resulted in less than ~50% toxicity in replicatively senescent HF043 fibroblasts after 48 hours treatment (Figure 6.7B). Interestingly, proliferating control cells at low CPD (<50) were more sensitive to both Y-27632 and PF-3758309 in the cell viability assay than replicatively senescent cells, perhaps reflecting the resistance to apoptosis of senescent fibroblasts, or a block of proliferation induced by cytoskeleton disruption in proliferating fibroblasts. However, this pattern of toxicity was not observed for CASIN, even though it acts upstream of PAK and ROCK (Figure 6.7B).

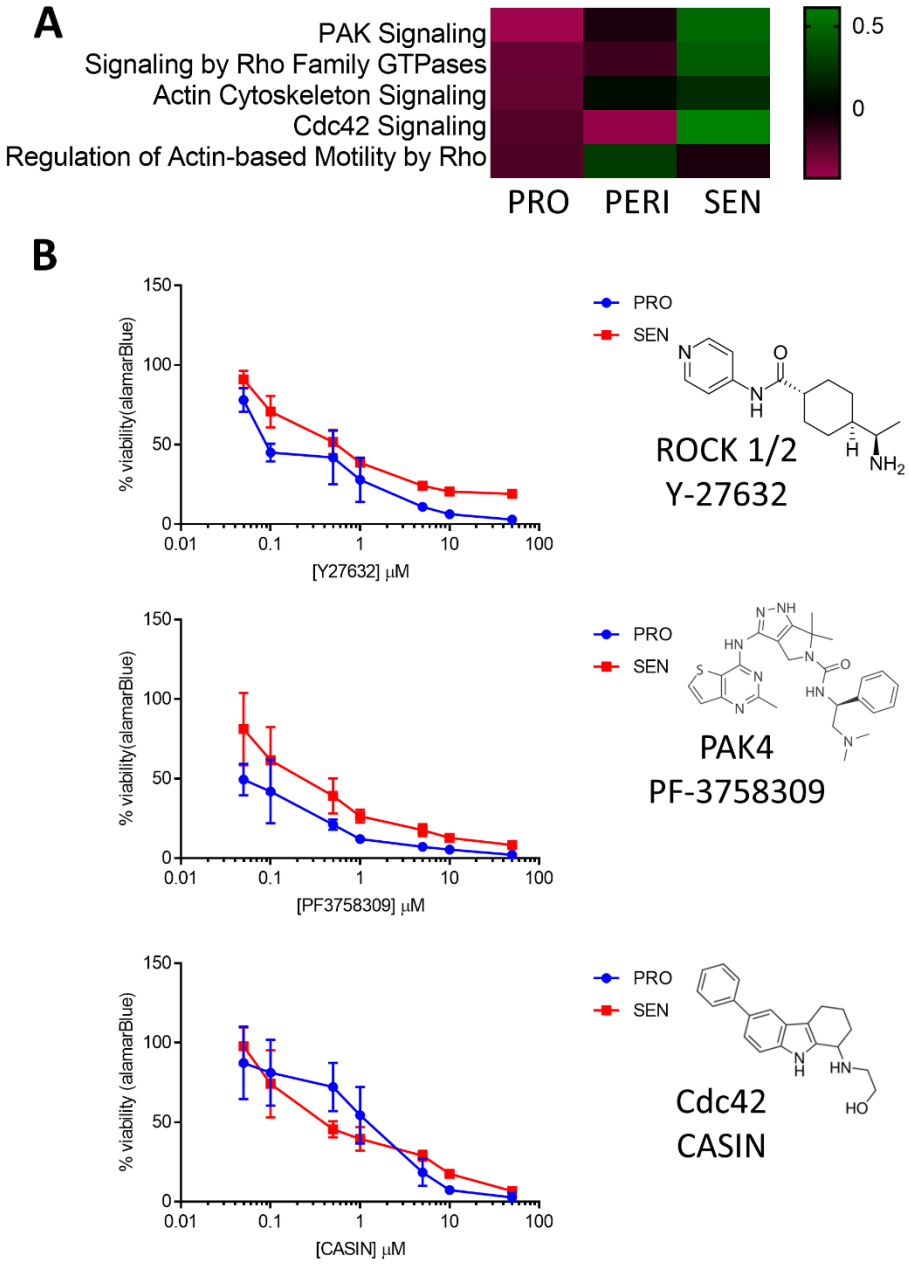


Figure 6.7 Cytoskeletal remodelling is a therapeutic target in senescence

A: Data is reproduced from Figure 6.2 highlighting changes to cytoskeletal remodelling pathways (z-scores shown normalised by mean of samples in each pathway). B: Proliferating (CPD <40) and replicatively senescent (CPD $\geq$ 90) HF043 fibroblasts were treated in a 96-well plate for 48 hours with a dose-range of each of three inhibitors of actin polymerisation: Y-27632, PF-3758309 and CASIN (structures and molecular targets shown). Cell viability was subsequently measured using the alamarBlue assay (representative data shown of n=3 experiments, error bars indicate SD between triplicate wells).

Having determined subtoxic doses, I therefore treated replicatively senescent primary human fibroblasts (HF043) and proliferating cell controls with 1 μM doses of each compound for 4 days prior to microscopy analysis (Figure 6.8, treated proliferating controls not shown for simplicity). Using rhodamine-phalloidin to examine actin filament distribution (Figure 6.8B), I saw large filamentous actin stress fibres in control senescent fibroblasts, compared to less intense actin staining in proliferating controls, where fibres predominantly occurred at cell edges, consistent with my previous microscopy results and the proteomics analysis (Figure 6.8B). This cytoskeletal reorganization in senescence was reflected by changes in cell morphology from the small, spindle-shape of proliferating cells to the enlarged, flattened morphology characteristic of senescent fibroblasts (Figure 6.8A, cells stained with SRB for morphological inspection). Upon treatment with the panel of inhibitors targeting actin modulators, I observed cytoskeletal re-organization and a reduction in stress fibres in senescent fibroblasts, especially notable following Y-27632 or CASIN treatment, where fibres were observed but only around the cell periphery (Figure 6.8B). Such cytoskeletal reorganization also correlated with morphological rejuvenation of the senescent fibroblasts towards a more spindle-like morphology reminiscent of the proliferating controls (Figure 6.8A). Moreover, drug treatment targeting actin reorganization in senescence led to a marked reduction in SA-β-gal staining, from intense blue staining in senescent control cells to a lower level of staining intensity usually observed in proliferating cells (Figure 6.8C). Hence actin dynamics are not simply a consequence of senescence but may act as a driver of certain senescence phenotypes.

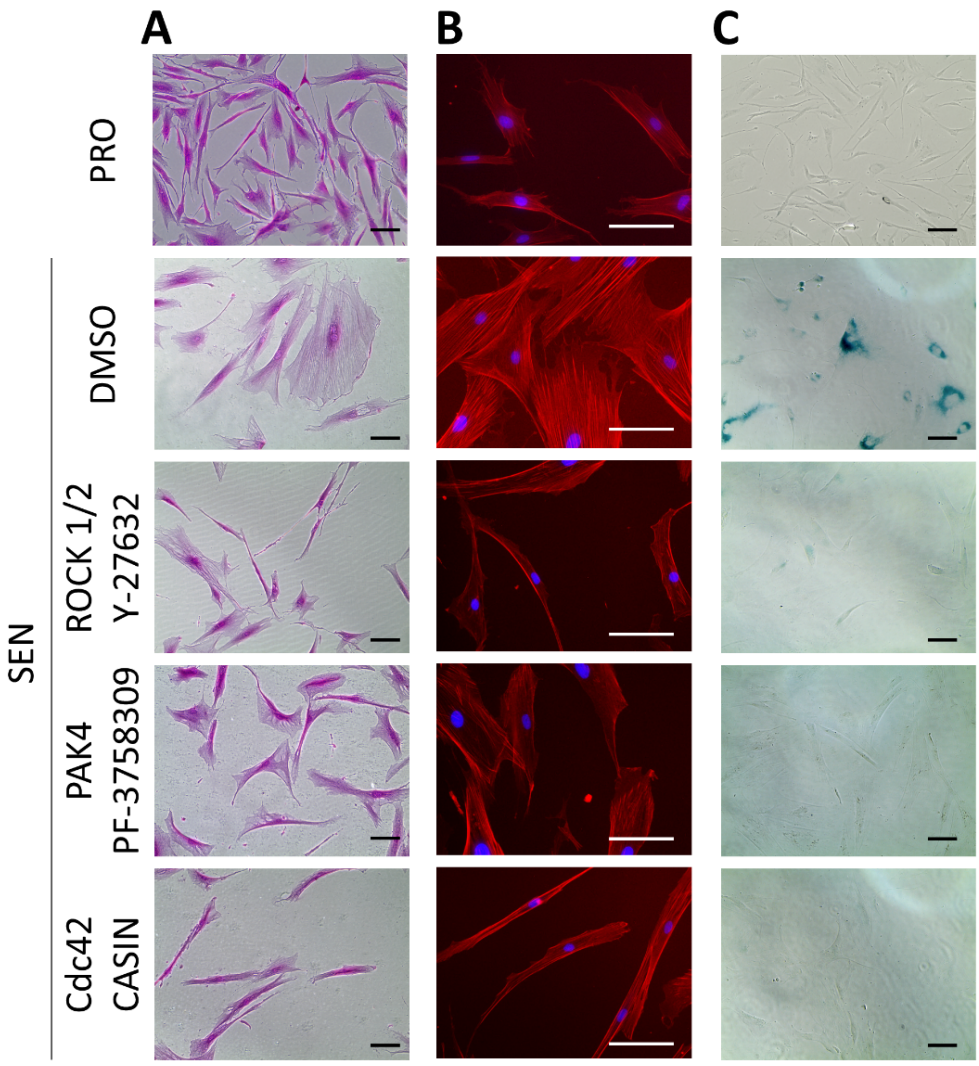


Figure 6.8 Inhibiting actin polymerisation through ROCK, PAK or Cdc42 disrupts phenotypes of senescence

Proliferating (CPD <40) and replicatively senescent (CPD ≥90) HF043 fibroblasts were treated for 4 days with DMSO vehicle control or 1 μM Y-27632, PF-3758309 or CASIN before examination of A: morphology following SRB staining, B: actin organization by rhodamine-phalloidin staining and C: lysosomal dysfunction by SA-β-gal staining. Representative images from n>3 experiments shown.

6.3.3.2. Targeting oxidative stress

To identify additional druggable targets in senescence, I used the online gene annotation resource Metascape to suggest commercially available compounds that target proteins that

my proteomics analysis suggested were significantly altered on senescence (Zhou et al., 2019). I then manually curated this list using the literature to assess whether certain compounds could be therapeutically useful (examples shown in Figure 6.9).

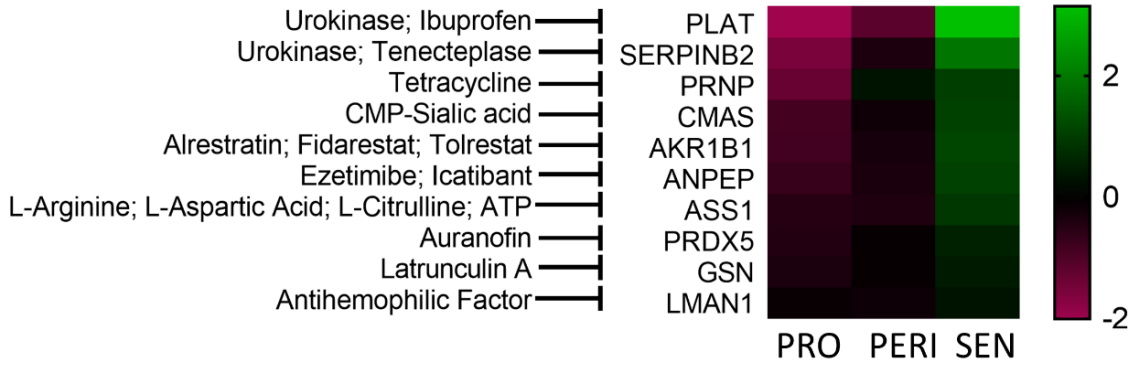


Figure 6.9 Possible therapeutic targets upregulated in senescence

Significant protein expression changes in replicative senescence were analysed using Metascape to suggest pharmacological inhibitors for individual therapeutic targets, with normalised protein expression data shown in a heatmap by replicative stage, normalized by mean expression values between samples.

In particular, I noted that the antioxidant protein PRDX5, targetable by auranofin (Figure 6.9, 6.10A), was significantly upregulated with increasing CPD. PRDX5 is a major player in the context of oxidative stress, presumably upregulated in senescence a compensatory mechanism for mitochondrial dysfunction and accumulation. Indeed, additional peroxiredoxin and thioredoxin family members and other antioxidant enzymes were also upregulated in– albeit not statistically significantly – with increased replicative age (Figure 6.10B, asterisks indicate significant changes in expression, see Table S6.1). The peroxiredoxins are a highly abundant family of antioxidant enzymes (PRDX1-6 in humans) which also control cytokine-induced peroxide levels. They function through oxidation of a redox-active cysteine within the enzyme active site, and subsequently rely on thioredoxin

(TXN) enzymes for reduction (Wood et al., 2003). Thioredoxins also interact with further proteins including AMPK and NFκB, where by reducing a disulphide bond, TRX1 promotes binding to DNA (Matthews et al., 1992). Indicative of a role for TRX1 in senescence and ageing, transgenic mice which overexpress thioredoxin show increased lifespan (Yoshida et al., 2005). Thanks to the protective effect of these enzymes, recent evidence has suggested that oxidative stress in senescence can be exploited as a senolytic target (Zhang et al., 2018).

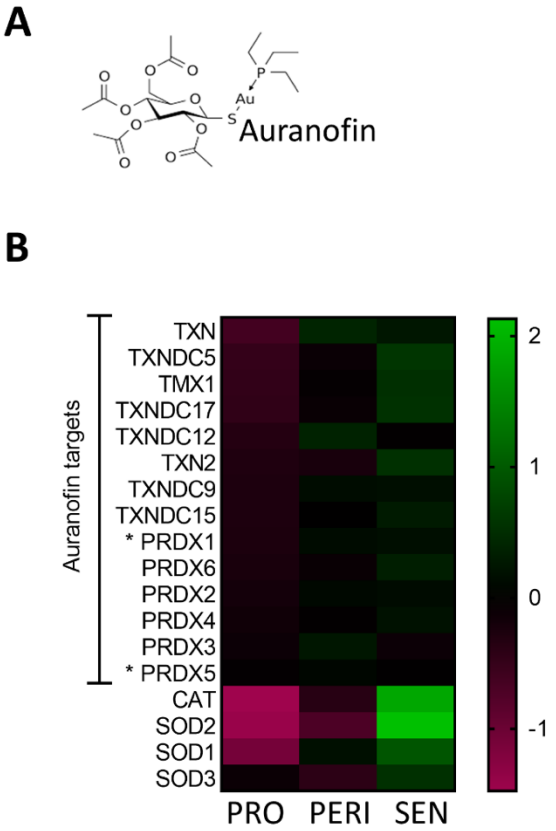


Figure 6.10 Upregulation of redox enzymes in replicative senescence

A: Auranofin structure. B: normalised expression (by mean between samples) of redox/ oxidative stress enzymes is shown by replicative stage (asterisk indicates proteins with significant expression changes according to student t-test, $p<0.01$ cut-off, see Table S6.1).

Auranofin is a redox enzyme inhibitor which operates through a thiol ligand; it has high affinity for both thiol and selenol groups in redox enzymes such as reductases and peroxiredoxins, to which it forms stable adducts thereby blocking enzyme activity, inducing

oxidative stress and apoptosis (Figure 6.10A). It has been approved as a safe, orally administered treatment for rheumatoid arthritis (RA) but is also a promising treatment for cancer, neurodegeneration and infectious disease. In RA, auranofin slows disease progression by suppressing inflammation and stimulating cell-mediated immunity. However, new and increasingly effective therapies such as the antibody infliximab have led to a decline in use, and auranofin was unsuitable for long-term use due to the relatively high rate of digestive side effects. Particular cell types that overexpress redox enzymes are vulnerable to off-target effects, suggesting that high ROS and redox enzyme-expressing senescent cells may be susceptible to auranofin.

First, I investigated whether auranofin induced oxidative stress in low CPD human primary fibroblasts (HF043) at a low, non-toxic dose for 48 hours, analysing mitochondrial ROS using the fluorescent stains Mitotracker CMXROS and DCFDA. I noted increased staining with both dyes in treated cells, suggestive of increased levels of ROS and oxidative stress, validating the mechanism of action in these primary fibroblasts (Figure 6.11).

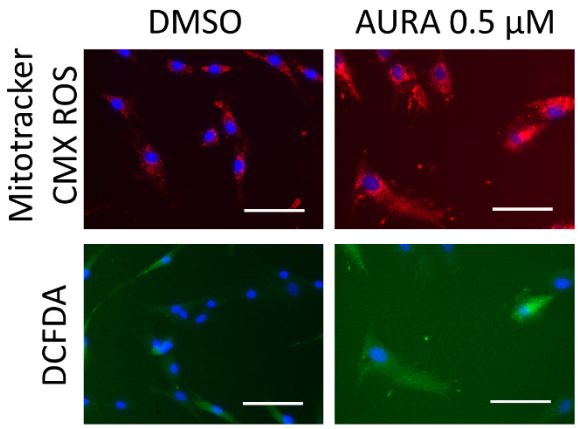


Figure 6.11 Auranofin induces oxidative stress in proliferating fibroblasts

Low CPD (<50) proliferating HF043 fibroblasts were treated with DMSO vehicle control or 0.5 µM auranofin for 48 hours in culture before examination of oxidative stress using Mitotracker CMX ROS and DCFDA staining, analysed by fluorescence microscopy. Representative data shown from n=3 independent experiments. Scale bar 100 µm.

Subsequently, I investigated whether auranofin had potentially senolytic activity. Proliferating, replicatively and DNA damage-induced senescent fibroblasts (HF043) were treated with a dose range of auranofin for 48 hours and viability was measured by alamarBlue reduction (Figure 6.12). Intriguingly, I noted that senescent fibroblasts (both RS and DDIS) were more sensitive to auranofin treatment than proliferating controls, suggesting a senolytic effect of auranofin treatment. I further confirmed this through fixing and staining treated fibroblasts with SRB; a dose of 0.5 μM greatly reduced cell number and induced cell rounding (suggestive of apoptosis) in senescent fibroblasts (Figure 6.12). Importantly, this suggests that targeting oxidative stress could be senolytic in multiple types of senescence, despite identification of the peroxiredoxin targets from a comparative proteomics screen of replicative senescence. In proliferating controls however, there was limited evidence of apoptosis at the same auranofin dose, but a reduction in cell number compared to untreated controls. This highlights the important caveat that even in healthy cells, redox enzymes are important in preventing oxidative stress; inhibiting such enzymes could block cell proliferation, or even perhaps induce senescence.

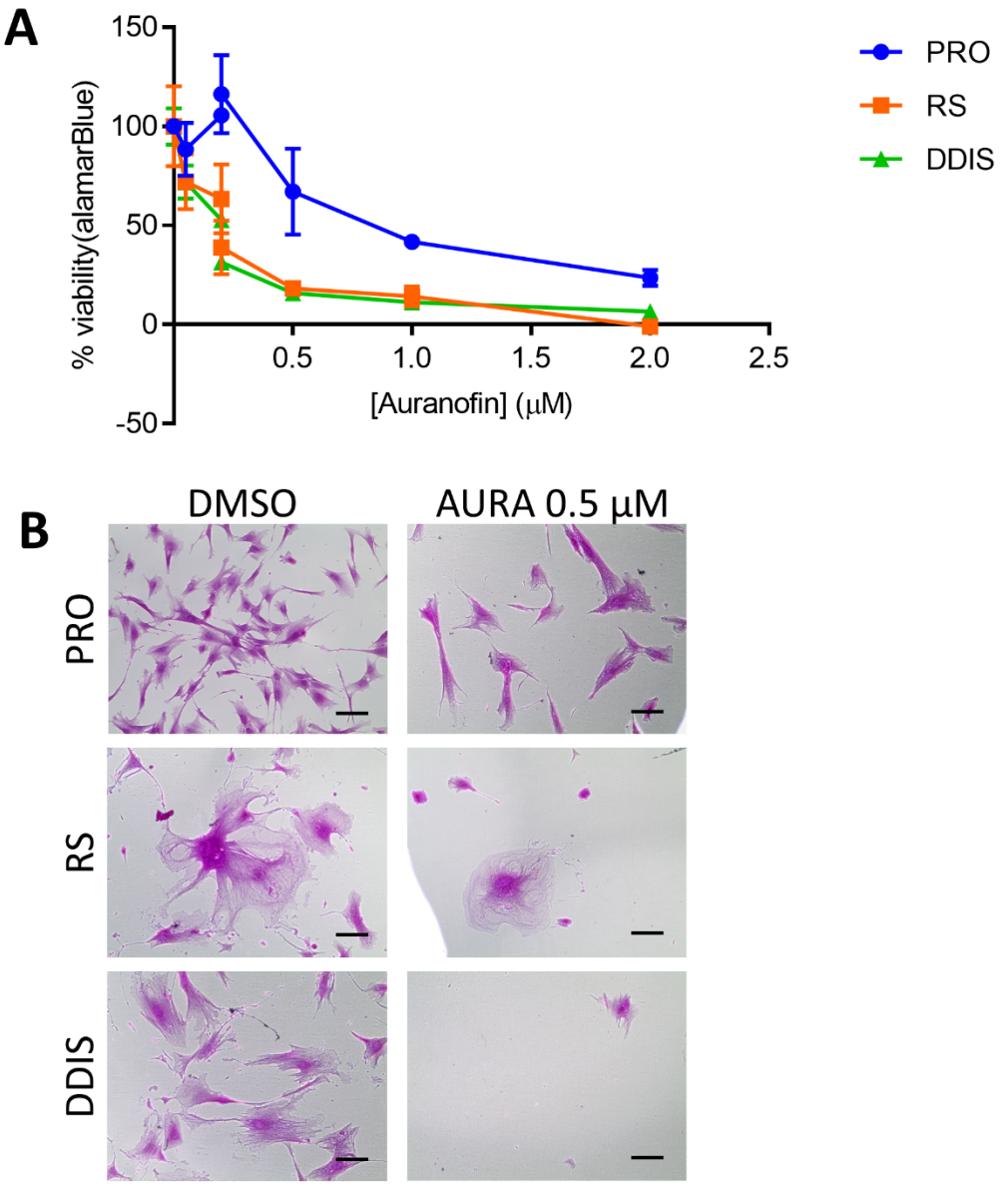


Figure 6.12 Targeting oxidative stress in senescence using auranofin is mildly senolytic

Proliferating CPD (<40), replicative senescent (CPD ≥90) and DNA damage induced senescent (7 day etoposide treated, CPD <40) HF043 fibroblasts were treated with a dose range of auranofin for 48 hours before analysis of cell viability by A: the alamarBlue assay and B: SRB staining and microscopic analysis. Representative data shown of n=3 experiments, error bars in A represent SD between triplicate repeats. Scale bar 100 μm.

6.4. Discussion

In this chapter, I have used comparative proteomics analysis to profile the molecular changes that occur in primary human fibroblasts during continuous culture towards replicative senescence, including changes in translational control, inflammatory signalling, protein ubiquitination, RNA processing and cytoskeletal remodelling. Furthermore, I observed that number of these important changes including inflammatory signalling, translational control, mitochondrial fission and cytoskeletal organization were disrupted in senescent samples by acute pan-mTOR inhibition, possibly indicating proteomic 'rejuvenation' as the molecular basis for previously observed effects of AZD8055 treatment at the cellular level (Chapter 4, Chapter 5). In addition, I identified oxidative stress and cytoskeletal organization as potential therapeutic targets in senescence, and showed selective toxicity to senescent fibroblasts upon pharmacological interference with oxidative stress tolerance proteins, and disruption of features of senescence using treatments to interfere with actin polymerisation.

6.4.1. Actin organization and senescence

Cell size and morphology are regulated by signaling pathways such as mTORC2 that impact on the complex and highly dynamic cytoskeletal network (Jacinto et al., 2004), which not only acts as a scaffold to provide cellular structural integrity but orchestrates an array of finely regulated cellular processes. These include directing cell motility, polarization, endocytosis, connection to the extracellular matrix, intracellular transport of organelles and vesicles, chromosomal segregation, cytokinesis and even transcription and translation (Miralles and Visa, 2006). The cytoskeleton comprises three major types of filaments, composed of actin microfilaments, microtubules made of tubulin, and intermediate filaments (such as vimentin) each constructed by polymerization of individual protein subunits. For example, following nucleation by factors such as the ARP2/3 complex, formin

and WASP proteins, individual actin monomers (i.e. globular actin) are polymerized using ATP into asymmetric actin filaments (filamentous actin) with one barbed (+, fast-growing) and one pointed (-, slow-growing) end to provide directionality and enable force generation. These filaments can be assembled into higher order structures including patches and cables to coordinate cellular functions. For example, actin cortical patches mediate endosome internalization, whilst actin cables mediate intracellular organelle transport using type V myosin molecules. Actin structures are controlled by the activity of formins such as the Rho GTPase family including Rho, Rac and Cdc42.

Interestingly, in the simple model of *S. cerevisiae* where there is only one gene for actin (ACT1), cytoskeletal reorganization has been linked to DNA repair, protein aggregation, oxidative stress, apoptosis and replicative ageing; indeed mutations that increase the dynamic nature of the actin cytoskeleton result in decreased levels of ROS, while deletion of the *S. cerevisiae* homologue of transgelin (which destabilizes cortical actin structures) also reduces oxidative stress and increases replicative lifespan (Gourlay et al., 2004).

Actin is also actively transported into and out of the nucleus by importin-9 (IPO9) and exportin-6 (XPO6) respectively, resulting in a finely regulated nuclear actin pool. In the cytoplasm, actin is predominantly found as part of polymerized filaments, but the nuclear actin pool is predominantly globular, though transient filaments have been observed, including in response to DNA damage. Actin-interacting proteins are implicated in DNA damage resolution: for example ARP2/3 coordinates DSB clustering and actin remodeling within the nucleus has also been shown to affect transcription, DNA replication and chromatin decondensation (Hurst et al., 2019). Consistent with a role for nuclear actin in DNA repair and replication, an increase in globular actin has been observed within the nuclei of senescent cells, appearing early (before SA-β-gal staining) in acutely-induced senescence, in conjunction with cofilin dephosphorylation and activation (which disassembles actin

filaments) and limited activity of its kinase LIMK (Kwak et al., 2004). Intriguingly, inducing nuclear export of globular actin in both primary and cancerous senescent cells resulted in senescence escape, with an increase in DNA synthesis and morphological rejuvenation observed together with p21 downregulation (Kwak et al., 2004), providing compelling evidence for nuclear actin in the onset of cellular senescence and further mechanistic implications for modulating senescence by targeting actin dynamics.

Further cytoskeletal changes beyond actin reorganization have also been observed in senescence. For example, the intermediate filament (IF) protein vimentin is strongly upregulated in senescent cells, resulting in a long, dense vimentin network within the reorganized senescent cytoskeleton (Nishio and Inoue, 2005) that also controls nuclear shape and integrity (Patteson et al., 2019). p53 has been observed to anchor to this upregulated vimentin network, highlighting a potential functional role for this upregulation (Nishio and Inoue, 2005). Notably, overexpression of vimentin in proliferating fibroblasts confers senescent morphology (Nishio et al., 2001). Furthermore, as revealed using a natural polyreactive antibody produced by senescent-cell-immunized BALB/c mice, senescent cells secrete an oxidized form of membrane-bound vimentin, detectable in the blood plasma of accelerated aged mice (Frescas et al., 2017). Vimentin has also been shown to form cross-linkage products with recombinogenic nuclear and mitochondrial DNA, suggesting it may protect against oxidative damage (Tolstonog et al., 2001). Collectively, these data suggest that regulation and modification of vimentin and actin cytoskeletal networks may play important roles in regulating senescent morphology, nuclear integrity, the DNA damage response, apoptosis and senescent cell clearance through humoral immunity, highlighting the multi-faceted roles of cytoskeletal organization in senescence. Therefore, targeting central proteins within actin reorganization networks altered at the onset of cell senescence results in disruption of several deleterious phenotypes of senescence, which warrant further mechanistic and *in vivo* exploration.

I previously reported that upon acute pan-mTOR inhibition in senescent cells, substantial actin stress fibres distributed within the cytoplasm are re-organized, accompanied by a shift from filamentous to globular actin. While mTOR activity regulates a multitude of cellular processes including autophagy and protein translation which may also be important in driving hypertrophy in senescence, there is an intriguing link between mTOR signaling and actin organization. Indeed, I observed substantial changes to several cytoskeletal remodeling pathways upon replicative senescence (Figure 6.3, 6.6, 6.7) that were disrupted by acute pan-mTOR inhibition. Indeed, rapamycin has previously been shown to inhibit tumour cell motility by preventing IGF-1-stimulated filamentous actin reorganization in cancer cells, as well as inhibiting phosphorylation of focal adhesion proteins including FAK and paxillin (Liu et al., 2008). Furthermore, mTORC1 and mTORC2 signaling have been shown to control the synthesis and activity of Rho GTPases including RhoA, Cdc42 and Rac1 respectively (Jacinto et al., 2004, Liu et al., 2010). Together, these data suggest that cytoskeletal organization may be altered in senescence, with a possible role for constitutive mTOR activity in driving this change.

In this chapter, I revealed that inhibitors of actin organization disrupt features of senescence (morphology, stress fibres and lysosomal dysfunction) in replicatively senescent fibroblasts (Figure 6.8). Indeed, these results are consistent with limited evidence from the literature: in salivary gland stem cells, ROCK1/2 inhibition using Y-27632 increased sphere formation, which was attributed to disrupting senescence, as reduced SA-β-gal staining was observed in concert with p16/p21 downregulation (Lee et al., 2015). Furthermore Y-27632 treatment has very recently been reported to induce functional recovery of mitochondria with metabolic reprogramming, changes in chromatin remodelling genes and alleviation of cell cycle arrest in replicatively senescent human fibroblasts, as well as improved wound healing *in vivo* (Park et al., 2018). In addition, Cdc42 activation has been observed in senescent mesenchymal stem cells (by increased levels of the GTP bound form) while following Cdc42 inhibition,

proliferation rates increased concurrently with decreases in SA-β-gal staining, ROS levels, p16 and ERK/JNK signalling (Umbayev et al., 2018). Cdc42 has also been revealed to play an important role in maintaining quiescence in adult HSCs *in vivo* (Yang et al., 2007). PAK4 has also been shown to be upregulated in senescence and implicated in senescence onset through ERK/MAPK signalling and upregulation of p16 and p19 in primary MEFs (Cammarano et al., 2005). However, despite literature reports of re-proliferation on PAK, ROCK or Cdc42 inhibition, I did not observe re-entry into the cell cycle in senescent fibroblasts upon treatment with any of the inhibitors. This may be due to the use of different experimental systems; I detected toxicity at > 1 μM doses (Figure 6.6B), yet other reports dosed replicatively senescent human fibroblasts with 5 μM concentrations of Y-27632 (Park et al., 2018).

Cytoskeletal reorganization inhibitors may be useful for targeting tumour growth, cellular transformation, invasion and metastasis in cancer therapy. For example, increased ROCK expression correlates negatively with patient survival, while Y-27632 and other ROCK inhibitors have shown promise in multiple cancer models including leukaemia (Burthem et al., 2007, Mali et al., 2011) and melanoma (Routhier et al., 2010). Notably however, as Y-27632 has a similar potency against both ROCK1/2 isoforms, genetic approaches are required to tease out the functional roles of each kinase in both tumour progression and senescence. However, both kinases share many direct substrates, and recent discoveries highlight that not all of these are directly involved in regulating cytoskeletal dynamics, such as the novel substrate eEF1a1 (elongation initiation factor 1-α-1, Couzens et al., 2014). Similarly, PAK4 activation is linked with worse prognosis in breast cancer and associated with increased PI3K/Akt signalling; dual inhibition was suggested to be a promising therapeutic approach (He et al., 2017). Indeed PAK4 has also been noted to regulate a senescence-like growth arrest in breast cancer through RELB (Costa et al., 2019). Further, it has also been linked to regulation of unexpected additional pathways beyond actin organization, including

p53 signalling (Murray et al., 2010). In addition, Cdc42 is commonly overexpressed or hyperactivated in cancer and treatment with CASIN has shown promise in colorectal cancer (Sakamori et al., 2014). The interplay between pro-tumorigenic effects of senescent cells in the local microenvironment and cancer cell proliferation is currently a major research topic, and the anti-cancer effects observed *in vivo* may reflect targeting senescent as well as tumour cells.

6.4.2. Oxidative stress and senescence

In this chapter, I found that senescent cells show increased activation of oxidative stress proteins and pathways (Figure 6.3, 6.4. 6.10), and that this could be exploited as a senolytic target, through inhibiting redox enzymes using auranofin. These findings are consistent with recent chemical proteomics evidence suggesting that one potential "Achilles' heel" of senescence could be the high levels of oxidative stress in senescent cells, kept in check only by robust upregulation of antioxidant proteins (Zhang et al., 2018). Substantial oxidative stress causes oxidative damage to cellular components including DNA, with mitochondrial DNA and G-rich nuclear DNA sequences such as telomeres particularly vulnerable (Von Zglinicki, 2000), exacerbated by the limited mitochondrial DNA repair capabilities and prevention of DNA repair within telomeres due to shelterin binding.

Indeed, the naturally derived senolytic agent piperlongumine exploits the high levels of oxidative stress in senescent cells through targeting OXR1 (amongst other targets, Zhang et al., 2018). OXR1 (oxidation resistance 1) is upregulated in senescence and functions as an antioxidant protein that also regulates the expression of a number of other antioxidant enzymes such as catalase. Direct binding of piperlongumine to OXR1 induces its ubiquitination and proteasome-dependent degradation, and depletion of OXR1 either by piperlongumine or by knockdown was shown to induce apoptosis in senescent but not control proliferating cells (Zhang et al., 2018). Thus, interfering with the protective

upregulation of specialized proteins which mitigate oxidative stress represents a way to render senescent cells vulnerable to apoptosis. However, the observed senolytic effect with auranofin shown here was mild in comparison with the potency of piperlongumine (Zhang et al., 2018). This could perhaps reflect the central role of OXR1 in coordinating the oxidative stress response, or result from activity of piperlongumine against other targets. A number of further compounds should be tested in future experiments for senolysis potential, such as the catalase inhibitor fomepizole and the peroxiredoxin inhibitor adenanthin. Concurrently, such experiments should investigate whether induction of senescence in proliferating cells is a potential risk of targeting oxidative stress.

However, repurposing old drugs is a reasonably straightforward, cheap and safe way of providing new treatments. Not only is drug design incredibly expensive and time consuming (costing $\geq$\$1.5 billion for discovery, development and registration of a compound, and taking >10 years), it has a high failure rate in clinical trials, often due to off-target effects or unacceptable side effect profiles. In repurposing, a large proportion of the cost has already been invested and the side effect profile is known, meaning only diseases where the profile is acceptable should be considered. Importantly, drug repurposing is also good for patients, as it can mean rapid adoption of approved drugs for new clinical uses, and lower risks for those entering clinical trials.

Further compounds targeting proteins I identified as upregulated on senescence above also warrant exploration, including the deubiquitinating enzyme UCHL1 inhibitor LDN57444. Furthermore, latrunculin compounds (A/B) targeting actin polymerization should be explored in targeting cytoskeletal changes in senescence, and using compounds such as CYT997 which induces tubulin depolymerization could be used to compare the roles and relative importance of tubulin and actin in senescence.

7. Altered actin organization networks in senescence direct intercellular organelle transfer

7.1. Introduction

Intercellular communication is crucial in regulating cellular function, for example in response to environmental changes or during development. Such interplay can be coordinated through secretion of soluble factors including chemokines, cytokines, growth factors and hormones, and their recognition by cell-surface receptors, or through secretion and internalization of extracellular vesicles. However, recent evidence suggests an alternative form of cell-cell communication can be mediated through intercellular membrane connections. Such connections, termed tunnelling nanotubes (TNTs) or intercellular bridges, have been characterized as long, fragile, open-ended and transient protrusions which mediate membrane continuity between connected cells. Since their initial description (Rustom et al., 2004), nanotubes have been observed connecting cells of the same or different cell types, with a particular prevalence detected in immune cells including macrophages, monocytes and NK cells (Dupont et al., 2018). The cargo shuttled within nanotubes includes nutrients, sterols, plasma membrane components, signalling molecules, proteins, RNA species and ions that passively diffuse between connected cells, alongside larger cargo such as whole organelles or protein complexes that require transport by myosin motors (Marzo et al., 2012).

Bridge formation can occur by two independent mechanisms: protrusion elongation and cell dislodgement. In protrusion elongation, one cell extends filopodia-like protrusions which subsequently connect with a second nearby cell. In cell dislodgement, two cells which are initially close move apart, leaving behind a long, thin membrane connection (Dupont et al., 2018). Both formation mechanisms result in nanotubes with diameters ranging from 50-1500 nm, spanning tens to hundreds of microns between connected cells. Bridge width may be determined by the presence of microtubules, which have been observed within ‘thick’

TNTs (in comparison with actin-only 'thin' nanotubes); it is possible that regulating nanotube width could control TNT cargo permeability by means of size exclusion (Önfelt et al., 2006).

Supporting the prevalence of TNTs in immune cells, expression of the MHC protein LST1 (highly expressed in macrophages and dendritic cells) induces TNT formation, through recruiting the actin cross-linking protein filamen alongside the small GTPase RalA to the plasma membrane, promoting its interaction with the exocyst complex, myosin and M-Sec/TNFaip2 (a marker of nanotube formation, Hase et al., 2009) leading to nanotube formation. Indeed, increased LST1 expression facilitates transfer of MHC class I complexes between cells through nanotubes (Schiller et al., 2013). Unsurprisingly given the universal requirement for F-actin in bridge structures, regulators of actin cytoskeletal dynamics including Rac1, Cdc42 and their respective downstream effectors WAVE and WASP are also implicated in bridge formation, as well as the myosin motor protein Myo10 (Hanna et al., 2017). Cdc42 expression, which also regulates filopodia formation, appears important for both bridge elongation and for intercellular cargo transport (Ohno et al., 2010).

Membrane lipid composition, particularly cholesterol levels which regulate membrane fluidity and mechanical strength, may be important for TNT formation and regulation (Delage and Zurzolo, 2013). In addition, there is evidence that advanced glycation end products (AGEs), specifically S100A4, are involved in nanotube formation: high concentrations of S100A4 have been reported to induce and attract outgrowth of TNTs (Sun et al., 2012). The AGE receptor (RAGE) when bound to AGEs induces local ROS production, which as well as regulating downstream gene expression through NFκB, may determine optimal TNT positioning. Indeed, in RAGE knockout mice, there is a strong reduction in detectable nanotubes, whilst CHO cells (which lack endogenous RAGE) are resistant to TNT formation under standard conditions (Sun et al., 2012).

Recent evidence has suggested that bridge formation occurs downstream of p53 upregulation (Wang et al., 2011), highlighting it as a possible stress response. Indeed, stresses such as H_2O_2 treatment or DNA damage induce TNT formation (Domhan et al., 2011) and intriguingly, transfer of mitochondria from healthy neighbouring cells to stressed cells via TNTs has been speculated to serve as a rescue mechanism for stress tolerance. For example, in cancer cells, intercellular mitochondrial transport allows cell survival even in extreme circumstances such as loss of mitochondrial functionality (Wang and Gerdes, 2015). As well as providing rescue from metabolic failure or mitochondrial dysfunction, mitochondrial transfer via TNTs has even been reported to result in cellular reprogramming (Koyanagi et al., 2005). Nanotube formation may even be involved in induction of apoptosis: the death signal Fas ligand has been noted to be shuttled via TNTs in T lymphocytes to induce cell death in target cells (Arkwright et al., 2010).

Furthermore, it has recently been reported that these intercellular membrane connections are increased upon induction of cell senescence. Indeed, cytoplasmic proteins were seen to transfer preferentially from senescent cells (compared with proliferating cells) to NK cells in co-culture, resulting in increased NK cell activation and cytotoxicity. Proteins implicated in actin re-organization were identified as preferentially transferred via intercellular bridges by proteomic analysis of transferred cargo. Furthermore, inhibiting the activity of such actin-regulating proteins including Cdc42 was shown to substantially reduce protein transfer and NK cytotoxicity (Biran et al., 2015).

The observations that Cdc42 is substantially upregulated and highly active in senescent vs. proliferating fibroblasts (Biran et al., 2015) is highly consistent with the prevalence of actin reorganization pathways and proteins in my proteomic profile of replicative senescence (Chapter 6). Furthermore, I also observed that inhibition of Cdc42 or associated downstream kinases PAK and ROCK disrupts filamentous actin stress fibres, restores lysosomal function

(decreases SA-β-gal) and restores 'youthful' morphology (Figure 6.7). In addition, actin organization networks strongly activated upon entry into senescence were also disrupted by acute mTORC inhibition (Figure 6.5), possibly consistent with previous data reporting a role for mTOR in regulating intercellular nanotubes (Lou et al., 2012, Desir et al., 2016).

7.2. Chapter aims

In this chapter I set out to address the following questions:

1. Are intercellular bridges observed in populations of senescent or proliferating fibroblasts?
2. What is the structural composition of intercellular bridges?
3. Is cargo transported between connected cells, and if so, what cargo?
4. What signalling pathways regulate the formation of direct intercellular connections?

To answer these questions, I used several types of microscopy analysis on a range of models of human cell senescence, in combination with pharmacological inhibitors of pathways implicated in intercellular communication and cellular senescence from my previous work.

7.3. Results

7.3.1. Actin- and tubulin-based intercellular bridges connect senescent cells

To assess the occurrence and investigate the composition of intercellular bridges in senescent and control proliferating human fibroblasts *in vitro*, I examined intercellular bridge occurrence in live, untreated cell populations using phase contrast microscopy (Figure 7.1). Within populations of senescent cells (RS, DDIS in HF043 and OIS in IMR90) I observed a substantial number of long, thin structures of considerable length (tens to hundreds of microns) directly connecting nearby cells (Figure 7.1, bridges indicated by arrowheads). In

contrast, such structures were infrequent within proliferating control populations, in agreement with previous data suggesting nanotube formation occurs in response to cellular stress (Biran et al., 2015).

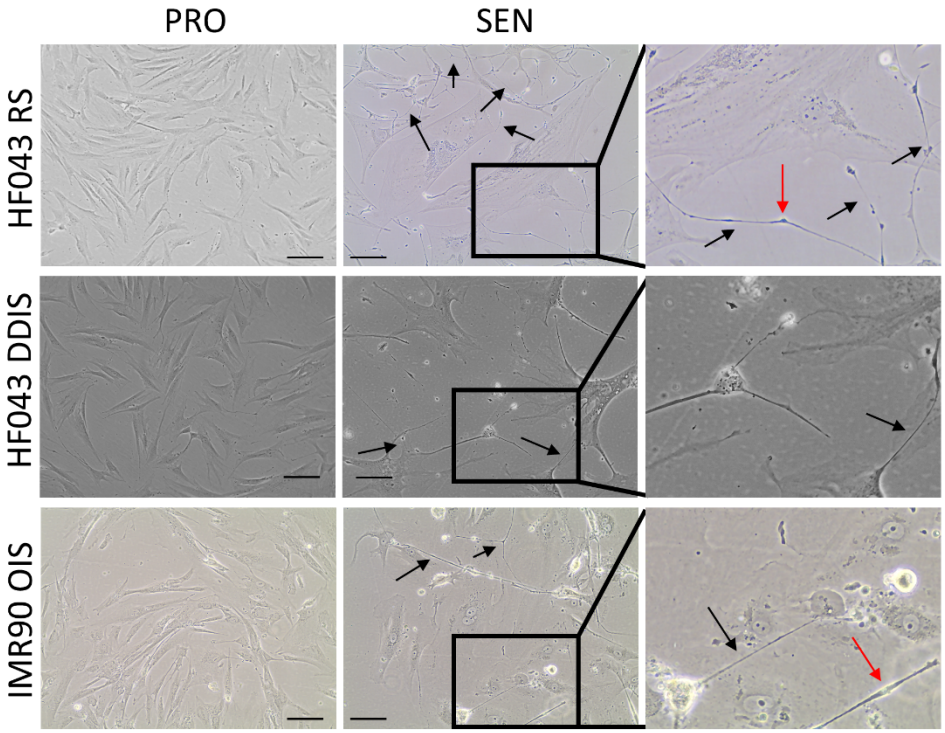


Figure 7.1 Senescent cells are connected by thin intercellular contacts *in vitro*

Low CPD (<40), replicatively senescent (CPD >90) and DNA damage induced senescent (7 day etoposide) HF043 fibroblasts alongside oncogene-induced senescent (7 day 4-OHT) and vehicle control IMR90 fibroblasts were observed live using an EVOS digital microscope for presence of intercellular bridges. Arrowheads indicate intercellular bridges, red arrowheads indicate bulky protrusions within nanotube. (Representative data shown of n>3 experiments.) Scale bar 100 μm.

To further investigate the constituent components of these thin, intercellular structures I used the fluorescent dyes rhodamine-wheat germ agglutinin (WGA) against the sugar O-Glc-NAc which is prevalent on mammalian membranes, and FITC-phalloidin and Tubulin Tracker Green to stain the actin cytoskeleton and polymerized tubulin, respectively. Using

fluorescence microscopy, I observed intercellular membrane-bound bridges within senescent cell populations reminiscent of those observed by phase contrast microscopy (Figure 7.1), which co-stained positively for both filamentous actin and polymerized tubulin (Figure 7.2). These data therefore suggest that senescent fibroblasts form 'thick' actin- and tubulin-based intercellular nanotubes to mediate cell-cell communication. Notably, the intercellular connections remained routinely observable despite formaldehyde fixation for phalloidin staining, though cells were not permeabilized to enable WGA membrane staining, resulting in lower permeability for phalloidin staining.

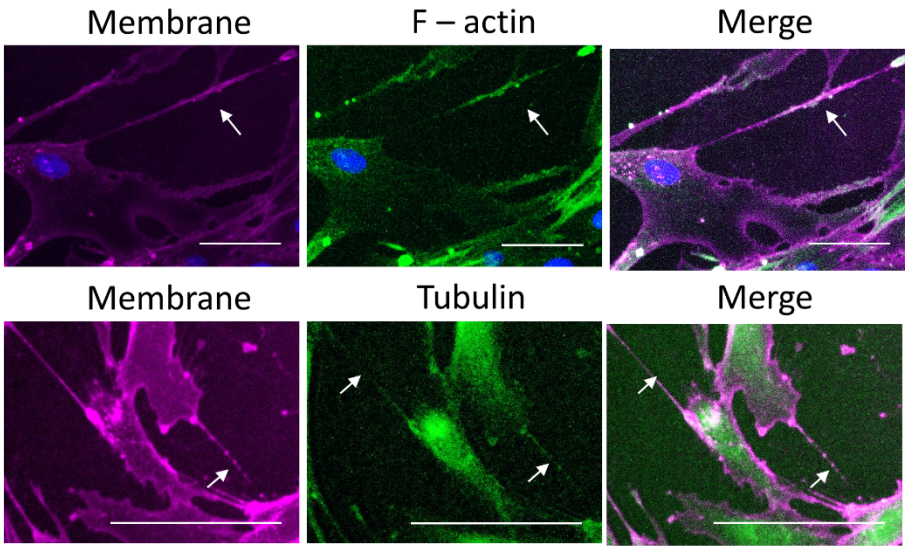


Figure 7.2 Senescent intercellular contacts are composed of membrane, actin and tubulin

Replicatively senescent HF043 fibroblasts (CPD >90) were stained with rhodamine-WGA (membrane) and Tubulin Tracker Green and imaged live, or fixed and stained with FITC-phalloidin (F-actin) before analysis by fluorescence microscopy. N=3, representative data shown. Arrowheads indicate intercellular bridges. DNA counter-stained with NucBlue Live. Scale bar 100 ɯm.

7.3.2. Senescent nanotubes support intercellular mitochondrial transport

Intercellular membrane bridges have been observed in a number of different cellular contexts as well as being observed *in vivo*. For example, viral particles including HIV have

been shown to infect neighbouring cells via these points of contact (Sowinski et al., 2008), and whole organelles such as mitochondria have been observed to transfer between cells through such bridges (Wang and Gerdes, 2015). As signalling hubs and the major source of oxidative stress, mitochondria play an important role in senescence (Correia-Melo et al., 2016). Senescent cells exhibit dramatic increases in mitochondrial load, perhaps to compensate for mitochondrial dysfunction, and the mitochondrial network becomes increasingly reticular through resistance to mitochondrial fission and mitophagy (see 1.3.3.2.1). Furthermore, the intercellular bridges between senescent fibroblasts I observed using phase contrast microscopy showed a number of swellings at various points along the nanotubes (red arrowheads, Figure 7.1). Previous work has indicated that such protrusions within nanotubes, termed 'gondolas' may account for nanotube widening to support vesicle or organelle transport (Veranič et al., 2008).

To investigate whether the intercellular membrane bridges I had observed between senescent cells contained mitochondria, I labelled mitochondria in senescent fibroblasts (again using RS and DDIS, HF043 and OIS, IMR90). To avoid labelling bias, I used a variety of mitochondrial dyes including the live stains Mitotracker Green, Mitotracker Red and CellLight Mitochondria GFP BacMam where GFP expression is driven exclusively in mitochondria under the 5'UTR of pyruvate dehydrogenase. I also conducted immunofluorescence for the mitochondrial transcription factor TFAM in fixed samples. In all cases, membranes were stained with fluorescent WGA. I observed that in all models of senescence investigated, small foci (Figure 7.3A, D) or even reticular networks (Figure 7.3B, E) positive for mitochondrial staining were evident in a substantial proportion of intercellular bridges, irrespective of the mitochondrial stain used, the model of senescence, or whether cells were imaged live or fixed (Figure 7.3).

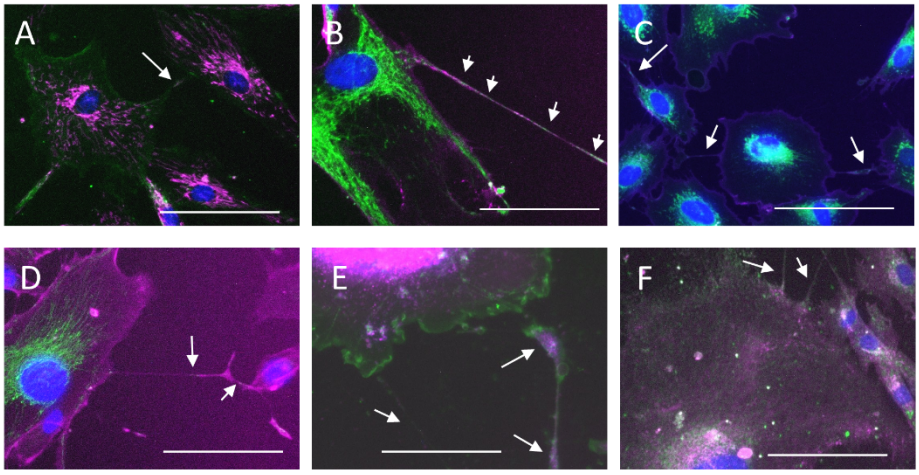


Figure 7.3 Mitochondria are present within senescent intercellular contacts

The presence of mitochondria in intercellular bridges was examined in a range of models of senescence using a range of staining methods as follows. A, B, C, D: replicatively senescent HF043 fibroblasts were stained with A: fluorescein-WGA and Mitotracker Red, B, C: rhodamine-WGA and Mitotracker Green, D: rhodamine-WGA and CellLight Mitochondria-GFP BacMam. E: IMR90 oncogene-induced senescent (OIS) fibroblasts were stained with fluorescein-WGA and Mitotracker Red. A-E were imaged live. F: etoposide-treated (DDIS) HF043 fibroblasts were fixed and stained for TFAM using immunofluorescence and rhodamine-WGA. Arrows indicate mitochondria within contacts. N>3, DNA stained with NucBlue Live. Scale bar 100 μm.

To assess whether such mitochondria are static or mobile within these intercellular bridges, time-lapse fluorescence microscopy of replicatively senescent HF043 fibroblasts stained with Mitotracker Red and fluorescein-WGA was conducted. Mitochondrial motility was observed within minutes of staining and mitochondria were seen to track along intercellular bridges (representative still images shown in Figure 7.4). These observations suggest that mitochondria are able to move within senescent intercellular bridges over the timescale of minutes to hours. The observation of unidirectional movement also suggests that mitochondrial motility may be regulated, rather than occurring by passive diffusion.

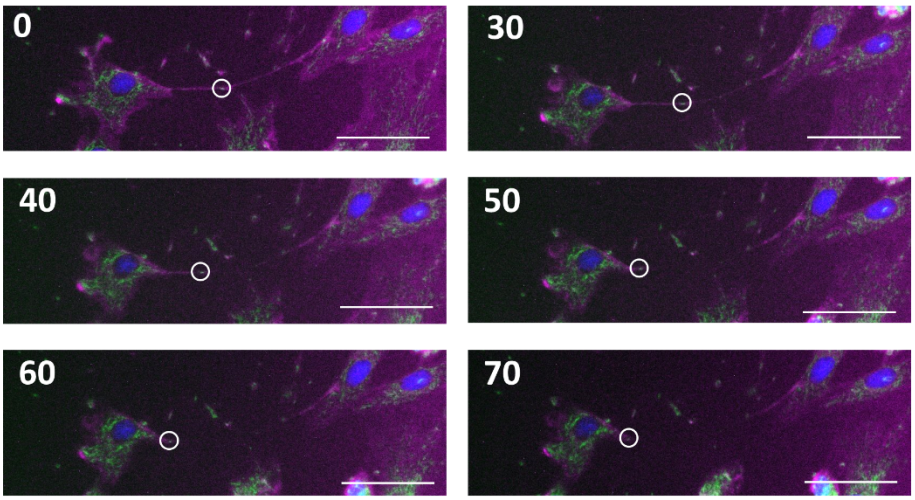


Figure 7.4 Mitochondria are motile within senescent intercellular contacts

Replicatively senescent HF043 fibroblasts were stained with Mitotracker Green and rhodamine-WGA (re-coloured magenta) imaged live using time-lapse fluorescence microscopy, with time points following the start of the observation period indicated in minutes, and the white circle highlighting a Mitotracker Green positive puncta. Representative images shown of n=3 experiments, DNA stained with NucBlue Live. Scale bar 100 μm; total movement detected here ~60 μm within 70 minutes, i.e. average rate of ~1μm/minute within the observation period.

To investigate whether this putative mitochondrial transport resulted in transfer of mitochondria between cells, I conducted a co-culture assay where separate populations of cells were stained with Mitotracker Green and Mitotracker Red respectively, then thoroughly washed before harvesting and co-seeding at a 1:1 ratio (Figure 7.5A, proliferating control cells shown immediately after seeding). Nuclei were counter-stained using the live dye NucBlue Live prior to imaging, and cells were examined over the course of co-culture for intercellular mitochondrial transfer. To exclude the possibility of dye leakage, conditioned media controls were included in each experiment whereby media was taken after 24 hours exposure to a stained single culture control well, incubated with unstained cells for 24 hours, and cells were then inspected for any fluorescent signal by microscopy; no evidence of dye leakage was detected (Figure 7.5B).

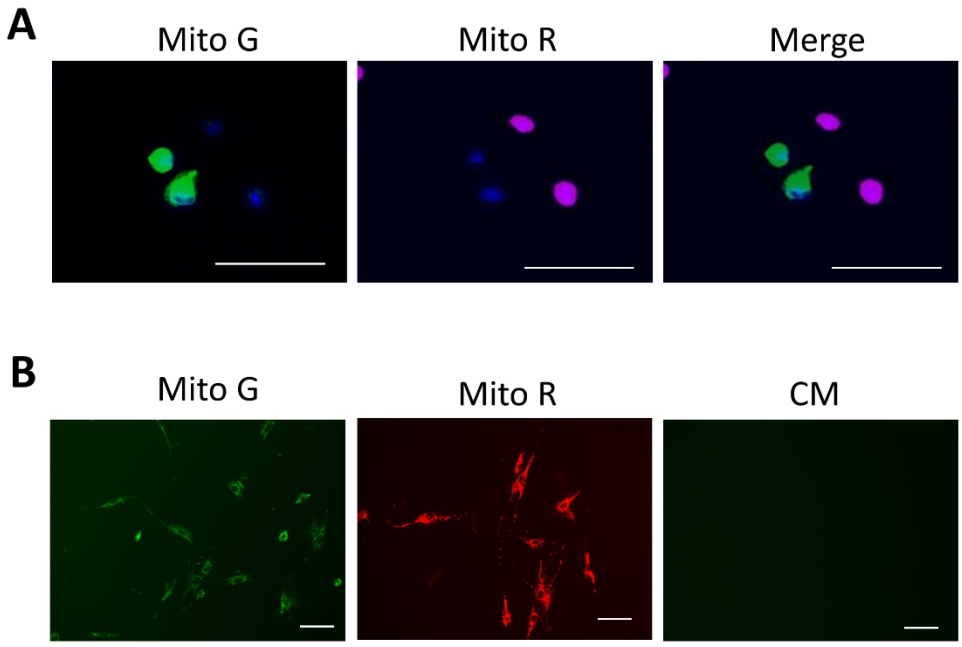


Figure 7.5 Co-culture assay for analysis of intercellular mitochondrial transfer

Proliferating and replicatively senescent HF043 fibroblasts were stained with Mitotracker Green or Red, washed thoroughly and then seeded into co-culture at 1:1 ratio before imaging for analysis of intercellular mitochondrial transfer, with DNA counter-stained with NucBlue Live. A: cells were imaged immediately following seeding into 1:1 co-culture (proliferating co-culture controls shown). B: 24 hour conditioned media from stained populations was incubated on unstained, control cells for a further 24 hours before imaging to inspect for fluorescence signal (proliferating controls shown for both Mitotracker Green and Red stains). N>3. Scale bar 100 μm.

After 24 hours of co-culture, I observed mitochondria-loaded bridges spanning alternately stained cells, together with distinct Mitotracker Red foci in predominantly Mitotracker green-stained cells and vice versa, strongly suggesting the hypothesis that mitochondria have been transported (Figure 7.6, PRO – PRO and SEN – SEN). While such intercellular transfer was observed within proliferating control co-cultures, dye co-localization was more pronounced within senescent co-cultures.

Intercellular mitochondrial transfer has been hypothesized as a rescue mechanism for stressed cells, including cancer cells that have lost mitochondrial functionality (Wang and Gerdes, 2015). However, mitochondria are important signalling hubs for oxidative stress, apoptosis and senescence, and senescent cells are known to influence their surrounding microenvironment in a plethora of ways including via paracrine pro-senescence signalling (Nelson et al., 2012, Acosta et al., 2013). To investigate directionality of intercellular mitochondrial transfer, I implemented the same double labelling Mitotracker Green/Red assay in 1:1 co-cultures of proliferating and senescent cells (Figure 7.6 PRO – SEN). After 24 hours of co-culture, I observed puncta of oppositely stained mitochondria within both proliferating and senescent fibroblasts, regardless of which population was stained with Mitotracker Green or Red, suggesting not only transfer of senescent mitochondria to proliferating cells, but also mitochondrial transfer from proliferating to senescent cells.

While other mechanisms such as vesicle secretion and uptake, or cell-cell fusion, could also account for intercellular mitochondrial trafficking, only a small proportion of senescent cells exhibited multiple nuclei per cell within the datasets analysed for Figure 7.6, suggesting low rates of cell-cell fusion within the analysed populations. Hence, my data suggest that these tubulin- and actin-based intercellular bridges may constitute an important mechanism of mitochondrial transfer and thus intercellular communication for senescent cells.

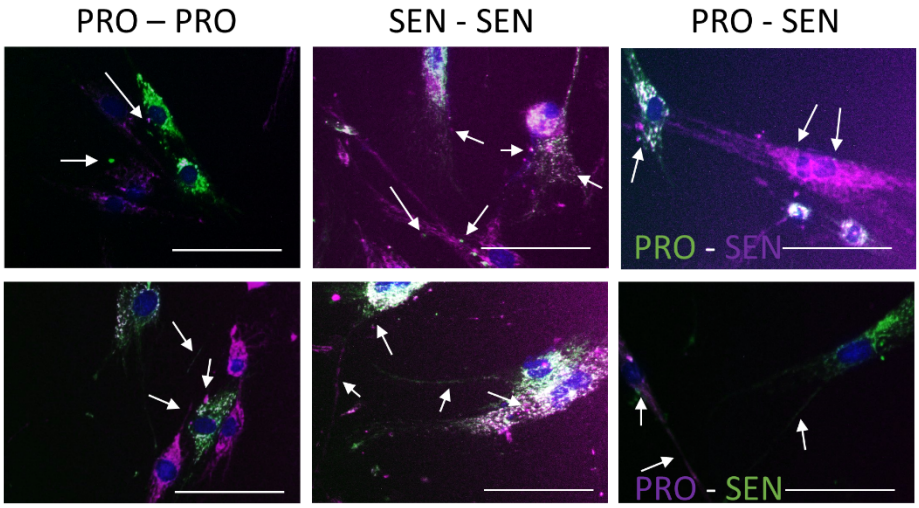


Figure 7.6 Co-culture assay reveals evidence of intercellular mitochondrial transfer

Co-cultures of proliferating/replicatively senescent HF043 fibroblasts pre-stained with Mitotracker Green or Red were set up as in Figure 7.5 and imaged following 24 hours co-incubation. Arrows indicate intercellular bridges or puncta of transferred mitochondria. N=3, DNA stained with NucBlue Live immediately prior to analysis. Scale bar 100 μm.

7.3.3. Direct intercellular communication in senescence is regulated by mTOR and Cdc42 signalling

As highlighted above, recent evidence has suggested that intercellular bridge structures between cancer cells can be regulated by mTOR signalling (Lou et al., 2012) and in senescent cells by proteins that regulate actin organization such as Cdc42 (Biran et al., 2015). Intriguingly, my proteomics analysis showed a substantial upregulation of the Cdc42 signalling network upon entry into replicative senescence, that was disrupted through acute mTOR inhibition (Chapter 6). Furthermore, my data demonstrated that acute pharmacological inhibition of either mTOR or Cdc42 in senescent fibroblasts rejuvenated senescent cell morphology, disrupted filamentous actin stress fibres and reduced lysosomal stress in senescent cells (Figure 6.7, Chapter 4).

I therefore tested whether the intercellular bridges observed here were regulated by Cdc42 or mTOR signalling, using the pharmacological inhibitors CASIN and AZD8055 to inhibit Cdc42 and mTOR respectively, in both senescent and proliferating control populations (Figure 7.7). To quantify intercellular bridge occurrence, I stained formaldehyde-fixed cell populations with fluorescein-WGA and NucBlue live for genomic DNA (I had previously observed that fixation improved the sharpness of cell staining without disrupting the intercellular bridge structures, results were also compared with live stained cells for verification, data not shown). The number of intercellular bridges (connected at both ends) was counted manually and number per cell determined by normalising against nuclear number (Figure 7.7).

I observed significantly more intercellular bridges within senescent compared with proliferating control populations (Figure 7.7), consistent with my earlier findings, with ~0.5 bridges per replicatively senescent cell (note a substantial proportion of cells exhibited several connections, while others had none). Inhibition of either Cdc42 or mTOR significantly reduced the number of bridges between senescent cells, both in replicatively senescent populations or those induced by DNA damage (Figure 7.7).

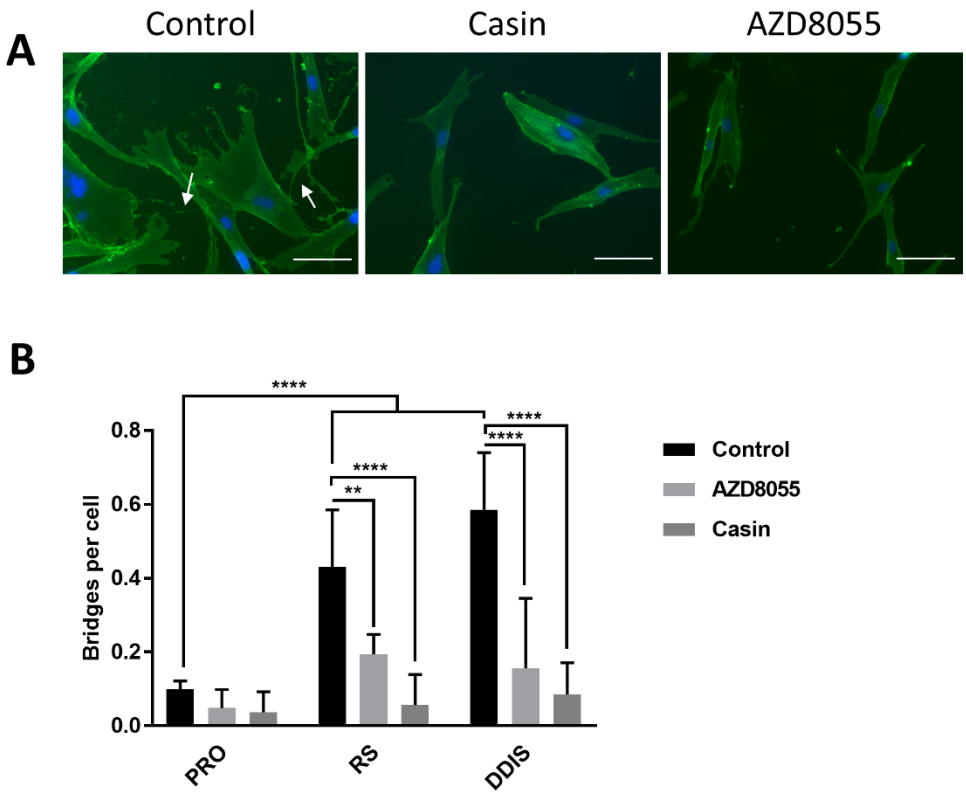


Figure 7.7 Cdc42 and mTOR signalling control formation of intercellular bridges in senescent cells

A: replicatively senescent (CPD≥90) and DNA damage-induced senescent (7 day, 20 μM etoposide) HF043 fibroblasts alongside low CPD proliferating controls were treated with the mTOR inhibitor AZD8055 (70 nM) or the Cdc42 inhibitor CASIN (2μM) for 24 hours before fixation and staining with fluorescein-WGA and NucBlue Live (DNA). Representative images of control and drug-treated replicatively senescent fibroblasts shown. Scale bar = 100 μm. B: intercellular bridges were manually quantified from >50 cells per replicate (n=3).

7.4. Discussion

Together, my proteomics observations (Chapter 6) indicate that Cdc42 signalling, implicated in the actin organization network, is elevated in senescent versus proliferating cells, and that Cdc42 may act downstream of constitutive mTOR activity in senescence. Proteins that

promote actin polymerization and stabilization play an important role in facilitating direct cell-cell contact via membrane-bound bridges, which had previously been shown to transport cytoplasmic proteins between cells (Biran et al., 2015). Using co-culture assays and live cell imaging, I reported here that not only do these bridges increase in frequency in senescence resulting from replicative exhaustion and also acute DNA damage or oncogene activation, but they are regulated by mTOR and Cdc42 signalling, and facilitate direct intercellular mitochondrial transfer.

Entry into senescence is accompanied by development of a number of distinctive phenotypes including epigenetic alterations, lysosomal and mitochondrial dysfunction, pro-inflammatory secretion and morphological transformation supported by hypertrophy and changes to actin organization networks. Furthermore, senescent cells are highly communicative, alerting immune cells to their presence for clearance (Ovadya et al., 2018), and regulating the proliferative capacity of surrounding healthy or cancerous cells positively and negatively (Gonzalez-Meljem et al., 2018, Nelson et al., 2012). While this interplay has largely been attributed to secretion of EVs and SASP factors, transient intercellular bridges supporting both protein (Biran et al., 2015) and organelle transfer (Figure 7.6) may also be important in mediating these effects.

The importance of mTOR in senescence may therefore extend to promoting direct intercellular communication through regulating formation of cell-cell communication channels (Figure 7.7), as well as regulating the SASP (Chapter 4, Herranz et al., 2015, Laberge et al., 2015) and the biogenesis and secretion of exosomes (Zou et al., 2019), whose production and secretion are amplified upon entry into senescence (Borghesan et al., 2019). Consequently, these findings highlight mTOR signalling as not only critical to the cell-autonomous coordination of senescence (Chapter 5) but in directing the non-cell-autonomous roles of cellular senescence.

While intercellular nanotubes appear to constitute a highly localized form of communication, it is important to note that these bridges often do not just connect two cells, but instead can form networks extending direct cell communication over larger distances. Furthermore, it is interesting to speculate that the cellular rationale behind the characteristic enlarged, flattened senescent morphology observed *in vitro* (and enlargement *in vivo*, Biran et al., 2017) is as a consequence of changes to actin networks including those mediated by Cdc42 signalling, which orchestrate intercellular communication to further influence the local microenvironment (Figures 6.7, 7.3).

7.4.1. Physiological relevance of direct intercellular senescent contacts

While my data above suggest that a substantial proportion of senescent cells form direct cell-cell bridges which can mediate intercellular mitochondrial transfer, it is important to note that these data were acquired in 2D, *in vitro* cell culture of skin fibroblasts. While further work is undoubtedly required to probe the physiological relevance of these findings, previous *in vivo* work has shown that intercellular contacts can both rescue compromised cells and spread disease or infection, suggesting context-dependent function or exploitation by invading pathogens. Indeed, TNTs between tumour cells can play important roles in pathogenesis and invasion, for example through intercellular transfer of the P-glycoprotein drug efflux pump to propagate multi-drug resistance (Pasquier et al., 2012), together with intercellular mitochondrial transport for cellular rescue. TNTs have been implicated in the intercellular spread of HIV (Sowinski et al., 2008), influenza (Kumar et al., 2017) and herpes viral particles as well as prions (Gousset et al., 2009) and protein aggregates implicated in neurodegenerative diseases (polyglutamine aggregates: Constanzo et al., 2013, α-synuclein: Wang et al., 2011, Abounit et al., 2016, and tau: Abounit et al., 2016). In the case of HIV infection, the viral Nef protein promotes actin remodelling to initiate TNT formation (Hashimoto et al., 2016). Subsequently, HIV particles can ‘surf’ along nanotubes to infect further immune cells, all while protected from extracellular detection or clearance by the

immune system (Sowinski et al., 2008). Indeed, time-lapse microscopy using fluorescently labelled viruses shows viral particle transmission through TNTs, which cannot be prevented by neutralizing antibodies that block intracellular viral entry (Kumar et al., 2017). Nanotubes may also play important physiological functions, for example in osteoclast differentiation (Takahashi et al., 2013), and have been observed *in vivo*, both in murine myeloid cells in the cornea (Chinnery et al., 2008) and in human malignant pleural mesothelioma (Lou et al., 2012). Hence the impact of intercellular nanotubes is therefore determined by the transferred cargo as well as the types and states of the connected cells.

While senescent cells are known to accumulate in tissues with chronological age and within tumours, they play important roles in development, tissue regeneration and in wound healing. Furthermore, the profile of cytokines, chemokines, matrix-remodelling enzymes and growth factors secreted in the SASP is highly heterogeneous between cell types and modes of senescence induction, perhaps underpinning the range of different paracrine responses to local induction of senescence. In these different physiological contexts, it is highly likely that senescent cells could exert a number of different impacts through direct intercellular bridges. Indeed, it is possible that within a tumour, intercellular bridges could participate in both rescuing cancer cells with dysfunctional mitochondria, but also in facilitating communication between senescent and immune cells to promote immune surveillance, as observed by Biran et al (2015). It is also important to note that senescent cells have actually been shown to evade immune surveillance, for example by HLA-E upregulation (Pereira et al., 2019), thus TNTs may enable evasion of immune detection through shuttling of surface markers.

7.4.2. Supercellularity in senescence: cell-cell bridges vs. cell-cell fusion

Through allowing bidirectional transport of cargo including whole organelles between connected cells, intercellular nanotubes may create temporary syncytia, or ‘supercellularity’.

Indeed, syncytia are permanently created through cell-cell fusion, an essential event in a number of developmental and physiological processes such as in mammalian muscle and osteoclast function, and in the formation of the placental syncytiotrophoblast (Cox and Redman, 2017). Similarly to pathogenic exploitation of nanotubes, a number of viruses exploit cell fusion to support their reproduction and dissemination. Cell fusion is coordinated through expression of fusogenic proteins (fusogens) such as the measles agent MV or ERVWE1, an endogenous retroviral locus present in the human genome which codes for the highly fusogenic glycoprotein responsible for formation of the placental syncytiotrophoblast. Intriguingly, cell fusion events have been linked to cellular senescence: the placental syncytiotrophoblast itself shows a number of markers of senescence, while expression of fusogens such as ERVWE1 or MV induces cell fusion and induction of cell cycle arrest and senescence (Chuprin et al., 2013). Through induction of senescence, fused cells coordinate a protection strategy to prevent division of multinucleate cells, while maintaining cell viability through resisting apoptosis, which may be important within the placental syncytiotrophoblast throughout pregnancy (Chuprin et al., 2013). It is interesting to speculate that through direct intercellular nanotubes, senescent cells could also relay danger signals to neighbouring cells and coordinate induction of paracrine senescence, just as cell fusion may induce senescence in syncytia.

7.4.3. Targeting intercellular nanotubes in disease

While syncytia are important in early mammalian development and intercellular bridges aid NK-mediated recognition of senescent cells (Biran et al., 2015), pathological effects of Cdc42/mTOR-regulated cell-cell bridges may be amenable to therapeutic intervention, for example using mTOR inhibitors or actin depolymerizing agents such as Cdc42 inhibitors. This approach may also be useful in cancer as well as in ageing, for example through blocking the transfer of healthy mitochondria from bystander cells to rescue dysfunctional tumour cells, or through blocking the spread of drug resistance channels. Indeed, neutralizing antibodies

against the adhesion molecule ICAM-1 in T-cell acute lymphoblastic leukaemia were shown to block transfer of healthy mitochondria from MSCs, thereby causing an increase in chemotherapy-induced cancer cell death (Wang et al., 2018). This approach may also be important in preventing the spread of pathogens such as HIV or protein aggregates implicated in neurodegeneration: inhibiting nanotube formation with latrunculin B was shown to prevent the spread of α-synuclein through healthy astrocytes in a model of Parkinson's disease propagation (Rostami et al., 2017).

Alternatively, it may be possible to exploit the beneficial properties of nanotubes, for example in treating diseases of organelle dysfunction, or by using intercellular mitochondrial transfer as a rescue strategy for compromised cells during stroke, when ischemic stress conditions may stimulate nanotube formation. In such circumstances, it may be possible to further promote nanotube formation by supplying a treatment that induces ROS, stabilizes microtubules or actin networks, or through inducing increased expression of trafficking adaptors in the mitochondria 'donor' cells. It may even be possible to exploit intercellular nanotubes as a drug delivery pathway in cancer therapy, as nanoparticles have been shown to be loaded into and move through TNTs (Kristl et al., 2013).

7.4.4. Future work

In this chapter, I used a range of microscopy and co-culture assays combined with molecular pathway analysis using pharmacological agents to probe the occurrence, composition, function and regulation of direct intercellular contacts and their relevance to cellular senescence. While I was able to manually quantify the number of bridges occurring per cell from microscopy images, analysing the levels of intercellular mitochondrial transfer was not possible. However, alongside distinct puncta of transferred mitochondria, I noted co-localization of Mitotracker Green and Red signals particularly within senescent cell population co-cultures, that could indicate not only uptake but fusion of mitochondria into

the cellular mitochondrial network. In the future, levels of mitochondrial transfer could be examined using Rho zero cells or cells induced to complete mitophagy (Correia-Melo et al., 2017) as 'acceptor' cells, though investigating fusion of transferred mitochondria to an acceptor cell reticular network would not be possible in such set-ups. Alternatively, rates of mitochondrial transfer could be analysed in co-cultures of two different populations of cells with distinguishable mitochondria, for example divergent by species and therefore measurable by immunofluorescence with a species-specific mitochondrial antibody, or by mitochondrial DNA sequence, which could be quantified by qPCR following cell sorting. However, species-specific membrane glycoproteins and receptors may be important in coordinating cell-cell contact.

Further, I did not investigate the molecular basis of mitochondrial transport along cell-cell bridges: while I and others have observed that actin organization through Cdc42 signaling is implicated in the formation of direct cell-cell contacts, I also noted that these contacts stained positively for tubulin. It would be highly interesting – perhaps using inhibitors of dynein molecular motors (for example ciliobrevin D or dynarrestin) – to investigate whether the mitochondrial motility I observed in these structures was dependent on actin or tubulin polymerization.

Furthermore, the above experiments did not address the functional status of transferred mitochondria. Senescent cells are known to accumulate dysfunctional mitochondria, and previous reports suggest that healthy mitochondria may be preferentially transferred to stressed cells (Wang and Gerdes, 2015). Measuring the O_2 consumption and activity of individual ETC components in senescent and proliferating cells following co-culture would therefore be informative as to whether healthy or dysfunctional mitochondria are preferentially transferred. Another important line of enquiry is whether the nanotube structures that senescent cells make with NK cells (Biran et al., 2015) also participate in

intercellular mitochondrial transfer, as well as analysing the impact of direct interaction between senescent and proliferating cells, e.g. through analysis of proliferation capacity in co-culture vs. in barrier trans-well formats. Moreover, it will be important to investigate the role of these intercellular connections in a physiologically relevant way, for example by *in vivo* analysis or in 3D culture formats (e.g. in hydrogels of appropriate rigidity reflecting 'young' and 'old' tissue structures). Indeed, recently published data analysing TNT formation in MSC spheroids showed intercellular transfer of cytosolic dyes, and intriguingly, inclusion of low passage MSCs with high passage cells was seen to abrogate p16 expression in spheroids, dependent on TNT formation. Hence, in this context TNTs appear to rescue proliferation potential of high passage cells, potentially overcoming senescence induction (Whitehead et al., 2019).

8. Discussion

8.1. Summary

In this thesis, I have demonstrated that acute treatment of primary fibroblasts with the SIRT1/2 inhibitor TnV6 results in p21 upregulation and G1-phase cell cycle arrest, with acquisition of features of senescence including DNA damage foci and pro-inflammatory secretion (Chapter 3, Walters and Cox, 2019). This finding not only improves our understanding of the role of sirtuin signalling in senescence but also provides an additional experimentally-inducible model of senescence.

I have also investigated the role of mTOR signalling in senescence, and demonstrated that constitutive mTOR activity in senescent fibroblasts regulates multiple senescent phenotypes including pro-inflammatory secretion (Chapter 4, Walters et al., 2016). I demonstrated that mTOR activity is required in coordinating the proliferation arrest associated with senescence, since pan-mTOR inhibition substantially extended the replicative capacity of wild-type and progeroid patient cells *in vitro*, as well as disrupting TnV6- and DNA damage-induced senescence (Chapter 5). Importantly, I noted that mTOR inhibition prevented upregulation of p21 in response to senescence-inducing stimuli, and had a mild but potentially important effect on stabilizing telomere length in progeroid and wild-type fibroblasts close to senescence. Hence, continued proliferation on pan-mTOR inhibition may result from inhibition of p21 elevation as well as potentially preventing p53 stabilization through delaying exhaustive telomere attrition (Chapter 5).

Using comparative proteomics, I generated a molecular profile of replicative senescence (Chapter 6), showing a predominance of cytoskeletal remodelling pathways activated in cell

senescence but suppressed on mTOR inhibition; these present potential therapeutic targets in senescence. Furthermore, I investigated how these pathways (in particular Cdc42 signalling) appear to regulate intercellular communication in senescence (Chapter 7). I observed direct cell-cell contacts mediating intercellular mitochondrial transfer in senescent cell populations in 2D cultures. Together, these data highlight mTOR signalling as a crucial regulator of the cell-autonomous and non-cell-autonomous aspects of cellular senescence.

8.1.1. Exploring the mechanism of mTOR-dependent regulation of cellular senescence

Fitting the data in this thesis into a molecular framework suggests an mTOR-centred mechanism through which senescence is orchestrated (Figure 8.1). Indeed, inducers of senescence such as telomere shortening, DNA damage or sirtuin inhibition act through the DDR and related cell cycle arrest pathways to upregulate p21 expression. The data presented here suggest that mTOR is critical in the upregulation of p21 for induction of proliferation arrest (Chapter 5) and for the development of important senescence phenotypes including mitochondrial accumulation, the appearance of CCFs and enlarged nuclear morphology indicative of breakdown of nuclear structure (Chapter 4) and possibly even telomere degradation (Chapter 5). The breakdown of nuclear structure and accumulation of dysfunctional mitochondria may act to reinforce the state of senescence, through CCFs activating cGAS-STING innate immune pathways and sustaining DNA damage signalling through ROS respectively. Hence mTOR regulates the cell-autonomous aspects of senescence. Furthermore, I have also presented evidence showing that mTOR activation regulates the non-cell-autonomous aspects of senescence, through regulating the pro-inflammatory SASP (suppression of IL-6 secretion, Chapter 4) and through regulating actin re-organization (Chapters 4, 6), which controls cell motility and metabolism as well as direct intercellular communication (Chapter 7). Importantly, this suggests mTOR signalling may impact important physiological functions of senescence, including senescent – immune

interplay, and the potentially deleterious induction of paracrine senescence. Collectively, these data as well as important findings from other groups (e.g. Laberge et al., 2015, Herranz et al., 2015) confirm mTOR as a critical regulator of cellular senescence.

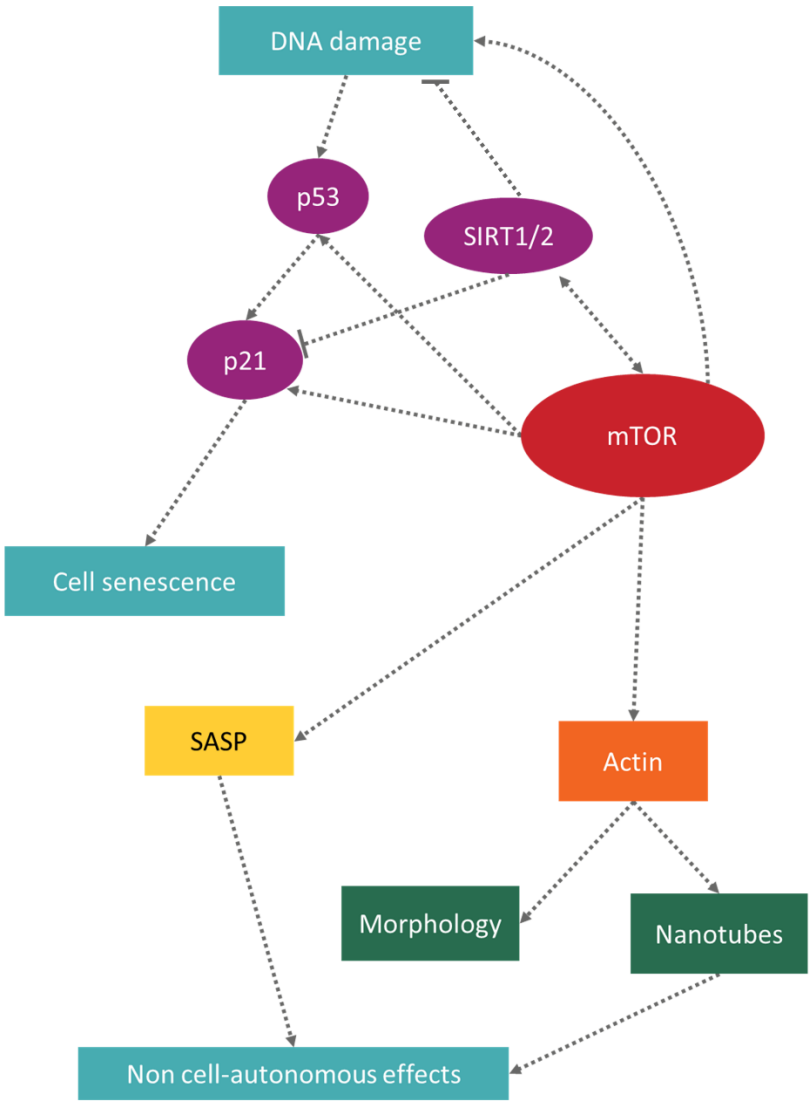


Figure 8.1 mTOR as a central regulator of cellular senescence

Schematic depicting induction of cellular senescence through stressors including sirtuin inhibition and DNA damage (such as telomere attrition). mTOR signalling may regulate both p53 stabilization and p21 upregulation as well as possibly regulating telomere stability, to enforce proliferation arrest and cell senescence, as well as regulating the non-cell-autonomous effects of senescence through regulating the SASP and intercellular communication through cell-cell bridges.

8.1.2. Importance of actin remodelling in cellular senescence

Data in this thesis have suggested significant roles of actin and cytoskeletal remodelling in senescence; such pathways may currently be under-appreciated in senescence, especially as actin is commonly used for normalization in both RNA and protein quantification. Indeed, only very recently has it been noted that actin is a poor loading control for qPCR experiments in senescent cells (Hernandez-Segura et al., 2019). However, I have shown that not only is actin remodelling important in determining senescent morphology but also in senescent cell function: direct intercellular bridges mediating mitochondrial transfer were regulated by Cdc42 activity which modulates actin polymerisation, and a shift from filamentous to globular actin was observed on mTOR inhibition, probably mediated through mTORC2 (Figure 4.4, 7.7). As the cell enlargement long-associated with senescence *in vitro* has also now been observed *in vivo* (Biran et al., 2017), the physiological consequences of this enlargement may soon become clear – perhaps in cooperating with cell cycle arrest pathways to prevent cytokinesis, in solidifying the barrier to tumorigenesis by hampering metastasis, in intracellular vesicle trafficking to mediate pro-inflammatory secretion, or indeed to communicate with the surrounding microenvironment via direct cell-cell bridges. However, changes to the cytoskeleton may also impact cell mechanics; accumulation of senescent cells *in vivo* for example in blood vessels or tissue epithelium could thus restrict tissue elasticity. Intriguingly, actin also has a role in regulating apoptosis. Indeed, the enzyme DNase I which binds nuclear DNA during apoptosis also binds with a very high affinity to globular actin, promoting actin depolymerization and then inhibiting DNase I in an autofeedback loop (a fluorescently-tagged DNase I was used to label G-actin, Figure 4.4). Further investigation will be required to ascertain whether cytoskeletal organization is implicated in senescent cell survival, and whether this could be exploited as a senolytic mechanism.

8.2. Future work

A number of follow-up experiments have been suggested in individual chapters, notably including further mining of the proteomic profile of replicative senescence for additional biological insights and therapeutic candidates (Chapter 6) and more thorough investigation of cell-cell bridges. Moreover, the research in this thesis has been completed entirely in primary human fibroblasts in 2D culture. Though I used a range of cell lines and models of senescence induction to account for heterogeneity, as our understanding of how cellular senescence is induced *in vivo* increases, it will be important to adjust these models accordingly. Notably, a thorough evaluation of TnV6-induced senescence in comparison with other models of senescence or senescent cells isolated from aged donors or disease niches will be critical in determining the suitability of this experimentally-amenable model system in, for example, drug-screening projects for senolytics and 'senomodifiers'. Of course, it will also be important to evaluate my findings (especially those relating to intercellular communication) in more physiologically relevant models such as 3D cultures involving multiple cell types, and in whole animal models.

In this thesis, I have chosen to investigate the role of a number of pathways in senescence using pharmacological inhibitors, instead of genetic manipulation. Firstly, this increases the translational relevance of this work; indeed, many compounds tested here have already been evaluated for their safety in humans in clinical trials for various conditions. Furthermore, where possible I used a panel of inhibitors (e.g. as in Figure 4.10) to decrease the likelihood of off-target effects being responsible for the observed biological outcomes. Secondly, I chose to use pharmacological modulation rather than genetic manipulation due to a number of issues with using transfection techniques in primary cells. Indeed, transfection involves putting DNA into the cytoplasm, and recent work has shown that cytoplasmic DNA sensing is extremely important in senescence (Ivanov et al., 2013, Dou et

al., 2017). Furthermore, transfection techniques using agents such as lipofectamine are not only stressful for cells, but their efficacy has been noted to change according to passage number (Lee et al., 2017), meaning knockdown efficiency may not be as experimentally reliable or as finely tuned as drug supplementation. However, further evaluation of these findings using techniques such as siRNA will be highly important, for example in teasing apart the signalling roles of each mTOR complex or downstream signalling targets.

8.2.1. mTORC1-specific inhibition

A major point of concern with pan-mTOR inhibitors, and indeed with long-term rapamycin treatment, is the potential side effects of mTORC2 inhibition. However, a number of recent publications have reported several compounds with marked selectivity for mTORC1 over mTORC2. The novel mTORC1-specific inhibitor DL001 is an analogue of rapamycin that also acts mechanistically through FKBP12 but has greatly improved selectivity; crucially, *in vivo* administration in mice revealed no metabolic or immune side effects (Schreiber et al., 2019). Further, several mTORC1-specific inhibitors including cinnarizine have been developed from a small molecule screen (Allen et al., 2018). In addition, the Rheb inhibitor NR1 has been shown to selectively block mTORC1 signalling *in vivo* (Mahoney et al., 2018).

Furthermore, as an important target in cancer in its own right, novel strategies for mTORC2-specific inhibition are being explored, including disruption of substrate recruitment by targeting the CRIM domain of mSin1, the binding partner of mTORC2 substrates including Akt (Murray and Cameron, 2017). The protein-protein interface between mTOR and Rictor in the mTORC2 complex has also been targeted to elicit mTORC2 inhibition (Benavides-Serrato et al., 2017).

I observed that pan-mTOR inhibitors were more effective than mTORC1 inhibition through rapamycin or deforolimus in disrupting phenotypes of senescence (Chapter 4); to investigate whether mTORC2 therefore plays an important role in senescence, as inferred through its

regulation of the cytoskeleton (Jacinto et al., 2004), I performed CRISPR knockout studies of Raptor and Rictor, the partner proteins of mTOR in mTORC1 and mTORC2 respectively. While extremely preliminary (n=1), I observed morphological changes reminiscent of pan-mTOR inhibition following Rictor (but not Raptor) knockout in primary fibroblasts at high CPD. To achieve the full benefits of mTOR inhibition, it is likely that suppressing mTORC1-dependent regulation of transcription, translation, autophagy and organelle biogenesis as well as suppressing mTORC2-dependent cytoskeletal regulation may be required. A thorough *in vitro* and *in vivo* workup of these different inhibitory mechanisms alongside rapamycin and ATP-competitive, pan-mTOR inhibition will therefore be required to discover the most effective strategies for targeting mTOR to tackle age-related disease without deleterious side effects, and to investigate the role of each complex in regulating senescence. Importantly, a range of dosing and treatment regimens should be investigated, as many of the adverse metabolic/pro-diabetic and immune-suppressive effects of rapamycin treatment may be attributable to the high doses required for cancer therapy; as previously mentioned, low doses of everolimus and the pan-mTOR/PI3K inhibitor BEZ235 have recently shown immunological benefit with few side effects in elderly humans (Mannick et al., 2018).

8.2.2. mTOR as senolytic target

Intriguingly, recent evidence has suggested that mTOR could be a senolytic target. In the absence of exogenous nutrients, Torin1 (a pan-mTOR inhibitor) was shown to induce senolysis of irradiated senescent fibroblasts *in vitro.* Thus starvation and mTOR inhibition appear to induce senolysis in a one-two punch mechanism, but senolysis was prevented by inhibition of autophagy. This was attributed to distinctive interplay between autophagy and mTOR in senescence, in which autophagy may contribute to persistent mTORC1 signalling in senescence through generation of free amino acids for mTORC1 activation at the lysosome (Carroll et al., 2017), though as discussed in section 1.3.4, there are inconsistencies in

reports examining levels of autophagy in senescence. Further preliminary data has also suggested that mTOR promotes senescent cell survival *in vivo*, by observing a reduced frequency of senescent hepatocytes following Torin1 treatment in NSG immunodeficient mice (which accumulate senescent cells at greatly increased rates, Kucheryavenko et al., 2019), but this needs further exploration and validation in wild-type mice. These findings are extremely interesting: in this thesis I have observed that mTOR signalling plays a central role in senescence regardless of mode of induction. A major caveat of current senolytic compounds is selectivity towards only certain models of senescence. Therefore, targeting mTOR for senolysis could present the opportunity to develop a broad-spectrum senolytic intervention.

8.2.3. Targeting mTOR to tackle bystander senescence *in vivo*

While senotherapies are currently being developed *in vitro* predominantly using the models of OIS, RS and DDIS, the contribution to the *in vivo* senescent cell burden of these programmes is not yet clear. However, recent research has highlighted the importance of targeting bystander senescence (or its induction) *in vivo.* There is convincing evidence for bystander senescence occurring *in vivo*, for example focal clustering of senescent cells was observed in the livers of aged mice (Nelson et al., 2012) and SASP-mediated accumulation of senescent cells has been seen around pre-neoplastic regions (Acosta et al., 2013). Furthermore, pro-senescence signalling can also be relayed systemically, possibly through EVs; intraperitoneal transplantation of low numbers of senescent cells ($0.5\text{-}1x10^6$) was shown to cause persistent, systemic physical dysfunction, attributed to deleterious impacts of the bystander effect beyond the site of transplantation (Xu et al., 2018).

Further evidence for the bystander effect has been produced from experiments in which labelled replicatively senescent MRC5 fibroblasts were transplanted into skeletal muscle and skin in mice, resulting in the appearance of senescent biomarkers after 3 weeks in murine

dermal fibroblasts and myofibres. Notably however, these results were produced in severely immunodeficient (NSG) mice where immunosurveillance is compromised due to defective macrophage, T, B and NK cell populations (da Silva et al., 2018); macrophages may normally clear such senescent cells, and they may also be targeted by NK action (Sagiv et al., 2013). Further, comparing the frequencies of senescent hepatocytes in wild-type vs. immunodeficient mice on ad libitum vs. dietary restriction (DR) diets allowed a crude assessment of the relative importance of cell-autonomous vs. bystander senescence, concluding that the bystander effect may play a major role in senescent cell accumulation *in vivo* (da Silva et al., 2018). However, a number of simplifying assumptions were made in this conclusion, and results may differ for highly proliferative tissues such as the gut epithelium. Importantly though, the bystander effect was reduced on DR, suggesting that 'senostatic' interventions that supress the bystander effect could be as effective as senolytics in reducing the senescent cell load *in vivo* and may have significant benefits even over relatively short timeframes. Further molecular candidates for targeting the bystander effect include the common SASP components and ROS-inducing cytokines TGFβ and IL-1β, which are critical in inducing bystander senescence in multiple models of primary senescence (Hubacova et al., 2012).

8.2.4. Targeting intercellular communication

A possible avenue for preventing induction of bystander senescence may be through blunting the non-cell-autonomous roles of senescence by targeting intercellular communication. For example, extracellular vesicles secreted from senescent cells have been shown to play a critical role in mediating paracrine senescence (Borghesan et al., 2019). Indeed, senescent cells secrete a greater volume of vesicles with altered contents. Single cell analysis of cells internalizing EVs also suggested increased uptake of EVs by senescent cells (Borghesan et al., 2019). Targeting the production, secretion or internalization of EVs is therefore a potential therapeutic avenue for decreasing the senescent cell burden *in vivo*.

Similarly, targeting the SASP with small molecules (such as mTOR inhibitors) that prevent its production and secretion, or therapies such as monoclonal antibodies that can blunt the impact of secreted factors (such as the anti-IL-6 antibody siltuximab) is a further strategy in targeting intercellular communication. Assays for SASP secretion that can be used in high throughput screening, such as the IL-6 reporter cell assay used in this thesis (Rolt et al., 2019), may therefore prove valuable in discovering novel SASP-suppressing compounds.

Furthermore, it may be possible to target direct intercellular communication in senescence, operating via continuous membrane-bound bridges under the regulation of actin organization, as I observed in Chapter 7. Compounds such as the Cdc42 inhibitor CASIN which target important regulatory proteins could be instrumental in this process, though off-target effects of these compounds, and potentially beneficial roles of bridges in senescence immunosurveillance (Biran et al., 2015) require careful consideration.

Indeed, inhibiting mTOR *in vivo* in both model organisms and clinical studies has produced extremely promising results in terms of extending healthy lifespan and tackling age-related decline (Harrison et al., 2009, Table 1.2). As discussed above, these results could be due to multi-faceted regulation of senescence by mTOR, including induction of senescent proliferation arrest, promotion of pro-inflammatory secretion and direct intercellular communication, causing bystander senescence, tackling senescence-associated mitochondrial dysfunction, re-potentiating the immune system (which could potentially promote immune surveillance, Mannick et al., 2018) and possibly even regulating senescent cell survival.

8.3. Perspectives

As the role of cellular senescence transitions from protector to antagonist with age, a number of different therapeutic avenues are being explored to blunt its deleterious effects

in elderly patients. As previously mentioned, there is highly promising pre-clinical and clinical evidence for the use of senolytic agents or DR mimetics such as mTOR inhibitors in tackling age-related disease. However, this impressive research does not mean that further avenues should not still be explored. While there are a number of differences between treating cancer cells and targeting senescent cells, therapies harnessing the power and selectivity of the immune system to treat tumours are now producing highly impressive results in the clinic. By analogy, such therapies could perhaps also be utilized to target senescent cells, with a view towards improving health in old age.

8.3.1. Enhancing immunosurveillance

Beyond the direct elimination of senescent cells using senolytic compounds, enhancing immune-mediated senescent cell clearance is now emerging as a potential therapeutic avenue (Burton and Stolzing, 2018). Indeed, senescent cells are highly immunogenic and subject to immune surveillance *in vivo*, though clearance appears to fail with advanced age, perhaps due to immune deficiency or evasion (Wilson et al., 2017). In theory, this approach may enable improved selectivity and efficacy in senescent cell elimination compared to small molecule administration.

Simplistically, age-related immune deficiency could be counteracted by re-potentiation of the aged immune system by an immune stimulator. For example, the stimulator polyI:C was shown to facilitate senescent cell clearance in fibrotic livers by NK cells (Krizhanovsky et al., 2008). However, this approach may be insufficiently specific for *in vivo* therapy. Further, age-related immune deficiency and compromised immune surveillance may be at least in part due to an increased proportion of senescent immune cells. Notably, statin administration appears to improve pneumonia recovery in the elderly through promoting neutrophil migration and function (Sapey et al., 2017). Further immune-rejuvenating therapies could involve the removal senescent immune cells from the blood either directly or through using

immune cell/HSC specific senolytics, or through rejuvenation of immune cells (e.g. by mTOR inhibition Mannick et al., 2014, 2018 or stimulation of autophagy, Puleston et al., 2014). Intriguingly, one year treatment with a cocktail including growth hormone and metformin, designed to stimulate thymic function, resulted in protective immunological changes and a reduction in patient epigenetic age, though no control group was included in the study (Fahy et al., 2019).

Immunotherapies currently in development for cancer treatment could also be repurposed to target senescent cells *in vivo*. Indeed, through the identification of cell surface markers specific to chronic senescent cells (currently the major stumbling block), immune-priming approaches could stimulate senescent cell clearance. For example, NKG2D ligands overexpressed in senescent cells (Sagiv et al., 2016) are also upregulated in many cancer cells, so approaches such as CAR-T could be adapted for senescent cell targeting. Excitingly, the cell surface protein DPP4 was shown to be upregulated on replicative senescence and has been successfully used as a target for antibody-dependent cell-mediated cytotoxicity (ADCC) against senescent cells, whereby NK cells are activated by antibodies, as used in cancer immunotherapy (Kim et al., 2017).

Ultimately, a vaccine which primes the aged immune system to target chronic senescent cells could be a highly effective intervention. Such a treatment would prevent the long-term persistence of senescent cells without compromising their beneficial roles. Further, a vaccine could result in enhanced continual senescent cell clearance without inducing mass removal of senescent cells upon administration of a senolytic treatment, which risks compromising tissue integrity. As in cancer immunotherapy, exposing chronic senescence-specific antigens to dendritic cells (DCs) would result in the expression of antigens on the DC cell surface for T cell recognition and activation, to promote T cell-mediated senescent cell clearance.

8.3.2. Therapeutic potential of targeting senescence in ageing

As a number of senotherapies enter clinical trials, we will soon be able to assess the therapeutic potential of targeting senescence to treat age-related decline in elderly patients. While the list of diseases in which senescence is implicated is continually increasing (Table 1.1) it is important to remember that other limiting but as yet undiscovered or underappreciated factors may also be involved in driving pathological ageing, including excessive glycation, ECM cross-linking and the chronic accumulation of latent pathogens. Furthermore, in model organism studies, the lifespan-extending effects of interventions such as DR markedly decline relative to maximum lifespan with increasing organismal complexity, and therefore any effects seen in humans may only be mild. However, an exciting number and breadth of interventions currently being tested could prove capable of reducing disease burden and improving quality of life in older age. As a critical regulator of cellular senescence, targeting mTOR signalling presents an exciting opportunity to treat a broad range of age-related diseases. Therefore, mTOR inhibitors warrant investigation in clinical trials for a range of age-related conditions, as well as in treating progeria.

9. References

1. Abad, M. *et al.* Reprogramming in vivo produces teratomas and iPS cells with totipotency features. *Nature* **502**, 340–345 (2013).
2. Abounit, S. *et al.* Tunneling nanotubes spread fibrillar α-synuclein by intercellular trafficking of lysosomes. *EMBO J.* **35**, 2120–2138 (2016).
3. Abounit, S., Wu, J. W., Duff, K., Victoria, G. S. & Zurzolo, C. Tunneling nanotubes: A possible highway in the spreading of tau and other prion-like proteins in neurodegenerative diseases. *Prion* **10**, 344–351 (2016).
4. Acosta, J. C. *et al.* Chemokine Signaling via the CXCR2 Receptor Reinforces Senescence. *Cell* **133**, 1006–1018 (2008).
5. Acosta, J. C. *et al.* A complex secretory program orchestrated by the inflammasome controls paracrine senescence. *Nat. Cell Biol.* **15**, 978–990 (2013).
6. Acosta, J. C., Snijders, A. P. & Gil, J. Unbiased Characterization of the Senescence-Associated Secretome Using SILAC-Based Quantitative Proteomics. in *Cell Senescence* 175–184 (2013). doi:10.1007/978-1-62703-239-1_11
7. Aguayo-Mazzucato, C. *et al.* Acceleration of β Cell Aging Determines Diabetes and Senolysis Improves Disease Outcomes. *Cell Metab.* **30**, 129-142.e4 (2019).
8. Ahmad, T. *et al.* Impaired mitophagy leads to cigarette smoke stress-induced cellular senescence: Implications for chronic obstructive pulmonary disease. *FASEB J.* **29**, 2912–2929 (2015).
9. Ahn, B., Lee, J. W., Jung, H., Beck, G. & Bohr, V. A. Mechanism of Werner DNA Helicase: POT1 and RPA Stimulates WRN to Unwind beyond Gaps in the Translocating Strand. *PLoS One* **4**, e4673 (2009).
10. Aird, K. M. *et al.* HMGB2 orchestrates the chromatin landscape of senescence-associated secretory phenotype gene loci. *J. Cell Biol.* **215**, 325–334 (2016).
11. Akbar, A. N., Henson, S. M. & Lanna, A. Senescence of T Lymphocytes: Implications for Enhancing Human Immunity. *Trends Immunol.* **37**, 866–876 (2016).
12. Alimbetov, D. *et al.* Suppression of the senescence-associated secretory phenotype (SASP) in human fibroblasts using small molecule inhibitors of p38 MAP kinase and MK2. *Biogerontology* **17**, 305–315 (2016).
13. Allen, S. A., Tomilov, A. & Cortopassi, G. A. Small molecules bind human mTOR protein and inhibit mTORC1 specifically. *Biochem. Pharmacol.* **155**, 298–304 (2018).
14. Althubiti, M. *et al.* Characterization of novel markers of senescence and their prognostic potential in cancer. *Cell Death Dis.* **5**, e1528-10 (2014).
15. Amano, H. *et al.* Telomere Dysfunction Induces Sirtuin Repression that Drives Telomere-Dependent Disease. *Cell Metab.* **29**, 1274-1290.e9 (2019).
16. Amano, M. *et al.* Phosphorylation and Activation of Myosin by Rho-associated Kinase (Rho-kinase). *J. Biol. Chem.* **271**, 20246–20249 (1996).
17. An, W.-L. *et al.* Up-Regulation of Phosphorylated/Activated p70 S6 Kinase and Its Relationship to Neurofibrillary Pathology in Alzheimer's Disease. *Am. J. Pathol.* **163**, 591–607 (2003).
18. Anisimov, V. N. *et al.* Rapamycin Extends Maximal Lifespan in Cancer-Prone Mice. *Am. J. Pathol.* **176**, 2092–2097 (2010).
19. Aparicio, O. M., Billington, B. L. & Gottschling, D. E. Modifiers of position effect are shared between telomeric and silent mating-type loci in S. cerevisiae. *Cell* **66**, 1279–1287 (1991).

20. Arkwright, P. D. *et al.* Fas stimulation of T lymphocytes promotes rapid intercellular exchange of death signals via membrane nanotubes. *Cell Res.* **20**, 72–88 (2010).
21. Ashburner, M. *et al.* Gene Ontology: tool for the unification of biology. *Nat. Genet.* **25**, 25–29 (2000).
22. Aslam, B., Basit, M., Nisar, M. A., Khurshid, M. & Rasool, M. H. Proteomics: Technologies and Their Applications. *J. Chromatogr. Sci.* **55**, 182–196 (2017).
23. Astle, M. V. *et al.* AKT induces senescence in human cells via mTORC1 and p53 in the absence of DNA damage: Implications for targeting mTOR during malignancy. *Oncogene* **31**, 1949–1962 (2012).
24. Baar, M. P. *et al.* Targeted Apoptosis of Senescent Cells Restores Tissue Homeostasis in Response to Chemotoxicity and Aging. *Cell* **169**, 132-147.e16 (2017).
25. Baker, D. J. *et al.* Naturally occurring p16 Ink4a-positive cells shorten healthy lifespan. *Nature* **530**, 184–189 (2016).
26. Baker, D. J. *et al.* Clearance of p16 Ink4a-positive senescent cells delays ageing-associated disorders. *Nature* **479**, 232–236 (2011).
27. Banerji, U. *et al.* First results from a phase I trial of AZD8055, a dual mTORC1 and mTORC2 inhibitor. *J. Clin. Oncol.* **29**, 3096–3096 (2011).
28. Basisty, N. *et al.* A Proteomic Atlas of Senescence-Associated Secretomes for Aging Biomarker Development. *bioRxiv* 604306 (2019). doi:10.1101/604306
29. Baus, F., Gire, V., Fisher, D., Piette, J. & Dulić, V. Permanent cell cycle exit in G2 phase after DNA damage in normal human fibroblasts. *EMBO J.* **22**, 3992–4002 (2003).
30. Beausejour, C. M. *et al.* Reversal of human cellular senescence: roles of the p53 and p16 pathways. *EMBO J.* **22**, 4212–4222 (2003).
31. Benavides-Serrato, A. *et al.* Specific blockade of Rictor-mTOR association inhibits mTORC2 activity and is cytotoxic in glioblastoma. *PLoS One* **12**, e0176599 (2017).
32. Bennett, J. E. *et al.* Contributions of diseases and injuries to widening life expectancy inequalities in England from 2001 to 2016: a population-based analysis of vital registration data. *Lancet Public Heal.* **3**, e586–e597 (2018).
33. Beuvink, I. *et al.* The mTOR Inhibitor RAD001 Sensitizes Tumor Cells to DNA-Damaged Induced Apoptosis through Inhibition of p21 Translation. *Cell* **120**, 747–759 (2005).
34. Biran, A. *et al.* Senescent cells communicate via intercellular protein transfer. *Genes Dev.* **29**, 791–802 (2015).
35. Biran, A. *et al.* Quantitative identification of senescent cells in aging and disease. *Aging Cell* **16**, 661–671 (2017).
36. Bird, J. L. E. *et al.* Recapitulation of Werner syndrome sensitivity to camptothecin by limited knockdown of the WRN helicase/exonuclease. *Biogerontology* **13**, 49–62 (2012).
37. Bischof, O. *et al.* Deconstructing PML-induced premature senescence. *EMBO J.* **21**, 3358–3369 (2002).
38. Blander, G. *et al.* Physical and Functional Interaction between p53 and the Werner's Syndrome Protein. *J. Biol. Chem.* **274**, 29463–29469 (1999).
39. Bodnar, A. G. *et al.* Extension of Life-Span by Introduction of Telomerase into Normal Human Cells. *Science (80-.).* **279**, 349–352 (1998).
40. Borghesan, M. *et al.* Small Extracellular Vesicles Are Key Regulators of Non-cell Autonomous Intercellular Communication in Senescence via the Interferon Protein IFITM3. *Cell Rep.* **27**, 3956-3971.e6 (2019).
41. Borodkina, A. V., Shatrova, A. N., Nikolsky, N. N. & Burova, E. B. The role of p38 MAP-kinase in stress-induced senescence of human endometrium-derived mesenchymal stem cells. *Cell tissue biol.* **10**, 365–371 (2016).
42. Borra, M. T. & Denu, J. M. Quantitative Assays for Characterization of the Sir2 Family of NAD+-Dependent Deacetylases. in *Methods in Enzymology* 171–187 (2003). doi:10.1016/S0076-6879(03)76011-X

43. Braig, M. *et al.* Oncogene-induced senescence as an initial barrier in lymphoma development. *Nature* **436**, 660–665 (2005).
44. Braumüller, H. *et al.* T-helper-1-cell cytokines drive cancer into senescence. *Nature* **494**, 361–365 (2013).
45. Bridger, J. M., Boyle, S., Kill, I. R. & Bickmore, W. A. Re-modelling of nuclear architecture in quiescent and senescent human fibroblasts. *Curr. Biol.* **10**, 149–152 (2000).
46. Brosh, R. M. *et al.* Functional and Physical Interaction between WRN Helicase and Human Replication Protein A. *J. Biol. Chem.* **274**, 18341–18350 (1999).
47. Brown, J. P., Wei, W. & Sedivy, J. M. Bypass of Senescence After Disruption of p21CIP1/WAF1 Gene in Normal Diploid Human Fibroblasts. *Science (80-.).* **277**, 831–834 (1997).
48. Browne, G. J. & Proud, C. G. A Novel mTOR-Regulated Phosphorylation Site in Elongation Factor 2 Kinase Modulates the Activity of the Kinase and Its Binding to Calmodulin. *Mol. Cell. Biol.* **24**, 2986–2997 (2004).
49. Buchwalter, A. & Hetzer, M. W. Nucleolar expansion and elevated protein translation in premature aging. *Nat. Commun.* **8**, 328 (2017).
50. Buj, R. *et al.* Suppression of p16 Induces mTORC1-Mediated Nucleotide Metabolic Reprogramming. *Cell Rep.* **28**, 1971-1980.e8 (2019).
51. Burnett, C. *et al.* Absence of effects of Sir2 overexpression on lifespan in C. elegans and Drosophila. *Nature* **477**, 482–485 (2011).
52. Burthem, J. *et al.* The ρ-kinase inhibitors Y-27632 and fasudil act synergistically with imatinib to inhibit the expansion of ex vivo CD34+ CML progenitor cells. *Leukemia* **21**, 1708–1714 (2007).
53. Burton, D. G. A. & Stolzing, A. Cellular senescence: Immunosurveillance and future immunotherapy. *Ageing Res. Rev.* **43**, 17–25 (2018).
54. Bussian, T. J. *et al.* Clearance of senescent glial cells prevents tau-dependent pathology and cognitive decline. *Nature* **562**, 578–582 (2018).
55. Caccamo, A., Majumder, S., Richardson, A., Strong, R. & Oddo, S. Molecular Interplay between Mammalian Target of Rapamycin (mTOR), Amyloid-β, and Tau. *J. Biol. Chem.* **285**, 13107–13120 (2010).
56. Cahu, J., Bustany, S. & Sola, B. Senescence-associated secretory phenotype favors the emergence of cancer stem-like cells. *Cell Death Dis.* **3**, e446–e446 (2012).
57. Calado, R. T. *et al.* A Spectrum of Severe Familial Liver Disorders Associate with Telomerase Mutations. *PLoS One* **4**, e7926 (2009).
58. Cammarano, M. S., Nekrasova, T., Noel, B. & Minden, A. Pak4 Induces Premature Senescence via a Pathway Requiring p16INK4/p19ARF and Mitogen-Activated Protein Kinase Signaling. *Mol. Cell. Biol.* **25**, 9532–9542 (2005).
59. Campisi, J. Senescent Cells, Tumor Suppression, and Organismal Aging: Good Citizens, Bad Neighbors. *Cell* **120**, 513–522 (2005).
60. Campisi, J. Aging, Cellular Senescence, and Cancer. *Annu. Rev. Physiol.* **75**, 685–705 (2013).
61. Canino, C. *et al.* SASP mediates chemoresistance and tumor-initiating-activity of mesothelioma cells. *Oncogene* **31**, 3148–3163 (2012).
62. Cao, K. *et al.* Rapamycin Reverses Cellular Phenotypes and Enhances Mutant Protein Clearance in Hutchinson-Gilford Progeria Syndrome Cells. *Sci. Transl. Med.* **3**, 89ra58-89ra58 (2011).
63. Cao, K. *et al.* Progerin and telomere dysfunction collaborate to trigger cellular senescence in normal human fibroblasts. *J. Clin. Invest.* **121**, 2833–2844 (2011).
64. Caramés, B. *et al.* Autophagy activation by rapamycin reduces severity of experimental osteoarthritis. *Ann. Rheum. Dis.* **71**, 575–581 (2012).

65. Caramés, B., Taniguchi, N., Otsuki, S., Blanco, F. J. & Lotz, M. Autophagy is a protective mechanism in normal cartilage, and its aging-related loss is linked with cell death and osteoarthritis. *Arthritis Rheum.* **62**, 791–801 (2010).
66. Caron, E. *et al.* A comprehensive map of the mTOR signaling network. *Mol. Syst. Biol.* **6**, 453 (2010).
67. Carroll, B. *et al.* Persistent mTORC1 signaling in cell senescence results from defects in amino acid and growth factor sensing. *J. Cell Biol.* **216**, 1949–1957 (2017).
68. Cascella, R. *et al.* Uncovering genetic and non-genetic biomarkers specific for exudative age-related macular degeneration: significant association of twelve variants. *Oncotarget* **9**, 7812–7821 (2018).
69. Chandra, T. *et al.* Global Reorganization of the Nuclear Landscape in Senescent Cells. *Cell Rep.* **10**, 471–483 (2015).
70. Chandra, T. *et al.* Independence of Repressive Histone Marks and Chromatin Compaction during Senescent Heterochromatic Layer Formation. *Mol. Cell* **47**, 203–214 (2012).
71. Chang, J. *et al.* Clearance of senescent cells by ABT263 rejuvenates aged hematopoietic stem cells in mice. *Nat. Med.* **22**, 78–83 (2016).
72. Chen, D. & Guarente, L. SIR2: a potential target for calorie restriction mimetics. *Trends Mol. Med.* **13**, 64–71 (2007).
73. Chen, D., Li, M., Luo, J. & Gu, W. Direct Interactions between HIF-1α and Mdm2 Modulate p53 Function. *J. Biol. Chem.* **278**, 13595–13598 (2003).
74. Chen, J., Lin, J. & Levine, A. J. Regulation of transcription functions of the p53 tumor suppressor by the mdm-2 oncogene. *Mol. Med.* **1**, 142–52 (1995).
75. Chen, J., Wu, X., Lin, J. & Levine, A. J. mdm-2 inhibits the G1 arrest and apoptosis functions of the p53 tumor suppressor protein. *Mol. Cell. Biol.* **16**, 2445–2452 (1996).
76. Chen, J. *et al.* Sirt6 overexpression suppresses senescence and apoptosis of nucleus pulposus cells by inducing autophagy in a model of intervertebral disc degeneration. *Cell Death Dis.* **9**, 56 (2018).
77. Chen, Q. M. *et al.* Involvement of Rb family proteins, focal adhesion proteins and protein synthesis in senescent morphogenesis induced by hydrogen peroxide. *J. Cell Sci.* **113 (Pt 2**, 4087–97 (2000).
78. Chen, Z. *et al.* Crucial role of p53-dependent cellular senescence in suppression of Pten-deficient tumorigenesis. *Nature* **436**, 725–730 (2005).
79. Cheng, L., Chen, J. & Mao, X. Everolimus vs. rapamycin for treating diabetic nephropathy in diabetic mouse model. *J. Huazhong Univ. Sci. Technol. [Medical Sci.* **31**, 457–462 (2011).
80. Cherif, H. *et al.* Curcumin and o-Vanillin Exhibit Evidence of Senolytic Activity in Human IVD Cells In Vitro. *J. Clin. Med.* **8**, 433 (2019).
81. Cheung, H.-H. *et al.* Telomerase Protects Werner Syndrome Lineage-Specific Stem Cells from Premature Aging. *Stem Cell Reports* **2**, 534–546 (2014).
82. Childs, B. G. *et al.* Senescent intimal foam cells are deleterious at all stages of atherosclerosis. *Science (80-.).* **354**, 472–477 (2016).
83. Childs, B. G. *et al.* Senescent cells: an emerging target for diseases of ageing. *Nat. Rev. Drug Discov.* **16**, 718–735 (2017).
84. Childs, B. G., Li, H. & van Deursen, J. M. Senescent cells: a therapeutic target for cardiovascular disease. *J. Clin. Invest.* **128**, 1217–1228 (2018).
85. Childs, B. G., Baker, D. J., Kirkland, J. L., Campisi, J. & van Deursen, J. M. Senescence and apoptosis: dueling or complementary cell fates? *EMBO Rep.* **15**, 1139–53 (2014).
86. Chinnery, H. R., Pearlman, E. & McMenamin, P. G. Cutting Edge: Membrane Nanotubes In Vivo: A Feature of MHC Class II + Cells in the Mouse Cornea. *J. Immunol.* **180**, 5779–5783 (2008).

87. Cho, K. A. *et al.* Morphological adjustment of senescent cells by modulating caveolin-1 status. *J. Biol. Chem.* **279**, 42270–42278 (2004).
88. Cho, S. & Hwang, E. S. Status of mTOR activity may phenotypically differentiate senescence and quiescence. *Mol. Cells* **33**, 597–604 (2012).
89. Choi, G. *et al.* Discovery of a potent small molecule SIRT1/2 inhibitor with anticancer effects. *Int. J. Oncol.* **43**, 1205–1211 (2013).
90. Chong, M. *et al.* CD36 initiates the secretory phenotype during the establishment of cellular senescence. *EMBO Rep.* **19**, e45274 (2018).
91. Choo, A. Y., Yoon, S.-O., Kim, S. G., Roux, P. P. & Blenis, J. Rapamycin differentially inhibits S6Ks and 4E-BP1 to mediate cell-type-specific repression of mRNA translation. *Proc. Natl. Acad. Sci.* **105**, 17414–17419 (2008).
92. Chresta, C. M. *et al.* AZD8055 Is a Potent, Selective, and Orally Bioavailable ATP-Competitive Mammalian Target of Rapamycin Kinase Inhibitor with In vitro and In vivo Antitumor Activity. *Cancer Res.* **70**, 288–298 (2010).
93. Chuprin, A. *et al.* Cell fusion induced by ERVWE1 or measles virus causes cellular senescence. *Genes Dev.* **27**, 2356–2366 (2013).
94. Collado, M. *et al.* Senescence in premalignant tumours. *Nature* **436**, 642–642 (2005).
95. Colman, R. J. *et al.* Caloric Restriction Delays Disease Onset and Mortality in Rhesus Monkeys. *Science (80-.).* **325**, 201–204 (2009).
96. Consortium, T. G. O. The Gene Ontology Resource: 20 years and still GOing strong. *Nucleic Acids Res.* **47**, D330–D338 (2019).
97. Coppé, J.-P., Kauser, K., Campisi, J. & Beauséjour, C. M. Secretion of Vascular Endothelial Growth Factor by Primary Human Fibroblasts at Senescence. *J. Biol. Chem.* **281**, 29568–29574 (2006).
98. Coppé, J.-P. *et al.* A Human-Like Senescence-Associated Secretory Phenotype Is Conserved in Mouse Cells Dependent on Physiological Oxygen. *PLoS One* **5**, e9188 (2010).
99. Coppé, J.-P. *et al.* Senescence-Associated Secretory Phenotypes Reveal Cell-Nonautonomous Functions of Oncogenic RAS and the p53 Tumor Suppressor. *PLoS Biol.* **6**, e301 (2008).
100. Correia-Melo, C., Ichim, G., Tait, S. W. G. & Passos, J. F. Depletion of mitochondria in mammalian cells through enforced mitophagy. *Nat. Protoc.* **12**, 183–194 (2017).
101. Correia-Melo, C. *et al.* Mitochondria are required for pro-ageing features of the senescent phenotype. *EMBO J.* **35**, 724–742 (2016).
102. Costa, T. D. F. *et al.* PAK4 suppresses RELB to prevent senescence-like growth arrest in breast cancer. *Nat. Commun.* **10**, 3589 (2019).
103. Costanzo, M. *et al.* Transfer of polyglutamine aggregates in neuronal cells occurs in tunneling nanotubes. *J. Cell Sci.* **126**, 3678–3685 (2013).
104. Couzens, A. L., Gill, R. & Scheid, M. P. Characterization of a modified ROCK2 protein that allows use of N6-ATP analogs for the identification of novel substrates. *BMC Biotechnol.* **14**, 2 (2014).
105. Cox, L. S. & Faragher, R. G. A. From old organisms to new molecules: integrative biology and therapeutic targets in accelerated human ageing. *Cell. Mol. Life Sci.* **64**, 2620–2641 (2007).
106. Cox, L. S. Live Fast, Die Young: New Lessons in Mammalian Longevity. *Rejuvenation Res.* **12**, 283–288 (2009).
107. Cox, L. S. & Lane, D. P. Tumour suppressors, kinases and clamps: How p53 regulates the cell cycle in response to DNA damage. *BioEssays* **17**, 501–508 (1995).
108. Cox, L. S. & Mattison, J. A. Increasing longevity through caloric restriction or rapamycin feeding in mammals: common mechanisms for common outcomes? *Aging Cell* **8**, 607–613 (2009).

109. Cox, L. S. & Redman, C. The role of cellular senescence in ageing of the placenta. *Placenta* **52**, 139–145 (2017).
110. Crabbe L, Verdun RE, Haggblom CI, K. J. Defective Telomere Lagging Strand Synthesis in Cells Lacking WRN Helicase Activity. *Science (80-.).* **306**, 1951–1953 (2004).
111. Cramer, L. P., Briggs, L. J. & Dawe, H. R. Use of fluorescently labelled deoxyribonuclease I to spatially measure G-actin levels in migrating and non-migrating cells. *Cell Motil. Cytoskeleton* **51**, 27–38 (2002).
112. Cruickshanks, H. A. *et al.* Senescent Cells Harbour Features of the Cancer Epigenome. *Nat. Cell Biol.* **15**, 1495–1506 (2013).
113. Cuervo, A. M. Autophagy and aging: keeping that old broom working. *Trends Genet.* **24**, 604–612 (2008).
114. Cunningham, J. T. *et al.* mTOR controls mitochondrial oxidative function through a YY1-PGC-1α transcriptional complex. *Nature* **450**, 736–740 (2007).
115. da Silva, P. F. L. *et al.* The bystander effect contributes to the accumulation of senescent cells in vivo. *Aging Cell* **18**, e12848 (2019).
116. D'Adda Di Fagagna, F. *et al.* A DNA damage checkpoint response in telomere-initiated senescence. *Nature* **426**, 194–198 (2003).
117. Dai, D.-F. *et al.* Altered proteome turnover and remodeling by short-term caloric restriction or rapamycin rejuvenate the aging heart. *Aging Cell* **13**, 529–539 (2014).
118. Dalle Pezze, P. *et al.* Dynamic Modelling of Pathways to Cellular Senescence Reveals Strategies for Targeted Interventions. *PLoS Comput. Biol.* **10**, e1003728 (2014).
119. Dang, W. The controversial world of sirtuins. *Drug Discov. Today Technol.* **12**, e9–e17 (2014).
120. Dang, W. *et al.* Histone H4 lysine 16 acetylation regulates cellular lifespan. *Nature* **459**, 802–807 (2009).
121. Davaapil, H., Brockes, J. P. & Yun, M. H. Conserved and novel functions of programmed cellular senescence during vertebrate development. *Development* **144**, 106–114 (2017).
122. Davalos, A. R. *et al.* p53-dependent release of Alarmin HMGB1 is a central mediator of senescent phenotypes. *J. Cell Biol.* **201**, 613–629 (2013).
123. Davis, T., Baird, D. M., Haughton, M. F., Jones, C. J. & Kipling, D. Prevention of Accelerated Cell Aging in Werner Syndrome Using a p38 Mitogen-Activated Protein Kinase Inhibitor. *Journals Gerontol. Ser. A Biol. Sci. Med. Sci.* **60**, 1386–1393 (2005).
124. Davis, T., Brook, A., Rokicki, M., Bagley, M. & Kipling, D. Evaluating the Role of p38 MAPK in the Accelerated Cell Senescence of Werner Syndrome Fibroblasts. *Pharmaceuticals* **9**, 23 (2016).
125. De Cecco, M. *et al.* L1 drives IFN in senescent cells and promotes age-associated inflammation. *Nature* **566**, 73–78 (2019).
126. Delage, E. & Zurzolo, C. Exploring the role of lipids in intercellular conduits: breakthroughs in the pipeline. *Front. Plant Sci.* **4**, 504 (2013).
127. Demaria, M. *et al.* An essential role for senescent cells in optimal wound healing through secretion of PDGF-AA. *Dev. Cell* **31**, 722–733 (2014).
128. Demidenko, Z. N. *et al.* Rapamycin decelerates cellular senescence. *Cell Cycle* **8**, 1888–1895 (2009).
129. Denoyelle, C. *et al.* Anti-oncogenic role of the endoplasmic reticulum differentially activated by mutations in the MAPK pathway. *Nat. Cell Biol.* **8**, 1053–1063 (2006).
130. Deracinois, B., Flahaut, C., Duban-Deweer, S. & Karamanos, Y. Comparative and Quantitative Global Proteomics Approaches: An Overview. *Proteomes* **1**, 180–218 (2013).
131. Desir, S. *et al.* Tunneling nanotube formation is stimulated by hypoxia in ovarian cancer cells. *Oncotarget* **7**, 43150–43161 (2016).

132. Di Micco, R. *et al.* Oncogene-induced senescence is a DNA damage response triggered by DNA hyper-replication. *Nature* **444**, 638–642 (2006).
133. Dierick, J.-F. *et al.* Stress-induced premature senescence and replicative senescence are different phenotypes, proteomic evidence. *Biochem. Pharmacol.* **64**, 1011–1017 (2002).
134. Dimri, G. P. *et al.* A biomarker that identifies senescent human cells in culture and in aging skin in vivo (replicative senescence/tumor suppression/18-galactosidase) Communicated by Arthur. *PNAS* **92**, 9363–9367 (1995).
135. Ding, R.-B., Bao, J. & Deng, C.-X. Emerging roles of SIRT1 in fatty liver diseases. *Int. J. Biol. Sci.* **13**, 852–867 (2017).
136. Diot, A. *et al.* A novel quantitative assay of mitophagy: Combining high content fluorescence microscopy and mitochondrial DNA load to quantify mitophagy and identify novel pharmacological tools against pathogenic heteroplasmic mtDNA. *Pharmacol. Res.* **100**, 24–35 (2015).
137. DiPaolo, J. A., Popescu, N. C., Alvarez, L. & Woodworth, C. D. Cellular and molecular alterations in human epithelial cells transformed by recombinant human papillomavirus DNA. *Crit. Rev. Oncog.* **4**, 337–60 (1993).
138. Domhan, S. *et al.* Intercellular Communication by Exchange of Cytoplasmic Material via Tunneling Nano-Tube Like Structures in Primary Human Renal Epithelial Cells. *PLoS One* **6**, e21283 (2011).
139. Dominguez, J., Mahalati, K., Kiberd, B., McAlister, V. C. & MacDonald, A. S. Conversion to rapamycin immunosuppression in renal transplant recipients: report of an initial experience. *Transplantation* **70**, 1244–1247 (2000).
140. Dos D. Sarbassov *et al.* Rictor, a Novel Binding Partner of mTOR, Defines a Rapamycin-Insensitive and Raptor-Independent Pathway that Regulates the Cytoskeleton. *Curr. Biol.* **14**, 1296–1302 (2004).
141. Dou, Z. *et al.* Cytoplasmic chromatin triggers inflammation in senescence and cancer. *Nature* **550**, 402–406 (2017).
142. Dou, Z. *et al.* Autophagy mediates degradation of nuclear lamina. *Nature* **527**, 105–109 (2015).
143. Dupont, M., Souriant, S., Lugo-Villarino, G., Maridonneau-Parini, I. & Vérollet, C. Tunneling Nanotubes: Intimate Communication between Myeloid Cells. *Front. Immunol.* **9**, 43 (2018).
144. Ebner, M., Sinkovics, B., Szczygieł, M., Ribeiro, D. W. & Yudushkin, I. Localization of mTORC2 activity inside cells. *J. Cell Biol.* **216**, 343–353 (2017).
145. Edwards, D. N., Orren, D. K. & Machwe, A. Strand exchange of telomeric DNA catalyzed by the Werner syndrome protein (WRN) is specifically stimulated by TRF2. *Nucleic Acids Res.* **42**, 7748–7761 (2014).
146. Eriksson, M. *et al.* Recurrent de novo point mutations in lamin A cause Hutchinson–Gilford progeria syndrome. *Nature* **423**, 293–298 (2003).
147. Fahy, G. M. *et al.* Reversal of epigenetic aging and immunosenescent trends in humans. *Aging Cell* e13028 (2019). doi:10.1111/acel.13028
148. Farr, J. N. *et al.* Targeting cellular senescence prevents age-related bone loss in mice. *Nat. Med.* **23**, 1072–1079 (2017).
149. Farr, J. *et al.* Senescent Osteocytes: Do They Cause Damage and Can They Be Targeted to Preserve the Skeleton? *J. Bone Miner. Res.* **31**, 1917–1919 (2016).
150. Feng, Z. *et al.* The Regulation of AMPK β1, TSC2, and PTEN Expression by p53: Stress, Cell and Tissue Specificity, and the Role of These Gene Products in Modulating the IGF-1-AKT-mTOR Pathways. *Cancer Res.* **67**, 3043–3053 (2007).
151. Ferbeyre, G. *et al.* PML is induced by oncogenic ras and promotes premature senescence. *Genes Dev.* **14**, 2015–27 (2000).

152. Fernández, Á. F. *et al.* Disruption of the beclin 1-BCL2 autophagy regulatory complex promotes longevity in mice. *Nature* **558**, 136–140 (2018).
153. Flynn, J. M. *et al.* Late-life rapamycin treatment reverses age-related heart dysfunction. *Aging Cell* **12**, 851–862 (2013).
154. Frescas, D. *et al.* Senescent cells expose and secrete an oxidized form of membrane-bound vimentin as revealed by a natural polyreactive antibody. *Proc. Natl. Acad. Sci.* **114**, E1668–E1677 (2017).
155. Freund, A., Laberge, R.-M., Demaria, M. & Campisi, J. Lamin B1 loss is a senescence-associated biomarker. *Mol. Biol. Cell* **23**, 2066–2075 (2012).
156. Fritze, C. E. Direct evidence for SIR2 modulation of chromatin structure in yeast rDNA. *EMBO J.* **16**, 6495–6509 (1997).
157. Fuhrmann-Stroissnigg, H. *et al.* Identification of HSP90 inhibitors as a novel class of senolytics. *Nat. Commun.* **8**, 422 (2017).
158. Fujikake, N., Shin, M. & Shimizu, S. Association Between Autophagy and Neurodegenerative Diseases. *Front. Neurosci.* **12**, 255 (2018).
159. Fumagalli, M. *et al.* Telomeric DNA damage is irreparable and causes persistent DNA-damage-response activation. *Nat. Cell Biol.* **14**, 355–365 (2012).
160. Fumagalli, M., Rossiello, F., Mondello, C. & d'Adda di Fagagna, F. Stable Cellular Senescence Is Associated with Persistent DDR Activation. *PLoS One* **9**, e110969 (2014).
161. Georgilis, A. *et al.* PTBP1-Mediated Alternative Splicing Regulates the Inflammatory Secretome and the Pro-tumorigenic Effects of Senescent Cells. *Cancer Cell* **34**, 85-102.e9 (2018).
162. Gevaert, A. B. *et al.* Endothelial Senescence Contributes to Heart Failure With Preserved Ejection Fraction in an Aging Mouse Model. *Circ. Hear. Fail.* **10**, e003806 (2017).
163. Ghosh, H. S., McBurney, M. & Robbins, P. D. SIRT1 Negatively Regulates the Mammalian Target of Rapamycin. *PLoS One* **5**, e9199 (2010).
164. Gingras, A.-C. *et al.* Regulation of 4E-BP1 phosphorylation: a novel two-step mechanism. *Genes Dev.* **13**, 1422–1437 (1999).
165. Gire, V. & Dulic, V. Senescence from G2 arrest, revisited. *Cell Cycle* **14**, 297–304 (2015).
166. Glück, S. *et al.* Innate immune sensing of cytosolic chromatin fragments through cGAS promotes senescence. *Nat. Cell Biol.* **19**, 1061–1070 (2017).
167. Godwin, J. W., Pinto, A. R. & Rosenthal, N. A. Macrophages are required for adult salamander limb regeneration. *Proc. Natl. Acad. Sci.* **110**, 9415–9420 (2013).
168. Gonzalez-Meljem, J. M., Apps, J. R., Fraser, H. C. & Martinez-Barbera, J. P. Paracrine roles of cellular senescence in promoting tumourigenesis. *Br. J. Cancer* **118**, 1283–1288 (2018).
169. Gourlay, C. W., Carpp, L. N., Timpson, P., Winder, S. J. & Ayscough, K. R. A role for the actin cytoskeleton in cell death and aging in yeast. *J. Cell Biol.* **164**, 803–809 (2004).
170. Gousset, K. *et al.* Prions hijack tunnelling nanotubes for intercellular spread. *Nat. Cell Biol.* **11**, 328–336 (2009).
171. Grabiner, B. C. *et al.* A Diverse Array of Cancer-Associated MTOR Mutations Are Hyperactivating and Can Predict Rapamycin Sensitivity. *Cancer Discov.* **4**, 554–563 (2014).
172. Guarente, L. Sir2 links chromatin silencing, metabolism, and aging. *Genes Dev.* **14**, 1021–6 (2000).
173. Guzman-Castillo, M. *et al.* Forecasted trends in disability and life expectancy in England and Wales up to 2025: a modelling study. *Lancet Public Heal.* **2**, e307–e313 (2017).
174. Gyurus, E., Kaposztas, Z. & Kahan, B. D. Sirolimus therapy predisposes to new-onset diabetes mellitus after renal transplantation: A long-term analysis of various treatment regimens. *Transplant. Proc.* **43**, 1583–1592 (2011).

175. Han, Z. *et al.* Role of p21 in Apoptosis and Senescence of Human Colon Cancer Cells Treated with Camptothecin. *J. Biol. Chem.* **277**, 17154–17160 (2002).
176. Hanahan, D. & Weinberg, R. A. The Hallmarks of Cancer. *Cell* **100**, 57–70 (2000).
177. Hanahan, D. & Weinberg, R. A. Hallmarks of Cancer: The Next Generation. *Cell* **144**, 646–674 (2011).
178. Hanna, S. J. *et al.* The Role of Rho-GTPases and actin polymerization during Macrophage Tunneling Nanotube Biogenesis. *Sci. Rep.* **7**, 8547 (2017).
179. Hansen, M. *et al.* Lifespan extension by conditions that inhibit translation in Caenorhabditis elegans. *Aging Cell* **6**, 95–110 (2007).
180. Harrison, D. E. *et al.* Rapamycin fed late in life extends lifespan in genetically heterogeneous mice. *Nature* **460**, 392–395 (2009).
181. Hase, K. *et al.* M-Sec promotes membrane nanotube formation by interacting with Ral and the exocyst complex. *Nat. Cell Biol.* **11**, 1427–1432 (2009).
182. Hashimoto, M. *et al.* Potential Role of the Formation of Tunneling Nanotubes in HIV-1 Spread in Macrophages. *J. Immunol.* **196**, 1832–1841 (2016).
183. Hayakawa, T. *et al.* SIRT1 Suppresses the Senescence-Associated Secretory Phenotype through Epigenetic Gene Regulation. *PLoS One* **10**, e0116480 (2015).
184. Hayflick, L. & Moorhead, P. S. The serial cultivation of human diploid cell strains. *Exp. Cell Res.* **25**, 585–621 (1961).
185. He, L.-F. *et al.* Activated-PAK4 predicts worse prognosis in breast cancer and promotes tumorigenesis through activation of PI3K/AKT signaling. *Oncotarget* **8**, 17573–17585 (2017).
186. Heasman, S. J. & Ridley, A. J. Mammalian Rho GTPases: new insights into their functions from in vivo studies. *Nat. Rev. Mol. Cell Biol.* **9**, 690–701 (2008).
187. Hédouin, S., Grillo, G., Ivkovic, I., Velasco, G. & Francastel, C. CENP-A chromatin disassembly in stressed and senescent murine cells. *Sci. Rep.* **7**, 42520 (2017).
188. Heitman, J., Movva, N. & Hall, M. Targets for cell cycle arrest by the immunosuppressant rapamycin in yeast. *Science (80-.).* **253**, 905–909 (1991).
189. Helman, A. *et al.* p16 Ink4a-induced senescence of pancreatic beta cells enhances insulin secretion. *Nat. Med.* **22**, 412–420 (2016).
190. Herbig, U. Cellular Senescence in Aging Primates. *Science (80-.).* **311**, 1257–1257 (2006).
191. Herbig, U., Jobling, W. A., Chen, B. P. C., Chen, D. J. & Sedivy, J. M. Telomere shortening triggers senescence of human cells through a pathway involving ATM, p53, and p21CIP1, but not p16INK4a. *Mol. Cell* **14**, 501–513 (2004).
192. Hernandez-Segura, A., Rubingh, R. & Demaria, M. Identification of stable senescence-associated reference genes. *Aging Cell* **18**, e12911 (2019).
193. Hernandez-Vallejo, S. J., Beaupere, C., Larghero, J., Capeau, J. & Lagathu, C. HIV protease inhibitors induce senescence and alter osteoblastic potential of human bone marrow mesenchymal stem cells: beneficial effect of pravastatin. *Aging Cell* **12**, 955–965 (2013).
194. Herranz, N. *et al.* mTOR regulates MAPKAPK2 translation to control the senescence-associated secretory phenotype. *Nat. Cell Biol.* **17**, 1205–1217 (2015).
195. Hickson, L. J. *et al.* Senolytics decrease senescent cells in humans: Preliminary report from a clinical trial of Dasatinib plus Quercetin in individuals with diabetic kidney disease. *EBioMedicine* **47**, 446–456 (2019).
196. Hirai, S. *et al.* Antitumor Effects of a Sirtuin Inhibitor, Tenovin-6, against Gastric Cancer Cells via Death Receptor 5 Up-Regulation. *PLoS One* **9**, e102831 (2014).
197. Hoare, M. *et al.* NOTCH1 mediates a switch between two distinct secretomes during senescence. *Nat. Cell Biol.* **18**, 979–992 (2016).

198. Holly, A. C. *et al.* Changes in splicing factor expression are associated with advancing age in man. *Mech. Ageing Dev.* **134**, 356–366 (2013).
199. Hong, S. *et al.* LARP1 functions as a molecular switch for mTORC1-mediated translation of an essential class of mRNAs. *Elife* **6**, e25237 (2017).
200. Hong, S., Zhao, B., Lombard, D. B., Fingar, D. C. & Inoki, K. Cross-talk between Sirtuin and Mammalian Target of Rapamycin Complex 1 (mTORC1) Signaling in the Regulation of S6 Kinase 1 (S6K1) Phosphorylation. *J. Biol. Chem.* **289**, 13132–13141 (2014).
201. Horvath, S. DNA methylation age of human tissues and cell types. *Genome Biol.* **14**, R115 (2013).
202. Huang, K. & Fingar, D. C. Growing knowledge of the mTOR signaling network. *Semin. Cell Dev. Biol.* **36**, 79–90 (2014).
203. Huang, W. *et al.* mTORC2 controls actin polymerization required for consolidation of long-term memory. *Nat. Neurosci.* **16**, 441–448 (2013).
204. Hubackova, S., Krejcikova, K., Bartek, J. & Hodny, Z. IL1-β and TGFβ-Nox4 signaling, oxidative stress and DNA damage response are shared features of replicative, oncogene-induced and drug-induced paracrine 'Bystander senescence'. *Aging (Albany. NY).* **4**, 932–951 (2012).
205. Hurez, V. *et al.* Chronic mTOR inhibition in mice with rapamycin alters T, B, myeloid, and innate lymphoid cells and gut flora and prolongs life of immune-deficient mice. *Aging Cell* **14**, 945–956 (2015).
206. Hurst, V., Shimada, K. & Gasser, S. M. Nuclear Actin and Actin-Binding Proteins in DNA Repair. *Trends Cell Biol.* **29**, 462–476 (2019).
207. Iadevaia, V., Liu, R. & Proud, C. G. MTORC1 signaling controls multiple steps in ribosome biogenesis. *Semin. Cell Dev. Biol.* **36**, 113–120 (2014).
208. Igarashi, M. & Guarente, L. mTORC1 and SIRT1 Cooperate to Foster Expansion of Gut Adult Stem Cells during Calorie Restriction. *Cell* **166**, 436–450 (2016).
209. Imai, S. & Guarente, L. It takes two to tango: NAD+ and sirtuins in aging/longevity control. *npj Aging Mech. Dis.* **2**, 16017 (2016).
210. Imai, Y. *et al.* Crosstalk between the Rb Pathway and AKT Signaling Forms a Quiescence-Senescence Switch. *Cell Rep.* **7**, 194–207 (2014).
211. Irani, K. *et al.* Mitogenic Signaling Mediated by Oxidants in Ras-Transformed Fibroblasts. *Science (80-.).* **275**, 1649–1652 (1997).
212. Ivanov, A. *et al.* Lysosome-mediated processing of chromatin in senescence. *J. Cell Biol.* **202**, 129–143 (2013).
213. Jacinto, E. *et al.* Mammalian TOR complex 2 controls the actin cytoskeleton and is rapamycin insensitive. *Nat. Cell Biol.* **6**, 1122–1128 (2004).
214. Jarrard, D. F. *et al.* p16/pRb pathway alterations are required for bypassing senescence in human prostate epithelial cells. *Cancer Res.* **59**, 2957–64 (1999).
215. Jascur, T. *et al.* Regulation of p21WAF1/CIP1 Stability by WISp39, a Hsp90 Binding TPR Protein. *Mol. Cell* **17**, 237–249 (2005).
216. Jaskelioff, M. *et al.* Telomerase reactivation reverses tissue degeneration in aged telomerase-deficient mice. *Nature* **469**, 102–106 (2011).
217. Jefferies, H. B., Reinhard, C., Kozma, S. C. & Thomas, G. Rapamycin selectively represses translation of the 'polypyrimidine tract' mRNA family. *Proc. Natl. Acad. Sci.* **91**, 4441–4445 (1994).
218. Jeon, O. H., David, N., Campisi, J. & Elisseeff, J. H. Senescent cells and osteoarthritis: a painful connection. *J. Clin. Invest.* **128**, 1229–1237 (2018).
219. Jeon, O. H. *et al.* Local clearance of senescent cells attenuates the development of post-traumatic osteoarthritis and creates a pro-regenerative environment. *Nat. Med.* **23**, 775–781 (2017).

220. Jia, K. & Levine, B. Autophagy is required for dietary restriction-mediated life span extension in C. elegans. *Autophagy* **3**, 597–599 (2007).
221. Jiao, R. *et al.* The Werner syndrome protein is required for recruitment of chromatin assembly factor 1 following DNA damage. *Oncogene* **26**, 3811–3822 (2007).
222. Jin, Y. *et al.* Tenovin-6-mediated inhibition of SIRT1/2 induces apoptosis in acute lymphoblastic leukemia (ALL) cells and eliminates ALL stem/progenitor cells. *BMC Cancer* **15**, 226 (2015).
223. Johmura, Y. *et al.* Necessary and sufficient role for a mitosis skip in senescence induction. *Mol. Cell* **55**, 73–84 (2014).
224. Joung, S. M. *et al.* Akt Contributes to Activation of the TRIF-Dependent Signaling Pathways of TLRs by Interacting with TANK-Binding Kinase 1. *J. Immunol.* **186**, 499–507 (2011).
225. Jun, J. Il & Lau, L. F. The matricellular protein CCN1 induces fibroblast senescence and restricts fibrosis in cutaneous wound healing. *Nat. Cell Biol.* **12**, 676–685 (2010).
226. Jung, S. H. *et al.* mTOR kinase leads to PTEN-loss-induced cellular senescence by phosphorylating p53. *Oncogene* **38**, 1639–1650 (2019).
227. Jurk, D. *et al.* Postmitotic neurons develop a p21-dependent senescence-like phenotype driven by a DNA damage response. *Aging Cell* **11**, 996–1004 (2012).
228. Jurk, D. *et al.* Chronic inflammation induces telomere dysfunction and accelerates ageing in mice. *Nat. Commun.* **5**, 4172 (2014).
229. Justice, J. N. *et al.* Senolytics in idiopathic pulmonary fibrosis: Results from a first-in-human, open-label, pilot study. *EBioMedicine* **40**, 554–563 (2019).
230. Kaeberlein, M., McVey, M. & Guarente, L. The SIR2/3/4 complex and SIR2 alone promote longevity in Saccharomyces cerevisiae by two different mechanisms. *Genes Dev.* **13**, 2570–2580 (1999).
231. Kaeberlein, M. *et al.* Regulation of Yeast Replicative Life Span by TOR and Sch9 in Response to Nutrients. *Science (80-.).* **310**, 1193–1196 (2005).
232. Kahyo, T., Mostoslavsky, R., Goto, M. & Setou, M. Sirtuin-mediated deacetylation pathway stabilizes Werner syndrome protein. *FEBS Lett.* **582**, 2479–2483 (2008).
233. Kamijo, T. *et al.* Tumor Suppression at the Mouse INK4a Locus Mediated by the Alternative Reading Frame Product p19 ARF. *Cell* **91**, 649–659 (1997).
234. Kang, T. W. *et al.* Senescence surveillance of pre-malignant hepatocytes limits liver cancer development. *Nature* **479**, 547–551 (2011).
235. Kapahi, P. *et al.* Regulation of lifespan in Drosophila by modulation of genes in the TOR signalling pathway. *Curr. Biol.* **14**, 885–890 (2004).
236. Kaplon, J. *et al.* A key role for mitochondrial gatekeeper pyruvate dehydrogenase in oncogene-induced senescence. *Nature* **498**, 109–112 (2013).
237. Kennedy, B. K. & Lamming, D. W. The Mechanistic Target of Rapamycin: The Grand ConducTOR of Metabolism and Aging. *Cell Metab.* **23**, 990–1003 (2016).
238. Kenyon, C. J. The genetics of ageing. *Nature* **464**, 504–512 (2010).
239. Kenyon, C., Chang, J. & Gensch, E. A C. elegans mutant that lives twice as long as wild type. *Nature* **366**, 461–464 (1993).
240. Kim, B. S., Lee, C.-H., Chang, G.-E., Cheong, E. & Shin, I. A potent and selective small molecule inhibitor of sirtuin 1 promotes differentiation of pluripotent P19 cells into functional neurons. *Sci. Rep.* **6**, 34324 (2016).
241. Kim, J., Kundu, M., Viollet, B. & Guan, K. L. AMPK and mTOR regulate autophagy through direct phosphorylation of Ulk1. *Nat. Cell Biol.* **13**, 132–141 (2011).
242. Kim, K. M. *et al.* Identification of senescent cell surface targetable protein DPP4. *Genes Dev.* **31**, 1529–1534 (2017).
243. Kim, L. C., Cook, R. S. & Chen, J. mTORC1 and mTORC2 in cancer and the tumor microenvironment. *Oncogene* **36**, 2191–2201 (2017).

244. Kimura, M. *et al.* Measurement of telomere length by the Southern blot analysis of terminal restriction fragment lengths. *Nat. Protoc.* **5**, 1596–1607 (2010).
245. Kloss, C. C., Condomines, M., Cartellieri, M., Bachmann, M. & Sadelain, M. Combinatorial antigen recognition with balanced signaling promotes selective tumor eradication by engineered T cells. *Nat. Biotechnol.* **31**, 71–75 (2013).
246. Kohli, L. *et al.* 4-Hydroxytamoxifen Induces Autophagic Death through K-Ras Degradation. *Cancer Res.* **73**, 4395–4405 (2013).
247. Kolesnichenko, M., Hong, L., Liao, R., Vogt, P. K. & Sun, P. Attenuation of TORC1 signaling delays replicative and oncogenic RAS-induced senescence. *Cell Cycle* **11**, 2391–2401 (2012).
248. Kolosova, N. G. *et al.* Prevention of Age-Related Macular Degeneration–Like Retinopathy by Rapamycin in Rats. *Am. J. Pathol.* **181**, 472–477 (2012).
249. Kong, X. *et al.* Interleukin-22 induces hepatic stellate cell senescence and restricts liver fibrosis in mice. *Hepatology* **56**, 1150–1159 (2012).
250. Koyanagi, M., Brandes, R. P., Haendeler, J., Zeiher, A. M. & Dimmeler, S. Cell-to-Cell Connection of Endothelial Progenitor Cells With Cardiac Myocytes by Nanotubes. *Circ. Res.* **96**, 1039–1041 (2005).
251. Kristl, J., Plajnšek, K. T., Kreft, M. E., Janković, B. & Kocbek, P. Intracellular trafficking of solid lipid nanoparticles and their distribution between cells through tunneling nanotubes. *Eur. J. Pharm. Sci.* **50**, 139–148 (2013).
252. Krizhanovsky, V. *et al.* Senescence of Activated Stellate Cells Limits Liver Fibrosis. *Cell* **134**, 657–667 (2008).
253. Krtolica, A., Parrinello, S., Lockett, S., Desprez, P.-Y. & Campisi, J. Senescent fibroblasts promote epithelial cell growth and tumorigenesis: a link between cancer and aging. *Proc. Natl. Acad. Sci.* **98**, 12072–12077 (2001).
254. Kruk, M. E. & Schwalbe, N. The relation between intermittent dosing and adherence: preliminary insights. *Clin. Ther.* **28**, 1989–95 (2006).
255. Kruse, S. E. *et al.* Age modifies respiratory complex I and protein homeostasis in a muscle type-specific manner. *Aging Cell* **15**, 89–99 (2016).
256. Kucharewicz, K. *et al.* Simultaneous induction and blockade of autophagy by a single agent. *Cell Death Dis.* **9**, 353 (2018).
257. Kucheryavenko, O., Nelson, G., von Zglinicki, T., Korolchuk, V. I. & Carroll, B. The mTORC1-autophagy pathway is a target for senescent cell elimination. *Biogerontology* **20**, 331–335 (2019).
258. Kuilman, T. *et al.* Oncogene-Induced Senescence Relayed by an Interleukin-Dependent Inflammatory Network. *Cell* **133**, 1019–1031 (2008).
259. Kumar, A. *et al.* Influenza virus exploits tunneling nanotubes for cell-to-cell spread. *Sci. Rep.* **7**, 40360 (2017).
260. Kwak, I. H., Kim, H. S., Choi, O. R., Ryu, M. S. & Lim, I. K. Nuclear accumulation of globular actin as a cellular senescence marker. *Cancer Res.* **64**, 572–80 (2004).
261. Laberge, R. M., Awad, P., Campisi, J. & Desprez, P. Y. Epithelial-mesenchymal transition induced by senescent fibroblasts. *Cancer Microenviron.* **5**, 39–44 (2012).
262. Laberge, R. M. *et al.* MTOR regulates the pro-tumorigenic senescence-associated secretory phenotype by promoting IL1A translation. *Nat. Cell Biol.* **17**, 1049–1061 (2015).
263. Lai, K. P. *et al.* S6K1 is a multifaceted regulator of Mdm2 that connects nutrient status and DNA damage response. *EMBO J.* **29**, 2994–3006 (2010).
264. Lain, S. *et al.* Discovery, In Vivo Activity, and Mechanism of Action of a Small-Molecule p53 Activator. *Cancer Cell* **13**, 454–463 (2008).
265. Lapasset, L. *et al.* Rejuvenating senescent and centenarian human cells by reprogramming through the pluripotent state. *Genes Dev.* **25**, 2248–2253 (2011).

266. Laplante, M. & Sabatini, D. M. Regulation of mTORC1 and its impact on gene expression at a glance. *J. Cell Sci.* **126**, 1713–1719 (2013).
267. Latorre, E. *et al.* Small molecule modulation of splicing factor expression is associated with rescue from cellular senescence. *BMC Cell Biol.* **18**, 31 (2017).
268. Lebel, M. & Leder, P. A deletion within the murine Werner syndrome helicase induces sensitivity to inhibitors of topoisomerase and loss of cellular proliferative capacity. *Proc. Natl. Acad. Sci.* **95**, 13097–13102 (1998).
269. Lebel, M., Spillare, E. A., Harris, C. C. & Leder, P. The Werner Syndrome Gene Product Co-purifies with the DNA Replication Complex and Interacts with PCNA and Topoisomerase I. *J. Biol. Chem.* **274**, 37795–37799 (1999).
270. Lee, C. H. *et al.* Constitutive mTOR activation in TSC mutants sensitizes cells to energy starvation and genomic damage via p53. *EMBO J.* **26**, 4812–4823 (2007).
271. Lee, J., Park, S. & Roh, S. Y-27632, a ROCK inhibitor, delays senescence of putative murine salivary gland stem cells in culture. *Arch. Oral Biol.* **60**, 875–882 (2015).
272. Lee, M., Chea, K., Pyda, R., Chua, M. & Dominguez, I. Comparative Analysis of Non-viral Transfection Methods in Mouse Embryonic Fibroblast Cells. *J. Biomol. Tech.* **28**, 67–74 (2017).
273. Lees, H., Walters, H. & Cox, L. S. Animal and human models to understand ageing. *Maturitas* **93**, 18–27 (2016).
274. Lehmann, B. D. *et al.* Senescence-associated exosome release from human prostate cancer cells. *Cancer Res.* **68**, 7864–7871 (2008).
275. Lenain, C., Gusyatiner, O., Douma, S., van den Broek, B. & Peeper, D. S. Autophagy-mediated degradation of nuclear envelope proteins during oncogene-induced senescence. *Carcinogenesis* **36**, 1263–1274 (2015).
276. Lenain, C. *et al.* Massive reshaping of genome-nuclear lamina interactions during oncogene-induced senescence. *Genome Res.* **27**, 1634–1644 (2017).
277. Leontieva, O. V. & Blagosklonny, M. V. Gerosuppression by pan-mTOR inhibitors. *Aging (Albany. NY).* **8**, 3535–3551 (2016).
278. Lerner, C. *et al.* Reduced mammalian target of rapamycin activity facilitates mitochondrial retrograde signaling and increases life span in normal human fibroblasts. *Aging Cell* **12**, 966–977 (2013).
279. Levy, M. Z., Allsopp, R. C., Futcher, A. B., Greider, C. W. & Harley, C. B. Telomere end-replication problem and cell aging. *J. Mol. Biol.* **225**, 951–960 (1992).
280. Lewis, D. A., Travers, J. B., Machado, C., Somani, A.-K. & Spandau, D. F. Reversing the aging stromal phenotype prevents carcinoma initiation. *Aging (Albany. NY).* **3**, 407–416 (2011).
281. Li, T. *et al.* Tumor Suppression in the Absence of p53-Mediated Cell-Cycle Arrest, Apoptosis, and Senescence. *Cell* **149**, 1269–1283 (2012).
282. Li, W. *et al.* Proteomics Analysis of Normal and Senescent NG108-15 Cells: GRP78 Plays a Negative Role in Cisplatin-Induced Senescence in the NG108-15 Cell Line. *PLoS One* **9**, e90114 (2014).
283. Lin, A. W. *et al.* Premature senescence involving p53 and p16 is activated in response to constitutive MEK/MAPK mitogenic signaling. *Genes Dev.* **12**, 3008–3019 (1998).
284. Lin, A.-L. *et al.* Chronic Rapamycin Restores Brain Vascular Integrity and Function Through NO Synthase Activation and Improves Memory in Symptomatic Mice Modeling Alzheimer's Disease. *J. Cereb. Blood Flow Metab.* **33**, 1412–1421 (2013).
285. Lipinski, M. M. *et al.* Genome-wide analysis reveals mechanisms modulating autophagy in normal brain aging and in Alzheimer's disease. *Proc. Natl. Acad. Sci.* **107**, 14164–14169 (2010).

286. Liu, B. *et al.* Resveratrol Rescues SIRT1-Dependent Adult Stem Cell Decline and Alleviates Progeroid Features in Laminopathy-Based Progeria. *Cell Metab.* **16**, 738–750 (2012).
287. Liu, D. & Hornsby, P. J. Senescent human fibroblasts increase the early growth of xenograft tumors via matrix metalloproteinase secretion. *Cancer Res.* **67**, 3117–3126 (2007).
288. Liu, J. *et al.* Impact of ER stress-regulated ATF4/p16 signaling on the premature senescence of renal tubular epithelial cells in diabetic nephropathy. *Am. J. Physiol. Physiol.* **308**, C621–C630 (2015).
289. Liu, L., Chen, L., Chung, J. & Huang, S. Rapamycin inhibits F-actin reorganization and phosphorylation of focal adhesion proteins. *Oncogene* **27**, 4998–5010 (2008).
290. Liu, L. *et al.* Rapamycin Inhibits Cytoskeleton Reorganization and Cell Motility by Suppressing RhoA Expression and Activity. *J. Biol. Chem.* **285**, 38362–38373 (2010).
291. Liu, W. *et al.* Mobilization of Hematopoitic Stem/Progenitor Cells by a Cdc42 Activity-Specific Inhibitor. *Blood* **112**, 68 LP – 68 (2008).
292. Liu, Y., Fallon, L., Lashuel, H. A., Liu, Z. & Lansbury, P. T. The UCH-L1 Gene Encodes Two Opposing Enzymatic Activities that Affect α-Synuclein Degradation and Parkinson's Disease Susceptibility. *Cell* **111**, 209–218 (2002).
293. Liu, Y. *et al.* Discovery of Inhibitors that Elucidate the Role of UCH-L1 Activity in the H1299 Lung Cancer Cell Line. *Chem. Biol.* **10**, 837–846 (2003).
294. Llanos, S., García-Pedrero, J. M., Morgado-Palacin, L., Rodrigo, J. P. & Serrano, M. Stabilization of p21 by mTORC1/4E-BP1 predicts clinical outcome of head and neck cancers. *Nat. Commun.* **7**, 10438 (2016).
295. Lloberas, N. *et al.* Mammalian Target of Rapamycin Pathway Blockade Slows Progression of Diabetic Kidney Disease in Rats. *J. Am. Soc. Nephrol.* **17**, 1395–1404 (2006).
296. López-Otín, C., Blasco, M. A., Partridge, L., Serrano, M. & Kroemer, G. The hallmarks of aging. *Cell* **153**, 1194 (2013).
297. Lou, E. *et al.* Tunneling Nanotubes Provide a Unique Conduit for Intercellular Transfer of Cellular Contents in Human Malignant Pleural Mesothelioma. *PLoS One* **7**, e33093 (2012).
298. Lu, P. D., Harding, H. P. & Ron, D. Translation reinitiation at alternative open reading frames regulates gene expression in an integrated stress response. *J. Cell Biol.* **167**, 27–33 (2004).
299. Lujambio, A. *et al.* Non-cell-autonomous tumor suppression by p53. *Cell* **153**, 449–460 (2013).
300. MacCallum, S. F. *et al.* Dysregulation of autophagy in chronic lymphocytic leukemia with the small-molecule Sirtuin inhibitor Tenovin-6. *Sci. Rep.* **3**, 1275 (2013).
301. Mahoney, S. J. *et al.* A small molecule inhibitor of Rheb selectively targets mTORC1 signaling. *Nat. Commun.* **9**, 548 (2018).
302. Mai, S., Klinkenberg, M., Auburger, G., Bereiter-Hahn, J. & Jendrach, M. Decreased expression of Drp1 and Fis1 mediates mitochondrial elongation in senescent cells and enhances resistance to oxidative stress through PINK1. *J. Cell Sci.* **123**, 917–926 (2010).
303. Maier, T., Güell, M. & Serrano, L. Correlation of mRNA and protein in complex biological samples. *FEBS Lett.* **583**, 3966–3973 (2009).
304. Maira, S.-M. *et al.* Identification and characterization of NVP-BEZ235, a new orally available dual phosphatidylinositol 3-kinase/mammalian target of rapamycin inhibitor with potent in vivo antitumor activity. *Mol. Cancer Ther.* **7**, 1851–1863 (2008).
305. Majumder, P. K. *et al.* mTOR inhibition reverses Akt-dependent prostate intraepithelial neoplasia through regulation of apoptotic and HIF-1-dependent pathways. *Nat. Med.* **10**, 594–601 (2004).

306. Majumder, S. *et al.* Lifelong rapamycin administration ameliorates age-dependent cognitive deficits by reducing IL-1β and enhancing NMDA signaling. *Aging Cell* **11**, 326–335 (2012).
307. Majumder, S., Richardson, A., Strong, R. & Oddo, S. Inducing Autophagy by Rapamycin Before, but Not After, the Formation of Plaques and Tangles Ameliorates Cognitive Deficits. *PLoS One* **6**, e25416 (2011).
308. Mali, R. S. *et al.* Rho Kinase Regulates the Survival and Transformation of Cells Bearing Oncogenic Forms of KIT, FLT3, and BCR-ABL. *Cancer Cell* **20**, 357–369 (2011).
309. Mannick, J. B. *et al.* mTOR inhibition improves immune function in the elderly. *Sci. Transl. Med.* **6**, 179 (2014).
310. Mannick, J. B. *et al.* TORC1 inhibition enhances immune function and reduces infections in the elderly. *Sci. Transl. Med.* **10**, eaaq1564 (2018).
311. Martin, G. M., Sprague, C. A. & Epstein, C. J. Replicative life-span of cultivated human cells. Effects of donor's age, tissue, and genotype. *Lab. Invest.* **23**, 86–92 (1970).
312. Marzo, L., Gousset, K. & Zurzolo, C. Multifaceted Roles of Tunneling Nanotubes in Intercellular Communication. *Front. Physiol.* **3**, (2012).
313. Matthews, J. R., Wakasugi, N., Virelizier, J.-L., Yodoi, J. & Hay, R. T. Thiordoxin regulates the DNA binding activity of NF-χB by reduction of a disulphid bond involving cysteine 62. *Nucleic Acids Res.* **20**, 3821–3830 (1992).
314. Mattison, J. A. *et al.* Caloric restriction improves health and survival of rhesus monkeys. *Nat. Commun.* **8**, 1–12 (2017).
315. Mattison, J. A. *et al.* Impact of caloric restriction on health and survival in rhesus monkeys from the NIA study. *Nature* **489**, 318–321 (2012).
316. McCarthy, A. R. *et al.* Tenovin-D3, a Novel Small-Molecule Inhibitor of Sirtuin SirT2, Increases p21 (CDKN1A) Expression in a p53-Independent Manner. *Mol. Cancer Ther.* **12**, 352–360 (2013).
317. Mercken, E. M. *et al.* SRT2104 extends survival of male mice on a standard diet and preserves bone and muscle mass. *Aging Cell* **13**, 787–796 (2014).
318. Meyer, K., Hodwin, B., Ramanujam, D., Engelhardt, S. & Sarikas, A. Essential Role for Premature Senescence of Myofibroblasts in Myocardial Fibrosis. *J. Am. Coll. Cardiol.* **67**, 2018–2028 (2016).
319. Mi, H., Muruganujan, A., Ebert, D., Huang, X. & Thomas, P. D. PANTHER version 14: more genomes, a new PANTHER GO-slim and improvements in enrichment analysis tools. *Nucleic Acids Res.* **47**, D419–D426 (2019).
320. Michaloglou, C. *et al.* BRAFE600-associated senescence-like cell cycle arrest of human naevi. *Nature* **436**, 720–724 (2005).
321. Miller, R. A. *et al.* Rapamycin, But Not Resveratrol or Simvastatin, Extends Life Span of Genetically Heterogeneous Mice. *Journals Gerontol. Ser. A* **66A**, 191–201 (2011).
322. Miloslavski, R. *et al.* Oxygen sufficiency controls TOP mRNA translation via the TSC-Rheb-mTOR pathway in a 4E-BP-independent manner. *J. Mol. Cell Biol.* **6**, 255–266 (2014).
323. Miralles, F. & Visa, N. Actin in transcription and transcription regulation. *Curr. Opin. Cell Biol.* **18**, 261–266 (2006).
324. Mitchell, S. J. *et al.* The SIRT1 Activator SRT1720 Extends Lifespan and Improves Health of Mice Fed a Standard Diet. *Cell Rep.* **6**, 836–843 (2014).
325. Miwa, S. *et al.* Decreased mTOR signalling reduces mitochondrial ROS in brain via accumulation of the telomerase protein TERT within mitochondria. *Aging (Albany. NY).* **8**, 2551–2567 (2016).
326. Mizunuma, M., Neumann-Haefelin, E., Moroz, N., Li, Y. & Blackwell, T. K. mTORC2-SGK-1 acts in two environmentally responsive pathways with opposing effects on longevity. *Aging Cell* **13**, 869–878 (2014).

327. Moore, M. *et al.* Ribosomal stress-induced senescence as a novel pro-senescence strategy for p16 positive basal-like breast cancer. *bioRxiv* 469445 (2018). doi:10.1101/469445
328. Morancho, B., Martínez-Barriocanal, Á., Villanueva, J. & Arribas, J. Role of ADAM17 in the non-cell autonomous effects of oncogene-induced senescence. *Breast Cancer Res.* **17**, 106 (2015).
329. Mori, H. *et al.* The mTOR pathway is highly activated in diabetic nephropathy and rapamycin has a strong therapeutic potential. *Biochem. Biophys. Res. Commun.* **384**, 471–475 (2009).
330. Morita, M. *et al.* MTORC1 controls mitochondrial activity and biogenesis through 4E-BP-dependent translational regulation. *Cell Metab.* **18**, 698–711 (2013).
331. Mosteiro, L. *et al.* Tissue damage and senescence provide critical signals for cellular reprogramming in vivo. *Science (80-.).* **354**, aaf4445 (2016).
332. Muñoz-Espín, D. Nanocarriers targeting senescent cells. *Transl. Med. Aging* **3**, 1–5 (2019).
333. Muñoz-Espín, D. *et al.* Programmed cell senescence during mammalian embryonic development. *Cell* **155**, 1104 (2013).
334. Muñoz-Espín, D. & Serrano, M. Cellular senescence: from physiology to pathology. *Nat. Rev. Mol. Cell Biol.* **15**, 482–496 (2014).
335. Murray, B. W. *et al.* Small-molecule p21-activated kinase inhibitor PF-3758309 is a potent inhibitor of oncogenic signaling and tumor growth. *Proc. Natl. Acad. Sci.* **107**, 9446–9451 (2010).
336. Murray, E. R. & Cameron, A. J. M. Towards specific inhibition of mTORC2. *Aging (Albany. NY).* **9**, 2461–2462 (2017).
337. Naing, A. *et al.* Abstract A168: First results from a phase I trial of AZD8055, a dual mTORC1 and mTORC2 inhibitor. in *Molecular Cancer Therapeutics* A168–A168 (American Association for Cancer Research, 2011). doi:10.1158/1535-7163.TARG-11-A168
338. Nakamura, H. *et al.* TCR Engagement Increases Hypoxia-Inducible Factor-1α Protein Synthesis via Rapamycin-Sensitive Pathway under Hypoxic Conditions in Human Peripheral T Cells. *J. Immunol.* **174**, 7592–7599 (2005).
339. Narita, M. *et al.* Spatial Coupling of mTOR and autophagy augments secretory phenotypes. *Science (80-.).* **332**, 966–70 (2011).
340. Narita, M. *et al.* Rb-mediated heterochromatin formation and silencing of E2F target genes during cellular senescence. *Cell* **113**, 703–716 (2003).
341. Nassour, J. *et al.* Defective DNA single-strand break repair is responsible for senescence and neoplastic escape of epithelial cells. *Nat. Commun.* **7**, 10399 (2016).
342. Nehlin, J. O., Skovgaard, G. L. & Bohr, V. A. The Werner Syndrome: A Model for the Study of Human Aging. *Ann. N. Y. Acad. Sci.* **908**, 167–179 (2006).
343. Nelson, D. M. *et al.* Mapping H4K20me3 onto the chromatin landscape of senescent cells indicates a function in control of cell senescence and tumor suppression through preservation of genetic and epigenetic stability. *Genome Biol.* **17**, 158 (2016).
344. Nelson, D. M., McBryan, T., Jeyapalan, J. C., Sedivy, J. M. & Adams, P. D. A comparison of oncogene-induced senescence and replicative senescence: implications for tumor suppression and aging. *Age (Omaha).* **36**, 9637 (2014).
345. Nelson, G. *et al.* A senescent cell bystander effect: senescence-induced senescence. *Aging Cell* **11**, 345–349 (2012).
346. Niccoli, T. & Partridge, L. Ageing as a Risk Factor for Disease. *Curr. Biol.* **22**, R741–R752 (2012).
347. Nishio, K. & Inoue, A. Senescence-associated alterations of cytoskeleton: extraordinary production of vimentin that anchors cytoplasmic p53 in senescent human fibroblasts. *Histochem. Cell Biol.* **123**, 263–273 (2005).

348. Nishio, K., Inoue, A., Qiao, S., Kondo, H. & Mimura, A. Senescence and cytoskeleton: Overproduction of vimentin induces senescent-like morphology in human fibroblasts. *Histochem. Cell Biol.* **116**, 321–327 (2001).
349. Oberdoerffer, P. *et al.* SIRT1 Redistribution on Chromatin Promotes Genomic Stability but Alters Gene Expression during Aging. *Cell* **135**, 907–918 (2008).
350. Ocampo, A. *et al.* In Vivo Amelioration of Age-Associated Hallmarks by Partial Reprogramming. *Cell* **167**, 1719-1733.e12 (2016).
351. Ogrodnik, M. *et al.* Cellular senescence drives age-dependent hepatic steatosis. *Nat. Commun.* **8**, 15691 (2017).
352. Ogrodnik, M. *et al.* Obesity-Induced Cellular Senescence Drives Anxiety and Impairs Neurogenesis. *Cell Metab.* **29**, 1233 (2019).
353. Oh, W. J. *et al.* MTORC2 can associate with ribosomes to promote cotranslational phosphorylation and stability of nascent Akt polypeptide. *EMBO J.* **29**, 3939–3951 (2010).
354. Ohno, H., Hase, K. & Kimura, S. Emerging secrets of tunneling nanotube formation. *Commun. Integr. Biol.* **3**, 231–233 (2010).
355. Oishi, N. *et al.* Hepatitis B virus X protein overcomes oncogenic RAS-induced senescence in human immortalized cells. *Cancer Sci.* **98**, 1540–1548 (2007).
356. Okamoto, H. *et al.* Trichostatin A, an Inhibitor of Histone Deacetylase, Inhibits Smooth Muscle Cell Proliferation via Induction of p21WAF1. *J. Atheroscler. Thromb.* **13**, 183–191 (2006).
357. Olive, M. *et al.* Cardiovascular Pathology in Hutchinson-Gilford Progeria: Correlation With the Vascular Pathology of Aging. *Arterioscler. Thromb. Vasc. Biol.* **30**, 2301–2309 (2010).
358. Önfelt, B. *et al.* Structurally Distinct Membrane Nanotubes between Human Macrophages Support Long-Distance Vesicular Traffic or Surfing of Bacteria. *J. Immunol.* **177**, 8476–8483 (2006).
359. Opresko, P. L. *et al.* POT1 Stimulates RecQ Helicases WRN and BLM to Unwind Telomeric DNA Substrates. *J. Biol. Chem.* **280**, 32069–32080 (2005).
360. Opresko, P. L. *et al.* The Werner Syndrome Helicase and Exonuclease Cooperate to Resolve Telomeric D Loops in a Manner Regulated by TRF1 and TRF2. *Mol. Cell* **14**, 763–774 (2004).
361. Ortells, M. C. *et al.* Transcriptional regulation of gene expression during osmotic stress responses by the mammalian target of rapamycin. *Nucleic Acids Res.* **40**, 4368–4384 (2012).
362. Ortiz-Montero, P., Londoño-Vallejo, A. & Vernot, J.-P. Senescence-associated IL-6 and IL-8 cytokines induce a self- and cross-reinforced senescence/inflammatory milieu strengthening tumorigenic capabilities in the MCF-7 breast cancer cell line. *Cell Commun. Signal.* **15**, 17 (2017).
363. Ouellette, M. M., McDaniel, L. D., Wright, W. E., Shay, J. W. & Schultz, R. A. The establishment of telomerase-immortalized cell lines representing human chromosome instability syndromes. *Hum. Mol. Genet.* **9**, 403–411 (2000).
364. Ovadya, Y. *et al.* Impaired immune surveillance accelerates accumulation of senescent cells and aging. *Nat. Commun.* **9**, 5435 (2018).
365. Pakos-Zebrucka, K. *et al.* The integrated stress response. *EMBO Rep.* **17**, 1374–1395 (2016).
366. Palacios, J. A. *et al.* SIRT1 contributes to telomere maintenance and augments global homologous recombination. *J. Cell Biol.* **191**, 1299–1313 (2010).
367. Park, J. T. *et al.* A crucial role of ROCK for alleviation of senescence-associated phenotype. *Exp. Gerontol.* **106**, 8–15 (2018).
368. Parrinello, S. Stromal-epithelial interactions in aging and cancer: senescent fibroblasts alter epithelial cell differentiation. *J. Cell Sci.* **118**, 485–496 (2005).

369. Parry, A. J. *et al.* NOTCH-mediated non-cell autonomous regulation of chromatin structure during senescence. *Nat. Commun.* **9**, 1–15 (2018).
370. Parry, A. J. & Narita, M. Old cells, new tricks: chromatin structure in senescence. *Mamm. Genome* **27**, 320–331 (2016).
371. Pasquier, J. *et al.* Different Modalities of Intercellular Membrane Exchanges Mediate Cell-to-cell P-glycoprotein Transfers in MCF-7 Breast Cancer Cells. *J. Biol. Chem.* **287**, 7374–7387 (2012).
372. Passos, J. F. *et al.* Feedback between p21 and reactive oxygen production is necessary for cell senescence. *Mol. Syst. Biol.* **6**, 1–14 (2010).
373. Passos, J. F. *et al.* Mitochondrial dysfunction accounts for the stochastic heterogeneity in telomere-dependent senescence. *PLoS Biol.* **5**, 1138–1151 (2007).
374. Patil, P. *et al.* Systemic clearance of p16 INK4a -positive senescent cells mitigates age-associated intervertebral disc degeneration. *Aging Cell* **18**, e12927 (2019).
375. Patteson, A. E. *et al.* Vimentin protects the structural integrity of the nucleus and suppresses nuclear damage caused by large deformations. *bioRxiv* 566174 (2019). doi:10.1101/566174
376. Pearson, M. *et al.* PML regulates p53 acetylation and premature senescence induced by oncogenic Ras. *Nature* **406**, 207–210 (2000).
377. Pei, J.-J. & Hugon, J. mTOR-dependent signalling in Alzheimer's disease. *J. Cell. Mol. Med.* **12**, 2525–2532 (2008).
378. Pereira, B. I. *et al.* Senescent cells evade immune clearance via HLA-E-mediated NK and CD8+ T cell inhibition. *Nat. Commun.* **10**, 2387 (2019).
379. Pichierri, P., Franchitto, A., Mosesso, P. & Palitti, F. Werner's Syndrome Protein Is Required for Correct Recovery after Replication Arrest and DNA Damage Induced in S-Phase of Cell Cycle. *Mol. Biol. Cell* **12**, 2412–2421 (2001).
380. Pirrie, L. *et al.* Discovery and Validation of SIRT2 Inhibitors Based on Tenovin-6: Use of a 1H-NMR Method to Assess Deacetylase Activity. *Molecules* **17**, 12206–12224 (2012).
381. Pitozzi, V. *et al.* Chronic Resveratrol Treatment Ameliorates Cell Adhesion and Mitigates the Inflammatory Phenotype in Senescent Human Fibroblasts. *Journals Gerontol. Ser. A Biol. Sci. Med. Sci.* **68**, 371–381 (2013).
382. Pluquet, O., Pourtier, A. & Abbadie, C. The unfolded protein response and cellular senescence. A Review in the Theme: Cellular Mechanisms of Endoplasmic Reticulum Stress Signaling in Health and Disease. *Am. J. Physiol. Physiol.* **308**, C415–C425 (2015).
383. Puleston, D. J. *et al.* Autophagy is a critical regulator of memory $CD8^+$ T cell formation. *Elife* **3**, 1–21 (2014).
384. Purushotham, A. *et al.* Hepatocyte-Specific Deletion of SIRT1 Alters Fatty Acid Metabolism and Results in Hepatic Steatosis and Inflammation. *Cell Metab.* **9**, 327–338 (2009).
385. Quan, T. *et al.* Elevated matrix metalloproteinases and collagen fragmentation in photodamaged human skin: impact of altered extracellular matrix microenvironment on dermal fibroblast function. *J. Invest. Dermatol.* **133**, 1362–6 (2013).
386. Reddy, S., Li, B. & Comai, L. Processing of human telomeres by the Werner syndrome protein. *Cell Cycle* **9**, 3137–3138 (2010).
387. Ritschka, B. *et al.* The senescence-associated secretory phenotype induces cellular plasticity and tissue regeneration. *Genes Dev.* **31**, 172–183 (2017).
388. Roberts, S., Evans, E. H., Kletsas, D., Jaffray, D. C. & Eisenstein, S. M. Senescence in human intervertebral discs. *Eur. Spine J.* **15**, 312–316 (2006).
389. Rodier, F., Campisi, J. & Bhaumik, D. Two faces of p53: aging and tumor suppression. *Nucleic Acids Res.* **35**, 7475–7484 (2007).

390. Rodier, F. *et al.* DNA-SCARS: distinct nuclear structures that sustain damage-induced senescence growth arrest and inflammatory cytokine secretion. *J. Cell Sci.* **124**, 68–81 (2011).
391. Rodier, F. *et al.* Persistent DNA damage signalling triggers senescence-associated inflammatory cytokine secretion. *Nat. Cell Biol.* **11**, 973–979 (2009).
392. Rodier, F., Zhou, D. & Ferbeyre, G. Cellular senescence, geroscience, cancer and beyond. *Aging (Albany. NY).* **10**, 2233–2242 (2018).
393. Rodriguez-Lopez, A. M., Jackson, D. A., Iborra, F. & Cox, L. S. Asymmetry of DNA replication fork progression in Werner's syndrome. *Aging Cell* **1**, 30–39 (2002).
394. Rodríguez-López, A. M. *et al.* Characterisation of the interaction between WRN, the helicase/exonuclease defective in progeroid Werner's syndrome, and an essential replication factor, PCNA. *Mech. Ageing Dev.* **124**, 167–74 (2003).
395. Rogakou, E. P., Boon, C., Redon, C. & Bonner, W. M. Megabase Chromatin Domains Involved in DNA Double-Strand Breaks in Vivo. *J. Cell Biol.* **146**, 905–916 (1999).
396. Rolt, A., Nair, A. & Cox, L. S. Optimisation of a screening platform for determining IL-6 inflammatory signalling in the senescence-associated secretory phenotype (SASP). *Biogerontology* **20**, 359–371 (2019).
397. Rossiello, F., Fumagalli, M. & di Fagagna, F. ImmunoFISH for Adherent Cultured Mammalian Cells. *BIO-PROTOCOL* **3**, e999 (2013).
398. Rossiello, F., Herbig, U., Longhese, M. P., Fumagalli, M. & d'Adda di Fagagna, F. Irreparable telomeric DNA damage and persistent DDR signalling as a shared causative mechanism of cellular senescence and ageing. *Curr. Opin. Genet. Dev.* **26**, 89–95 (2014).
399. Rostami, J. *et al.* Human Astrocytes Transfer Aggregated Alpha-Synuclein via Tunneling Nanotubes. *J. Neurosci.* **37**, 11835–11853 (2017).
400. Routhier, A. *et al.* Pharmacological inhibition of Rho-kinase signaling with Y-27632 blocks melanoma tumor growth. *Oncol. Rep.* **23**, 861–7 (2010).
401. Ruas, M. & Peters, G. The p16INK4a/CDKN2A tumor suppressor and its relatives. *Biochim. Biophys. Acta - Rev. Cancer* **1378**, F115–F177 (1998).
402. Rubinsztein, D. C., Mariño, G. & Kroemer, G. Autophagy and aging. *Cell* **146**, 682–695 (2011).
403. Rustom, A. Nanotubular Highways for Intercellular Organelle Transport. *Science (80-.).* **303**, 1007–1010 (2004).
404. Ryu, S. J., Oh, Y. S. & Park, S. C. Failure of stress-induced downregulation of Bcl-2 contributes to apoptosis resistance in senescent human diploid fibroblasts. *Cell Death Differ.* **14**, 1020–1028 (2007).
405. Sacco, F. *et al.* Tumor Suppressor Density-enhanced Phosphatase-1 (DEP-1) Inhibits the RAS Pathway by Direct Dephosphorylation of ERK1/2 Kinases. *J. Biol. Chem.* **284**, 22048–22058 (2009).
406. Sagiv, A. *et al.* Granule exocytosis mediates immune surveillance of senescent cells. *Oncogene* **32**, 1971–1977 (2013).
407. Saha, B., Cypro, A., Martin, G. M. & Oshima, J. Rapamycin decreases DNA damage accumulation and enhances cell growth of WRN-deficient human fibroblasts. *Aging Cell* **13**, 573–575 (2014).
408. Saintigny, Y., Makienko, K., Swanson, C., Emond, M. J. & Monnat, R. J. Homologous Recombination Resolution Defect in Werner Syndrome. *Mol. Cell. Biol.* **22**, 6971–6978 (2002).
409. Saitou, M. *et al.* An evolutionary transcriptomics approach links CD36 to membrane remodeling in replicative senescence. *bioRxiv* 294512 (2018). doi:10.1101/294512
410. Sakaguchi, M. *et al.* Inhibition of mTOR signaling with rapamycin attenuates renal hypertrophy in the early diabetic mice. *Biochem. Biophys. Res. Commun.* **340**, 296–301 (2006).

411. Sakamori, R. *et al.* CDC42 Inhibition Suppresses Progression of Incipient Intestinal Tumors. *Cancer Res.* **74**, 5480–5492 (2014).
412. Sanders, J. L. & Newman, A. B. Telomere Length in Epidemiology: A Biomarker of Aging, Age-Related Disease, Both, or Neither? *Epidemiol. Rev.* **35**, 112–131 (2013).
413. Sanders, Y. Y. *et al.* Histone modifications in senescence-associated resistance to apoptosis by oxidative stress. *Redox Biol.* **1**, 8–16 (2013).
414. Santagata, S. *et al.* Tight coordination of protein translation and HSF1 activation supports the anabolic malignant state. *Science (80-.).* **341**, (2013).
415. Sarbassov, D. D. *et al.* Prolonged Rapamycin Treatment Inhibits mTORC2 Assembly and Akt/PKB. *Mol. Cell* **22**, 159–168 (2006).
416. Saretzki, G. Extra-telomeric Functions of Human Telomerase: Cancer, Mitochondria and Oxidative Stress. *Curr. Pharm. Des.* **20**, 6386–6403 (2014).
417. Sarvothaman, S., Undi, R. B., Pasupuleti, S. R., Gutti, U. & Gutti, R. K. Apoptosis: role in myeloid cell development. *Blood Res.* **50**, 73 (2015).
418. Satoh, A. *et al.* Sirt1 Extends Life Span and Delays Aging in Mice through the Regulation of Nk2 Homeobox 1 in the DMH and LH. *Cell Metab.* **18**, 416–430 (2013).
419. Savage, N. New tricks from old dogs join the fight against ageing. *Nature* **552**, S57–S59 (2017).
420. Schafer, M. J. *et al.* Exercise prevents diet-induced cellular senescence in adipose tissue. *Diabetes* **65**, 1606–1615 (2016).
421. Schafer, M. J. *et al.* Cellular senescence mediates fibrotic pulmonary disease. *Nat. Commun.* **8**, 14532 (2017).
422. Schiller, C. *et al.* LST1 promotes the assembly of a molecular machinery responsible for tunneling nanotube formation. *J. Cell Sci.* **126**, 767–777 (2013).
423. Schreiber, K. H. *et al.* A novel rapamycin analog is highly selective for mTORC1 in vivo. *Nat. Commun.* **10**, 3194 (2019).
424. Schreiber, K. H. *et al.* Rapamycin-mediated mTORC2 inhibition is determined by the relative expression of FK506-binding proteins. *Aging Cell* **14**, 265–273 (2015).
425. Schuler, M., Bossy-Wetzel, E., Goldstein, J. C., Fitzgerald, P. & Green, D. R. p53 Induces Apoptosis by Caspase Activation through Mitochondrial Cytochrome c Release. *J. Biol. Chem.* **275**, 7337–7342 (2000).
426. Schulze, C. *et al.* Stiffening of Human Skin Fibroblasts with Age. *Biophys. J.* **99**, 2434–2442 (2010).
427. Seiter, K. *et al.* Severe toxicity following induction chemotherapy for acute myelogenous leukemia in a patient with Werner's syndrome. *Leuk. Lymphoma* **46**, 1091–1095 (2005).
428. Selman, C. *et al.* Ribosomal Protein S6 Kinase 1 Signaling Regulates Mammalian Life Span. *Science (80-.).* **326**, 140–144 (2009).
429. Seluanov, A. *et al.* Change of the Death Pathway in Senescent Human Fibroblasts in Response to DNA Damage Is Caused by an Inability To Stabilize p53. *Mol. Cell. Biol.* **21**, 1552–1564 (2001).
430. Selvarajah, J., Elia, A., Carroll, V. A. & Moumen, A. DNA damage-induced S and G2/M cell cycle arrest requires mTORC2-dependent regulation of Chk1. *Oncotarget* **6**, 19–21 (2015).
431. Seo, G. J. *et al.* TRIM56-mediated monoubiquitination of cGAS for cytosolic DNA sensing. *Nat. Commun.* **9**, 613 (2018).
432. Serrano, M., Lin, A. W., McCurrach, M. E., Beach, D. & Lowe, S. W. Oncogenic ras provokes premature cell senescence associated with accumulation of p53 and p16(INK4a). *Cell* **88**, 593–602 (1997).
433. Shahni, R. *et al.* Signal transducer and activator of transcription 2 deficiency is a novel disorder of mitochondrial fission. *Brain* **138**, 2834–2846 (2015).

434. Shamanna, R. A., Croteau, D. L., Lee, J.-H. & Bohr, V. A. Recent Advances in Understanding Werner Syndrome. *F1000Research* **6**, 1779 (2017).
435. Sharma, N., Chakrabarti, S. & Grover, S. Gender differences in caregiving among family - caregivers of people with mental illnesses. *World J. Psychiatry* **6**, 7 (2016).
436. Sharpless, N. E. *et al.* p16(INK4a) and p53 deficiency cooperate in tumorigenesis. *Cancer Res.* **62**, 2761–5 (2002).
437. Shay, J. W., Pereira-Smith, O. M. & Wright, W. E. A role for both RB and p53 in the regulation of human cellular senescence. *Exp. Cell Res.* **196**, 33–39 (1991).
438. Sheridan, C. Drug developers switch gears to inhibit STING. *Nat. Biotechnol.* **37**, 199–201 (2019).
439. Shih, J.-W. *et al.* Critical roles of RNA helicase DDX3 and its interactions with eIF4E/PABP1 in stress granule assembly and stress response. *Biochem. J.* **441**, 119–129 (2012).
440. Shiratori, M. *et al.* WRN helicase accelerates the transcription of ribosomal RNA as a component of an RNA polymerase I-associated complex. *Oncogene* **21**, 2447–2454 (2002).
441. Sinclair, D. A. & Guarente, L. Extrachromosomal rDNA Circles— A Cause of Aging in Yeast. *Cell* **91**, 1033–1042 (1997).
442. Sofiadis, S. *et al.* HMGB1 as a rheostat of chromatin topology and RNA homeostasis on the path to senescence. *bioRxiv Genomics* 1–33 (2019). doi:10.1101/540146
443. Sowinski, S. *et al.* Membrane nanotubes physically connect T cells over long distances presenting a novel route for HIV-1 transmission. *Nat. Cell Biol.* **10**, 211–219 (2008).
444. Spilman, P. *et al.* Inhibition of mTOR by Rapamycin Abolishes Cognitive Deficits and Reduces Amyloid-β Levels in a Mouse Model of Alzheimer's Disease. *PLoS One* **5**, e9979 (2010).
445. Stanfel, M. N., Shamieh, L. S., Kaeberlein, M. & Kennedy, B. K. The TOR pathway comes of age. *Biochim. Biophys. Acta - Gen. Subj.* **1790**, 1067–1074 (2009).
446. Steensel, B. van & Henikoff, S. Identification of in vivo DNA targets of chromatin proteins using tethered Dam methyltransferase. *Nat. Biotechnol.* **18**, 424–428 (2000).
447. Stoeger, T., Gerlach, M., Morimoto, R. I. & Nunes Amaral, L. A. Large-scale investigation of the reasons why potentially important genes are ignored. *PLOS Biol.* **16**, e2006643 (2018).
448. Storer, M. *et al.* Senescence is a developmental mechanism that contributes to embryonic growth and patterning. *Cell* **155**, 1119 (2013).
449. Sun, L. *et al.* WRN is recruited to damaged telomeres via its RQC domain and tankyrase1-mediated poly-ADP-ribosylation of TRF1. *Nucleic Acids Res.* **45**, 3844–3859 (2017).
450. Sun, X. *et al.* Tunneling-nanotube direction determination in neurons and astrocytes. *Cell Death Dis.* **3**, e438–e438 (2012).
451. Sunami, Y. *et al.* Inhibition of the NAD-Dependent Protein Deacetylase SIRT2 Induces Granulocytic Differentiation in Human Leukemia Cells. *PLoS One* **8**, e57633 (2013).
452. Sundin, T. & Hentosh, P. InTERTesting association between telomerase, mTOR and phytochemicals. *Expert Rev. Mol. Med.* **14**, e8 (2012).
453. Sung, J. Y., Lee, K. Y., Kim, J. R. & Choi, H. C. Interaction between mTOR pathway inhibition and autophagy induction attenuates adriamycin-induced vascular smooth muscle cell senescence through decreased expressions of p53/p21/p16. *Exp. Gerontol.* **109**, 51–58 (2017).
454. Swinney, D. C. Phenotypic vs. Target-Based Drug Discovery for First-in-Class Medicines. *Clin. Pharmacol. Ther.* **93**, 299–301 (2013).
455. Szekely, A. M., Chen, Y.-H., Zhang, C., Oshima, J. & Weissman, S. M. Werner protein recruits DNA polymerase delta to the nucleolus. *Proc. Natl. Acad. Sci.* **97**, 11365–11370 (2000).

456. Takahashi, A. *et al.* DNA damage signaling triggers degradation of histone methyltransferases through APC/C Cdh1 in senescent cells. *Mol. Cell* **45**, 123–131 (2012).
457. Takahashi, A., Ohtani, N. & Hara, E. Irreversibility of cellular senescence: dual roles of p16INK4a/Rb-pathway in cell cycle control. *Cell Div.* **2**, 10 (2007).
458. Takahashi, A. *et al.* Mitogenic signalling and the p16INK4a–Rb pathway cooperate to enforce irreversible cellular senescence. *Nat. Cell Biol.* **8**, 1291–1297 (2006).
459. Takahashi, A. *et al.* Exosomes maintain cellular homeostasis by excreting harmful DNA from cells. *Nat. Commun.* **8**, 1–14 (2017).
460. Takahashi, A. *et al.* Tunneling nanotube formation is essential for the regulation of osteoclastogenesis. *J. Cell. Biochem.* **114**, 1238–1247 (2013).
461. Takasugi, M. *et al.* Small extracellular vesicles secreted from senescent cells promote cancer cell proliferation through EphA2. *Nat. Commun.* **8**, 1–11 (2017).
462. Takauji, Y. *et al.* Restriction of protein synthesis abolishes senescence features at cellular and organismal levels. *Sci. Rep.* **6**, 18722 (2016).
463. Talaei, F., van Praag, V. M. & Henning, R. H. Hydrogen sulfide restores a normal morphological phenotype in Werner syndrome fibroblasts, attenuates oxidative damage and modulates mTOR pathway. *Pharmacol. Res.* **74**, 34–44 (2013).
464. Tan, J.-K., Jaafar, F. & Makpol, S. Proteomic profiling of senescent human diploid fibroblasts treated with gamma-tocotrienol. *BMC Complement. Altern. Med.* **18**, 314 (2018).
465. Tanaka, Y. & Chen, Z. J. STING Specifies IRF3 Phosphorylation by TBK1 in the Cytosolic DNA Signaling Pathway. *Sci. Signal.* **5**, ra20–ra20 (2012).
466. Tennen, R. I. & Chua, K. F. Chromatin regulation and genome maintenance by mammalian SIRT6. *Trends Biochem. Sci.* **36**, 39–46 (2011).
467. Teo, Y. V. *et al.* Notch Signaling Mediates Secondary Senescence. *Cell Rep.* **27**, 997-1007.e5 (2019).
468. Thompson, P. J. *et al.* Targeted Elimination of Senescent Beta Cells Prevents Type 1 Diabetes. *Cell Metab.* **29**, 1045-1060.e10 (2019).
469. Thoreen, C. C. *et al.* A unifying model for mTORC1-mediated regulation of mRNA translation. *Nature* **485**, 109–113 (2012).
470. Tiku, V. *et al.* Small nucleoli are a cellular hallmark of longevity. *Nat. Commun.* **8**, 16083 (2017).
471. Tivey, H. S. E., Brook, A. J. C., Rokicki, M. J., Kipling, D. & Davis, T. p38 MAPK stress signalling in replicative senescence in fibroblasts from progeroid and genomic instability syndromes. *Biogerontology* **14**, 47–62 (2013).
472. Toledo, L. I. *et al.* A cell-based screen identifies ATR inhibitors with synthetic lethal properties for cancer-associated mutations. *Nat. Struct. Mol. Biol.* **18**, 721–727 (2011).
473. Tolstonog, G. V., Shoeman, R. L., Traub, U. & Traub, P. Role of the Intermediate Filament Protein Vimentin in Delaying Senescence and in the Spontaneous Immortalization of Mouse Embryo Fibroblasts. *DNA Cell Biol.* **20**, 509–529 (2001).
474. Torres, R. A. & Lewis, W. Aging and HIV/AIDS: pathogenetic role of therapeutic side effects. *Lab. Investig.* **94**, 120–128 (2014).
475. Toulany, M. *et al.* Function of erbB receptors and DNA-PKcs on phosphorylation of cytoplasmic and nuclear Akt at S473 induced by erbB1 ligand and ionizing radiation. *Radiother. Oncol.* **101**, 140–146 (2011).
476. Truban, D., Hou, X., Caulfield, T. R., Fiesel, F. C. & Springer, W. PINK1, Parkin, and Mitochondrial Quality Control: What can we Learn about Parkinson's Disease Pathobiology? *J. Parkinsons. Dis.* **7**, 13–29 (2017).
477. Turaga, R. V. N., Massip, L., Chavez, A., Johnson, F. B. & Lebel, M. Werner syndrome protein prevents DNA breaks upon chromatin structure alteration. *Aging Cell* **6**, 471–481 (2007).

478. Tyanova, S. & Cox, J. Perseus: A Bioinformatics Platform for Integrative Analysis of Proteomics Data in Cancer Research. in *Cancer Systems Biology* 133–148 (2018). doi:10.1007/978-1-4939-7493-1_7
479. Uehata, M. *et al.* Calcium sensitization of smooth muscle mediated by a Rho-associated protein kinase in hypertension. *Nature* **389**, 990–994 (1997).
480. Umbayev, B. *et al.* Elevated levels of the small GTPase Cdc42 induces senescence in male rat mesenchymal stem cells. *Biogerontology* **19**, 287–301 (2018).
481. Uphoff, C. C. & Drexler, H. G. Detecting Mycoplasma contamination in cell cultures by polymerase chain reaction. *Methods Mol. Med.* **88**, 319–26 (2004).
482. Uphoff, C. C. & Drexler, H. G. Comparative PCR analysis for detection of mycoplasma infections in continuous cell lines. *In Vitro Cell. Dev. Biol. Anim.* **38**, 79–85 (2002).
483. Urfer, S. R. *et al.* A randomized controlled trial to establish effects of short-term rapamycin treatment in 24 middle-aged companion dogs. *GeroScience* **39**, 117–127 (2017).
484. van Leeuwen, I. M. M., Rao, B., Sachweh, M. C. C. & Lain, S. An evaluation of small-molecule p53 activators as chemoprotectants ameliorating adverse effects of anticancer drugs in normal cells. *Cell Cycle* **11**, 1851–1861 (2012).
485. van Os, N. J. H. *et al.* Health risks for ataxia-telangiectasia mutated heterozygotes: a systematic review, meta-analysis and evidence-based guideline. *Clin. Genet.* **90**, 105–117 (2016).
486. van Tuyn, J. *et al.* Oncogene-Expressing Senescent Melanocytes Up-Regulate MHC Class II, a Candidate Melanoma Suppressor Function. *J. Invest. Dermatol.* **137**, 2197–2207 (2017).
487. Vande Berg, J. S. *et al.* Cultured pressure ulcer fibroblasts show replicative senescence with elevated production of plasmin, plasminogen activator inhibitor-1, and transforming growth factor-β1. *Wound Repair Regen.* **13**, 76–83 (2005).
488. Vaseva, A. V. & Moll, U. M. The mitochondrial p53 pathway. *Biochim. Biophys. Acta - Bioenerg.* **1787**, 414–420 (2009).
489. Vellai, T. *et al.* Influence of TOR kinase on lifespan in C. elegans. *Nature* **426**, 620–620 (2003).
490. Veranič, P. *et al.* Different Types of Cell-to-Cell Connections Mediated by Nanotubular Structures. *Biophys. J.* **95**, 4416–4425 (2008).
491. Vézina, C., Kudelski, A. & Sehgal, S. N. Rapamycin (AY-22,989), a new antifungal antibiotic. I. Taxonomy of the producing streptomycete and isolation of the active principle. *J. Antibiot. (Tokyo).* **28**, 721–726 (1975).
492. Vichai, V. & Kirtikara, K. Sulforhodamine B colorimetric assay for cytotoxicity screening. *Nat. Protoc.* **1**, 1112–1116 (2006).
493. Volonte, D. *et al.* Oxidative stress-induced inhibition of Sirt1 by caveolin-1 promotes p53-dependent premature senescence and stimulates the secretion of interleukin 6 (IL-6). *J. Biol. Chem.* **290**, 4202–4214 (2015).
494. Vulliamy, T. *et al.* The RNA component of telomerase is mutated in autosomal dominant dyskeratosis congenita. *Nature* **413**, 432–435 (2001).
495. Walters, H. E. & Cox, L. S. mTORC inhibitors as broad-spectrum therapeutics for age-related diseases. *Int. J. Mol. Sci.* **19**, 1–33 (2018).
496. Walters, H. E., Deneka-Hannemann, S. & Cox, L. S. Reversal of phenotypes of cellular senescence by pan-mTOR inhibition. *Aging (Albany. NY).* **8**, 231–244 (2016).
497. Walters, H. E. & Cox, L. S. Generation of a novel model of primary human cell senescence through Tenovin-6 mediated inhibition of sirtuins. *Biogerontology* **20**, 303–319 (2019).
498. Wang, B. *et al.* 14-3-3 Proteins Reduce Cell-to-Cell Transfer and Propagation of Pathogenic α-Synuclein. *J. Neurosci.* **38**, 8211–8232 (2018).

499. Wang, B., Hendricks, D. T., Wamunyokoli, F. & Parker, M. I. A Growth-Related Oncogene/CXC Chemokine Receptor 2 Autocrine Loop Contributes to Cellular Proliferation in Esophageal Cancer. *Cancer Res.* **66**, 3071–3077 (2006).
500. Wang, C. *et al.* DNA damage response and cellular senescence in tissues of aging mice. *Aging Cell* **8**, 311–323 (2009).
501. Wang, E. Senescent human fibroblasts resist programmed cell death, and failure to suppress bcl2 is involved. *Cancer Res.* **55**, 2284–92 (1995).
502. Wang, F. *et al.* S6K-STING interaction regulates cytosolic DNA–mediated activation of the transcription factor IRF3. *Nat. Immunol.* **17**, 514–522 (2016).
503. Wang, G. *et al.* Rad As a Novel Regulator of Excitation–Contraction Coupling and β-Adrenergic Signaling in Heart. *Circ. Res.* **106**, 317–327 (2010).
504. Wang, J. *et al.* Cell adhesion-mediated mitochondria transfer contributes to mesenchymal stem cell-induced chemoresistance on T cell acute lymphoblastic leukemia cells. *J. Hematol. Oncol.* **11**, 11 (2018).
505. Wang, L. *et al.* A pH probe inhibits senescence in mesenchymal stem cells. *Stem Cell Res. Ther.* **9**, 343 (2018).
506. Wang, X. & Gerdes, H.-H. Transfer of mitochondria via tunneling nanotubes rescues apoptotic PC12 cells. *Cell Death Differ.* **22**, 1181–1191 (2015).
507. Wang, Y., Cui, J., Sun, X. & Zhang, Y. Tunneling-nanotube development in astrocytes depends on p53 activation. *Cell Death Differ.* **18**, 732–742 (2011).
508. Whitehead, J. *et al.* Tunneling Nanotubes Mediate the Expression of Senescence Markers in Mesenchymal Stem/Stromal Cell Spheroids. *Stem Cells* epub (2019). doi:10.1002/stem.3056
509. Wiley, C. D. *et al.* Mitochondrial Dysfunction Induces Senescence with a Distinct Secretory Phenotype. *Cell Metab.* **23**, 303–314 (2016).
510. Wilkinson, J. E. *et al.* Rapamycin slows aging in mice. *Aging Cell* **11**, 675–682 (2012).
511. Wilson, D., Jackson, T., Sapey, E. & Lord, J. M. Frailty and sarcopenia: The potential role of an aged immune system. *Ageing Res. Rev.* **36**, 1–10 (2017).
512. Wong, W. T. *et al.* Treatment of Geographic Atrophy With Subconjunctival Sirolimus: Results of a Phase I/II Clinical Trial. *Investig. Opthalmology Vis. Sci.* **54**, 2941 (2013).
513. Wood, J. G. *et al.* Sirtuin activators mimic caloric restriction and delay ageing in metazoans. *Nature* **430**, 686–689 (2004).
514. Wood, Z. A., Schröder, E., Robin Harris, J. & Poole, L. B. Structure, mechanism and regulation of peroxiredoxins. *Trends Biochem. Sci.* **28**, 32–40 (2003).
515. Xie, J. & Proud, C. G. Signaling crosstalk between the mTOR complexes. *Translation* **2**, e28174 (2014).
516. Xu, M. *et al.* Transplanted Senescent Cells Induce an Osteoarthritis-Like Condition in Mice. *Journals Gerontol. Ser. A Biol. Sci. Med. Sci.* glw154 (2016).
517. Xu, M. *et al.* Targeting senescent cells enhances adipogenesis and metabolic function in old age. *Elife* **4**, e12997 (2015).
518. Xu, M. *et al.* Senolytics improve physical function and increase lifespan in old age. *Nat. Med.* **24**, 1246–1256 (2018).
519. Yang, H. & Fogo, A. B. Cell Senescence in the Aging Kidney. *J. Am. Soc. Nephrol.* **21**, 1436–1439 (2010).
520. Yang, H. *et al.* mTOR kinase structure, mechanism and regulation. *Nature* **497**, 217–223 (2013).
521. Yang, L. *et al.* Rho GTPase Cdc42 coordinates hematopoietic stem cell quiescence and niche interaction in the bone marrow. *Proc. Natl. Acad. Sci.* **104**, 5091–5096 (2007).
522. Yang, N. C. & Hu, M. L. The limitations and validities of senescence associated-β-galactosidase activity as an aging marker for human foreskin fibroblast Hs68 cells. *Exp. Gerontol.* **40**, 813–819 (2005).

523. Yang, Y. *et al.* Rapamycin Prevents Early Steps of the Development of Diabetic Nephropathy in Rats. *Am. J. Nephrol.* **27**, 495–502 (2007).
524. Ye, X. *et al.* Downregulation of Wnt Signaling Is a Trigger for Formation of Facultative Heterochromatin and Onset of Cell Senescence in Primary Human Cells. *Mol. Cell* **27**, 183–196 (2007).
525. Yoon, J. S., Moon, J. S., Kim, Y.-W., Won, K. C. & Lee, H. W. The Glucotoxicity Protecting Effect of Ezetimibe in Pancreatic Beta Cells via Inhibition of CD36. *J. Korean Med. Sci.* **31**, 547 (2016).
526. Yosef, R. *et al.* p21 maintains senescent cell viability under persistent DNA damage response by restraining JNK and caspase signaling. *EMBO J.* **36**, 2280–2295 (2017).
527. Yosef, R. *et al.* Directed elimination of senescent cells by inhibition of BCL-W and BCL-XL. *Nat. Commun.* **7**, 11190 (2016).
528. Yosihda, T., Nakamura, H., Masutani, H. & Yodoi, J. The Involvement of Thioredoxin and Thioredoxin Binding Protein-2 on Cellular Proliferation and Aging Process. *Ann. N. Y. Acad. Sci.* **1055**, 1–12 (2005).
529. Yousefzadeh, M. J. *et al.* Fisetin is a senotherapeutic that extends health and lifespan. *EBioMedicine* **36**, 18–28 (2018).
530. Yu, C.-E. *et al.* Positional Cloning of the Werner's Syndrome Gene. *Science (80-.).* **272**, 258–262 (1996).
531. Yu, Q. *et al.* DNA-Damage-Induced Type I Interferon Promotes Senescence and Inhibits Stem Cell Function. *Cell Rep.* **11**, 785–797 (2015).
532. Yuan, H. *et al.* Activation of stress response gene SIRT1 by BCR-ABL promotes leukemogenesis. *Blood* **119**, 1904–1914 (2012).
533. Yun, M. H. Cellular senescence in tissue repair: every cloud has a silver lining. *Int. J. Dev. Biol.* **62**, 591–604 (2018).
534. Yun, M. H., Davaapil, H. & Brockes, J. P. Recurrent turnover of senescent cells during regeneration of a complex structure. *Elife* **4**, 1–16 (2015).
535. Zglinicki, T. von. Role of oxidative stress in telomere length regulation and replicative senescence. *Ann. N. Y. Acad. Sci.* 99–110 (2000).
536. Zhang, R., Chen, W. & Adams, P. D. Molecular Dissection of Formation of Senescence-Associated Heterochromatin Foci. *Mol. Cell. Biol.* **27**, 2343–2358 (2007).
537. Zhang, R. *et al.* Formation of macroH2A-containing senescence-associated heterochromatin foci and senescence driven by ASF1a and HIRA. *Dev. Cell* **8**, 19–30 (2005).
538. Zhang, X. *et al.* Oxidation resistance 1 is a novel senolytic target. *Aging Cell* **17**, e12780 (2018).
539. Zhang, Y. Tunneling-nanotube. *Commun. Integr. Biol.* **4**, 324–325 (2011).
540. Zhou, Y. *et al.* Metascape provides a biologist-oriented resource for the analysis of systems-level datasets. *Nat. Commun.* **10**, 1523 (2019).
541. Zhu, D., Wu, J., Spee, C., Ryan, S. J. & Hinton, D. R. BMP4 Mediates Oxidative Stress-induced Retinal Pigment Epithelial Cell Senescence and Is Overexpressed in Age-related Macular Degeneration. *J. Biol. Chem.* **284**, 9529–9539 (2009).
542. Zhu, Y. *et al.* Identification of a novel senolytic agent, navitoclax, targeting the Bcl-2 family of anti-apoptotic factors. *Aging Cell* **15**, 428–435 (2016).
543. Zhu, Y. *et al.* The Achilles' heel of senescent cells: from transcriptome to senolytic drugs. *Aging Cell* **14**, 644–658 (2015).
544. Zirkel, A. *et al.* HMGB2 Loss upon Senescence Entry Disrupts Genomic Organization and Induces CTCF Clustering across Cell Types. *Mol. Cell* **70**, 730-744.e6 (2018).
545. Zou, W. *et al.* Exosome Release Is Regulated by mTORC1. *Adv. Sci.* **6**, 1801313 (2019).

10. Supplementary Material

Supplementary Table S6.1

Comparison	Gene name	Protein name	(-Log$_{10}$) Student's T-test p-value	Student's T-test Difference
PRO_SEN				
UP IN SEN	COL8A1	Collagen alpha-1(VIII) chain;Vastatin	2.85964	-7.06191
	PLAT	Tissue-type plasminogen activator	2.31365	-5.14948
	GM2A	Ganglioside GM2 activator;Ganglioside GM2 activator isoform short	3.18475	-4.81496
	CST1	Cystatin-SN	2.27277	-4.07895
	ASAP1	Arf-GAP with SH3 domain, ANK repeat and PH domain-containing protein 1	2.62886	-3.87989
	MSI2	RNA-binding protein Musashi homolog 2	2.87287	-3.78826
	SERPINB2	Plasminogen activator inhibitor 2	2.885	-3.49015
	FBXO2	F-box only protein 2	2.09852	-3.22466
	MOXD1	DBH-like monooxygenase protein 1	2.07771	-2.71604
	TRIM56	E3 ubiquitin-protein ligase TRIM56	2.92714	-2.4205
	PRNP	Major prion protein	2.50313	-2.3271
	PRAMEF	PRAME family member	2.07992	-2.23141
	WFS1	Wolframin	2.23429	-2.17331
	SMARCE1	SWI/SNF-related matrix-associated actin-dependent regulator of chromatin subfamily E member 1	2.12025	-2.1639
	AKR1B1	Aldose reductase	2.01287	-1.96096
	CMAS	N-acylneuraminate cytidylyltransferase	2.36286	-1.9119
	CDH2	Cadherin-2	2.12593	-1.87829
	ANPEP	Aminopeptidase N	3.07378	-1.76558
	RPAP1	RNA polymerase II-associated protein 1	2.35956	-1.55951
	DHRS7	Dehydrogenase/reductase SDR family member 7	2.74282	-1.51234
	UCHL1	Ubiquitin carboxyl-terminal hydrolase isozyme L1	2.46569	-1.27264
	CSTF2T	Cleavage stimulation factor subunit 2 tau variant	2.11628	-1.20541
	PRDX5	Peroxiredoxin-5, mitochondrial	2.65969	-0.987014
	GSN	Gelsolin	2.19403	-0.771281
	RCN2	Reticulocalbin-2	2.23843	-0.74861

	PRDX1	Peroxiredoxin-1	2.42542	-0.428336
DOWN IN SEN	RPL22L1	60S ribosomal protein L22-like 1	2.05514	5.5161
	CLDN11	Claudin-11	3.35659	5.47769
	CTHRC1	Collagen triple helix repeat-containing protein 1	2.22664	4.99429
	RAB3IL1	Guanine nucleotide exchange factor for Rab-3A	3.07084	3.36656
	PDGFRA	Platelet-derived growth factor receptor alpha	2.61149	3.14735
	CLTCL1	Clathrin heavy chain 2	2.77081	2.68148
	ZC3H7A	Zinc finger CCCH domain-containing protein 7A	2.12425	2.44499
	ITFG1	T-cell immunomodulatory protein	2.24886	2.42135
	CALD1	Caldesmon	2.20706	2.17244
	PRPSAP2	Phosphoribosyl pyrophosphate synthase-associated protein 2	2.0995	2.11579
	PPFIBP1	Liprin-beta-1	2.41862	1.89268
	DAXX	Death domain-associated protein 6	2.0485	1.82497
	SPATS2L	SPATS2-like protein	3.03395	1.80517
	STRN4	Striatin-4	2.27274	1.78463
	COPZ1	Coatomer subunit zeta-1	2.50448	1.48302
	SF3B3	Splicing factor 3B subunit 3	2.50565	1.33681
	CHD4;CHD5	Chromodomain-helicase-DNA-binding protein 4;Chromodomain-helicase-DNA-binding protein 5	2.43974	1.01654
	HNRNPL	Heterogeneous nuclear ribonucleoprotein L	2.28821	0.916333
	SYDE1	Rho GTPase-activating protein SYDE1	2.34358	0.864642
	HNRNPUL1	Heterogeneous nuclear ribonucleoprotein U-like protein 1	2.59137	0.769681
	HNRNPC	Heterogeneous nuclear ribonucleoproteins C1/C2	4.9255	0.714842
PERI_SEN				
UP IN SEN	COL8A1	Collagen alpha-1(VIII) chain;Vastatin	3.19549	-5.51271
	CD36	Platelet glycoprotein 4	2.03468	-4.77225
	PLAT	Tissue-type plasminogen activator	2.04879	-4.27939
	CST1	Cystatin-SN	2.97138	-3.12357
	FBXO2	F-box only protein 2	2.40809	-2.73428
	ANPEP	Aminopeptidase N	3.06657	-1.37525
	ASS1	Argininosuccinate synthase	2.61803	-1.28256
	RTN4	Reticulon-4	2.31017	-0.814491
	LMAN1	Protein ERGIC-53	4.04625	-0.463817
DOWN IN SEN	CRIP2	Cysteine-rich protein 2	2.05726	3.48959
	LBR	Lamin-B receptor	2.2519	3.04515

	HMGB2	High mobility group protein B2	2.87424	2.96112
	RTN4	Reticulon-4	2.49457	2.94702
	PRPSAP2	Phosphoribosyl pyrophosphate synthase-associated protein 2	2.40172	2.74261
	ITFG1	T-cell immunomodulatory protein	3.26468	2.71754
	STAT2	Signal transducer and activator of transcription 2	2.04155	2.54545
	RALGPS2	Ras-specific guanine nucleotide-releasing factor RalGPS2	2.07185	2.52807
	TRMT1	tRNA (guanine(26)-N(2))-dimethyltransferase	2.13054	2.40749
	USP39	U4/U6.U5 tri-snRNP-associated protein 2	2.13106	2.34236
	SNX18	Sorting nexin-18	2.26643	1.99307
	HTATSF1	HIV Tat-specific factor 1	2.17556	1.93234
	CPSF6	Cleavage and polyadenylation specificity factor subunit 6	2.16921	1.56691
	RBM3	Putative RNA-binding protein 3	2.22029	1.24224
	G6PD	Glucose-6-phosphate 1-dehydrogenase	2.06995	1.22854
	COPZ1	Coatomer subunit zeta-1	2.04355	1.21268
	SRPR	Signal recognition particle receptor subunit alpha	2.31528	1.18969
	NAV1	Neuron navigator 1	2.20546	1.11333
	HNRNPL	Heterogeneous nuclear ribonucleoprotein L	2.19358	0.771263
	PA2G4	Proliferation-associated protein 2G4	2.01764	0.741189
	CRABP2	Cellular retinoic acid-binding protein 2	2.45676	0.726133
PRO_PERI				
UP IN PERI	ATE1	Arginyl-tRNA--protein transferase 1	2.20338	-3.54398
	ARPP19	cAMP-regulated phosphoprotein 19	2.12536	-3.25906
	MIEN1	Migration and invasion enhancer 1	2.57713	-3.15883
	LIMA1	LIM domain and actin-binding protein 1	2.43484	-1.79783
	INPP5K	Inositol polyphosphate 5-phosphatase K	2.40762	-1.16415
	AKAP11	A-kinase anchor protein 11	2.19212	-0.787334
	CRABP2	Cellular retinoic acid-binding protein 2	2.74575	-0.740908
DOWN IN PERI	HCFC1	Host cell factor 1	2.74635	0.969767
	SEPT5	Septin-5	2.41914	1.77278

Supplementary Table S6.1 Statistical hits of pairwise comparisons from comparative proteomics of replicative senescence.

Supplementary Table S6.2

Comparison	Gene name	Protein name	(-Log_{10}) Student's T-test p-value	Student's T-test Difference
PRO ± AZD8055				
UP ON AZD8055	COL8A1	Collagen alpha-1(VIII) chain;Vastatin	2.268856287	2.155943871
	AGFG1	Arf-GAP domain and FG repeat-containing protein 1	2.230368853	1.370090485
	PHPT1	14 kDa phosphohistidine phosphatase	2.086373329	1.164999008
	ANPEP	Aminopeptidase N	2.348256111	0.822317123
	TPR	Nucleoprotein TPR	2.362705708	0.513710022
	CMPK1	UMP-CMP kinase	2.647693396	0.440823555
	MYL9	Myosin regulatory light polypeptide 9	2.103111982	0.361738205
DOWN ON AZD8055				
	PSMB8	Proteasome subunit beta type-8	3.287923574	-1.721815109
	HIBCH	3-hydroxyisobutyryl-CoA hydrolase, mitochondrial	3.057844162	-1.500289917
	EPHX1	Epoxide hydrolase 1	2.528011799	-1.236840248
	SAR1A	GTP-binding protein SAR1a	2.488519192	-1.16901207
	COL6A1	Collagen alpha-1(VI) chain	2.16920948	-0.870118141
	FAM162A	Protein FAM162A	2.111553431	-0.443446159
PERI ± AZD8055				
UP ON AZD8055	PRKAB1	5-AMP-activated protein kinase subunit beta-1	2.225982904	2.607385635
	CRIP2	Cysteine-rich protein 2	2.074705124	2.099671602
	VAMP2	Vesicle-associated membrane protein 2	2.208615303	1.416007042
	SMARCE1	SWI/SNF-related matrix-associated actin-dependent regulator of chromatin subfamily E member 1	2.2407341	1.399971366
	MGARP	Protein MGARP	2.38444066	1.256875396
	CLMP	CXADR-like membrane protein	2.191079617	1.220062852
	IGF2BP2	Insulin-like growth factor 2 mRNA-binding protein 2	2.431643724	0.935033798
	ANPEP	Aminopeptidase N	2.748897076	0.869091034
	HP1BP3	Heterochromatin protein 1-binding protein 3	2.615540743	0.842790604
	H2AFY	Core histone macro-H2A.1	2.027689934	0.754719436
	TMEM43	Transmembrane protein 43	2.132051945	0.714179993
	MYADM	Myeloid-associated differentiation marker	2.204995871	0.683201492
	ESYT2	Extended synaptotagmin-2	2.03438139	0.605337799
	LMBRD1	Probable lysosomal cobalamin transporter	2.25659132	0.567186356
	LMNB1	Lamin-B1	2.018817663	0.391370773
DOWN ON AZD8055	ASCC2	Activating signal cointegrator 1 complex subunit 2	2.749554873	-1.754846931

	STAT2	Signal transducer and activator of transcription 2	2.021143675	-1.489892364
	SELENBP1	Selenium-binding protein 1	2.498142242	-1.319455504
	ERAP2	Endoplasmic reticulum aminopeptidase 2	2.399851799	-1.265826583
	PPP4R1	Serine/threonine-protein phosphatase 4 regulatory subunit 1	2.228532553	-1.255233765
	LRRC40	Leucine-rich repeat-containing protein 40	2.059760809	-1.108135819
	LIMA1	LIM domain and actin-binding protein 1	2.005773306	-0.98149997
	POR	NADPH--cytochrome P450 reductase	2.098381281	-0.889744461
	PGD	6-phosphogluconate dehydrogenase, decarboxylating	2.940891743	-0.755226135
	CORO1B	Coronin-1B	2.958579779	-0.665555298
	WDR82	WD repeat-containing protein 82	2.236100912	-0.642587006
	PA2G4	Proliferation-associated protein 2G4	2.359664679	-0.575607955
	NECAP2	Adaptin ear-binding coat-associated protein 2	2.116609573	-0.509569824
	ILF3	Interleukin enhancer-binding factor 3	2.379317284	-0.450717926
	DDX3X	ATP-dependent RNA helicase DDX3X	2.183496714	-0.442045838
	CAT	Catalase	2.081552982	-0.432378143
	ETFB	Electron transfer flavoprotein subunit beta	2.015107632	-0.362941742
	IMMT	Mitochondrial inner membrane protein	2.118208647	-0.17040889
SEN ± AZD8055				
UP ON AZD8055	WASL	Neural Wiskott-Aldrich syndrome protein	2.216403484	1.43123436
	KIF2A	Kinesin-like protein KIF2A	2.149124146	1.376105666
	TGM2	Protein-glutamine gamma-glutamyltransferase 2	2.8456738	1.18062079
	EVA1B	Protein eva-1 homolog B	2.239509583	1.157167435
	ANPEP	Aminopeptidase N	2.153449297	0.843577683
	ITGA2	Integrin alpha-2	2.085857868	0.721862793
	CTSD	Cathepsin D;Cathepsin D light chain;Cathepsin D heavy chain	2.402604818	0.665993989
	WDR3	WD repeat-containing protein 3	2.031283379	0.357647896
DOWN ON AZD8055	FADS2	Fatty acid desaturase 2	2.133281946	-2.445489883
	TUBB2B	Tubulin beta-2B chain	2.25515151	-0.757843018
	FAM45A;FAM45B	Protein FAM45A;Protein FAM45B	3.215917349	-0.537092209
	RMDN2	Regulator of microtubule dynamics protein 2	2.09863472	-0.4061203

Supplementary Table S6.2 Statistical hits of pairwise comparisons from comparative proteomics of pan-mTOR inhibition